

University of Nottingham
UK | CHINA | MALAYSIA

Identifying factors that control medulloblastoma cell migration using a model of brain-CSF dissemination

Macha Anne-Marie Jeanine Aldighieri

Thesis submitted to the University of Nottingham for the degree of

Doctor of Philosophy

June 2020



Children's
Brain Tumour
Research Centre

Abstract

Introduction

Medulloblastoma is the most common type of malignant paediatric brain tumour, accounting for 10% of cancer deaths in children. While survival rates have improved in recent years, metastatic spread poses a significant challenge to therapy success. Current therapies also cause irreparable damage to the surrounding brain leading to a decreased quality of life in surviving patients, consequently there is a need for new targeted therapy options. One of the routes for dissemination of metastatic cells is invasion into the leptomeninges, a process during which cells cross basement membrane barriers as they travel from the primary tumour niche into the metastatic niche in the cerebrospinal fluid (CSF). The pathways involved in dissemination and metastasis remain elusive, and a better understanding is crucial to developing targeted therapies. This project aimed to develop an *in vitro* model system to mimic key characteristics of cell migration from the brain to the CSF, and identify novel candidate genes driving medulloblastoma metastasis.

Methods

An *in vitro* culture model representing certain features of the basement membrane interface between the brain parenchyma and the CSF was developed in order to isolate cells for transcriptomic analysis from three compartments: (a) non-metastatic suspension cells, (b) early metastatic adherent cells, and (c) metastatic migrated cells. Differentially expressed genes in these three compartments were identified by Next Generation 3^{I} UPX RNA Seq. The prognostic role of candidates was assessed by analysis of a large medulloblastoma gene expression dataset (Cavalli et al., 2017) on the R2: Genomics Analysis and Visualization Platform (http://r2.amc.nl). SORCS2 expression was validated in medulloblastoma cell lines by qRT-PCR and western blotting, and a possible function assessed *in vitro* after siRNA knockdown.

Results

A trans-well migration assay format was modified to represent certain features of the basement membrane, collagen IV and laminin 111 were used as a basement membrane-like coating, and cells were induced to migrate towards artificial CSF supplemented with FBS. The transcripts *SORCS2, CORO2B* and *LMNB1-DT* were identified as candidates that may drive the process of migration. The gene *SORCS2* demonstrated a significant increase in expression as Group 3 medulloblastoma cells progressed through the stages of migration, from the suspension compartment to the adherent compartment and then to the migration compartment. The transcripts *CORO2B* and *LMNB1-DT* were upregulated in cells in the adherent compartment. The expression of *SORCS2, CORO2B* and *LMNB1-DT* correlated with poor patient outcome and metastatic recurrence in medulloblastoma patients. *SORCS2* was selected for further *in vitro* investigation as it most significantly correlated with an early poor survival trend in patients with metastatic tumours. *SORCS2* gene and protein expression was confirmed in Group 3 and Group 4 cell lines. The results from *in vitro* experiments did not allow significant conclusions relating to *SORCS2* function in migration to be drawn, however they offer preliminary data encouraging further investigation.

Conclusions

This non-biased, model-led, target identification approach identified genes of interest *SORCS2* and *CORO2B*, and lncRNA *LMNB1-DT*, in migrating medulloblastoma cells. *SORCS2* encodes a brain-specific transmembrane receptor in the VPS10 family of sorting proteins previously linked to actin dynamics in neuronal growth cones, and was implicated in the migratory behaviour of basal-like breast carcinoma. The analyses in this project suggested a link between *SORCS2*, metastasis, and tumour recurrence in medulloblastoma. The other candidates identified by these analyses warrant further validation and may shed light on the metastatic process in medulloblastoma. A better understanding of the processes and pathways that drive malignancy is a starting point for a push towards improving efficacy of our treatment options while reducing toxicity.

Acknowledgements

I would like to thank the following people for their help and support throughout my PhD project.

To my supervisor Dr Beth Coyle, thank you for giving me the opportunity to work on this project as a member of your lab, and believing in my abilities as a researcher. I am grateful for your understanding and guidance over the last few years. To my supervisors Prof Anna Grabowska and Dr Ian Kerr, I would like to sincerely thank you for all your advice and encouragements. To all my supervisors, I am deeply appreciative of the kindness and dedication that you have shown me during the last 4 years.

I also want to express my gratitude to my colleagues, who became my support network during my time as a student. To Dr Franziska Linke, thank you for your invaluable advice and for your friendship. I cannot imagine my PhD journey without you by my side. To my dear friends Sophie, Hannah, Christine, Alice, Louisa and James, I could not have asked for a better lab group. You have stood by me through all the challenges, and helped me forward every step of the way. To my wonderful fellow CBTRC students and friends, thank you for creating such a joyful and caring working environment filled with laughter and yummy snacks. A special thank you to Matt, Jasper, James, Josh, Catherine, Phoebe, Alina, Andie, Louise and Michaela.

To all the members of CBTRC, thank you for a memorable time as part of our lively, friendly community. I will fondly remember our bake-offs, Christmas parties and samosa-fuelled social events.

Finally, I would like to thank the Stoneygate Trust for funding this work.

To my beloved parents, Maman et Papa, your unwavering love and support have made me the woman and scientist I am today.

Table of contents

Abstract i

Acknowledgements iii

Table of contents iv

List of tables xiv

List of figures xvi

List of common abbreviations 1

Chapter 1 Introduction 3

1.1 Paediatric medulloblastoma 3

1.1.1 Epidemiology of medulloblastoma 3

1.2 Medulloblastoma classification 5

1.2.1 Histological subgroups 5

1.2.2 Molecular subgroups 7

1.2.2.1 WNT 7

1.2.2.2 SHH 7

1.2.2.3 Group 3 8

1.2.2.4 Group 4 8

1.2.3 Molecular subtypes 9

1.2.3.1 WNT 10

1.2.3.2 SHH 10

1.2.3.3 Group 3 11

1.2.3.4 Group 4 12

1.3 Cerebellar location and origins 13

1.4 Diagnosis and treatment 18

1.4.1 Clinical symptoms and staging 18

1.4.2 Treatment 19

1.4.3 Impacts on quality of life 20

1.5 The leptomeninges and CSF circulation 21

1.6 Metastasis 23

1.6.1 General cancer metastasis 23

1.6.1.1 The metastatic cascade 23

1.6.1.2 Control of cell migration 24

1.6.2 Medulloblastoma leptomeningeal metastasis 26

1.6.2.1 Leptomeningeal metastasis 26

1.6.2.2 Invasion into the leptomeninges 27

1.6.2.3 Haematogenous metastasis 28

1.6.3 Invading basement membranes in the brain 28

1.7 *In viv*o and *in vitro* models 30

1.7.1 *In vivo* models of medulloblastoma 30

1.7.2 *In vitro* models of medulloblastoma 32

1.7.2.1 Primary cultures and cell lines 32

1.7.2.2 3D in vitro cultures 33

1.7.2.3 Hydrogel-based 3D cultures 34

1.7.2.4 More complex 3D culture systems 35

1.7.2.5 In vitro models of migration 36

1.8 Hypothesis and aims 39

Chapter 2 Materials & Methods 40

2.1.1 Cell lines used 40

2.1.2 Standard cell culture 40

2.1.2.1 Standard cell culture media 40

2.1.2.2 Recovering cells from liquid nitrogen cryo-storage 41

2.1.2.3 Mycoplasma testing and cell line authentication 41

2.1.2.4 Sub-culturing cell lines 41

2.1.2.5 Preparing stocks for cryo-storage 42

2.1.2.6 Preparing cell pellets for molecular analysis 43

2.1.2.7 Cell counting 43

2.2 Cell culture in 3D 44

2.2.1 Basement membrane extract hydrogel culture 44

2.2.2 Plating BME in 96-well microplates 44

2.2.3 Plating BME in a chemotaxis u-slide 45

2.3 Cell culture imaging 45

2.3.1 Widefield imaging of 3D cultures in a 96-well microplate 45

2.3.2 Time-lapse imaging of 3D cultures in a chemotaxis µ-slide 46

2.4 Assessing cell viability 46

2.5 Migration and invasion assays *in vitro* 47

2.5.1 Chemotaxis migration assay 47

2.5.1.1 Serum starvation 47

2.5.2 Quantification of migration assay 47

2.5.2.1 Metabolic activity assay 47

2.5.2.2 Staining 49

2.5.3 Isolation of cells from migration assays for molecular analysis 49

2.5.3.1 Basement membrane ECM coating 49

2.5.3.2 Collecting cells for molecular analysis 50

2.6 Molecular techniques 50

2.6.1 RNA extraction 50

2.6.1.1 From 3D culture in BME 50

2.6.1.2 From cell pellets 51

2.6.2 Measuring RNA concentration and purity 51

2.6.2.1 RNA samples isolated from BME 51

2.6.2.2 RNA samples from migration assays for 3’ UPX RNA-seq 51

2.6.2.3 RNA samples from standard cell pellets for qRT-PCR analysis 51

2.6.3 Analysing gene expression 52

2.6.3.1 cDNA synthesis 52

2.6.3.2 Primer design 52

2.6.3.3 qRT-PCR 53

2.6.3.4 Gene expression analysis 54

2.6.4 Protein extraction 54

2.6.5 Measuring protein concentration 54

2.6.6 Analysing protein expression 55

2.6.6.1 Protein sample preparation 55

2.6.6.2 SDS gel preparation 55

2.6.6.3 Gel electrophoresis 55

2.6.6.4 Transfer 56

2.6.6.5 Western blotting 56

2.6.6.6 Western blot development 57

2.6.6.7 Western blot quantification 57

2.7 Transfection of cells in standard culture 58

2.7.1 Transfection with GFP vector 58

2.7.1.1 Transfection efficiency 58

2.7.2 siRNA knockdown of gene expression 58

2.7.2.1 Transfection efficiency 59

2.8 Patient tissue IHC 59

2.8.1 Patient TMAs 59

2.8.2 IHC 60

2.8.2.1 Preparation and rehydration 60

2.8.2.2 Antigen Retrieval 60

2.8.2.3 Peroxidase quenching and blocking 60

2.8.2.4 Antibody incubation 61

2.8.2.5 Antibody detection 61

2.8.3 TMA imaging and scoring 62

2.9 Next Generation Sequencing: 3′ UPX RNA-seq 62

2.9.1.1 Library preparation 62

2.9.1.2 Primary sequence analysis 63

2.9.1.3 Differential gene expression analysis 63

2.10 Gene Ontology analysis 65

2.11 Identifying patterns of gene expression 65

2.12 Patient dataset analysis 66

2.13 Figures and statistical analysis 66

Chapter 3 Developing an *in vitro* model of the brain-CSF interface to capture migrating cells 67

3.1 Introduction 67

3.2 Optimising growth and migration conditions for a range of cell lines in BME 69

3.2.1 Optimising matrix concentration 73

3.2.2 Optimising culture medium 80

3.2.3 Observing cell migration of a metastatic cell line in BME through time-lapse microscopy 85

3.3 A trans-well migration assay to model the basement membrane 89

3.3.1 BME as a basement membrane coating 90

3.3.2 Optimising a chemokine gradient to induce cell migration 95

3.3.3 Using a combination of collagen IV and Laminin as a basement membrane coating 106

3.3.4 Optimising the time point at which to isolate cell samples 107

3.3.5 Isolating cells from three compartments for molecular analysis 109

3.4 Summary 111

Chapter 4 Identifying new markers of migration and metastasis through analysis of transcriptomic differences between cells from an optimised *in vitro* model 113

4.1 Introduction 113

4.2 Sample preparation 116

4.3 Analysis 118

4.3.1 Mapping the sequencing data 118

4.3.2 Differential expression analysis 121

4.3.3 Sample classes 122

4.3.4 Visualization of genes with large magnitude changes 124

4.3.5 Differentially expressed genes between cell compartments 127

4.4 Identifying patterns of gene expression 131

4.4.1 Patterns of gene expression across cell lines 131

4.4.2 Patterns of gene expression across cell compartments 137

4.5 Identifying target genes involved in migration and metastasis 143

4.5.1 Gene expression in patients by subgroup 146

4.5.2 Gene expression in patients by metastatic status 151

4.5.3 Patient survival 155

4.6 Summary 161

Chapter 5 Proposing a novel role for SORCS2 in medulloblastoma migration and metastasis 162

5.1 Introduction 162

5.2 Expression of genes of interest in patients 165

5.2.1 SORCS2, LMNB1 and CORO2B RNA is expressed in medulloblastoma patients 165

5.2.2 Gene expression in metastatic tumours may be associated with poor patient outcome 173

5.2.3 SORCS2 protein is expressed in medulloblastoma patient tissue 177

5.3 SORCS2 is expressed in Group 3 and group 4 medulloblastoma cell lines 186

5.4 Optimising transfection and knockdown in Group 3 cell lines 190

5.4.1 Optimising transient transfection and siRNA knockdown of SORCS2 . 190

5.5 Knockdown of SORCS2 seems to reduce cell migration, but not cell viability in Group 3 cell lines 195

5.6 Summary 200

Chapter 6 Discussion 202

6.1 Main Findings 202

6.2 Developing an *in vitro* model of medulloblastoma 203

6.2.1 Addressing the need to identify the subset of clones that drives metastatic dissemination 203

6.2.2 Addressing the need to investigate the poorly understood TME of leptomeningeal metastasis 204

6.2.3 Pros and cons of the model 207

6.2.3.1 Pros: 207

6.2.3.2 Cons: 209

6.2.4 Future directions 214

6.2.4.1 Conclusions 216

6.3 Identifying novel markers of migration and metastasis using NGS 217

6.3.1 Advantages of the study 217

6.3.2 Disadvantages of the study 218

6.3.3 Candidates of interest identified by the analysis of 3′ RNA-seq data ... 221

6.3.3.1 CORO2B 221

6.3.3.2 LMNB1 222

6.3.3.3 Conclusions 223

6.4 Investigating a novel role for SORCS2 in brain tumour cell migration 225

6.4.1 SORCS2 function in neural cells 225

6.4.2 SORCS2 in growth cone motility 226

6.4.3 SORCS2 in cellular trafficking 228

6.4.4 Functional overlap with Sortilin 231

6.4.4.1 Therapeutic targeting of SORT1 and SORCS2 231

6.4.4.2 A function for SORT1 and SORCS2 in extracellular vesicles 232

6.4.5 Future Directions 233

6.4.5.1 Defining SORCS2 localization in migrating cells 233

6.4.5.2 Inhibiting SORCS2 expression and function in vitro and in vivo ... 234

6.4.5.3 Investigating SORCS2 pathways in cell migration 234

6.5 Conclusion 237

Publications 238

Conferences & meetings 238

Prizes and awards 238

References 239

Appendices 261

List of tables

Table 1.1 Summary of most common integrated medulloblastoma diagnoses based on the 2016 WHO classification, reproduced from Louis *et al*., 2016. 4

Table 1.2 The 4 molecular subgroups of medulloblastoma according to the most recent WHO consensus. 6

Table 1.3 Chang's staging system for medulloblastoma. 19

Table 2.1 Soluble factors tested as chemokines. 47

Table 2.2 ECM gel or components used to coat trans-well inserts. 50

Table 2.3 cDNA synthesis master mix. 52

Table 2.4 qPCR master mix. 53

Table 2.5 Gel composition. 55

Table 2.6 Primary antibodies used. 56

Table 2.7 Secondary antibodies used. 56

Table 2.8 Luminol Solution 57

Table 2.9 Peroxide Solution. 57

Table 2.10 Sodium citrate buffer composition. 60

Table 2.11 Primary antibodies used. 61

Table 2.12 Secondary antibodies used. 61

Table 3.1 Medulloblastoma cell lines used in this project. 71

Table 3.2 Summary table showing the percent (% of seeded cell number) of Group 3 cells that migrated in response to each chemokine in Figure 3.14. 98

Table 3.3 Summary table showing percentage migration increase (%) from Figure 3.15, in the presence of one soluble chemokine in 2% FBS, compared to 2% FBS as a baseline. 102

Table 3.4 Comparing the composition of two aCSF solutions to CSF. 104

Table 3.5 Summary table showing migration increase (%) through the optimised migration model compared to 5 x 10^4 cells as a baseline. 110

Table 4.1 The RNA samples selected for the RNA-Seq study. 117

Table 4.2 Overarching analysis of UPX sequencing data. 120

Table 4.3 GSEA Migrated > Adherent across 3 cell lines. 129

Table 4.4 GSEA Migrated > Suspension across 3 cell lines. 130

Table 4.5 List of upregulated and downregulated genes 136

Table 4.6 Genes upregulated in the migrated compartment. 144

Table 4.7 Genes upregulated in the adherent compartment. 145

Table 5.1 The scoring guide followed in order to quantify SORCS2 staining. 179

List of figures

Figure 1.1 MRI features of medulloblastoma subgroups. 14

Figure 1.2 Medulloblastoma tumour subgroups are located in defined areas of the cerebellum, and arise from different cell types. 16

Figure 1.3 The composition of the leptomeninges. 22

Figure 1.4 The metastatic cascade 24

Figure 1.5 The parenchymal basement membrane at the interface between the brain and leptomeninges. 30

Figure 1.6 Established medulloblastoma cell lines organised by molecular subgroup. 33

Figure 1.7 Cell migration and invasion models. 37

Figure 3.1 Medulloblastoma cell lines in standard culture. 72

Figure 3.2 BME supports short-term growth of CHLA-01R-MED. 76

Figure 3.3 BME supports short-term growth of CHLA-01-MED. 77

Figure 3.4 BME supports short-term growth of CHLA-01R-MED. 78

Figure 3.5 BME supports short-term growth of CHLA-01-MED. 79

Figure 3.6 BME does not support short-term growth of Group 3 cell line D458-MED. 82

Figure 3.7 BME supports short-term growth of Group 3 cell line D283-MED with added growth factors. 83

Figure 3.8 BME supports short-term growth of Group 3 cell line HD-MB03 with or without added growth factors. 84

Figure 3.9 Time-lapse microscopy captures CHLA-01R-MED cell migration in BME. 87

Figure 3.10 A modified Boyden chamber migration assay to capture cells from three compartments. 90

Figure 3.11 Collagen IV, but not BME, allows migration of cells through the migration model. 92

Figure 3.12 Collagen IV coating permits modest migration of Group 4 cell lines. 93

Figure 3.13 Medium supplemented with 10% FBS induced the highest number of migrating cells across three Group 3 cell lines. 97

Figure 3.14 Individual soluble factors do not induce migration. 101

Figure 3.15 aCSF enables migration to be separated from proliferation. 105

Figure 3.16 Combination of collagen IV and Laminin 111 results in optimisation of a trans-well migration model. 108

Figure 3.17 Group 3 cells migrated through the optimised brain-CSF migration model. 110

Figure 3.18 Summary schematic of the optimised brain-CSF migration model. 112

Figure 4.1 3′ UPX RNA-Seq workflow 115

Figure 4.2 Principal Component Analysis (PCA) plot for all samples. 123

Figure 4.3 Heatmap and unsupervised clustering for all samples. 125

Figure 4.4 Volcano plots to visualize the results of differential expression analysis. 126

Figure 4.5 Genes overexpressed in the migrated compartment. 133

Figure 4.6 Genes overexpressed in the Adherent compartment. 134

Figure 4.7 Genes overexpressed in the suspension compartment..... 135

Figure 4.8 Genes following the pattern S<A<M 139

Figure 4.9 Genes following the pattern S<A>M 140

Figure 4.10 Genes following the pattern S<(A=M) 141

Figure 4.11 Genes following the pattern S>A>M 142

Figure 4.12 CORO2B and LMNB1 are associated with Group 3 subgroup. RASSF3 and DNAJC27 are associated with WNT subgroup. 148

Figure 4.13 GREB1L and METTL15 are associated with SHH. PARG, RN7SK and TMEM117 are associated with Group 4. TRPM3 and FREM2 are associated with WNT. 149

Figure 4.14 Genes expressed in both the adherent and migrated compartments are differentially expressed in medulloblastoma subgroups..... 150

Figure 4.15 Expression of CORO2B and LMNB1 are associated with metastatic tumours. 152

Figure 4.16 Expression of the genes GREB1L and METTL15 in the migrated compartment are associated with non-metastatic tumours..... 153

Figure 4.17 Expression of the gene GCNT1 is associated with non-metastatic tumours. 154

Figure 4.18 Patients with high expression of CORO2B and LMNB1 followed a negative survival trend, although this was not significant. Patients with high expression of RASSF3 had worst survival than patients with low expression. Patients with low expression of DNAJC27 followed a negative survival trend, although this was not significant..... 157

Figure 4.19 Patients with high expression of GREB1l, METTL15, PARG and RN7SK followed a positive survival trend, although this was not significant. 158

Figure 4.20 Patients with high expression of TMEM117 followed a positive survival trend, although this was not significant. Patients with high expression of TRPM3 had significantly better survival than patients with low expression. Patients with high expression of FREM2 followed a negative survival trend, although this was not significant. 159

Figure 4.21 Patients with high expression of SORCS2 or GCNT1 followed a worst survival trend, although this was no significant. 160

Figure 5.1 Gene expression across medulloblastoma molecular subgroups. 166

Figure 5.2 SORCS2 expression in 12 medulloblastoma subtypes. 168

Figure 5.3 LMNB1 expression in 12 medulloblastoma subtypes. 169

Figure 5.4 CORO2B expression in 12 medulloblastoma subtypes. 170

Figure 5.5 Variation in gene expression were observed in Group 3 tumours in patients with non-metastatic (M0) or metastatic (M+) tumours. 172

Figure 5.6 Patients with high SORCS2 and CORO2B followed poor survival trends in Group 3 patients. 175

Figure 5.7 Patients with high expression of SORCS2 and metastatic tumours had the worst outcome. 176

Figure 5.8 Examples of SORCS2 protein expression scores following the guide in Table 5.1. 179

Figure 5.9. Areas of SORCS2 staining that were not scored. 180

Figure 5.10 Interesting types of tissue in the TMAs. 181

Figure 5.11 SORCS2 expression was not significantly correlated with patient clinical characteristics. 184

Figure 5.12 Survival of patients included in the TMA analysis. 185

Figure 5.13 SORCS2 gene expression in medulloblastoma cell lines. 187

Figure 5.14 SORCS2 protein expression in medulloblastoma cell lines. 189

Figure 5.15 Summary of the optimised transfection and migration/viability assay setup. 191

Figure 5.16 siRNA reduces SORCS2 RNA expression with varying efficiency in HD-MB03 cells 193

Figure 5.17 SORCS2 protein expression is decreased by siRNA in HD-MB03 cells. 194

Figure 5.18 A decrease in SORCS2 expression decreased cell migration but did not impact cell viability in HD-MB03. 196

Figure 5.19 SORCS2 protein decreases after siRNA knockdown. 197

Figure 5.20 A decrease in SORCS2 expression decreased cell migration and increased cell viability in D283-MED. 199

Figure 6.1 The primary tumour niche in the brain parenchyma and metastatic niche in the leptomeninges differ in composition and structure. 205

Figure 6.2 Summary of a possible complex 3D culture model representing the brain-leptomeninges interface. 215

Figure 6.3 SORCS2 forms a receptor complex that binds proNGF and causes growth cone collapse. 227

Figure 6.4 SORCS2 function in EAAT3 transporter sorting. 229

List of common abbreviations

2D	two-dimensional
3D	three-dimensional
aCSF	artificial cerebrospinal fluid
aCSF	artificial cerebrospinal fluid
ADHD	Attention deficit hyperactivity disorder
BDNF	Brain derived neurotrophic factor
BME	Basement membrane extract
ChIP-Seq	Chromatin immunoprecipitation sequencing
CNS	Central nervous system
CORO2B	Coronin 2B
CSF	cerebrospinal fluid
CSI	Cranio-spinal irradiation
CVBM	cerebrovascular basement membrane
ECM	extracellular matrix
EGFR	Epidermal growth factor receptor
FDR	Benjamini-Hochberg false Discovery rate method
GEO	Gene expression omnibus
GluCN	Glutamatergic cerebellar nuclei
GO	Gene ontology
GSEA	Gene set enrichment analysis
HA	Hyaluronic acid
HGF	Hepatocyte growth factor
HSPGs	heparan sulphate proteoglycans
IHC	immunohistochemistry
KD	Gene knock down
LCA	Large cell-anaplastic medulloblastoma
LCM	Laser-capture microdissection
LMNB1	lamin B1
lncRNA	Long non-coding RNA
LRT	Likelihood ratio test
MBEN	Medulloblastoma with extensive nodularity
mRNA	messenger RNA
MSigDB	Molecular signatures database
NGF	Nerve growth factor
NGS	Next generation sequencing
NSCLC	Non-small cell lung cancer
OCSC	Organotypic cerebellum slice culture
$P75^{NTR}$	p75 neurotrophic receptor
PCA	Principal component analysis
PDX	Patient-derived xenograft
proBDNF	pro brain derived neurotrophic factor
proNGF	pro nerve growth factor
QC	Quality control
SHH	Sonic hedgehog
SNCAIP	Synuclein Alpha Interacting Protein
SORCS2	sortilin related VPS10 domain containing receptor 2
SORT1	sortilin
TLDA	TaqMan Low-Density Array
TMA	Tumour microarray
TME	Tumour micro-environment
TrkB	Tropomyosin-related kinase B
UBC	Unipolar brush cell
UMI	Unique molecular index

VST	Variance stabilizing transformation
WNT	Wingless

Chapter 1 Introduction

1.1 Paediatric medulloblastoma

1.1.1 Epidemiology of medulloblastoma

Tumours of the brain and central nervous system (CNS) are the second most common cancer types in children, accounting for ~26% of childhood cancers (Cancer Research UK and National Registry of Childhood Tumours). Within this statistic, malignant brain tumours are the leading cause of death as a result of cancer in children, and medulloblastoma (MB) is the most common malignant brain tumour in children (Cancer Research UK). Medulloblastomas belong to the class of embryonal tumours of the CNS (Louis et al., 2016). While medulloblastomas can occur at any age, children (1-9 years) are 10 times more likely to be diagnosed than adults (>19 years) (Smoll and Drummond, 2012). In the United States, medulloblastoma had an incidence of ~5 cases per 1 million individuals between 2011 and 2015 (Ostrom et al., 2018). In the childhood demographic, males are 1.58 times more likely to be diagnosed with medulloblastoma than females (Smoll and Drummond, 2012). In addition to gender, heritable factors are the only known risk factors associated with medulloblastoma. For example, Gorlin syndrome, Curry-Jones syndrome and Greig cephalopolysyndactyly syndrome which are linked to elements of the sonic hedgehog (SHH) signalling pathway (Smith et al., 2014, Twigg et al., 2016, Tommerup et al., 1983), as well as familial adenomatous polyposis (FAP) syndrome linked to WNT signalling (Cohen, 1982).

Medulloblastoma tumours occur in the posterior fossa of the brain, located in or around the cerebellum and brainstem. Historically, medulloblastoma tumours were histologically defined based on tissue characteristics as classic, desmoplastic/nodular, medulloblastoma with extensive nodularity (MBEN), and large cell/ anaplastic (LCA). In 2012, a consensus conference proposed 4 subgroups of medulloblastoma (SHH, WNT, Group 3 and Group 4) based on their molecular classification (Taylor et al., 2012), and these were integrated into the WHO classification alongside the histological variants (Louis et al., 2016). This integration

of histopathological features of the tumours with the molecular characteristics yielded a novel risk-stratification system for medulloblastomas (Table 1.1). The classification of medulloblastoma is dynamically-evolving as novel 'omics methods are integrated with clinical characteristics to further adapt risk-stratification and treatment of these tumours. Tumour dissemination and survival are inconsistent across the different types of medulloblastoma, and a detailed understanding of the biology and its clinical implications is needed.

Table 1.1 Summary of most common integrated medulloblastoma diagnoses based on the 2016 WHO classification, reproduced from Louis *et al*., 2016.

Molecular subgroup	**Histological subgroup**	**Prognosis**	
		Occurrence	***risk***
WNT	Classic	most common histology for WNT	Low-risk,
	LCA	Very rare	uncertain clinicopathological significance
SHH, TP53-mutant	Classic	Uncommon	high risk
	LCA	In children 7-17 years	High risk
	Desmoplastic/nodular	Very rare	uncertain clinicopathological significance
SHH, TP53-WT	Classic	/	Standard risk
	LCA	/	uncertain clinicopathological significance
	Desmoplastic/nodular	In infants and adults	Low risk in infants
	MBEN	/	Low risk in infants
Group 3	Classic	/	Standard risk
	LCA	/	High risk
Group 4	Classic	Most common histology for Group 4	Standard risk
	LCA	rare	uncertain clinicopathological significance

/ = no information available
LCA= large cell/ anaplastic
MBEN = medulloblastoma with extensive nodularity

1.2 Medulloblastoma classification

The definition of 4 molecular subgroups with biologically and clinically relevant inter-tumoural heterogeneity (Table 1.2) has significantly influenced how pre-clinical studies are done and clinical protocols have been adapted. The ongoing study of inter- and intra-tumoural heterogeneity in these tumours will continue to impact the diagnosis, risk-stratification and treatment of medulloblastoma patients.

1.2.1 Histological subgroups

The diagnosis of medulloblastoma is based on histopathological evaluation of the tumour in order to distinguish it from other types of paediatric tumours that can occur in the posterior fossa. Tumours with classic histology are the most common (McManamy et al., 2007), but desmoplastic tumours are more frequent in infants (<3 years) (Rutkowski et al., 2009). Desmoplastic tumours are also most common in adult patients (Giordana et al., 2005). Large cell histology (LCA) correlates with poor prognosis and metastasis at diagnosis (Giangaspero et al., 1992, Brown et al., 2000). However, as this histology is rare, it is combined with anaplastic classification, but anaplastic tumours are not always associated with a poor outcome. While these histological subgroups are still used in the clinic today, the molecular classification has also become an important criteria for risk stratification and research with the aim of developing more targeted therapies for high risk patients.

Table 1.2 The 4 molecular subgroups of medulloblastoma according to the most recent WHO consensus.

Subgroups		**WNT**	**SHH**	**Group 3**	**Group 4**
Frequency (%) Northcott et al 2012		10%	30%	25%	35%
Metastasis (%)		~5-10%	~15-20%	~40-45%	~35-40%
5-year survival (%)		~95%	~75%	~50%	~75%
Molecular driver events Hovestadt et al 2020		**Mutations**: *CTNNB1, DDX3X, SMARCA4*	**Mutations**: *TP53, PTCH1, KMT2S, SUFU, SMO, BCOR, TERT*	**Mutations** : *KBTBD4, SMARCA4, CTDNEP1, KMT2D*	**Mutations** : *KDM6A, ZMYM3, KMT2C*
			Amplifications: *MYCN, GLI2*	**Amplifications** : *MYC*	/
			Deletions: *PTEN, SUFU*	**Activation** : *GFI1, GFI1B*	**Activation** : *PRDM6*
Primary tumour Zapotocky et al 2018 & Patay et al 2015	*location*	Lateralized from the brain stem and cerebellum	Cerebellar hemispheres	4th ventricle / midline	4th ventricle / midline
	Size	≥ 35 mm	≥ 35 mm	< 35 mm	≥ 35 mm
Metastasis Zapotocky et al 2018	*location*	No metastatic WNT tumours were identified in the study	Infratentorial, spinal	Supratentorial infratentorial, spinal	Supratentorial, suprasellar, infratentorial, spinal
	character	Rare	Nodular	Nodular and laminar	Laminar
Subtypes	*Cavalli et al 2017*	WNTα, WNTβ	SHHα, SHHβ, SHHγ, SHHδ	Group 3α, Group 3β, Group 3γ	Group 4α, Group 4β, Group 4γ
	Schwalbe et al 2017	/	SHH-infant (iSHH-I, iSHH-II), SHH-child	MBGr3-HighRisk, MBGr3-Low-Risk	MBGrp4-HighRisk, MBGrp4-LowRisk
	Northcott et al 2017	/	/	Group 3 only: II, III, IV Group 3 & 4: I, V, VII	Group 4 only: VI, VIII Group 3 & 4: I, V, VII
	Sharma et al 2019	/	/	Group 3 only: II, III, IV Group 3 & 4: I, V, VI, VII	Group 4 only: VIII Group 3 & 4: I, V, VI, VII

/ = no information available

1.2.2 Molecular subgroups

1.2.2.1 WNT

The WNT subgroup represents 10% of all patients with MB, and also has the most favourable outcome with a 5-year survival of 95% (Northcott et al., 2019, Hovestadt et al., 2019a). This subgroup typically has classic histology, and the occurrence of metastasis at diagnosis is rare (~5-10%) (Northcott et al., 2012a). This subgroup also has a clearly defining hallmark event, somatic mutations in *CTNNB1* in 85-90% of patients. These mutations include 33 missense mutations in the ubiquitination recognition motif, as well as mutations at phosphorylation sites (Robbins et al., 2018). *CTNNB1* encodes the protein β-catenin, and somatic activating mutations result in stabilized β-catenin accumulating in the nucleus and the constitutively active WNT signalling. WNT-responsive genes are responsible for cell growth and proliferation in these tumours (Ellison et al., 2005, Ellison et al., 2011, Kool et al., 2012). Patients who do not have the *CTNNB1* somatic activation often have germline variants in adenomatous polyposis coli (*APC*) (Waszak et al., 2018). Up to 85% of patients also have loss of one copy of chromosome 6 (monosomy 6) (Northcott et al., 2012b).

1.2.2.2 SHH

SHH represents 30% of all medulloblastoma cases, with ~15-20% metastatic at diagnosis, and a 5-year survival rate of 75% (Northcott et al., 2012a). 40% of SHH patients have classic histology, 40% have desmoplastic/nodular histology, and the remaining 20% have LCA histology. The hallmark genetic event in SHH tumours are mutations and focal somatic copy-number alterations in genes of the SHH signalling pathway. The most common loss-of-function mutations or deletions occur in patched 1 (*PTCH1*) in 43% of patients, which has 7 known mutations (Pugh et al., 2012). Mutations or amplifications are also found in suppressor of fused homolog (*SUFU*), smoothened (*SMO*), glioma-associated oncogene homolog 1 (*GLI1*), glioma-associated oncogene family zinc finger 2 (*GLI2*) and MYCN proto oncogene (*MYCN*)

(Kool et al., 2014, Northcott et al., 2017). In the current WHO guidelines SHH is further subdivided on the basis of tumour protein 53 (*TP53*) somatic mutations (TP53-WT or TP53-mutant). 22 inactivating TP53 mutations have been identified, with most in the DNA binding domain of the p53 protein (Pfaff et al., 2010). Tumours with mutations in *TP53* have poorer survival that TP53-WT, are most common in older children compared to infants (Kool et al., 2014, Northcott et al., 2017, Schwalbe et al., 2017).

1.2.2.3 Group 3

Group 3 medulloblastomas occur in 25% of patients, and are the most commonly metastatic, with 40-45% of patients presented with metastatic tumours at diagnosis. This subgroup also has the poorest 5-year survival, only 50% of patients reach this landmark (Northcott et al., 2012a). *MYC* amplification is found in 17% of patients and is associated with poor survival. Enhancer hijacking results in the upregulation of *GFI1* and *GFI1*B, which regulate cell fate in the hematopoietic system under normal conditions, in 12-15% of Group 3 and Group 4 patients (Northcott et al., 2014, Northcott et al., 2017). Enhancer hijacking is structural variant-dependent gene activation, where a translocation event leads to the overexpression of oncogenes.

Group 3 has the smallest primary tumours compared to other subgroups, and it has been reported that primary tumours are smaller in the presence of metastases (Zapotocky et al., 2018). This suggests an early metastatic event as a result of tumour invasion into the leptomeningeal space rather than growth and passive shedding into the flow of CSF. There is a need for better understanding of the processes of metastasis and dissemination in order to specifically treat these patients with the worst prognosis.

1.2.2.4 Group 4

Group 4 is the most commonly occurring subgroup of medulloblastoma, accounting for 35% of cases, yet it remains one of the least well understood (Northcott et al.,

2019, Hovestadt et al., 2019a). Within the current 4 consensus subgroups, 35-40% of Group 4 patients have metastasis at diagnosis and there is a 75% 5-year survival rate (Northcott et al., 2012a), however the ongoing subdivision of this subgroup and Group 3 is revealing differing rates of metastasis and survival in newly-defined subtypes (Sharma et al., 2019). Notable genetic alterations in Group 4 include *MYCN,* orthodenticle homeobox 2 (*OTX2*) and cell division protein kinase 6 (*CDK6*) amplifications in 6% of patients, and isochromosome 17q (an abnormal chromosome 17 with duplication of the long arm and loss of the short arm). In 17% of patients, PR/SET domain 6 (*PRDM6*) is overexpressed as a result of enhancer hijacking associated with synuclein alpha interacting protein (*SNCAIP*) (Northcott et al., 2017). *PRDM6* encodes a chromatin-modifying protein, but its function in Group 4 pathology has not been defined.

1.2.3 Molecular subtypes

Intra-subgroup and inter-subgroup heterogeneity is an area of active study in the medulloblastoma field. Several published studies have reported novel molecularly-defined subtype classifications (Table 1.2) for all medulloblastoma subgroups. These studies employed different analysis methods on independent patient samples, and therefore reported different classifications. Most recently, a joint meta-analysis of Group 3 and Group 4 tumours using published datasets from several of these studies (Schwalbe et al., 2017, Northcott et al., 2017, Cavalli et al., 2017) was undertaken (Sharma et al., 2019). This study reported 8 subtypes of Group3/Group 4 medulloblastoma, some consisting of only one subgroup and others a combination of both.

The key recent advances in medulloblastoma subtyping will be summarised in this introduction. However, most of the practical work in this project was performed before or in parallel with the latest publications. This project was therefore designed to investigate the Group 3 and Group 4 subgroups (Louis et al., 2016), and some of the data was analysed against one of the more recently published subtype classifications (Cavalli et al., 2017). The dataset by Cavalli *et al.* is the largest medulloblastoma

dataset encompassing subtype classification available for analysis using the R2 Genomics Analysis and Visualization Platform (r2platform.com).

1.2.3.1 WNT

WNT is known to be largely homogeneous in its gene expression and methylation profile, but the study by Cavalli *et al*. reported 2 subtypes differentiated by the age of patients at diagnosis and the frequency of monosomy 6. The median age at diagnosis for WNT-α is 10 years old, these have loss of 1 copy of chromosome 6 which is characteristic of WNT tumours, while WNT-β is enriched in patients with a median age of 20 without monosomy 6 (Cavalli et al., 2017).

1.2.3.2 SHH

The biological and clinical heterogeneity found in SHH tumours has resulted in its subdivision into several subtypes.

1) Cavalli *et al.* reported 4 independent subtypes, SHHα, SHHβ, SHHγ, and SHHδ (Cavalli et al., 2017). SHHα and SHHδ occur in children and adolescents, while SHHβ and SHHγ are associated with infants. In addition, a third of SHHα are enriched for *TP53* mutation and have poorer survival compared to SHHδ. Among the infants, SHHβ patients have poorer outcome than SHHγ.
2) Schwalbe *et al*. described 2 subtypes of medulloblastoma based on age distribution of patients: SHH-infant and SHH-child (Schwalbe et al., 2017). The infant subgroup can be further divided into iSHH-I and iSHH-II. The iSHH-I subtype occurs most frequently in young infants and is enriched for *SUFU* mutations and chromosome 2 gain, while iSHH-II is enriched for *SMO* mutations as well as mutations in chromatin-modifying genes. Following a trial investigating treatment with chemotherapy alone (no cranio-spinal irradiation), it was reported that infants with iSHH-II had improved

progression-free survival compared to iSHH-I (75% compared to 28%) (Robinson et al., 2018).

iSHH-I and iSHH-II described by the Schwalbe *et al.* study correspond to Cavalli and colleagues' SHHβ and SHHy subtypes respectively, and the survival trends reported by both studies are in agreement (Northcott et al., 2019). This supports the adapting of risk-stratification guidelines for treatment as medulloblastoma classification continues to expand, to reduce the toxicity associated with therapeutic options such as cranio-spinal irradiation in patients who may not need it.

1.2.3.3 Group 3

Several studies have reported varying subtypes in Group 3 MB.

1) In 2011, Cho *et al*. reported 2 subtypes: c1 characterized by *MYC* amplification and poor outcome, and c5 characterized by aneuploidy and a more favourable outcome (Cho et al., 2011).
2) Schwalbe *et al.* also described 2 Group 3 subtypes based on outcome; MBGrp3-HighRisk had *MYC* amplification and a poorer outcome than MBGrp3-LowRisk, characterised by chromosome 10 loss (Schwalbe et al., 2017).
3) Cavalli *et al.* reported 3 subtypes for Group 3; Group 3α had the best overall survival, Group 3β was characterized by *GFI* oncogene activation, and Group 3γ was characterised by *MYC* amplification and had the worst overall survival (42%). They found that Group 3α and Group 3γ were frequently metastatic at diagnosis, while Group 3β were infrequently metastatic (Cavalli et al., 2017).
4) Northcott *et al.* analysed Group 3 and Group 4 tumours together, and identified 8 subtypes (I-VIII). Subtypes II, III and IV represent Group 3 tumours. Subtypes I, V and VII represent a combination of Group 3 and Group 4 (Northcott et al., 2017).

1.2.3.4 Group 4

3 independent studies have reported varying classifications of Group 4 subtypes.

1) Schwalbe *et al.* reported 2 Group 4 subtypes based on high or low risk: MBGrp4-HighRisk and MBGrp4-LowRisk. The high risk group had a lower (36%) 10-year overall survival than the low risk group (72%). Overexpressed genes differed between the subtypes, for example *PRDM6* was overexpressed in the high risk group compared to the low risk group.
2) Cavalli *et al.* identified 3 subtypes of Group 4 tumours: Group 4α, Group 4β and Group 4γ. They did not identify significant differences in survival or metastasis at diagnosis between these subtypes. Group 4α is characterised by *MYCN* amplification, while Group 4β is enriched for *SNCAIP* duplications. They reported *CDK6* amplifications in both subtypes 4α and 4γ.
3) Northcott *et al.* reported 8 subtypes across Group 3 and Group 4 medulloblastoma. Within these, they described subtypes VI and VIII as Group 4. Subtypes I, V and VII represent a combination of Group 3 and Group 4. The gene *PRDM6* was also up-regulated in Group 4 tumours, and they reported this was associated with duplication of *SNCAIP* (Northcott et al., 2017).

The joint meta-analysis by Sharma *et al*. on data from three of the aforementioned studies (Cavalli et al., 2017, Schwalbe et al., 2017, Northcott et al., 2017), described 8 subtypes characterising Group 3 and Group 4 tumours (Sharma et al., 2019).

- Subtypes I, V, VI and VII are a combination of Group 3 and 4 tumours. Subtype I is characterized by amplification of the *OTX2* oncogene, and activation of *GFI* oncogene. Subtype V has amplifications of *MYC* and *MYCN* and modest outcomes.
- Subtypes II, III and IV remain Group 3 only, and within these II and III have *MYC* amplifications and poor outcomes.

- Subtype VIII is the only subtype composed only of Group 4 tumours, with favourable 5-year survival, but a unique trend of late relapse leading to death.

Group 3 and Group 4 tumours have been more challenging to characterise than WNT and SHH subgroups due to the reduced frequency of driver mutations in major signalling pathways. However, research over the last several years has begun to uncover characteristics of these subgroups that may eventually lead to a re-classification based on the subtypes discussed above. For example, Group 3 and Group 4 have the lowest correlation between mRNA expression and protein expression, which suggests that post-transcriptional mechanisms may be highly significant in driving their pathogenesis (Archer et al., 2018, Rivero-Hinojosa et al., 2018). The ultimate goal is improved survival and reduced toxicity in these high-risk patients, which may be accomplished through a more targeted treatment based on integrated molecular classification.

1.3 Cerebellar location and origins

Medulloblastoma primary tumours occur in the cerebellum, located in the posterior fossa region of the brain. Tumour location is determined by MRI imaging, and the 4 subgroups have distinct location and contrast enhancement. In the transverse plane (imaged from the top down) WNT tumours are found either at the midline, or off-midline (Figure 1.1 A). Patay *et al.* defined WNT location as a curved triangular zone (Figure 1.2 A) that includes the foreamen of Luschka, the cerebellopontine angle cistern, the cisterna magna and the fourth ventricle (Patay et al., 2015). The majority of SHH tumours are found in cerebellar hemispheres (Figure 1.1 B A), and have rarely been reported to invade the brainstem (Perreault et al., 2014, Raybaud et al., 2015). Group 3 and Group 4 tumours are found at the midline, in the immediate vicinity of the 4^{th} ventricle of the cerebrospinal fluid ventricular system (Figure 1.2 A). In addition, Group 3 tumours show enhancement while Group 4 tumours do not (Figure 1.1 C and D). Figure 1.1 A-D gives examples of subgroup tumour locations

viewed on the transverse plane, while Figure 1.2 A summarises the localisation of MB tumours from a sagittal view. The inter-tumoural heterogeneity of medulloblastoma subgroups suggests that these tumours also originate from distinct cell types or developmental lineages (Gibson et al., 2010, Pei et al., 2012, Vladoiu et al., 2019, Hovestadt et al., 2019b).

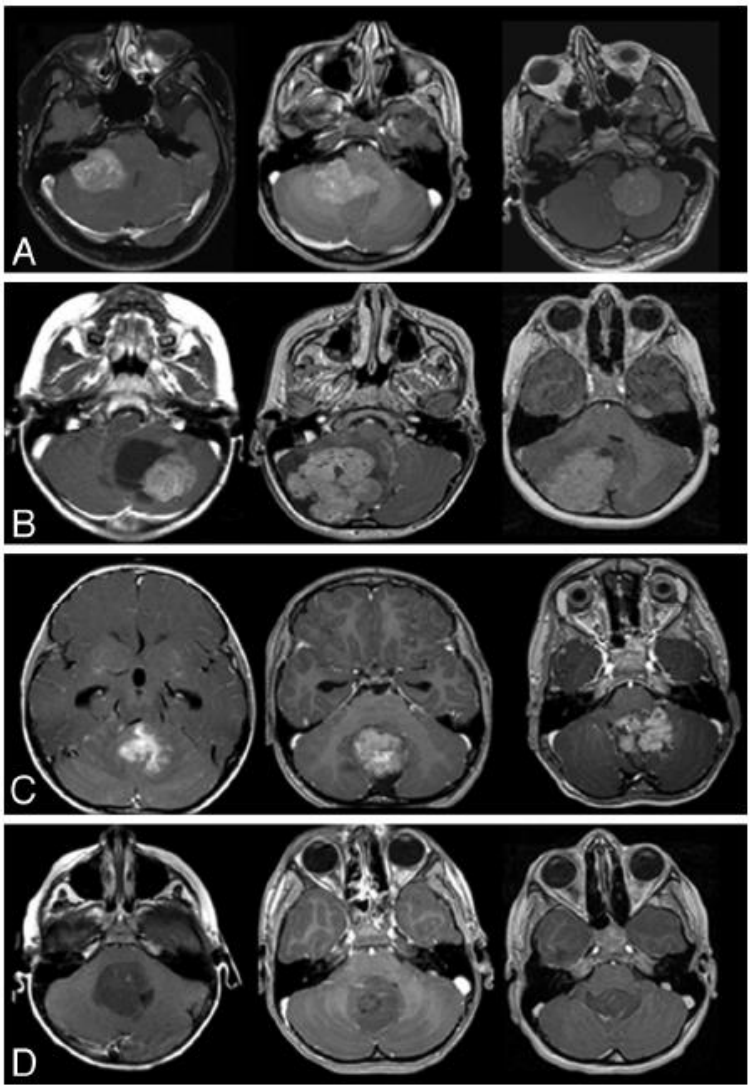


Figure 1.1 MRI features of medulloblastoma subgroups.

A) WNT tumours are found in the cerebellar peduncle/cerebellopontine angle cistern. **B)** SHH tumours are found in the cerebellar hemispheres. **C)** Group 3 tumours are found at the midline in the 4th ventricle and are enhanced against the brain parenchyma. **D)** Group 4 tumours are found at the midline and 4th ventricle but are not enhanced against the brain parenchyma. This figure is a reproduction from Perreault *et al*., 2014.

The cerebellum is responsible for sensory-motor processing and the control of fine movement. It is home to half the mature neurons in the CNS and is organised in 3 layers (Figure 1.2 B). The layer nearest the white matter is made up of excitatory granule cells and other cell types including unipolar brush cells (UBCs). The middle layer is a monolayer of Purkinje cells, which extend their Purkinje tree axons into the third layer nearest the pia matter. The third layer is a molecular layer of granule cell axons and glutamatergic Purkinje cell dendritic trees. External signals are received by the UBCs, transmitted to the granule cells, whose T-shaped axons synapse with Purkinje trees (Butts et al., 2014). During development, stem and radial glial progenitor cells that line the fourth ventricle give rise to Purkinje cells, interneurons and glial cells, while progenitors in the upper rhombic lip generate granule lineage cells. Understanding the neurobiology and anatomy of the developing brain can inform researchers of the transcriptional landscape of malignancies such as medulloblastoma (Martirosian et al., 2016).

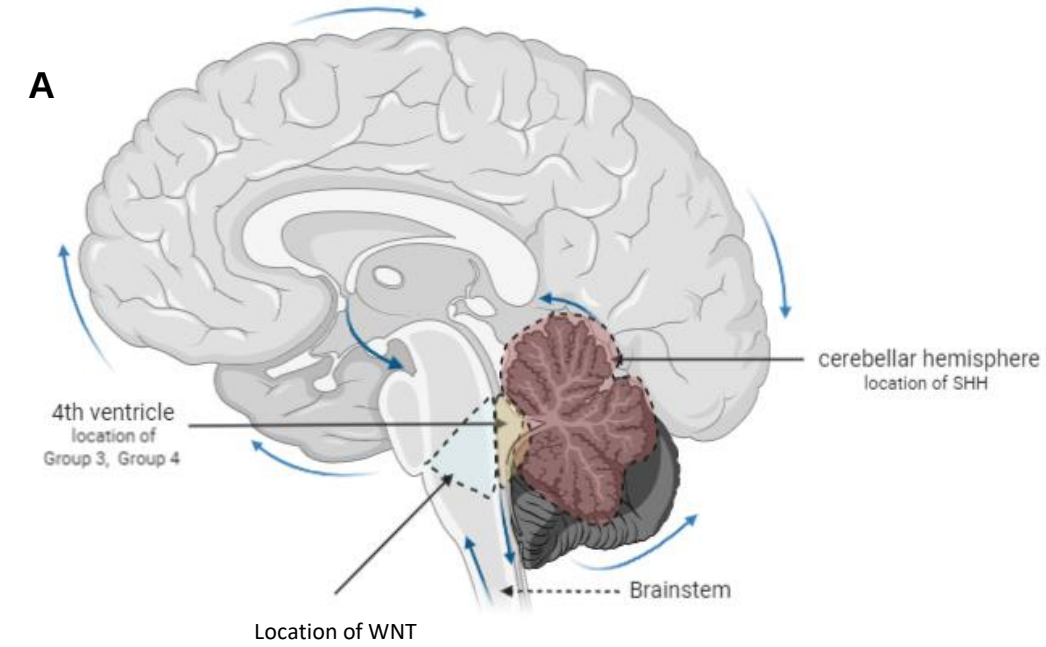


Figure 1.2 Medulloblastoma tumour subgroups are located in defined areas of the cerebellum, and arise from different cell types.

A) A sagittal view of the most common diagnostic locations for medulloblastoma tumours according to subgroup. The blue arrows indicate flow of CSF through the ventricles and in the leptomeninges. This schematic was adapted from Northcott *et al*., 2019. **B)** The cerebellum is made up of 3 layers as labelled on the schematic. Each layer is characterised by a particular cell type of cell structure, some of which may give rise to medulloblastoma tumours. This schematic was adapted from Butts *et al*, 2014.

Over the last decade, probable progenitor cells have been reported for each of the 4 subgroups. This has confirmed that the distinct subgroups stem from distinct progenitors. SHH tumours are formed by cells in the external granule layer of the cerebellum, while WNT tumours are formed from cells of the lower rhombic lip of the developing brain stem (Gibson et al., 2010). Group 4 tumours likely arise from glutamatergic cerebellar nuclei (GluCN) or unipolar brush cells, which are glutamatergic interneurons that derive from the upper rhombic lip. Two studies reported that Group 3 tumours may arise from nestin-positive cerebellar stem cells, which can give rise to a variety of differentiated cell types (Pei et al., 2012, Vladoiu et al., 2019). This would explain why it has been challenging to identify one overarching signalling pathway that drives and defined Group 3 tumours. However, it has also been reported that Group 3 tumours may arise from cells of non-cerebellar origin (Hovestadt et al., 2019b).

Subgroup differences also influence the localisation and characteristics of metastases. This was recently reported by Zapotocky and colleagues in a study characterising 40 metastatic medulloblastoma patient MRIs (5 SHH, 16 group 3 and 19 Group 4) (Zapotocky et al., 2018). The study identified both a nodular pattern and laminar pattern of metastasis in Group 4 tumours while SHH tumours predominantly formed nodules and Group 3 tumours predominantly metastasized as laminar coating. The study also observed specific Group 4 characteristics. These tumours commonly formed suprasellar metastases, and when the primary tumour was not contrast-enhanced, the metastases did not appear contrast-enhanced either. They also reported that Group 3 had the smallest primary tumours, in some cases even smaller than the metastatic lesions in the same patients. They suggested that this may be a result of an early clonal event causing metastatic dissemination in Group 3, an observation in agreement with the poor prognosis of metastatic Group 3 patients. Studies such as this one aim to improve the diagnosis of medulloblastoma for adapted management of patients, and encourage further research into the leptomeningeal metastasis characteristics of these tumours.

1.4 Diagnosis and treatment

1.4.1 Clinical symptoms and staging

Medulloblastoma is diagnosed based on the patient's clinical symptoms, MRI scans of the brain and spine to identify the primary tumours and any macro-metastases, CSF cytology to identify any micro-metastases, and the integrated analysis of histology and molecular features as described above. An increase in intracranial pressure related to hydrocephalus can cause non-specific symptoms of brain tumours including headaches, vomiting, problems with balance and coordination, and fatigue (https://www.headsmart.org.uk/). A delay in diagnosis of children under 18 months may occur as a result of the intracranial pressure going unnoticed for longer as these babies' skull sutures are not fully closed (Wilne et al., 2007, Northcott et al., 2019). Specific symptoms of MB include ataxia, an impact on motor skills such as handwriting, and problems with the eyes and vision. Spinal metastases can also lead to back pain and affect the patient's gait. However, "sugar coating" spinal metastasis is often asymptomatic.

Twenty to thirty percent of children will present with metastasis at diagnosis, and others will develop metastatic recurrence during the course of the disease (Zapotocky et al., 2018). Metastatic dissemination, as mentioned above, is also subgroup-specific. Medulloblastoma tumours are assigned a stage following Chang's classification (Chang et al., 1969) based on MRI imaging and CSF cytology. This system classes patients into 5 incremental groups (M0-M4) based on the presence and extent of metastases (Table 1.3). Metastasis most commonly occurs within the CNS, but can, on rare occasions, occur outside it. A recent study reported haematogenous spread of medulloblastoma in a mouse model for the first time (Garzia et al., 2018), implicating the circulatory system in the process of metastasis.

Table 1.3 Chang's staging system for medulloblastoma.

Metastatic stage	Characteristics
M0	no evidence of subarachnoid or haematogenous metastases
M1	tumours cells in the CSF
M2	nodular metastases in the cerebellum, subarachnoid space, or ventricles
M3	nodular metastases in the spinal subarachnoid space
M4	extraneuroaxial metastases

1.4.2 Treatment

The standard of care for medulloblastoma patients, which results in the best survival for non-high risk patients, is maximal surgical resection of the primary tumour. A surgical sample is obtained at the time of total tumour resection, and used for histological and molecular analysis and staging. Surgery is followed by cranio-spinal irradiation (CSI) of the entire brain and spine axis, with boost irradiation of the posterior fossa or tumour bed, and multi-agent adjuvant chemotherapy. Radiotherapy used on young patients include CT based conformal radiation therapy (3DCRT) (Gupta and Ahmad, 2019), intensity-modulated radiation therapy, conformal 3D photon therapy (Deutsch et al., 1996, Clair et al., 2004) and proton beam radiation therapy (Indelicato et al., 2016). Combinations of the chemotherapeutic agents cisplatin, carboplatin, vincristine, cyclophosphamide and lomustine are administered in cycles. The radiation and adjuvant therapy protocols and dosages vary between countries, and are adapted based on risk-stratification of the patient. Following this protocol, children over the age of 3 with non-metastatic medulloblastoma, who do not exhibit any residual tumour on MRI post-surgery, have a 5-year survival rate of 80%. This is reduced to 60% in children with metastatic disease or residual tumour detected on MRI post-surgery. If patients experience a recurrence after initial therapy, their 5 year survival drops to <10% even if the primary tumour was standard risk (Northcott et al., 2019). Patients under the age of three (considered "infants") cannot receive CSI as it is considered too damaging. Within these general statistics, the subgroups and subtypes of medulloblastoma have a more significant impact on

survival than the differences in trial designs (Ramaswamy et al., 2016). It is therefore a key research aim to reduce toxicity and maintain survival by further adapting treatments to the risk-stratification system.

Patients with metastasis at diagnosis, patients with residual tumour after surgery, and infants are considered high risk. Currently, the standard of care is that these patients, except the infants >3 years old, receive stronger craniospinal radiotherapy. Adapted protocols are being investigated in order to reduce the neurotoxicity associated with total-brain irradiation (Gajjar et al., 2006, Jakacki et al., 2012, von Bueren et al., 2016). Other studies are investigating the replacement of CSI with intraventricular administration of chemotherapy (Rutkowski et al., 2009). This treatment protocol would allow bypass of the blood-brain barrier (BBB) and target tumour cells that may be flowing freely in the leptomeninges or in the nearby parenchyma. As it is administered directly to the site of treatment, lower doses can be used to reduce systemic toxicity effects (Walker et al., 2020). In paediatric leukaemia and lymphoma, intra-CSF administration of chemotherapy has replaced CSI due to its reduced neurotoxicity and the prevention of CNS relapse in these haematogenous malignancies (Schrappe et al., 2013, Gaynon et al., 2010). Despite these efforts, new therapies are desperately needed for high-risk patients, and to reduce the sequelae associated with CSI. Research guided by unique tumour profiles may lead to novel therapies for use over the clinic in the next several years.

1.4.3 Impacts on quality of life

The location of the tumours and consequences of surgery can cause impairments in motor skills and behaviour. In particular, cerebellar mutism syndrome (CMS) occurs more frequently in medulloblastoma patients compared to other cerebellar tumours, affecting the patients' speech and mood among other neuropsychological impairment (Gudrunardottir et al., 2016). Over the last few decades, advances in surgical techniques and adjuvant therapies have improved the survival rates for patients with medulloblastoma. However, this has also resulted in toxic and life-altering side effects in survivors. Children receiving treatment can experience acute neurological

neuropsychological and physical disabilities, and these can remain in survivors. Cranio-spinal irradiation will inevitably cause neurological damage that will impact the patients' cognitive function (Moxon-Emre et al., 2014). The consequences of this neurological and psychological damage can also result in hearing loss (Hua et al., 2008), hormonal deficiencies (Gurney et al., 2006), and infertility (Byrne et al., 2004). A major aim of ongoing research is the identification of treatment regimens that are curative while limiting the long-term side effects that reduce the patients' quality of life.

1.5 The leptomeninges and CSF circulation

The brain and spinal cord are seamlessly encapsulated in a protective tissue coating composed of three layers (Figure 1.3) (Barshes et al., 2005). The outermost layer is the dura matter, anchored to the skull and the bones of the spinal cord. Below it is the arachnoid matter, a highly-vascularized web of tissue. The arachnoid matter is composed of arachnoid barrier cells and arachnoid trabecular cells, interconnected through a basement membrane. Below the arachnoid matter is the subarachnoid space, where the CSF flows. Arachnoid barrier cells have an abundance of tight junctions, adherens junctions and desmosomes which stop large molecules from diffusing from the circulatory system into the CSF. The last layer of the leptomeninges is the pia matter, attached to the brain parenchyma and spinal cord, and made up of modified fibroblasts. The main area of interest for medulloblastoma, is the subarachnoid CSF compartment where tumour cells can circulate around the brain and spine in order to disseminate and colonize secondary metastatic sites.

The CSF is a plasma ultra-filtrate, produced in the choroid plexus in the brain's ventricular system (Cushing, 1925). CSF flows through the fourth ventricle, located adjacent to the cerebellum, and then freely around the subarachnoid space. While the CSF is filtered from blood plasma, most water-soluble molecules and cells from the blood are separated from the CSF by the BBB. The CSF's main components are NA^{+}, CL^{-}, $HCO3^{-}$, K^{+}, Mg^{+}, $Ca2^{+}$, O_2, and glucose. The CSF also contains substances such as vitamin C, folate, ions, and RNAs that are essential for brain health. The

CSF is also poorer in molecules including growth factors, and the variety of cell types found in brain tissue. For example, plasma has ~7g of protein per 100 mL, while CSF has ~0.025g of protein per 100 mL, mostly made up of albumin that diffuses from plasma into CSF (Spector et al., 2015). It is still unknown how tumour cells transition from one microenvironment to another, survive, and colonize in the subarachnoid space.

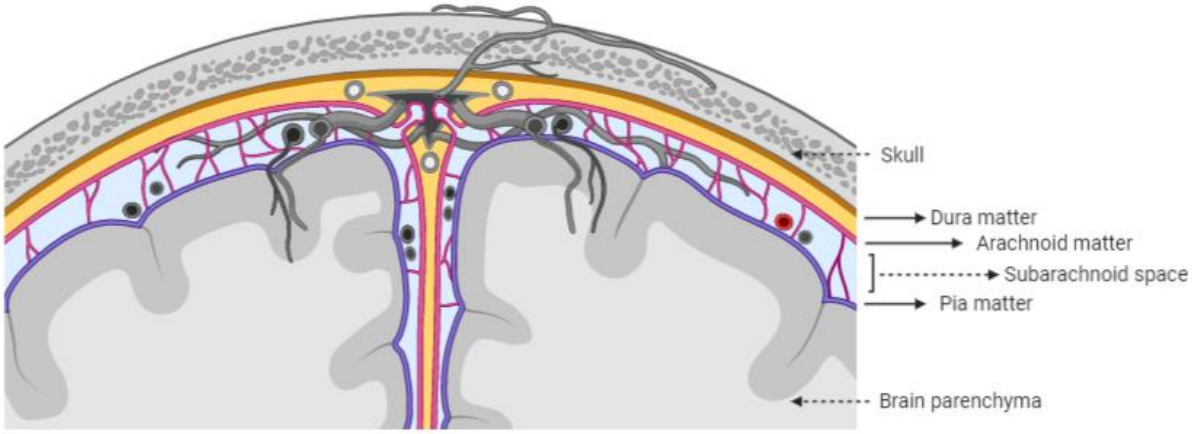


Figure 1.3 The composition of the leptomeninges.

The leptomeninges that encapsulates and cushions the brain and spinal cord is composed of 3 layers. Between the arachnoid matter and subarachnoid matter, the CSF flows in the subarachnoid space. This is the most common metastatic niche for medulloblastoma.

1.6 Metastasis

1.6.1 General cancer metastasis

The word “metastasis” comes from the combination of the Greek prefix “meta” meaning change, and “stasis” meaning a state of equilibrium. By definition, it is the process of spreading to a secondary site and formation of macroscopic tumours. In 2000, Hanahan and Weinberg defined a framework of characteristics for cancer cells; one of which was invasion and metastasis (Weinberg and Hanahan, 2000, Hanahan and Weinberg, 2011). This is a hallmark restricted to a subset of cells from the primary tumour able to invade through a basement membrane and disseminate to a near or distant metastatic site. Recently, Welch and Hurst reported 4 hallmarks of metastasis: 1) motility and invasion, 2) modulating the environment, 3) plasticity, and 4) colonization (Welch and Hurst, 2019). Another review by Fares and colleagues described a 5-step metastatic cascade: 1) invasion, 2) intravasation, 3) circulation, 4) extravasation, and 5) colonization (Figure 1.4) (Fares et al., 2020).

1.6.1.1 The metastatic cascade

The most common route for solid tumours to disseminate is through haematogenous spread. First, a subset of metastatic clones from the primary tumour invade into the surrounding environment through single-cell or collective migration. Some cells have the ability to infiltrate the circulatory system (intravasation), possibly through the same mechanisms as immune cells. In the vasculature, cells can roll on the endothelium and form cell aggregates with other tumour cells or haematogenous cells (emboli). Metastatic cells are then able to arrest at the extravasation location and modulate the environment of the secondary pre-metastatic niche. Finally, cells colonize the tissue and form macroscopic lesion which can in turn restart the metastatic cascade (Welch and Hurst, 2019, Fares et al., 2020).

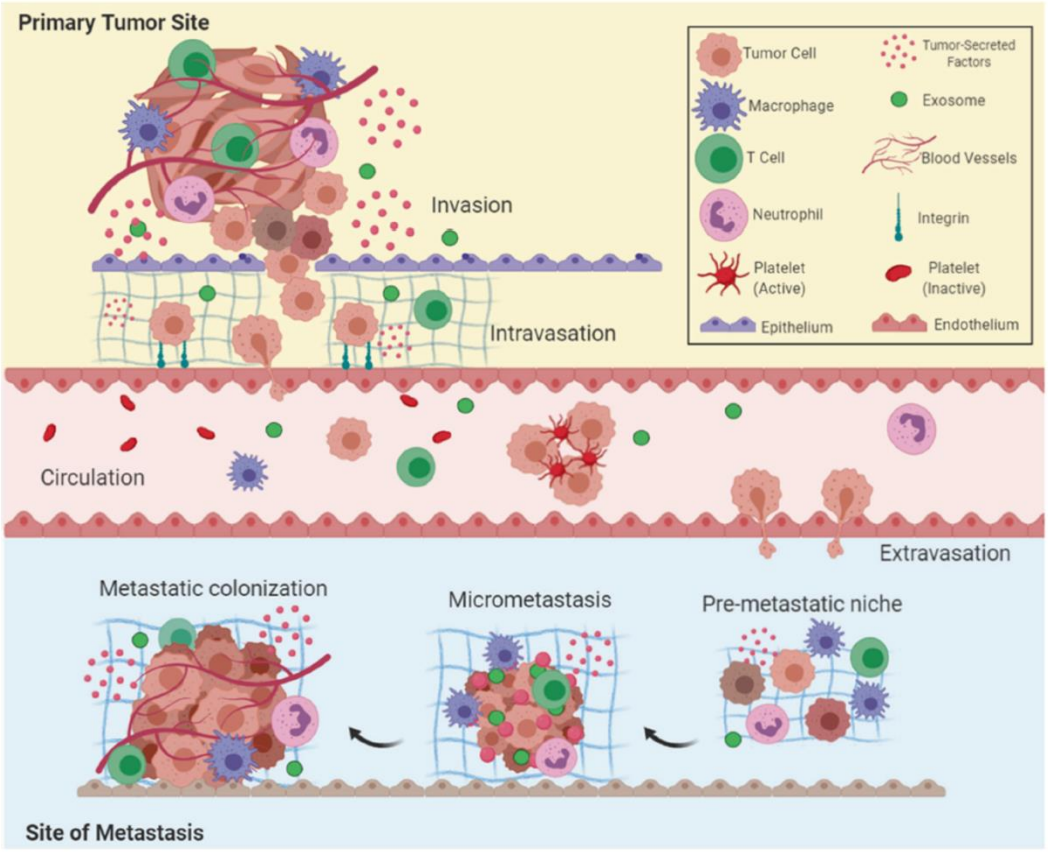


Figure 1.4 The metastatic cascade

Metastatic sub-clones **invade** into tissue surrounding the primary tumour. **Intravasation** allows cells to enter the circulatory system, and **circulate** through blood or lymph vessels. **Extravasation** allows tumour cells to exit the circulatory system where they prepare the pre-metastatic niche and **colonise** the secondary site. This figure is a reproduction from Fares et al., 2020.

1.6.1.2 Control of cell migration

In order to migrate, cells alter their cytoskeletal and cytoplasmic structures, allowing them to modify their cell shape and respond to chemo-attractant or chemo-repulsive stimuli. This results in directional migration towards localized or gradients of signals. Cell motility occurs individually in the absence of cell-cell interactions, or as collective cell migration when cell-cell junctions mediate communication and cohesion (Friedl and Gilmour, 2009). The mode of migration is determined by intracellular determinants (cytoskeletal organisation, cell-cell adhesion, cell-ECM adhesion and cell deformability) as well as environmental determinants. The cell-intrinsic

determinants include cytoskeletal organisation which directs cell membrane structures and interactions with the ECM.

Actin dynamics (assembly and disassembly) lead to the formation of different membrane protrusions ranging from basic “blebbing” that mediate amoeboid migration (Paluch and Raz, 2013), to the more specialized lamellipodia, filopodia and invadopodia. These actin structures are regulated through cross-linking by proteins such as fascin, and polymerisation of actin and actin-associated proteins by small GTPases including Rac and Cdc42 (Te Boekhorst et al., 2016). Migrating cells can also adapt to characteristics of their tissue environment including physical properties (dimensions, space, topography) as well as macromolecular composition and organisation. For example, cells experience molecular and structural changes when they transition from one tissue type to another, such as when metastatic cells exit the circulatory system into a secondary tissue niche (Kienast et al., 2010, Te Boekhorst et al., 2016).

Haematogenous invasion has been characterised by a change in cell morphology to a spindle shape, leading to the hypothesis that these cells de-differentiate into mesenchymal cells. This process was named cancer epithelial to mesenchymal transition (EMT) as it shares characteristics with EMT observed during normal development (Thiery, 2002). This process is characterised by the downregulation of adherens junctions, tight junctions and desmosomes due to the conversion of E-cadherin to N-cadherin. This leads to the loss of the epithelial phenotype and dissociation of cells from the epithelial mass. EMT transformation gives cells the ability to migrate, reduce cell-cell adhesion, and stem-like properties that enable population at the metastatic site (Mani et al., 2008).

Similar intra-cellular and cell-ECM factors to the ones described above may be driving the process of metastasis in medulloblastoma. Although medulloblastomas are not of epithelial origin, the recent confirmation that these tumours are capable of haematogenous spread has sparked interest into researching EMT-like pathways that may be driving medulloblastoma invasiveness.

1.6.2 Medulloblastoma leptomeningeal metastasis

Medulloblastoma patients with metastasis at diagnosis or metastasis at recurrence are considered high risk, and have high mortality rates. The frequency of metastatic events differs significantly between medulloblastoma subgroups. It has also been shown that the molecular subgroup of the primary tumour is conserved in the metastatic disease (Ramaswamy et al., 2013). Molecular characteristics of metastases can be found in a small sub-clone population in the primary tumour (Wu et al., 2012, Morrissy et al., 2016), but disseminated tumours will also develop changes from their primary tumour. For example, *MYC* and *MYCN* amplifications and P53 pathway defects are found at relapse (Hill et al., 2015).

1.6.2.1 Leptomeningeal metastasis

Since most metastatic medulloblastoma tumours remain within the CNS, it has long been assumed that the process of medulloblastoma metastasis occur through passive shedding into the CSF system (Fults et al., 2019). This assumption has however never been experimentally confirmed, and the understanding of how cells metastasize from the primary tumour and disseminate within and outside the CNS remains poor. Within the primary tumour niche in the brain parenchyma, cells interact with brain ECM components and growth factors, and are surrounded by other neural cell types such as neurons and astrocytes. The medulloblastoma metastatic niche in the subarachnoid space of the leptomeninges is a stark contrast with the cerebellum's environment. The difficulty in obtaining tissue samples to study the metastatic niche has meant that we have a poor understanding of this environment (Van Ommeren et al., 2019).

A leptomeningeal dissemination cascade has been proposed whereby medulloblastoma cells proceed through 3 stages: initiation, dispersal, and colonization (Fults et al., 2019). This is similar to the metastatic cascade (Fares et al., 2020), but medulloblastoma cells circulate through the subarachnoid space rather than the vascular system. In the initiation stage, MB cells infiltrate the CSF, and then

enter the second stage of survival and dispersal around the leptomeninges. Finally, disseminated cells implant into the secondary metastatic site in order to colonize it (Fults et al., 2019). Cell migration and invasiveness are essential for the leptomeningeal dissemination cascade to begin, and this has been experimentally provoked through the ectopic expression of *MYC* (Zhou et al., 2010). There are several mechanisms by which primary tumour cells are thought to invade the meninges; by direct invasion into the CSF, invasion into blood vessels, or through surgery (O'Meara et al., 2007).

1.6.2.2 Invasion into the leptomeninges

As medulloblastoma is located close to the meninges, metastatic cells may grow into, or invade directly into the subarachnoid space, allowing cells to travel around the neuroaxis carried by the flow of CSF. In order to migrate through the brain parenchyma, cells must increase motility signals and remodel their cytoskeletons. Hepatocyte growth factor (HGF) and its receptor c-Met are molecular components of epithelial to mesenchymal transition that induce cell scattering and motility (Birchmeier et al., 2003). HGF is a known inducer of EMT which has been reported to induce EMT in aggressive SHH tumours *in vivo* (Li et al., 2005, Abounader and Laterra, 2005, Binning et al., 2008). *In vivo* studies have also implicated the transcription factors *Myc* and *Lhx1* in the activation of various aspects of the leptomeningeal dissemination cascade (Zhou et al., 2010).

It has been reported that signalling between stromal cells and tumour cells through the CXCR4/CXCL12/WIP1 signalling pathway may guide medulloblastoma cells to their metastatic niche. CXCR4 is a receptor that has been shown to direct tumour cells to a metastatic niche through signalling by its ligand CXCL12 (Burger and Kipps, 2006). CXCL12 has also been shown to induce migration of medulloblastoma cells *in vitro*. The same study reported that WIP1, a known oncogene, impacts the localization of CXCR4 receptor in medulloblastoma cells (Buss et al., 2012, Buss et al., 2015). While in the leptomeninges, disseminating cells likely silence apoptotic

machinery that would normally be induced by the challenges in the metastatic environment, including sheer stress from fluid flow and osmotic gradients. Anti-apoptotic signalling that may aid metastatic cells to survive has been linked to loss of *TP53* or expression of Bcl-2 (Kawauchi et al., 2012, Jenkins et al., 2016).

1.6.2.3 Haematogenous metastasis

The most common route of leptomeningeal metastasis for tumours that originate outside the CNS is via haematogenous spread, where tumour cells circulating in the blood invade into the highly-vascularized arachnoid matter. Recently, a study provided the first *in vivo* evidence that medulloblastoma cells may also disseminate through the circulatory system. While a molecular mechanism has not been confirmed, the study suggested that the CCL2/CCR2 signalling axis may mediate medulloblastoma cell trafficking out of the haematogenous circulation as it does with leukocytes under normal conditions (Garzia et al., 2018, Lim et al., 2016b).

Finally, it is possible for leptomeningeal dissemination to occur during surgery (O'Meara et al., 2007). If a brain tumour obstructs the flow of CSF, this causes hydrocephalus, an increase in intracranial pressure. This requires immediate surgical intervention, and shunt is placed to drain the CSF into the abdominal cavity. This can lead to peritoneal metastasis.

1.6.3 Invading basement membranes in the brain

The basement membrane is an extracellular matrix that covers the basal layer of all endothelial and epithelial cells, providing support for the cells and separating different tissue compartments (Pozzi et al., 2017). The components of the basement membrane also provide cues to induce differentiation and migration in its surrounding cells. In normal conditions, basement membranes act as barriers to cells whose function does not require them to cross basement membranes. The ability to migrate through the limits of the basement membrane is an important feature that

distinguishes malignant from benign tumours (Rowe and Weiss, 2008, Welch and Hurst, 2019).

The basement membranes in different tissue types are composed of a variety of marcomolecules: collagens, laminins, nidogens, and heparin-sulphate proteoglycans (HSPGs). In the brain, basement membranes are primarily composed of type IV collagen, laminin-111, nidogens, the (HSPG perlecan, agrin and fibronectin (Morris et al., 2014). The formation of the basement membrane occurs through self-assembly of supramolecular networks of laminin-111 and collagen IV. Laminin polymers initiate the membrane formation, acting as a template for other components, and anchoring the basement membrane to the cellular cytoskeleton through integrin binding (Yurchenco and Cheng, 1993). Collagen IV then assembles through interactions with integrins, or directly with the laminin networks. The two networks are bridged by recombinant Nidogen-1 (Fox et al., 1991) and HSPGs such as perlecan to create a stable network of matrix components (Timpl, 1996). At the basement membrane, astrocytic end feet also contribute to the barrier (Sofroniew, 2015).

Some of the main basement membranes in the CNS are:

1) the parenchymal basement membrane, a collective name for the meningeal epithelial basement membrane and the astroglial basement membrane, which separates the brain parenchyma from the pia matter (Figure 1.5) (Sofroniew, 2015)

2) The basement membrane separating the subarachnoid space from the bottom layer of barrier cells in the arachnoid matter (Barshes et al., 2005).

3) The cerebrovascular basement membrane (CVBM) which defines the borders of blood vessels in the brain (Hallmann et al., 2005, Sofroniew, 2015). The BBB is a permeable limit between the circulatory system and the brain or CSF made up of endothelial cells that prevent any water-soluble molecules from diffusing from the bloodstream, while allowing active transport of nutrients to the CNS. The CVBM contributes to the BBB around endothelial cells of blood vessels. The blood-CSF

barrier (BCSFB) is found between epithelial cells of the choroid plexus and cells of the arachnoid matter.

Exactly how invasion occurs in medulloblastoma is not known, but in order to extend into the CSF, medulloblastoma cells would have to extend through the corrugated cerebellum and therefore cross one of more basement membranes.

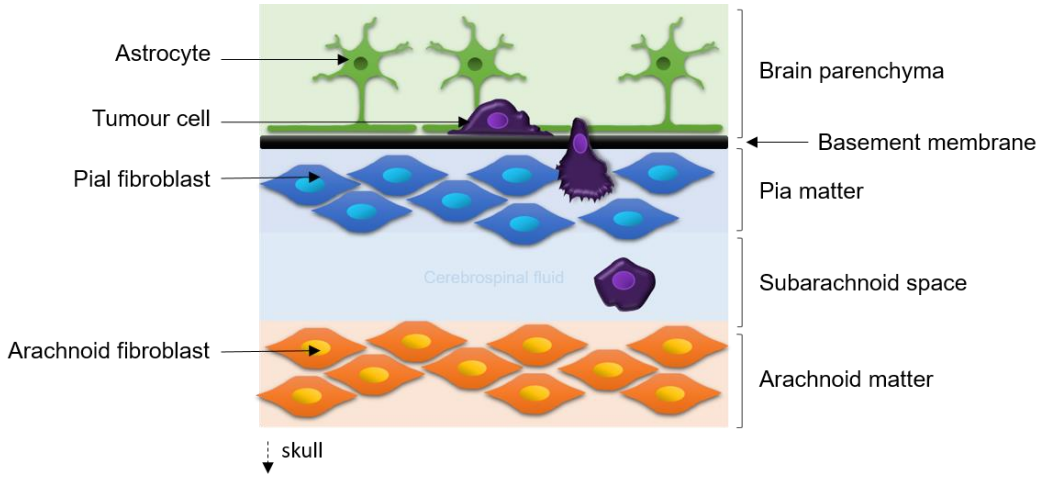


Figure 1.5 The parenchymal basement membrane at the interface between the brain and leptomeninges.

This figure was adapted from Sofroniew M.V., 2015.

1.7 *In vivo* and *in vitro* models

1.7.1 *In vivo* models of medulloblastoma

Mouse models have been an essential tool in identifying the cells of origin, molecular drivers, and varying phenotypes of medulloblastoma. Patient-derived xenograft (PDXs) are made by culturing primary tumour cells *in vivo*. Models can be orthotopic xenografts where established medulloblastoma cell lines are implanted into the mouse cerebellum in order to model the equivalent location in the human brain. Transgenic mouse models are achieved by inducing random or specific genetic events in the animal in order to replicate tumour characteristics and behaviour. *In*

vivo studies performed in the last decade have let to improved understanding of medulloblastoma metastasis.

WNT: All the currently published models for WNT medulloblastoma are transgenic mouse models that rely on mutations in *Ctnnb1* and *Tp53* to develop tumours (Gibson et al., 2010, Robinson et al., 2012).

SHH: The bulk of medulloblastoma *in vivo* model work has been done on SHH tumours, and several transgenic models have been reported. For example, deletion of SHH pathway gene *Ptch1* in combination with *Tp53* deletion results in the development of MB tumours in 100% of animals (Wetmore et al., 2001). The *Sleeping Beauty* transposon system (Ivics et al., 1997) has been adapted in a SHH mouse model and has substantiated the hypothesis that clonal selection leads to MB metastasis (Wu et al., 2012). This model can be described as a “cut and paste” process where transposase excises a transposable element and integrates it into a new location. The random mutagenic approach can be used to identify genes that contain insertions more frequently than the background rate, which are assumed to be altered to confer a benefit to tumour cells.

Group 3: Several transgenic mouse models of Group 3 MB have been reported, all relying on the overexpression of *Myc* or *Mycn*. *Myc* overexpression in combination with Tp53 loss-of-function in stem/progenitor cell populations results in a Group 3-like medulloblastoma (Pei et al., 2012, Kawauchi et al., 2012). However, this is not entirely representative of human Group 3 genotypes, as *TP53* mutations are considered more indicative of SHH and WNT tumours (Zhukova et al., 2013). An orthotopic model overexpressing Group 3 oncogenes *GFI1* and *GFI1B* in conjunction with *MYC* overexpression in neural stem cells resulted in aggressive cerebellar tumours with metastatic dissemination (Northcott et al., 2014). While *MYC* overexpression only accounts for 17% of Group 3 tumours, and there is still a need for non-*MYC in vivo* models.

Group 4: While Group 4 tumours are the most commonly occurring medulloblastoma subgroup, there are no transgenic models of Group 4 in the literature. This may change in the future as the classification of medulloblastoma subtypes evolves, and the origin of distinct tumour types are identified.

1.7.2 *In vitro* models of medulloblastoma

1.7.2.1 Primary cultures and cell lines

A heterogeneous mix of cells derived from patients or *in vivo* models can be passaged *in vitro* to make primary cultures. These can also be passaged in mice in order to retain more of their original heterogeneity. An established cell line results from primary cell cultures that have been immortalised or become continuous cultures through repeated passaging *in vitro*. Standard cell culture using established cell lines made to adhere to a plastic surface has been used to screen potential cancer drugs since the 1950s (Eagle and Foley, 1958, Hirschberg, 1958). These cell lines offer a simple model to work with, although they may be the result of clonal selection from the primary culture and may only represent a subset of genetic and phenotypic characteristics of the tumour of origin. Culturing cells *in vitro* has been reported to alter the genetic profiles of medulloblastoma cell lines in comparison with patient tumours (Lin and Chang, 2008). A review by Ivanov and colleagues classified the existing established cell lines for medulloblastoma (Ivanov et al., 2016). The majority of these lines were derived from Group 3 tumours, a handful represent SHH tumours, and there is only one and two cell lines derived from WNT and Group 4 tumours respectively (the Group 4 lines are a matched pair from the same patient) (Figure 1.6).

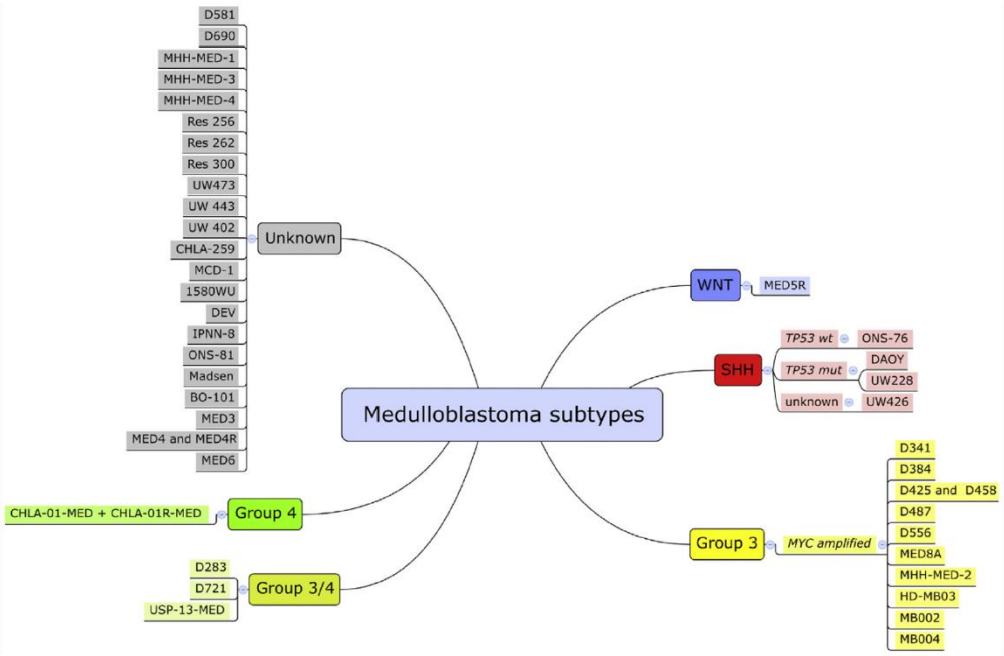


Figure 1.6 Established medulloblastoma cell lines organised by molecular subgroup.

This figure is a reproduction from Ivanov *et al*., 2016.

1.7.2.2 3D in vitro cultures

Cells cultured *in vitro* are typically grown in conventional polystyrene flasks, which are stiffer than any tissue in the body. The standard 2D cell culture approach does not take into account the 3D environment of tumours such as their multi-dimensional architecture, the contribution of the stroma, and the essential ECM. This can result in data that is non-predictive of *in vivo* responses and prevent pre-clinical studies from translating into clinical trials. Some of the caveats of 2D cultures can be overcome by culturing cells in 3D in order to recapitulate some of the complex architecture and extracellular factors that can influence tumours (Edmondson et al., 2014). The development of specialized 3D culture methods that maintain key characteristics of the patient TME may lead to bridging the gap between pre-clinical *in vitro* studies, pre-clinical *in vivo* studies, and clinical trials. Although there is no single widely-adopted 3D culture method to date, 3D *in vitro* cultures have been reported in several published studies.

The simplest methods to grow cells in 3D include the hanging drop or the use of spinner flasks to allow cells to aggregate, create cell-cell interactions, and secrete ECM components. 3D tumour spheroid culture (Sutherland et al., 1971) is another method to grow reproducible cell aggregates, and is a valuable method for high-throughput screens. Spheroids are spherical cell aggregates of controlled volume that can be culture suspended in medium or encapsulated in an ECM matrix. Tumour spheroids are a useful tool to study the secretion of ECM, the interaction of cells with surrounding matrix, or the invasion of cells from the spheroid into the matrix (Vinci et al., 2015). Spheroids can also be co-cultured to study the role of different cell types including stem cells. In addition, spheroids typically have a hypoxic core as a result of a gradient of oxygen, carbon dioxide, nutrients and waste within the 3D structure (Lin and Chang, 2008). A common application of spheroid models is drug screening, as spheroids are less sensitive to drugs and better resemble the *in vivo* response than 2D cultures (Friedrich et al., 2009). Although more representative of tumours than 2D culture, spheroids grown suspended in medium still lack the support of the ECM. In order to improve these models further, they can be cultured on top of, or embedded in a gel matrix.

1.7.2.3 Hydrogel-based 3D cultures

There is an array of natural and synthetic gel matrices available, each with different characteristics that are adaptable to individual experiment needs. One of the most commonly used gels is basement membrane extract (BME) purified from Engelbreth-Holm-Swarm (EHS) murine tumours, derived from the parietal endoderm of the mouse yolk sack (Orkin et al., 1977). The most commonly used BMEs include Matrigel™ (Hughes et al., 2010) and Cultrex® BME, and most closely resemble the basement membrane. Embedding tumours spheroids in these 3D gel matrices allows them to proliferate, differentiate and migrate in ways that are not sustained by a liquid, ECM-free environment. Characteristics of organ-specific ECMs such as stiffness, composition of ECM proteins such as laminin and collagens, and co-culture with stromal cell types all play a key role in influencing cell behaviour.

In 2D, cell migration occurs on only one surface. The leading edge of the migrating cell advances, and the lateral space allows the cell to spread in an unconfined manner (Starke et al., 2014). By culturing cells on or within a 3D matrix, the structure and composition of the matrix can influence cells on all surfaces. Cells encapsulated in a 3D matrix will need to use different strategies for movement compared to those in 2D. Topology and stiffness influence cell migration, and cells will follow random or organised paths formed by the structure of the ECM. Different substrate stiffness can also push and compress cells in a way that mimics tissue. As a result, global gene expression will differ between cells cultured in 2D or 3D (Liu et al., 2006). The brain is one of the softest organs in the body with an elastic modulus of 1-2 kPa (Budday et al., 2015). The choice of matrix model should take into account this characteristic in order to influence global gene expression, global gene expression, and cell differentiation in a brain-dependent manner. These changes will ultimately affect the data collected such as the cells' invasion patterns and drug responses.

1.7.2.4 More complex 3D culture systems

The use of organotypic tissue slices also provides a complex and representative model of specific tumour environments. Patient or animal tissue sections can be precision-cut, maintained for up to a week, and used to culture tumour spheroids in 3D. Organotypic brain slice culture has been used in medulloblastoma research. One group treated medulloblastoma cells cultured on an organotypic brain slice with a SMO inhibitor (Chadwick et al., 2015), while another study compared the penetration of nanoparticles into cell monolayers, 3D spheroids and organotypic brain slice culture (Meng et al., 2016). Another study implanted medulloblastoma spheroids onto an *ex vivo* organotypic cerebellar slice culture and imaged infiltration and dissemination using immunofluorescence (Neve et al., 2017). Organotypic brain slice cultures are a promising example of how 3D culture advances could bridge the gap between *in vitro* and *in vivo* pre-clinical studies.

Models can be taken further to more closely resemble the cellular microenvironment and tumour architecture of cancers while maintaining physiological levels of oxygen, temperature and pH through the use of microfluidic devices. Delivery of external stimuli is prevented by the lack of vascularization in 3D culture models, and microfluidic devices offer an automated solution to some of these. These types of models also allow perfusion to mimic the effects of circulatory system to overcome the drawbacks of having non-vascularized cell culture models. In the last 5 years "organ-on-a-chip" microfluidic systems have been developed to represent not only the structure, but the complex functions of different organs (Huh et al., 2010, Bhatia and Ingber, 2014, Bein et al., 2018).

1.7.2.5 In vitro models of migration

The use of *in vitro* 2D and 3D migration assays to study tumour cell migration and invasion has been reviewed by Zimmerman, Box and Eccles (Figure 1.7) (Zimmermann et al., 2013). The most basic migration assay is the "scratch wound" assay where a pipette tip is used to scratch a confluent monolayer of adherent cells, or cells are cultured around a ring which is removed to allow migration into the "clear" area. The "wound" closure is then imaged over time to quantify migration. This technique can be automated for better reproducibility and use in high throughput screens. However, the method also has several caveats, including a lack of resemblance to *in vivo* models or tissue of origin, and it quantifies only one type of migration in a population of cells where there may be other migratory properties.

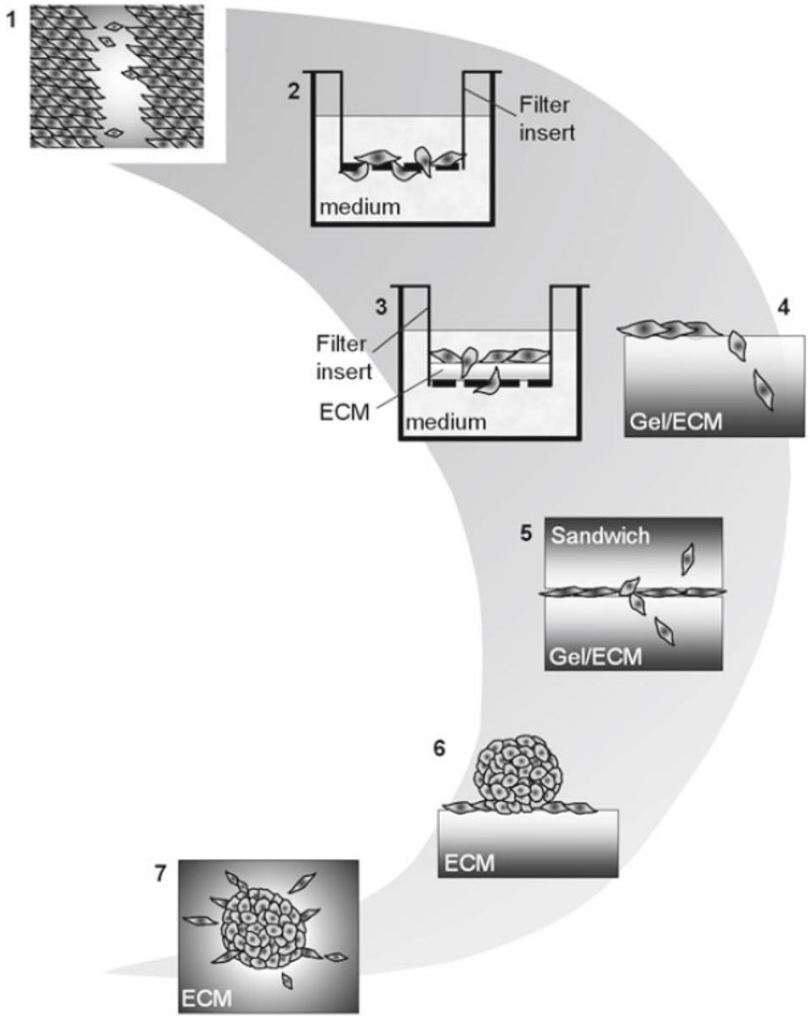


Figure 1.7 Cell migration and invasion models.

Zimmerman and colleagues ranked existing *in vitro* cell migration and invasion assays based on their degrees of 2- or 3-dimensionality. **1)** The “scratch wound” assay quantifies cell migration into a cell-free area. **2)** The 2-D chemotaxis assay quantifies cell migration through a trans-well filter. **3)** The trans-well filter can be coated in ECM to model invasion into a 3D matrix. **4)** Cells seeded on the surface of a 3D matrix can invade in one direction, while **5)** cells sandwiched between two layers of 3D matrix can migrate up or down. **6)** Cells cultured in a 3D tumour spheroids can be seeded on a 3D matrix or **7)** embedded in 3D matrix to quantify cell invasion. This figure is a reproduction from Zimmermann *et al*., 2013.

Another 2D assay to study cell migration is through the induction of chemotaxis, the directional cell migration that occurs when in the presence of an extracellular chemokine gradient. This is done in Boyden chambers (Boyden, 1962). Trans-well assays, based on the Boyden chamber design, feature two chambers separated by a semi-permeable membrane. Cells are seeded in the top of the assay to quantify migration towards a chemo attractive gradient. The invasive potential of cells can be quantified by coating the membranes in ECM proteins or matrix, or a feeder layer of stromal cells such as fibroblasts (Albini et al., 1987). This provides a 3D environment for cells seeded on top of a layer of matrix, or sandwiched between two layers of matrix. During dynamic invasion, cells degrade the ECM in the surrounding tissue. The secretion of proteases such as metalloproteinases by invasive cells has been extensively investigated using this chemo-invasion assay (Albini et al., 2004). BME has been used in the past as the main *in vitro* invasion assay to identify drivers of medulloblastoma metastasis including the PDGFRA-Akt-ERK pathway (Abouantoun and MacDonald, 2009), GLI2 and ARNT (Jenkins et al., 2014), and NICD1, the active form of NOTCH1, (Kahn et al., 2018).

3D spheroid cultures can also be adapted to investigate cell invasion into a matrix. This is done by transferring tumour spheroids onto an ECM-coated surface, or embedding the spheroid in ECM. Cell invasion out of the spheroid can then be imaged and quantified. Invading cells produce invadopodia cell protrusion that extend into the matrix (Vinci et al., 2012). Vinci et al have optimised 3D spheroid models using glioblastoma cell lines that enable reproducible quantification of tumour cell invasion, drug-screening, and the analysis of molecular changes in the analysed spheroids following these assays (Vinci et al., 2015).

Through further modifications, the assays described have the potential to more closely resemble a specific organ environment, including physical interactions and signal molecules that are essential for specialised cell function. Overall, *in vivo* models are ethically-challenging, expensive, do not allow for high-throughput screening of therapeutic agents, and are currently not representative of all subgroups

and subtypes. In addition, 2D cell culture does not recapitulate a tumour's architecture or microenvironment. Developing clinically-relevant 3D models *in vitro* could replace, reduce and refine the use of animals and bridge the gap between pre-clinical models and clinical trials.

1.8 Hypothesis and aims

The major cause of mortality in infants and children with medulloblastoma is metastasis. There is therefore an urgent need to better understand this tumour process and identify driver molecules so that novel therapeutic options can be implemented in clinical treatment of these patients. The mechanisms by which cells invade from the primary tumour niche to the metastatic niche in the leptomeninges remain unclear. This project will focus on the interface that highly-invasive medulloblastoma cells likely invade through between the primary tumour niche in the cerebellum parenchyma and the CSF in the leptomeninges.

I will test the hypothesis that cells develop transcriptomic changes as they migrate through the basement membrane, and transition from non-migratory, to adherent, and finally migratory phenotypes. I will then test the hypothesis that transcripts upregulated as cells become migratory have a function in cell migration. This project aims to investigate the initiation stage of the leptomeningeal dissemination cascade (Fults et al., 2019).

Aim 1: Develop an *in vitro* model representing the interface between the brain and the CSF for capture and molecular analysis of migrating cells.

Aim 2: Identify new markers of migration and metastasis in medulloblastoma by sequencing the transcriptome of migrating cells in the *in vitro* model.

Aim 3: Validate the expression and function of these new markers *in vitro* and in medulloblastoma patients.

Chapter 2 Materials & Methods

2.1.1 Cell lines used

CHLA-01-MED (ATCC® CRL-3021™) and CHLA-01R-MED (ATCC® CRL-3034 ™) cells were a kind gift from Professor Geoff Pilkington (University of Portsmouth, United Kingdom). D458-MED cells were a kind gift from John R. Silber (University of Washington Seattle, United States of America). HD-MB03 cells (DSMZ ACC 740) were a kind gift from Dr Till Milde (DKFZ, Heidelberg, Germany). ONS-76 cells (ATCC® HTB-186™) were a kind gift from Dr Annette Kunkele (Charite Universitatsmedizin, Berlin, German). MDA-MB-231 breast cancer cells were a kind gift from Dr Cathy Merry (University of Nottingham, United Kingdom). D283-MED cells (ATCC®HTB-185™) and DAOY cells (ATCC® HTB-186™) were purchased from ATCC.

Characteristics of all medulloblastoma cell lines used can be found in Table 3.1.

2.1.2 Standard cell culture

2.1.2.1 Standard cell culture media

D283-MED, D458-MED, DAOY and MDA-MB-231 cells were cultured in Dulbecco's Modified Eagle Medium (DMEM; Fisher Scientific 11574446) supplemented with 10% foetal bovine serum (FBS; HyClone, SH30541.03).

HD-MB03 and ONS76 cells were cultured in RPMI-1640 medium (Sigma-Aldrich R8758) supplemented with 10% FBS.

CHLA-01-MED and CHLA-01R-MED cells were cultured in DMEM/F-12 medium (Fisher Scientific 11520396) supplemented with 2% B-27 supplement (Gibco, 17504044), 20 ng/mL recombinant human epidermal growth factor (EGF; Gibco, PHG0315), and 20 ng/mL recombinant human basic fibroblast growth factor (FGF; Gibco, PHG0266).

2.1.2.2 Recovering cells from liquid nitrogen cryo-storage

Cryo-vials of cells were thawed quickly in a 37°C water bath. The cell suspension in freezing medium was then centrifuged for 7 minutes at 100 x *g*. The supernatant was removed, and the cell pellet washed in room temperature sterile Hank's balanced salt solution (HBSS; Gibco, 24020117). The cell pellet was then resuspended in fresh culture medium warmed to 37°C and transferred to a cell culture flask.

All human cell lines were grown in a 37°C incubator with 5% CO_2 (New Brunswick, Galaxy 170R).

2.1.2.3 Mycoplasma testing and cell line authentication

Mycoplasma testing was routinely performed on a sample of medium that had been in contact with the cells for at least 3 days in culture. Screening for Mycoplasma was done using the PlasmoTestTM Mycoplasma Detection Kit (InvivoGen rep-pt1). All cell lines used in this thesis were culture antibiotic-free.

The cell lines used in this thesis were not authenticated during the course of this project.

2.1.2.4 Sub-culturing cell lines

CHLA-01-MED and CHLA-01R-MED are suspension cell lines, and were grown in non-treated cell culture flasks (Eppendorf, 0030711017). D283 MED, D458 MED, DAOY, ONS76, MDA-MB-231 and HD-MB03 are semi-adherent cell lines, and were grown in tissue culture treated flasks (Eppendorf, 0030711114).

Suspension cell lines

Suspension cell lines CHLA-01-MED and CHLA-01R-MED form large clusters of cells, smaller clusters, and single suspension cells. The cells were sub-cultured by removing volumes of cell suspension and replacing with a larger volume of fresh medium once or twice a week. Once a week, the cell suspension was centrifuged for

7 minutes at 100g and resuspended in ¼ conditioned medium, ¾ fresh medium. The passages were in a range of 1:2 to 1:10 depending on needs.

Semi-adherent cell lines

Semi-adherent cell lines consist of adherent cells, semi-adherent cell clusters and suspension single cells and small cell clusters. The cells were sub-cultured by collecting the cell suspension, and 10 mL of HBSS was used to wash the flask. The adherent cells were then incubated for 5 minutes with 2 mL of warmed 1X trypsin-EDTA (Sigma, LH-SIG2044). The trypsin-EDTA treated cells were added to the cell suspension, and centrifuged for 7 minutes at 100g. The cell pellet was then resuspended in fresh medium and seeded into a new flask. D458 MED and D283 MED were split in a range of 1:2 to 1:5.

Adherent cell lines

Adherent cell lines DAOY, ONS76 and MDA-MB-231 (breast cancer) were sub-cultured by disposing the culture medium, and then following the protocol described above for semi-adherent cell lines.

2.1.2.5 Preparing stocks for cryo-storage

Cells were passaged as described previously, and the desired amount was collected in a 50 mL falcon and centrifuged for 7 minutes at 800 rpm. The supernatant was removed, and the cell pellet resuspended in freezing medium. Freezing medium was either 1) made from 90% FBS and 10% Dimethyl Sulfoxide (DMSO; Sigma D2650), and filter-sterilized, OR 2) CELLBANKER 2 freezing medium (AMSBIO, 11891). 1 mL or 0.5 mL of cells in freezing medium was transferred to cryogenic vials and placed in a Mr Frosty (if using FBS and DMSO freezing medium), or placed directly in -80°C (if using CELLBANKER 2 freezing medium). The samples were stored for 24 hours at -80°C before being transferred to the liquid nitrogen store.

2.1.2.6 Preparing cell pellets for molecular analysis

The cell suspension was centrifuged for 5 minutes at 3,000 rpm in a micro-centrifuge, and the supernatant was discarded. The cell pellet was washed twice in 1 mL of PBS, and centrifuged again. After the final wash, the PBS was carefully removed, and the dry pellet was snap frozen in liquid nitrogen. The samples were immediately transferred to a -80°C freezer.

2.1.2.7 Cell counting

Suspension cell lines

A representative aliquot was taken from the flask and centrifuge for 7 minutes at 100g. The cell pellet was resuspended in 1 mL of Accutase cell detachment solution (AT104-500). The cells were resuspended 10 times with a 1 mL pipette, then incubated for 10 minutes in the cell detachment solution. At the end of the incubation, the cells were resuspended 10 times with a 1 mL pipette. The incubation in Accutase serves to break apart tight clusters of cells to allow counting. 10 µl of cells were combined with 10 µl of Trypan blue stain. 10 µL was counted using a haemocytometer (Hawksley) on a light microscope (Olympus CK2). The number of cells per mL was calculated using the formulae below.

Semi-adherent and adherent cell lines

Cells were cultured as described previously, and the cell pellet resuspended in 1 mL of medium. 10 µL of cells were combined with 10 µL of Trypan blue, a vital stain which selectively colours dead cells blue. 10 µL of cells and Trypan blue suspension was pipetted onto a glass counting chamber (Hawksley) and counted by eye on a brightfield microscope (Olympus CK2). The number of cells per mL was calculated using the following formulae:

$$(\#\ of\ live\ cells) / 4 = Cells\ per\ square$$

$$(Cells\ per\ square) \times (Dilution\ factor: 2) \times (1 \times 10^4) = Cells\ per\ mL$$

$$\frac{(Cells\ per\ ml)}{(Cells\ wanted\ per\ well\ )(number\ of\ wells)} = \frac{1{,}000\ \mu l}{x}$$

2.2 Cell culture in 3D

2.2.1 Basement membrane extract hydrogel culture

The cell lines CHLA-01-MED, CHLA-01R-MED, D283-MED and D458-MED were cultured in 3D using basement membrane extract (Cultrex® BME, Pathclear®: Trevigen 3432-005-01). BME is formulated to be 12-18 mg/mL. The lot used in these experiments was #33645G15, with a concentration of 16.15 mg/mL. Cultrex® BME is soluble form of basement membrane purified from Engelbreth-Holm-Swarm (EHS) tumours, which occur in the mouse yolk sac. The main components in BME are laminin, collagen IV, the HSPG perlecan and entactin. The BME also contains growth factors (FGF, EGF, TGF-β, PDGF, IGF). For these experiments, the BME was diluted to 2.5 mg/mL or 10 mg/mL in culture medium following the manufacturer's protocol.

BME was stored at -80°C for long term storage. Aliquots of BME were then frozen at -20°C for up to 3 months as recommended by the manufacturer. BME is liquid at 4°C, and solidifies at temperatures above 15°C. The BME aliquots were thawed overnight on ice at 4°C, and kept on ice during use.

2.2.2 Plating BME in 96-well microplates

A black walled-clear bottom plate 96-well microplate (BrandTech 781671), was warmed on a plate warmer at 37°C before use, and the outer wells of the plate filled with 200 µL of phosphate buffered saline (PBS) to create a humidity chamber and prevent the gels from drying.

Before plating, cells were counted as described above, and the desired number of cells was centrifuged for 5 minutes at 3,000 rpm. The cell pellets were resuspended in medium to a concentration of 10 mg/mL. The cell suspension in BME was resuspended gently with a pipette. 100 µl was immediately plater per well. The plate was then incubated for 30 minutes to 1 hour at 37°C. Following the incubation, 50 µl

of medium was added to the top of every well. The cells were fed by replacing the culture medium on top of the BME gel every 2-3 days.

For some experiments, a thin layer of BME was used to coat the wells of a 96-well microplate, and cell suspension was plated on top. The BME was diluted to a concentration of 10 mg/mL with culture medium, and 50 µl was plated onto the bottom of each well, shaken by hand to distribute the BME. The plate was incubated for 4 hours at 37 °C to set the BME before cell suspension was added.

2.2.3 Plating BME in a chemotaxis u-slide

The chemotaxis µ-slide (ibidi, 80326), was placed in a 10 cm petri dish (Corning) and a wet tissue was placed around the edges of the petri dish to create a humid chamber.

The manufacturer's manual instructions were followed. 6 µL of cell suspension in BME diluted to 10 mg/mL was added to the central observation area. The chemotaxis chamber slide was then incubated at 37°C for 30 minutes. Following the incubation, a total of ~60 µL of medium was added to each reservoir. A gradient of chemoattractant was created by adding medium without chemoattractant to the reservoir on the right, and adding medium with chemoattractant to the reservoir on the left. The chamber slide was then incubated at 37°C for 1 hour before imaging.

2.3 Cell culture imaging

2.3.1 Widefield imaging of 3D cultures in a 96-well microplate

Cells embedded in BME were plated in triplicate wells for each condition. The same triplicate wells used for cell viability assays described above were imaged using a Nikon Eclipse Ti inverted microscope, on the Widefield setting. Images were taken at set XY coordinates selected on Day 1. Sequential stacks of images taken along a vertical axis through each well (z-stacks) were aligned and focused using NIS-Elements to create composite images for each day. These images were used to assess the phenotype of cells in 3D BME over time, and were assessed visually for

signs of cell migration, proliferation, and cell death. Images were taken periodically, until the phenotypic features of the cells and PrestoBlue® cell viability indicated that the majority of cells had died. The area of cell clusters was measured using the open access software imageJ (Fiji) image analysis software (https://imagej.nih.gov/ij/).

2.3.2 Time-lapse imaging of 3D cultures in a chemotaxis µ-slide

Cells embedded in BME were plated in the three observation areas on each slide. The chamber slides were imaged in a Leica DMIRE2 Microscope, using the Widefield setting. The microscope was set up in an incubator chamber with a temperature of 37°C, and a CO_2 chamber was placed over the slide to create an environment with 5% CO_2. The open source microscopy software µManager (https://micro-manager.org/wiki/LeicaDMI) was used to set up time-lapse imaging of the slide over 48 hours. Two positions were manually selected in each of the three observation areas on the slide, making up a total of 6 points being imaged. One image was taken at each point every 30 minutes.

2.4 Assessing cell viability

PrestoBlue® cell viability reagent for microplates (ThermoFisher, A13261) was diluted 1:5 in medium without FBS or growth factors. 50 µl of 1:5 PrestoBlue® was added to each well, creating a final 1:10 dilution. The plate was incubated for 1 hour in the dark at 37°C. A 1 hour incubation time was chosen based on a standard curve performed on a range of optimisation times between 10 minutes and 2 hours as recommended by the manufacturer. After incubation, a bottom read was perform on a FLUOstar Omega plate reader (BMG labtech).

PrestoBlue® uses a cell's reducing power to convert resazurin to the fluorescent molecule resorufin. Resazurin is a cell-permeable compound that is non-fluorescent, and upon entering the cell, becomes a fluorescent red molecule. This reagent is used to measure metabolic activity. Fluorescent resorufin has an Excitation of 560 nm and an Emission of 590 nm. In order to quantify cell viability, the medium in each well of 96-well plate was replaced by 50 ul of medium without FBS or growth factors.

2.5 Migration and invasion assays *in vitro*

2.5.1 Chemotaxis migration assay

Cell migration and invasion assays were performed in a modified Boyden chamber assay using trans-well insert with 8 µm pores (Greiner Bio-One Thincert, 662638) in 24-well plates.

2.5.1.1 Serum starvation

Cells were incubated overnight in reduced FBS conditions (medium with 2% FBS) then passaged and counted as described in section 2.1.2.5.

5 x 10^4 cells were seeded onto each insert in 24-well trans-well inserts (~6.5 mm in diameter) in 100 µl of medium devoid of FBS. 600 µl of medium with 10% FBS or selected soluble factors (see table below) was added to the receiver wells. Alternatively, artificial cerebrospinal fluid (aCSF; TOCRIS 3525) supplemented with 0.8 mg/mL glucose and 10% FBS was added to the receiver well of each insert, making sure no air bubbles remained between the insert and the receiver well. The plates were incubated for 48-72 hours at 37ºC.

Table 2.1 Soluble factors tested as chemokines.

Soluble factor	Concentration
IGF1	100 ng/mL
Netrin-1	800 ng/mL
SHH	10 nM
EGF	20 ng/mL
FGF	20 ng/mL
HGF	20 ng/mL
CXCL12	1 µg/mL

2.5.2 Quantification of migration assay

2.5.2.1 Metabolic activity assay

Cell migration was quantified following the “Cell Migration, Chemotaxis and Invasion Assay Protocol” established by Corning.

(https://www.corning.com/catalog/cls/documents/protocols/an_Chemotaxis_protocol.pdf).

Standard curve

A standard curve of known cell numbers was set up for every biological replicate, with a range of 0 to 5 x 10^4 cells in 1X cell dissociation solution (AMSBIO, 3455-096-05). Calcein acetoxymethyl ester (Calcein AM; Source Bioscience, ABE3994) was diluted in cell dissociation solution at a ratio of 2.4 µl of calcein AM per 1 mL of 1X cell dissociation solution, and 50 µl was distributed to each well of the standard curve. The plate was incubated for 1 hour at 37ºC in the dark. After incubation, a bottom read was performed on a FLUOstar Omega plate reader (BMG labtech) at Excitation 485, Emission 520 and gain set to 1500.

Calcein AM is a cell permeable compound which is hydrolysed by esterases in metabolically-active cells, cleaving the AM group and converting the compound to a green fluorescent calcein.

Quantifying migrated cells

After 48-72 hours of migration, non-migrated cells were cleaned from the filters with a cotton swap and the medium was removed from the bottom well. Calcein AM was diluted in 1X cell dissociation solution at a ratio of 1.2 µl of Calcein AM for 1 mL of 1X cell dissociation solution, and 300 µl was added to the bottom well of each trans-well insert. The plate was incubated for 1 hour at 37ºC in the dark. After incubation, the sides of the plate were tapped to dissociate any remaining cells from the bottom of the filters, and the cells in suspension were transferred to a black-walled clear bottom 96-well plate (Brandtech). The plate was centrifuged for 5 minutes at 1,500 rpm to concentrate the cells at the bottom of the well, and 150 ul was removed before reading. A bottom read was perform on a FLUOstar Omega plate reader (BMG labtech) at Excitation 485, Emission 520 and gain set to 1500.

2.5.2.2 Staining

After 48-72 hours of migration, non-migrated cells were cleaned from the filters with a cotton swap and the medium was removed from the bottom well. The inserts were transferred to a 24-well plate containing 4% PFA for 10 minutes in order to fix the migrated cells on the bottom of the filters. The inserts were then washed in PBS and transferred to a plate containing haemotoxilin stain for 1 minute, followed by eosin for 10 minutes. The inserts were washed twice in PBS between stains and following the eosin stain. The inserts were dried overnight at room temperature. A scalpel was used to cut the filter off of the insert, placed on a glass slide with the bottom facing up, and a coverslip attached with DPX glue. The slides were allowed to dry before imaging on a light microscope.

2.5.3 Isolation of cells from migration assays for molecular analysis

2.5.3.1 Basement membrane ECM coating

For invasion across BME, the filters were coated with 20 µl BME (see Table 2.2 for concentrations). Migration assays were incubated for 48 hours before quantification of migration was performed by staining.

For migration assays across basement membrane components, the inserts were coated with collagen IV 24 hours prior to the start of the experiment. 50 µl of collagen IV was added to each insert, and the sides of the plate tapped to distribute evenly. The plates were dried overnight at room temperature in a tissue culture hood, then placed in the incubator until the experiment setup. On the day of the experiment, 50 µl of laminin 111 was added to each well and the sides of the plate tapped to evenly distribute. The inserts were dried for 1 hour at room temperature in a tissue culture hood, but the laminin was not allowed to dry fully. After 1 hour, the remaining liquid was pipetted off the inserts before adding cells. Uncoated duplicate controls and no chemokine triplicate controls were included for each condition.

Table 2.2 ECM gel or components used to coat trans-well inserts.

ECM coating	Product details	Concentration
BME Pathclear®	Cultrex 3432-005-01	2.5 mg/mL or 10mg/mL
Collagen IV from human placenta	Sigma C55333	200 µg/mL in H_2O
Collagen IV from mouse	Cultrex 3410-010-01	200 µg/mL in H_2O
Laminin 1 from mouse	Cultrex 3400-010-02	100 ug/µl in PBS

2.5.3.2 Collecting cells for molecular analysis

At the end of the migration period, suspension cells were collected by pipetting the medium from the top of the insert and gently washing with 100 uL of HBSS. The aCSF was gently removed from the bottom of the receiver plate and discarded. 100 µl of Cell Dissociation Solution was added to the top of the insert, and 300 µl to the receiver plate. Inserts were incubated for 10 minute at 37ºC. The sides of the plate were tapped to dissociate any cells, and cells were collected from the top of the insert or the bottom receiver well with 1 HBSS wash. 6 wells were pooled for each cell line, and the cells were centrifuged then snap frozen to store pellets for later molecular analysis.

2.6 Molecular techniques

2.6.1 RNA extraction

2.6.1.1 From 3D culture in BME

The supernatant medium was aspirated from the top of the BME layer, and a volume of Cell Recovery Solution (Corning, 354253) that was twice the volume of BME was added to each well. The BME layer was broken up by repeat pipetting, and all the content of the well was transferred to an Eppendorf. All wells containing the same conditions were pooled into the same Eppendorf. A second, equal volume of cell recovery solution was added to each well and pooled with the rest of the sample. The tubes were incubated on ice, in a 4°C cold room for 1 hour to solubilise the BME in the cell recovery solution. The miRNeasy Micro kit (Qiagen, 217084) was used following the manufacturer's manual. Samples were stored at -80°C until use.

2.6.1.2 From cell pellets

RNA samples from snap-frozen standard cell pellets and cell pellets isolated from the migration assays for 3′ UPX RNA Seq were extracted using the Machery-Nagel NucleoSpin RNA Plus kit (Machery-Nagel 740984.50) following the manufacturer's protocol. The RNA was eluted twice in the same 30 µl of RNAse free water, for a final volume of 30 µl. Samples were stored at -80°C until use.

2.6.2 Measuring RNA concentration and purity

2.6.2.1 RNA samples isolated from BME

RNA concentration and purity were assessed on a Nanodrop 2000C instrument. The desired 260/280 values should be ~2.0 and 260/230 values in a range between 2.0-2.2.

2.6.2.2 RNA samples from migration assays for 3′ UPX RNA-seq

The concentration and quality of a selection of RNA samples for 3′ UPX RNA Seq were assessed using the Agilent 2100 Bioanalyzer system. The Bioanalyzer RNA assays estimate the concentration of RNA in a sample and identifies degradation. The Bioanalyzer pico kit can detect mRNA 250-5000 pg/µl, while the nano kit can detect mRNA 25-250 ng/µl. Sample quality was defined by a measure of RNA degradation using the RNA integrity number (RIN) algorithm (Schroeder et al., 2006). A RIN number is between 1 and 10, where 10 is the highest possible RNA quality.

2.6.2.3 RNA samples from standard cell pellets for qRT-PCR analysis

RNA concentration was measured using the Qubit RNA broad range kit (Thermo Fisher Scientific Q10210) or Qubit high sensitivity kit (Thermo Fisher Scientific Q32852) in a Qubit 4® Fluorometer instrument. The broad range assay quantifies RNA concentrations within the 20-1000 ng/µl range, while the high sensitivity assay quantifies RNA concentrations 250 pg/µl to 100 ng/µl.

2.6.3 Analysing gene expression

2.6.3.1 cDNA synthesis

All sample preparation steps were performed on ice. 1 µg of RNA was first combined with a Random Primers and dNTPs mix (Table 2.3) and heated to 65°C for 5 minutes. Tubes were incubated on ice for 1 minute. Following this, the mix containing 5X First Strand, DTT, RNAseOUT recombinant ribonuclease inhibitor and SuperScript III Reverse Transcriptase was added. No reverse transcriptase controls (NRTs) were run in parallel, replacing SuperScript III RNAse-free H_2O.

Table 2.3 cDNA synthesis master mix.

Reagent	For 1 reaction (µl)
Random primers 250ng/µl (Invitrogen, 48190-011)	1
dNTPs 10mM (Bioline, BIO-39044)	1
5X First Strand Buffer (Invitrogen 18080093)	4
DTT 0.1M (Invitrogen 18080093)	1
RNaseOUT (Thermo Fisher Scientific 10777019)	1
SuperScript III Reverse Transcriptase (Invitrogen 18080093)	1

The samples were placed in a thermal cycler with the following programme:

- 5 minutes at 25 ºC
- 60 minutes at ºC
- 15 minutes at ºC

cDNA samples (50 ng/µl) were then diluted to 10 ng/µl in RNAse-free H_2O (Stratech PCR-258L-JEN) and stored at -80°C until use.

2.6.3.2 Primer design

Primer pairs for *SORCS2* were designed using NCBI Primer Blast (https://www.ncbi.nlm.nih.gov/tools/primer-blast/).

The following open access online tools were used to predict the formation of primer dimers and hairpin structures.

- Oligonucleotide Properties Calculator (http://biotools.nubic.northwestern.edu/OligoCalc.html)
- OligoAnalyzer (https://eu.idtdna.com/pages/tools/oligoanalyzer)

A standard PCR with temperature gradient was performed to verify the products of each primer set. This was visualised by agarose gel electrophoresis using the molecular weight marker Quick-Load® Purple 100bp DNA ladder (NEB N0551S).

The efficiency of the final primers was calculated through qRT-PCR of a dilution series of control RNA. D283-MED RNA was used following positive Western Blot protein expression.

Gene	Forward primer 5′ to 3′	Reverse primer 5′ to 3′
SORCS2	TGGTGCTGTTTGTCATCGGG	TGGTGCTGTTTGTCATCGGG
GAPDH	ATGTTCGTCATGGGTGTGAA	GTCTTCTGGGTGGCAGTGAT
HPRT	ATTATGCTGAGGATTTGGAAAGGG	GCCTCCCATCTCCTTCATCAC

2.6.3.3 qRT-PCR

qRT-PCR was performed using a Bio-Rad CFX384 Touch Real-Time PCR Detection System and the primers described above. All preparation steps were performed on ice.

Table 2.4 qPCR master mix.

Reagent	Volume per reaction (µl)
iQ™ SYBR® Green Supermix (Bio-Rad 1708884)	5
Forward primer (150 nM)	1.5
Reverse primer (15 0nM)	1.5
cDNA (10 ng/µl)	2

Non-template controls (NTCs) were run on 2 µl of RNAse-free H_2O and no reverse transcriptase controls (NRTs) on 2 µl of NRT mix. The plate was sealed and briefly centrifuged to pool reagents in the well before running the programme below.

- Initial denaturation step:3 minutes at 94 ºC
- Then 40x cycles of:

    - 30 seconds at 94ºC
    - 60 seconds at 60ºC
- Final extension step: 5 minutes at 72 ºC
- Primer melt curve

2.6.3.4 Gene expression analysis

Real-time PCR data was analysed using CFX Maestro™ software. ΔCt was calculated by subtracting the average housekeeping gene expression from the expression of the gene of interest. Gene expression was plotted as $2^{-\Delta Ct}$ using GraphPad Prism 8 software.

2.6.4 Protein extraction

NP-40 lysis buffer was prepared using the following method and stored at -20°C for up to 1 year.

- 150 mM sodium chloride
- 0.5% NP-40
- 50 mM Tris pH 7.4
- 1mM EDTA

Aliquots of lysis buffer were thawed for each protein extraction, and 10X cOmplete Mini EDTA-free protease inhibitor cocktail (Sigma 11836170001) was added fresh at a 1:10 ratio. The cell pellets were resuspended in 50-100 µl of lysis buffer and incubated for 30 minutes on ice, vortexing every 10 minutes. Next, the lysates were centrifuged at 14000 x *g* for 15 minutes in a pre-cooled 4ºC centrifuge.

2.6.5 Measuring protein concentration

Protein concentration was measured using a Bradford Assay. Bovine serum albumin (BSA) stock solution (100 µ/mL) was stored at -20°C and thawed for each experiment. A BSA dilution series was prepared (0-100 µ/mL) to derive a standard curve of protein concentration. Bradford reagent was diluted in H_2O at a 1:5 mL ratio and stored at 4ºC for up to 3 months. 50 µl of BSA standard or protein lysate was combined with 200 µl of Bradford solution and incubated in the dark at room

temperature for 5 minutes. The colorimetric assay read was perform on a FLUOstar Omega plate reader (BMG labtech) at OD_{595nm}.

2.6.6 Analysing protein expression

2.6.6.1 Protein sample preparation

In a fume cupboard, protein lysates of known concentrations were diluted to 1.5 µg/µl in lysis buffer and Laemmli sample buffer containing β-mercaptoethanol. Samples were used immediately or stored at -80°C until use.

2.6.6.2 SDS gel preparation

Separating gels were prepared according to the target protein size using. For SORCS2, 7.5- 8% gels cast in 1.5mm molds were used.

Table 2.5 Gel composition.

Reagent	7.5 – 8% separating gel	Stacking gel
1M Tris	pH 8.8, 3.9 mL	pH 6.8, 0.65 ml
H_2O	3.4 mL	3.58 mL
Acrylamide 30%	3.5 mL	0.67 mL
Sodium dodecyl sulfate (SDS) 10%	100 µl	50 µl
Ammonium Persulfate (APS) 10%	100 µl	50 µl
N,N,N′,N′-tetramethylethane-1,2-diamine (TEMED)	10 µl	5 µl

2.6.6.3 Gel electrophoresis

20 µl of protein was loaded into each well of the gel, 5 µl of Amersham™ ECL™ Rainbow™ Marker Full range (Sigma RPN800E) was run in parallel as a molecular weight marker, and all free wells were filled with sample buffer. Samples were run in a vertical electrophoresis tank (Bio-Rad) at 20 mA and maximum Volts through the stacking gel, then 40 mA and maximum Volts through the separating gel.

2.6.6.4 Transfer

The Amersham™ Hybond® Western blotting PVDF membrane (Scientific Lab Supplies 10600023) was activated for 30 seconds in methanol, 3 minutes in water, and 10 minutes in transfer buffer. The protein was transferred onto the membrane for 1 hour at 4ºC, maximum mA and 100 Volts. After transfer, the binding capacity of the membrane was increased by drying for 10 minutes, followed by a rehydration step in TBS-tween wash buffer.

2.6.6.5 Western blotting

Membranes were incubated in primary antibody overnight at 4ºC in 50 mL falcon tubes rolling continuously. The next day, the blots were washed 3x for 10 minutes in TBS-tween. The blots were incubated in secondary antibody for 1 hour at room temperature, rolling continuously. Following this, the blots were washed 3x for 10 minutes in TBS-tween.

Table 2.6 Primary antibodies used.

Protein	Species	Concentration	Development
SORCS2 (R&D Systems, AF4238)	sheep	1 µg/mL in milk	Signal fire ECL 3 minutes
GAPDH (Cell Signalling, CS2118)	rabbit	1:1,000 in BSA	Homemade ECL 2 minutes
β-TUBULIN (Cell Signalling, CS2128)	rabbit	1:1,000 in BSA	Homemade ECL 3 minutes

Table 2.7 Secondary antibodies used.

Antibody	Concentration
anti-sheep IgG HRP-conjugated (R&D Systems, HAF016)	1:1,000
anti-mouse IgG HRP-conjugated (Cell Signalling, CS7076)	1:2,000
anti-rabbit IgG HRP-conjugated (Cell Signalling, CS7074)	1:2,000

2.6.6.6 Western blot development

The blots were incubated with enhanced chemiluminescence (ECL) solution. Signalfire Elite (Cell Signalling 12757S) or a homemade ECL solution were used. Homemade ECL was made by combining equal-parts luminol solution and peroxide solution (see details in Table 2.8 and Table 2.9). The blots were imaged using a LAS 4000 mini Biomolecular imager (GE Healthcare) immediately after ECL incubation and digital images were saved.

Table 2.8 Luminol Solution

	Stock	Final concentration	For 50 mL
Tris/HCL pH 8.8	1M (10X)	100 mM	5 mL
Luminol	500 mM (200X)	2.5 mM	0.25 mL
4-IPBA	400 mM (100X)	4 mM	0.5 mL
H_2O			44.25 mL

Table 2.9 Peroxide Solution

	Stock	Final concentration	For 50 mL
Tris/HCL pH 8.8	1M (10X)	100 mM	5 mL
H_2O_2	30% (~9.88M)	10.6 mM	46.6 µl
H_2O			45 mL

2.6.6.7 Western blot quantification

Protein concentration was quantified by area measurements using imageJ image analysis software. This method compares the intensity of bands by creating histograms representing the brightness of the band. These are converted to numerical values by measuring the area of the curve in the histogram for each band. The values for the protein of interest are then normalized using values from their corresponding housekeeping protein band. Quantification was only performed on blots with more than 2 biological replicates, as specified in the figure legends.

2.7 Transfection of cells in standard culture

2.7.1 Transfection with GFP vector

Cells were transfected using the Mouse Neural Stem Cell Nucleofector™ Kit (Lonza VPG-1004) in a Nucleofector™ 2b device (Lonza AAB-1001). For transfection efficiency experiments, 0.5 x 10^5 or 1 x 10^6 cells were nucleofected with pmaxGFP® vector using programme A0-33 following the manufacturer's instructions. GFP transfected-cells were imaged on a fluorescent microscope (Nikon) at 24h, 48h, 72h and 96h post-nucleofection.

2.7.1.1 Transfection efficiency

Transfection efficiency was determined using the ImageJ plugin "cell counter" by counting the total number of cells in the brightfield image, followed by the total number of fluorescent cells, and calculating the proportion of fluorescent cells.

2.7.2 siRNA knockdown of gene expression

To achieve gene knockdown of *SORCS2*, ON-TARGET Plus SMARTpool siRNA for *SORCS2* 5nMol (Dharmacon L-013162-00-0005) or ON-TARGET Plus Non-targeting Pool 5nMol (Dharmacon D-001810-10-05) were nucleofected into 1 x 10^6 cells using the method described in section 2.7.1.

Immediately after nucleofection, cells were allowed to settle for at least 5 hours before the medium was replaced with reduced serum (2% FBS) overnight. At 24 hours post-nucleofection, the cells were used to seed 1) a migration assay, 2) a parallel viability assay. In addition, some nucleofected cells were cultured in a 6-well plate for cell pellet collection.

A cell viability measurement (see section 2.4) and a cell pellet for molecular analysis (see section 2.1.2.4) were taken every 24 hours. The migration assay was performed as described in Section 2.5.

2.7.2.1 Transfection efficiency

Transfection efficiency was determined by quantifying the expression of the knocked down gene using qRT-PCR (see section 2.6.3).

- First, ∆ct was calculated by subtracting the mean expression of the housekeeping gene from the mean expression of the gene of interest.
- ∆∆Ct was then determined using the formula:
  (∆ct non-transfected control) – (∆ct knocked down gene)
- $2^{-(\Delta\Delta Ct)}$ was calculated.
- Finally, (1-∆∆Ct) x 100 was calculated to determine % knockdown.

2.8 Patient tissue IHC

2.8.1 Patient TMAs

Protein immunohistochemistry (IHC) was used to detect SORCS2 protein expression in patient tissue microarrays (TMAs). The TMAs represented patients treated at Birmingham and Nottingham University Hospitals between 1985 and 2012. Clinical details of patients included in tissue microarrays (TMA) obtained from the Children's Brain Tumour Research Centre (CBTRC) were previously published by several studies (Dubuc et al., 2013, Othman et al., 2014, Yao et al., 2020). The study and the experimental protocols required, were reviewed and approved by the National Research Ethics Service Committee East Midlands – Nottingham 2 and the Ethics Committee of the Burdenko Neurosurgical Institute (Ethical vote number 563/6-16). The study was in accordance with the ethical standards laid down in an appropriate version of the 1975 Declaration of Helsinki, as revised in 1983. For all patients, informed consent was obtained from the patient, or a parent and/or legal guardian where the patient was under 18 years of age, prior to their inclusion in the study.

4 TMAs from Birmingham cohorts were stained:

- MRS-MB-1b

- MRS-MB-2b
- MRS-MB-3b
- MRS-MB-4b

2 TMAs from Nottingham cohorts were stained:

- 11-07ME1b
- 11-07ME2b

2.8.2 IHC

2.8.2.1 Preparation and rehydration

Slides were baked in an oven overnight to melt the wax. Slides were deparaffinised in xylene for 15 minutes, followed by rehydration in a series of ethanol baths (100%, 95% 80%, 70%). Slides were briefly rinsed in running tap water.

2.8.2.2 Antigen Retrieval

Heat induced antigen retrieval was performed by immersing the slides in sodium citrate buffer (Table 2.10) in a steamer for 40 minutes. Slides were briefly rinsed in PBS. The slides were then placed in a humidified chamber and the tissue sections were circled with a hydrophobic pen.

Table 2.10 Sodium citrate buffer composition.

Reagent	For 1 L
Citric acid monohydrate	2.1 g
Sodium hydroxide (pH 6.0)	~13 mL
Tween 20	0.5 mL
Distilled H_2O	Up to 1 L

2.8.2.3 Peroxidase quenching and blocking

Endogenous peroxidase activity suppression was performed using peroxidase suppressor (Thermo Fisher Scientific 35000) for 30 minutes. Slides were washed in

PBS, then blocked with Universal Blocker™ blocking buffer (Thermo Fisher Scientific 1859332) for 30 minutes.

2.8.2.4 Antibody incubation

Primary antibody diluted in blocking buffer was then incubated on the slides overnight. The positive control tissue slides were also incubated with primary antibody, while negative control slides were incubated with blocking buffer only.

Table 2.11 Primary antibodies used.

Primary Antibody	Species	Dilution	Positive control
SORCS2 (Novus Biologicals, NBP2-56711)	Rabbit	15 µg/ml	Hippocampus

The next day, slides were washed in PBS, then incubated in biotinylated secondary antibody for 1 hour. The slides were washed in PBS.

Table 2.12 Secondary antibodies used.

Secondary Antibody	Dilution
Goat anti rabbit Biotin Conjugate (Thermo Fisher Scientific, 65-6140)	1:500

The Ultra-sensitive avidin and biotynilated HRP (ABC) peroxidase staining kit (Thermo Fisher Scientific, 32020) was used to amplify the signal from biotinylated secondary antibody. Avidin was combined with Biotinylated HRP 30 minutes before use following the manufacturer's instructions. The ABC reagent was then applied to the slides and incubated for 30 minutes. Slides were washed in PBS.

2.8.2.5 Antibody detection

Antibody detection was performed using diaminobenzidine (DAB) Substrate Kit (Cell Signalling, 8059) following the manufacturer's instructions. SignalStain® DAB chromogen concentrate was diluted in SignalStain® DAB diluent and incubated on the slides for 10-15 minutes. Slides were washed in PBS and briefly rinsed in water. Harris Modified Haematoxylin (Thermo Fisher Scientific 1859352) was added to the slides for 1-5 minutes and then washed in water. Slides were dehydrated in ethanol

(95% then 100%) followed by xylene. Mounting medium and a coverslip were applied and set at room temperature.

2.8.3 TMA imaging and scoring

Whole slides were imaged by the Nottingham University Hospitals Trust Imaging Unit at the Queen's Medical Centre on a Nanozoomer instrument (Hamatsu) at x40 magnification. The cores were independently scored by two blinded observers without knowledge of the clinical information associated with each tumour core. The SORCS2 expression score was averaged for each core, and then for each patient tumour. The protein expression scores and patient data were analysed using IBM SPSS® Statistics.

2.9 Next Generation Sequencing: 3′ UPX RNA-seq

RNA was extracted from these three cell compartments as described above and sent to Qiagen for quality control and sequencing.

2.9.1.1 Library preparation

The library preparation was done using the QIAseq UPX 3′ Transcriptome kit (QIAGEN, 333088) at QIAGEN in Hilden, Germany. During library preparation, each RNA molecule is tagged with a unique molecular index (UMI) barcode. After cDNA synthesis and amplification, quality control was performed to determine sample concentration and purity on a TapeStation 4200 (Agilent) or Bioanalyzer system (Agilent) and the libraries were pooled then quantified by qPCR. The library pools were sequenced on a NextSeq500 instrument, producing raw data. Raw data was de-multiplexed and FASTQ files were generated for each sample using bcl2fastq software (Illumina).

2.9.1.2 Primary sequence analysis

Raw data analysis was performed by bioinformaticians at QIAGEN. First, the raw sequencing data FASTQ files were uploaded to the QIAGEN GeneGlobe bioinformatics tool (https://geneglobe.qiagen.com/gb/). Cells were de-multiplexed using the unique cell IDs. The 3′ poly-A region was then trimmed off and reads were aligned to the human reference genome GRCh38 (RefSeq accession number GCF_000001405.39) using STAR splice aware aligner (Dobin et al., 2013).

The aligned reads were annotated to gene regions, and the UMIs were counted for each gene. External RNA Controls Consortium (ERCC) spike-ins were used as a standard.

2.9.1.3 Differential gene expression analysis

R package DESeq2 (Love et al., 2014) software was used for differential analysis of UMI count data.

The input is count data as a table which reports, for each sample, the number of MTs that have been assigned to each gene. The differential expression analysis in DESeq2 uses a generalized linear model of the form:

$$K_{ij} \sim NB(\mu_{ij}, a_i)$$

$$\mu_{ij} = s_j q_{ij}$$

$$log_2(q_{ij}) = x_j . \beta_i$$

In this model, counts K_{ij} for gene i, sample j are modelled using a negative binomial distribution with fitted mean μ_{ij}, and a gene-specific dispersion parameter a_i. The fitted mean is composed of a sample-specific size factor s_j and a parameter q_{ij} proportional to the expected true concentration of fragments for sample j. The coefficients β_i give the log_2 fold changes for gene i for each column of the model

matrix X. The model can be generalised to use sample- and gene-dependent normalization factors s_{ij}.

The dispersion parameter a_i defines how far we expect the observed count will be from the mean value, which depends both on the size factor s_j and the covariate-dependent part q_{ij} as defined above.

$$Var(K_{ij}) = E[(K_{ij} - \mu_{ij})^2] = \mu_{ij} + a_i\mu_{ij}^2$$

DESeq2 creates an artificial reference sample by taking the geometric means of counts from all genes, and calculates a ratio of the raw counts to their respective geometric means. After this, the software calculates a normalization factor which is the median of all ratios per samples, and the raw counts are divided by the corresponding normalization factor of that sample.

Principal components analysis

Principal Component Analysis (PCA) is a method used in unsupervised analysis to reduce the dimension of large data sets. The PCA was performed on all samples using the DESeq2 transformed counts (using variance stabilizing transformation) of all genes.

Heatmap and unsupervised clustering

The measure of distance quantifies dissimilarity between sample data for numerical computation. Euclidean distance was used as a distance metric, this is the square root of sum of attribute differences. Euclidean distance is:

$$\sqrt{(\mathbf{x1} - \mathbf{x2})2 + (\mathbf{y1} - \mathbf{y2})2}$$

where the first point is (x1,y1)(x1,y1) and the second point is (x2,y2).

Complete linkage was used for hierarchical clustering, this defines the cluster distance between two clusters to be the maximum distance between their individual components.

Volcano plots

The plot is constructed by plotting -log10(p-value) on the y-axis, and the log2 of the expression fold change between the two experimental groups on the x-axis.

2.10 Gene Ontology analysis

Gene Ontology (GO) was performed using Gene Set Enrichment Analysis (https://www.gsea-msigdb.org/gsea/index.jsp) (Subramanian et al., 2005, Mootha et al., 2003). This publicly-available software from the University of California San Diego and the Broad Institute (software.broadinstitute.org/gsea) determined whether gene lists identified through differential gene expression analysis overlap with gene sets on a Molecular Signatures Database (MSigDB). Gene sets used in this project include Gene Ontology “biological processes” and “molecular function” gene sets (Consortium, 2019, Ashburner et al., 2000). Significance of the overlap with the GO gene sets was calculated using an uncorrected p-value and a Benjamini-Hochberg False Discovery Rate adjusted p-value (FDR q-value) to correct for multiple testing.

2.11 Identifying patterns of gene expression

The results of differential expression analysis were filtered using the log2 fold change threshold of ≥+/-1, the p-value <0.05, and the mean normalized count >10. Gene lists were filtered in Microsoft® Excel® by using the “Sort & Filter” option and ranking genes from smallest to largest. Genes were first ranked based on the log2 fold change, then by p-value, and finally by mean of normalized count. Genes were then classed as either upregulated, downregulated or unchanged.

The lists of genes produced as described were input into the Gene List Venn Diagram online tool (http://genevenn.sourceforge.net/), and Venn Diagrams were

generated showing the number and lists of genes overlapping between 3 categories. This was done to compare the 3 cell lines, as well as the 3 migration compartments within each cell line. By looking at different combinations of lists, different patterns of expression were defined.

2.12 Patient dataset analysis

The expression of genes in medulloblastoma patients was assessed by analysis of a large medulloblastoma patient dataset (Cavalli et al., 2017) using the R2 Genomics Analysis and Visualization Platform (r2platform.com).

First, the “View a Gene” function was used in a single dataset to analyse the expression of one gene at a time in all samples of the selected dataset. Each sample is annotated with clinical data, which can be grouped to form a “track” to filter the data. Gene expression was transformed to log2 and separated into tracks based on “subgroup” or “met status” (metastatic status). Expression for each sample in the dataset was obtained by viewing the “data table” and input into GraphPad Prism 8 to create boxplots.

The KaplanScan feature was used to generate Kaplan Meier survival curves using the Cavalli *et al.,* dataset. This finds the most significant gene expression cut-off point through a logrank test in order to separate patients into 2 groups (high and low expression).

The Principal Component Analysis (PCA) Meta Analysis feature was used to generate PCA plots using the Cavalli *et al.,* dataset.

2.13 Figures and statistical analysis

All graphs were generated and statistical tests performed using GraphPad Prism 8 software (https://www.graphpad.com/scientific-software/prism/). Significant differences were calculated using one-way ANOVA with Tukey’s multiple comparisons or an unpaired t-test using SEM, as specified in each figure legend.

Chapter 3 Developing an *in vitro* model of the brain-CSF interface to capture migrating cells

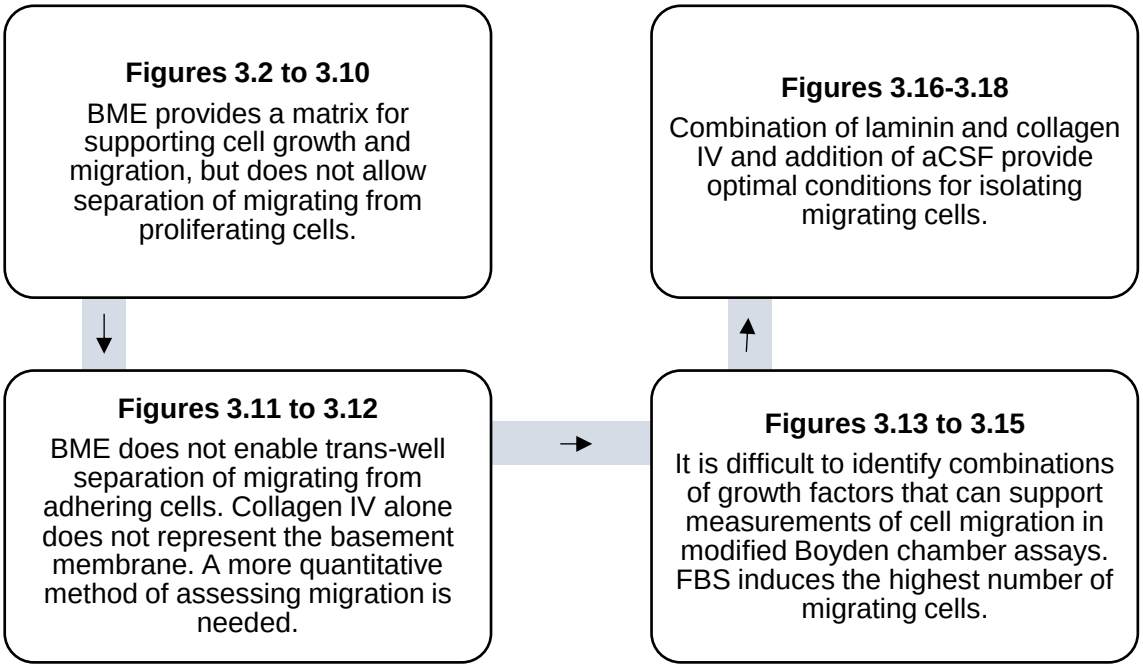
3.1 Introduction

Aim 1: Develop an *in vitro* model representing the interface between the brain and the CSF for capture and molecular analysis of migrating cells.

The standard 2-dimensional (2D) cell culture approach does not take into account the 3-dimensional (3D) environment of tumours, and is therefore not a representative model when trying to mimic biological events. Cell architecture, as well as the stroma and the essential extracellular matrix (ECM), contribute to a cell's ability to migrate. While these characteristics are not represented in standard 2D culture, they can be restored by growing cells in 3D within or on top of ECM components they would normally encounter in the brain. In order to model migration, this project aims to mimic the important aspects of the interface between the brain and the cerebrospinal fluid (CSF) circulating in the leptomeninges, one of the possible paths of dissemination and metastasis for medulloblastoma (O'Meara et al., 2007).

The basement membrane is a specialized extracellular matrix lamina that provides structural support and functional cues to nearby cells. The main components of the basement membrane are type IV collagens, laminins, nidogens and HSPGs (Rowe and Weiss, 2008). The formation of the basement membrane occurs through self-assembly of supramolecular networks (Pozzi et al., 2017). Cells will cross the basement membrane through the course of normal development, in response to inflammation and during immune surveillance, as well as during neoplastic processes such as cancer metastasis. As the cerebellum has a corrugated architecture, the tumour may cross the basement membrane one or more times as it extends towards the meninges in order to disseminate in the CSF. Cells capable of migrating through a basement membrane barrier likely have advantages provided by transcriptional changes as they migrate.

This chapter describes the optimisation experiments performed in order to develop an *in vitro* model that induced cell migration and allowed the collection of migrating cells for further molecular analysis. The key conclusions from each stage of optimisation are summarised in the Overview Figure.



Overview Figure. Conclusions from the optimisation experiments detailed in this chapter are summarised in four key steps, and the corresponding figures are listed.

3.2 Optimising growth and migration conditions for a range of cell lines in BME

The cell lines selected for this project represent the medulloblastoma subgroups Group 3 and Group 4, and within the subgroups, cells of metastatic or primary tumour origins. Each cell line has different growth characteristics under their normal growth conditions in 2D standard culture. The clinical information from the patient of origin as well as cell line details with references are summarised in Table 3.1.

- The cell line D283-MED has been classed as both Group 3 and Group 4 by different methods, and was isolated from metastases in the ascetic fluid. D283-MED cells grow as single cells adherently or in suspension, and when grown to confluence can form small clusters containing a few cells that grow either in suspension or semi-adherently (Figure 3.1 A).
- The cell line HD-MB03 is classed as Group 3, and was isolated from the primary tumour of a patient with metastatic medulloblastoma (Table 3.1). HD-MB03 cells grow as adherent monolayers, and when grown to confluence can have single cells or small cell clusters growing in suspension or semi-adherently (Figure 3.1 B).
- The cell line D458-MED is classed as Group 3, and was isolated from metastatic cells in the patient's CSF and grows as a semi-adherent monolayer with some cells in suspension (Figure 3.1 C). It has a matched pair cell line, D425-MED, isolated from the same patient's primary tumour, although this cell line was not available in our laboratories at the time this project was undertaken.
- Two Group 4 cell lines were used in this project, the matched pair CHLA-01-MED and CHLA-01R-MED, isolated from a primary tumour and a malignant pleural effusion of the same patient respectively (Table 3.1). CHLA-01-MED cells grow as large clusters in suspension, and some single cells in suspension. The clusters are of uneven shapes and sizes with rough edges (Figure 3.1 D). CHLA-01R-MED cells grow in more compact, spherical

clusters and have fewer single cells in suspension when compared to CHLA-01-MED (Figure 3.1 E).

Table 3.1 Medulloblastoma cell lines used in this project.

Three cell lines classed as Group 3 and two cell lines classed as Group 4 were used at different stages of this project.

*These cell lines have a matched primary a metastatic pair from the same patient.

Cell line	Clinical information	Subgroup	Origin	Behaviour in standard culture	Reference
D283-MED	3 year old male with a mass in the vermis, peritoneal metastasis and malignant ascites (M2).	Group 3 by Gene Set Enrichment Analysis (Sengupta et al., 2014) Group 4 by IHC (Snuderl et al., 2013)	Ascetic fluid and tissue from laparotomy	Semi-adherent	Friedman et al., 1985
HD-MB03	3 year old male with a large cell anaplastic mass in midline, spinal metastasis and CTCs in CSF (M3).	Group 3 by IHC and gene expression profiling (Milde et al., 2012)	Primary tumour	Semi-adherent	Milde et al., 2012
D458-MED	6 year old male with a mass in the posterior fossa, and tumour cells in the CSF 6 months after diagnosis (M+).	Group 3 by gene expression profiling (Weeraratne et al., 2012)	Metastatic cells from CSF	Semi-adherent	He et al., 1991
CHLA-01-MED*	8 year old male with a mass in posterior fossa and diffuse leptomeningeal disease (M3).	Group 4 by TaqMan Low Density Array (Xu et al., 2015)	Primary tumour	Suspension	Xu et al., 2015
CHLA-01R-MED*	8 year old male with symptomatic malignant pleural and peritoneal effusions.	Group 4	Malignant pleural effusion in the lungs	Suspension	Xu et al., 2015

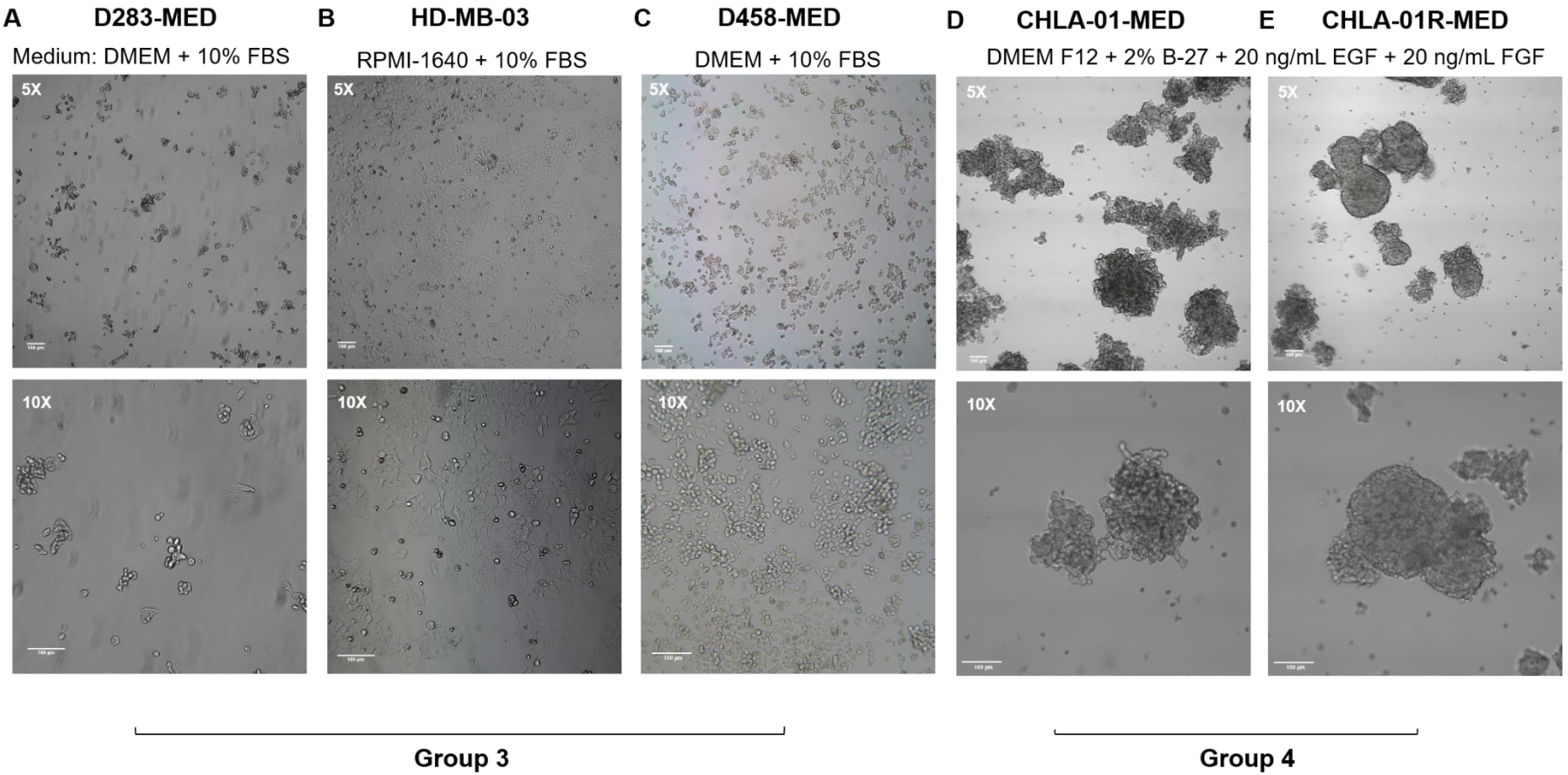


Figure 3.1 Medulloblastoma cell lines in standard culture.

Brightfield images at 5X (top row) and 10X (bottom row) magnification of Group 3 (D283-MED, HD-MB03, and D458-MED) and Group 4 (CHLA-01-MED and CHLA-01R-MED) cell lines cultured to confluence in standard culture medium (scale bar 100µm). A) The D283-MED cell line was cultured in DMEM medium supplemented with 10% FBS. Cells grew as single cells adherently or in suspension, with small clusters containing a few cells that grew either in suspension or semi-adherently. B) The HD-MB03 cell line was cultured in RPMI-1640 medium supplemented with 10% FBS. Cells grew as an adherent monolayer, and had single cells or small cell clusters growing in suspension or semi-adherently. C) The D458-MED cell line was cultured in DMEM medium supplemented with 10% FBS. Cells grew as a semi-adherent monolayer with some cells in suspension. D) and E) The CHLA-01-MED and CHLA-01R-MED cell lines were cultured in DMEM F12 medium supplemented with 2% B-27, 20 ng/mL EGF and 20 ng/mL FGF. CHLA-01-MED cells grew as large clusters of uneven shapes and sizes with rough edges in suspension, and CHLA-01R-MED cells grew as compact, spherical clusters.

3.2.1 Optimising matrix concentration

This project first hypothesized that BME could be used to recapitulate some of the complex architecture and extracellular factors that can influence tumour cells to migrate. BME is a soluble form of basement membrane purified from Engelbreth-Holm-Swarm (EHS) tumours, which occur in the mouse yolk sac. The main components in BME are laminin, collagen IV, and the HSPGs perlecan and entactin, and also contains growth factors. BME has been used to culture cancer cells and assess their migratory and invasive potentials across many cancers including breast cancer (Tang et al., 2019, Lim et al., 2016a) and Glioblastoma (Wang et al., 2019, Sun et al., 2015).

The concentration to which the matrix is diluted affects the amounts of each component, although the exact concentration of each is not known. The manufacturer recommends concentrations below 9 mg/mL for non-gelling culture conditions and above 9 mg/mL for gelling culture conditions. The non-gelling concentration of 2.25 mg/mL and has been used in published studies to support growth of different cancer types (Onion et al., 2016, Saunders et al., 2017). A 3D culture model where medulloblastoma cells were encapsulated in BME at a concentration of 2.25 mg/mL has been previously optimised in our lab by Aishah Nasir (A. Nasir., 2016). This previous work reported differences in migration between low risk cell lines and metastatic medulloblastoma cell lines in our lab (A. Nasir, unpublished data). With the aim of adapting this culture model for the cell lines HD-MB03, CHLA-01-MED and CHLA-01R-MED, the first step taken was to further optimise the culture conditions to allow maintained cell viability and observe for signs of cell migration.

The Group 4 cell lines CHLA-01-MED and CHLA-01R-MED grow in suspension in standard culture, forming 3D structures without the presence of surrounding ECM (Figure 3.1 D and E). It was hypothesized that seeding these cell clusters in BME would provide cells with the necessary support and signals to migrate. In order to assess the effect of different BME concentrations on MB cell survival, MB long-term culture viability and cell cluster growth were compared between 2.25 mg/ml and 10

mg/ml BME concentrations. The cultures were set up as described in section 2.2.2, and the cells were fed by replacing the culture medium on top of the BME gel every 2-3 days.

Both cell lines remained viable for 8 days regardless of BME concentration, and showed phenotypic changes that differed from their 2D phenotypes (see Figure 3.1 E compared to Figure 3.2 A, and Figure 3.1 D compared to Figure 3.3 A). In the high-gelling concentration, the CHLA-01R-MED clusters (Figure 3.2 A Day 1 red arrows) lost their smooth edges with the cells around the edges of large clusters becoming elongated, and more mesenchymal-like in terms of cell shape (Figure 3.2 A Day 3 red arrows). Some cell clusters grew and merged, and some clusters dissociated after over 2 weeks in culture (Figure 3.2 A Day 17 blue arrow). In the low gelling concentrations, cell clusters dissociated into a monolayer after 3 or 4 days (Figure 3.2 B yellow arrows and Figure 3.4 C). This may be due to cell clusters sinking to the bottom of the well when seeded in a non-gelling matrix, and forming an adherent monolayer at the bottom of the well. There were some phenotypic changes noticeable in CHLA-01-MED cell clusters in BME as well, but to a lower extent.

Metabolic activity was assayed as a measure of cell viability on the same days the images were taken. In BME, CHLA-01R-MED metabolic activity increased in the first 8 days before steadily dropping off until the end of the experiment at day 22 (Figure 3.4 A). The metabolic activity increased in the CHLA-01-MED cell line for the first 8 days before decreasing, but this decrease was slower than CHLA-01R-MED cells (Figure 3.5 A). In the high gelling concentration, it was possible to follow the same cell cluster for the duration of the experiment (Figure 3.3 A red arrows and Figure 3.5 B), although clusters appeared to dissociate after 1 week (Figure 3.3 A blue arrows, Figure 3.5 B red symbols). However, in the non-gelling concentration, clusters dissociated and grew as a monolayer from day 4 (Figure 3.3 B yellow arrow), losing their initial cluster structure and could therefore not be measured after dissociating (Figure 3.5 C).

These long-term culture experiments in BME revealed that some clusters can either grow at a slow, steady rate, while others grow fast over 1 week. Some clusters begin to dissociate after 1 week in culture, and cannot be monitored for longer periods. This is especially true for cells grown in 2.25mg/mL where clusters appear to dissociate into adherent monolayers

In summary, a gelling condition of 10 mg/mL where cells do not dissociate into a monolayer on the bottom of the well was determined to be better suited to the observation of cell phenotypes in the matrix. This decision was made after 2 biological replicates for each cell line.

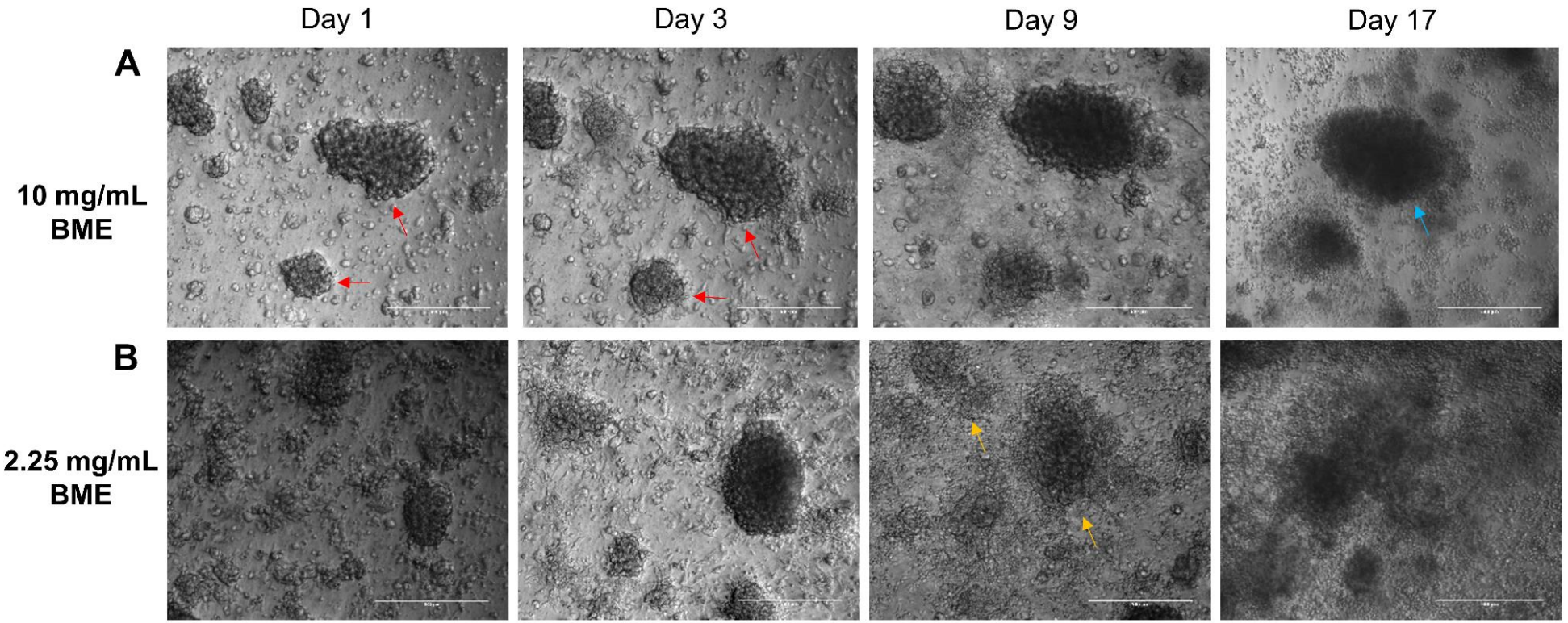


Figure 3.2 BME supports short-term growth of CHLA-01R-MED.

A) Group 4 cell line CHLA-01R-MED cells were cultured in BME at a high-gelling (10 mg/mL) or **B)** low-gelling (2.25 mg/mL) concentration and observed for 17 days (scale bar=500µm). The culture medium on top of the BME was replaced every 2-3 days. Red arrows indicate cell clusters, blue arrows indicate dissociating cell clusters, and yellow arrows indicate monolayers. Cells were imaged using a Nikon Eclipse Ti inverted microscope, on the Widefield setting (n=2).

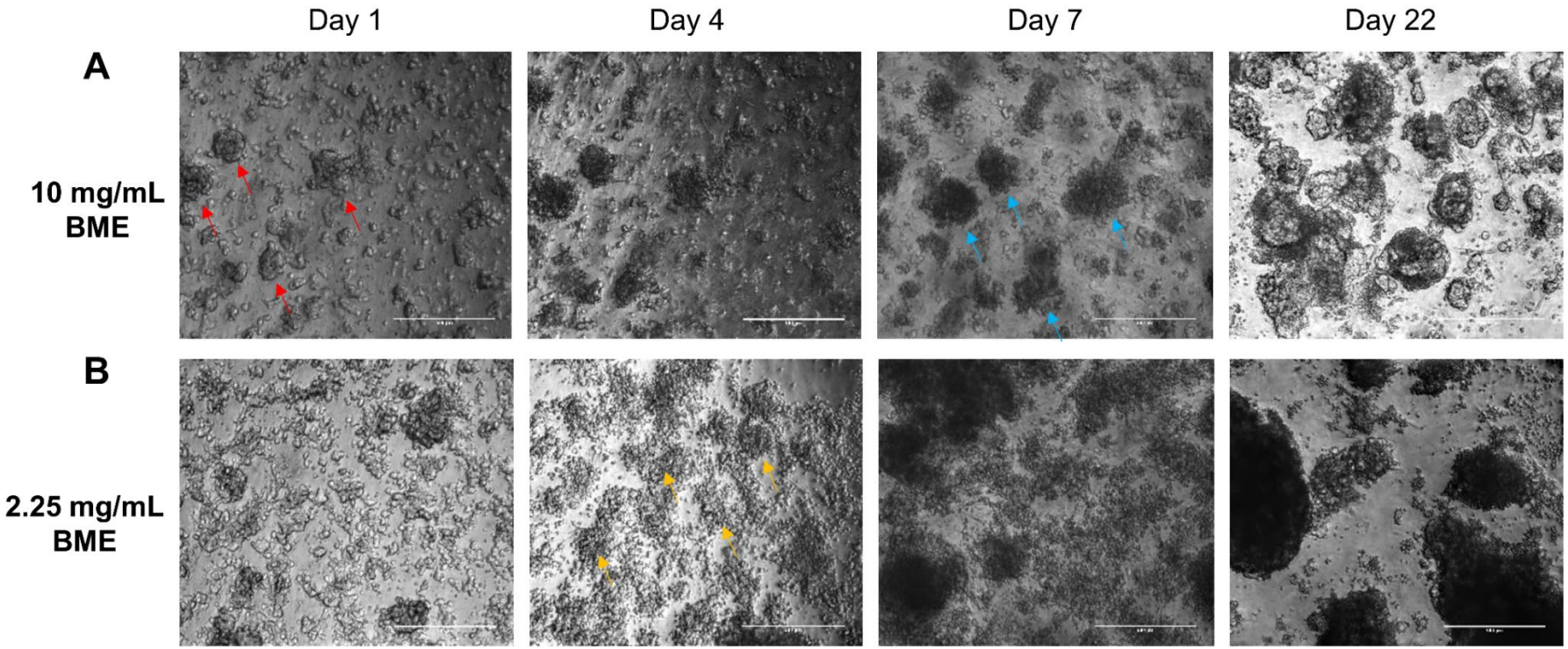


Figure 3.3 BME supports short-term growth of CHLA-01-MED.

A) CHLA-01-MED cells were cultured in BME at high-gelling (10 mg/mL) concentration and observed for 22 days (scale bar=500μm). The culture medium on top of the BME was replaced every 2-3 days. **B)** CHLA-01-MED cells were cultured in BME at a non-gelling (2.25 mg/mL) concentration. Red arrows indicate cell clusters, blue arrows indicate dissociating cell clusters, and yellow arrows indicate monolayers. Cells were imaged using a Nikon Eclipse Ti inverted microscope, on the Widefield setting (n=2).

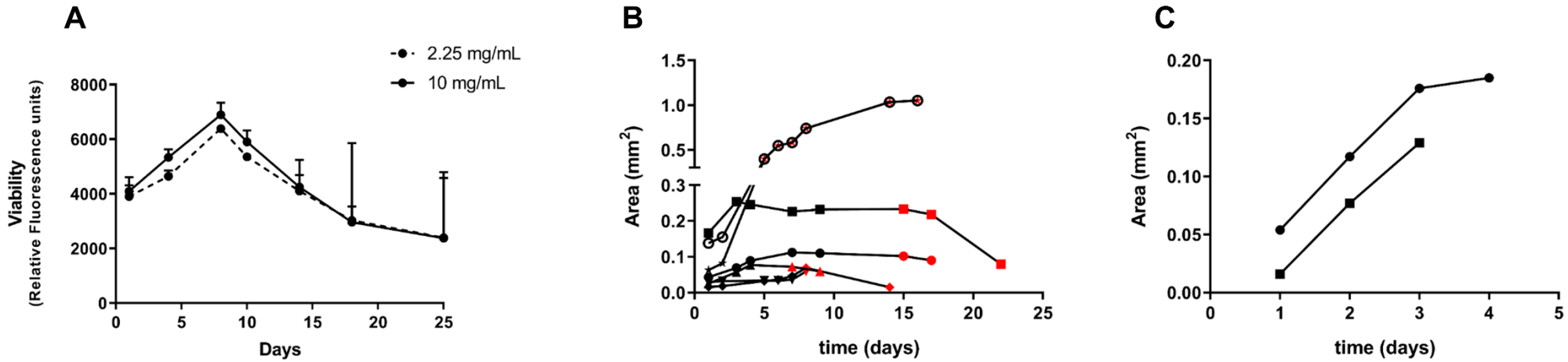


Figure 3.4 BME supports short-term growth of CHLA-01R-MED.

A) The metabolic activity of the cells was assayed by replacing the medium on top of the BME with PrestoBlue cell viability reagent diluted 1:10 in culture medium (see section 2.4 for details). **B)** The area of cell clusters in the 10 mg/mL BME condition was measured to determine cell cluster growth in 10mg/ml BME. Each symbol shape represents a separate cell cluster. The red symbols indicate time points where the clusters started to disintegrate and fall apart. Exemplary growth of 7 clusters has been measured (n=2 with at least 3 measured clusters per image). **C)** The area of cell clusters in the 2.25 mg/mL BME condition was measured to determine cell cluster growth in 10mg/ml BME. Each symbol shape represents a separate cell cluster. 2 clusters were measured (n=1).

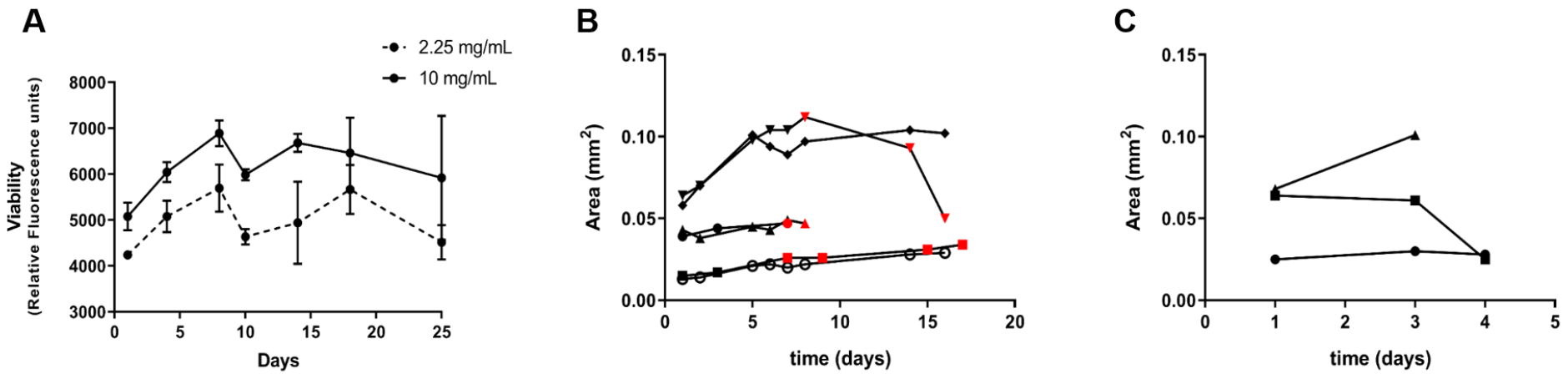


Figure 3.5 BME supports short-term growth of CHLA-01-MED.

A)) The metabolic activity of the cells was assayed by replacing the medium on top of the BME with PrestoBlue cell viability reagent diluted 1:10 in culture medium (see section 2.4 for details). **B** The area of cell clusters in the 10 mg/mL BME condition was measured to determine cell cluster growth. Each symbol shape represents a separate cell cluster. The red symbols indicate time points where the clusters started to disintegrate and fall apart. Exemplary growth of 6 clusters/nodules has been measured (n=2 with at least 2 measured clusters per image). **C)** The area of cell clusters in the 2.25 mg/mL BME condition was measured to determine cell cluster growth. Each symbol shape represents a separate cell cluster. Growth of 3 clusters was measured (n=1).

3.2.2 Optimising culture medium

The culture medium used may contribute to cell viability as well as the phenotypic and migratory differences of the same cell line cultured in 2D or in 3D. It is also important to keep the culture conditions consistent in order to analyse the RNA expression in different cell lines downstream, as expression may be changed by variations in growth factors in the medium. The Group 4 cell lines CHLA-01-MED and CHLA-01R-MED are standardly cultured in medium supplemented with B27, EGF and bFGF, while the Group 3 cell lines D283-MED, D458-MED and HD-MB03 are grown in medium supplemented with FBS. In order to select one medium condition for 3D culture, cell phenotype and viability were assess when cultured with different supplements. Each medium tested was used to dilute the BME to 10 mg/mL, and added on top of the gel in each well.

When cultured in BME, D458-MED cells did not grow into clusters regardless of whether FBS or B27 and growth factors were present, and cells did not appear viable in either condition after Day 1 (Figure 3.6 A and B). In medium supplemented with B27 and growth factors, metabolic activity measurements remained stable until day 10, while in medium with FBS, cell viability decreased after day 1 (Figure 3.6 C). The metabolic activity measurements of cells in medium supplemented with B27 and growth factors does not match the images taken on the same days, where cells do not appear viable on days 3 or 10. However as this experiment was only performed once, no conclusions can be drawn.

The cell lines HD-MB03 and D283-MED formed densely packed, spherical aggregates with smooth edges or remained as single cells (Figure 3.7 A and B and Figure 3.8 A and B). D283-MED cells remained viable for up to 4 days in both mediums. Viability then decreased in medium with FBS and remained more stable until day 8 in medium with B27 and growth factors (Figure 3.7 C). However, these cells only formed spherical aggregates in DMEM F12 supplemented with growth factors. HD-MB03 viability increased for 4 days then remained stable until day 8 in medium with B27 and growth factors, however cell viability decreased in medium with

FBS after day 4 (Figure 3.8 C). HD-MB03 cells formed spherical aggregates in both medium types. The HD-MB03 cell line formed spherical cell aggregates from day 1, while D283 MED aggregates appeared from day 3. It could not be concluded whether the spherical aggregates seen were formed mainly from migration, proliferation, or a combination of both from this experiment alone. In order to determine the mechanism by which clusters form, the cells in BME would have to be imaged continuously. Individual clusters could not be recognized in the sequential images, and it was therefore not possible to measure cluster growth over time.

Taking into account the observation of cell images and the metabolic activity in the culture medium conditions described above, DMEM F12 supplemented with B-27 supplement, EGF and bFGF appeared to maintain cell viability and the appearance of cell clusters in the Group 4 and Group 3 cell lines cultured in BME, except D458-MED. However, as these results only represent 1 replicate for Group 3 cell lines, no conclusions can be drawn. The concentration of each soluble factor (EGF, FGF B27 or FBS) recommended for standard culture was used in the experiments presented, but no other concentrations were tested. Dose response curves or step down changes in media were not performed.

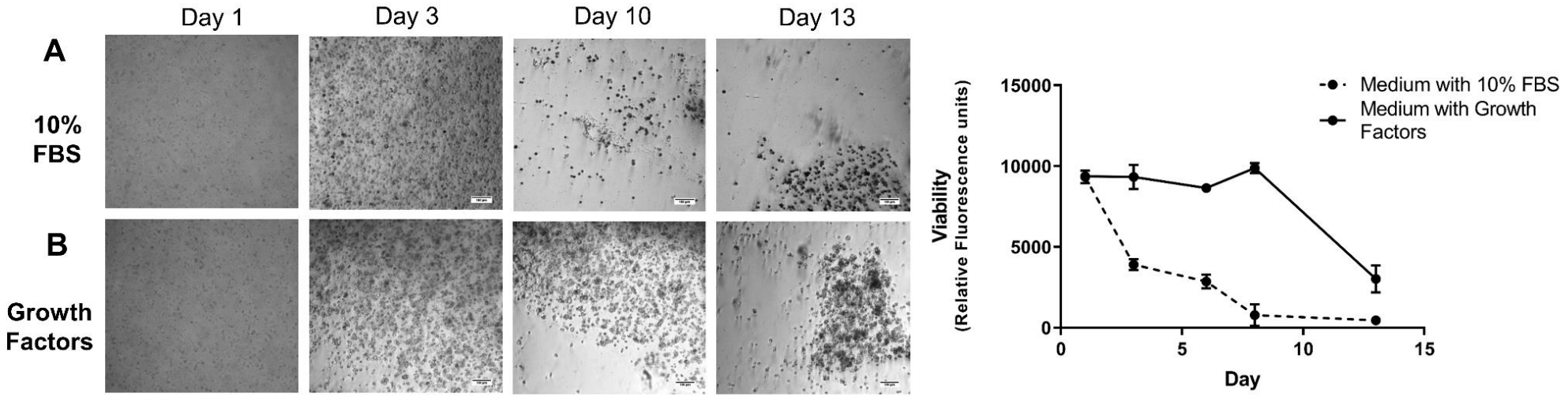


Figure 3.6 BME does not support short-term growth of Group 3 cell line D458-MED.

A) Group 3 cell line D458-MED cells were cultured in BME at a high-gelling concentration (10 mg/mL) in medium containing 10% FBS and observed for 13 days (scale bar=100µm). The medium was replaced every 2-3 days. **B)** Group 3 cell line D458-MED cells were cultured in BME at a high-gelling (10 mg/mL) in medium with 2% B-27, 20 ng/mL FGF and 20 ng/mL EGF. **C)** The metabolic activity of the cells was assayed on the same day as images were taken using PrestoBlue cell viability reagent for the duration of the experiment. n=1

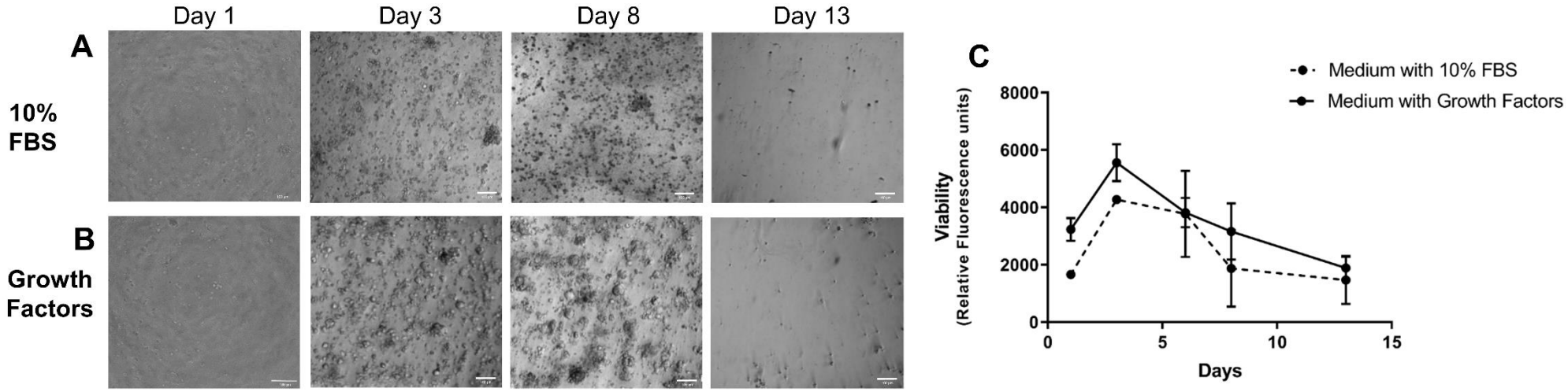


Figure 3.7 BME supports short-term growth of Group 3 cell line D283-MED with added growth factors.

A) cells were cultured in BME at a high-gelling concentration (10 mg/mL) in medium containing 10% FBS and observed for 13 days (scale bar=100µm). The medium was replaced every 2-3 days. **B)** Group 3 cell line D283-MED cells were cultured in BME at a high-gelling (10 mg/mL) in medium with 2% B-27, 20 ng/mL FGF and 20 ng/mL EGF. **C)** The metabolic activity of the cells was assayed on the same day as images were taken using PrestoBlue cell viability reagent for the duration of the experiment. n=1

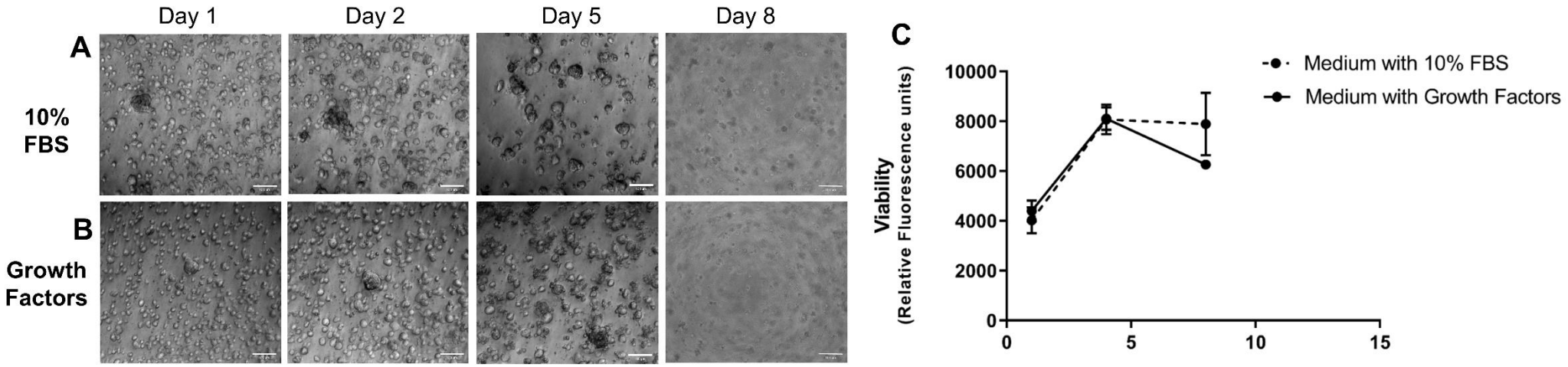


Figure 3.8 BME supports short-term growth of Group 3 cell line HD-MB03 with or without added growth factors.

A) Group 3 cell line HD-MB03 cells were cultured in BME at a high-gelling concentration (10 mg/mL) in medium with 10% FBS and observed for 8 days (scale bar=100µm). **B)** Group 3 cell line D283-MED cells were cultured in BME at a high-gelling (10 mg/mL) in medium with 2% B-27, 20 ng/mL FGF and 20 ng/mL EGF. Images on day 8 were taken on a microscope with less definition, clusters are therefore less visible, but still present. **C)** The metabolic activity of the cells was assayed on the same day as images were taken using PrestoBlue cell viability reagent for the duration of the experiment. n=1

3.2.3 Observing cell migration of a metastatic cell line in BME through time-lapse microscopy

The metastatic cell line CHLA-01R-MED showed the most promising phenotypes indicative of cell migration in sequential images taken over 1 week (Figure 3.2). This cell line was therefore chosen for time-lapse microscopy to confirm whether the observed changes in phenotype were due to migration or proliferation in 3D BME culture conditions and to investigate whether growth factors in the medium, or the cell secretome, could act as chemoattractants to induce cell migration.

CHLA-01-R-MED cells in undissociated clusters were embedded in 3D BME and plated into a chemotaxis chamber (see Chapter 2 for details). Three different medium conditions were tested to determine whether soluble growth factors and/or factors secreted by cell clusters induced directional cell migration:

1) medium with no supplements or cells
2) conditioned medium containing growth factors but no cells
3) conditioned medium containing growth factors and cells

The time-lapse images revealed that cell migration occurred after 24 hours. Single-cells were imaged migrating from one point to another in the matrix. A range of migrational behaviours was observed in all three conditions (Figure 3.9). Large clusters in close proximity to each other formed extensions to bridge the gap and begin merging into a larger cluster (red arrows). Single cells appeared to migrate from their location of seeding towards clusters or towards other single cells, adopting a more elongated shape (yellow arrows). Finally, single cells in close proximity to each other formed physical interactions with each other, and with nearby large clusters (blue arrows). These results suggested that both proliferation and migration may contribute to cell clusters fusing into larger clusters as had been observed in the experiments in section 3.2.1. However, as these observations were based on only one replicate, this is not a significant conclusion.

The aim of inducing directional cell migration towards define soluble factors or the cell secretome was not accomplished, since the differences in cell migration behaviours could have been due to chance based on how close or far clusters were initially seeded. None of the medium conditions resulted in directional migration towards the reservoirs containing growth factors, conditioned medium, or conditioned medium with cell clusters in suspension.

It was determined that while migration events may occur when cells are embedded in BME, migrating cells could not be isolated for further analysis in the current experimental format.

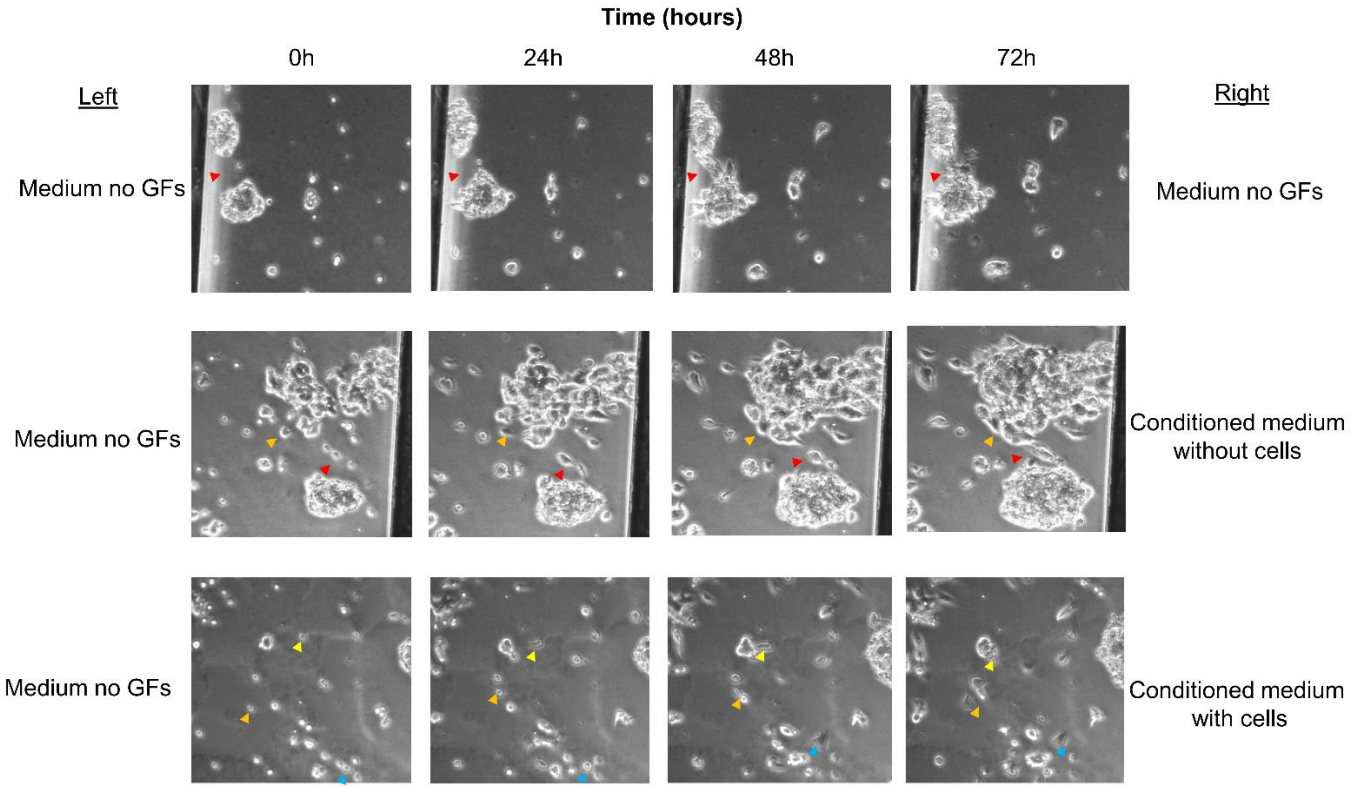


Figure 3.9 Time-lapse microscopy captures CHLA-01R-MED cell migration in BME.

CHLA-01R-MED cells were cultured in BME at high-gelling concentration (10 mg/mL) in a chamber slide. Either medium without growth factors (DMEM F12) or medium conditioned by cells or medium containing cells was placed in the side reservoirs. The slide was imaged for 72h and videos captured. Images captured from the video showed some cells formed bridges between clusters (red arrows,) single cells migrated towards other single cells or cell clusters (yellow arrows) and some cells adopted a more mesenchymal shape when interacting with other cells (blue arrows). n=1

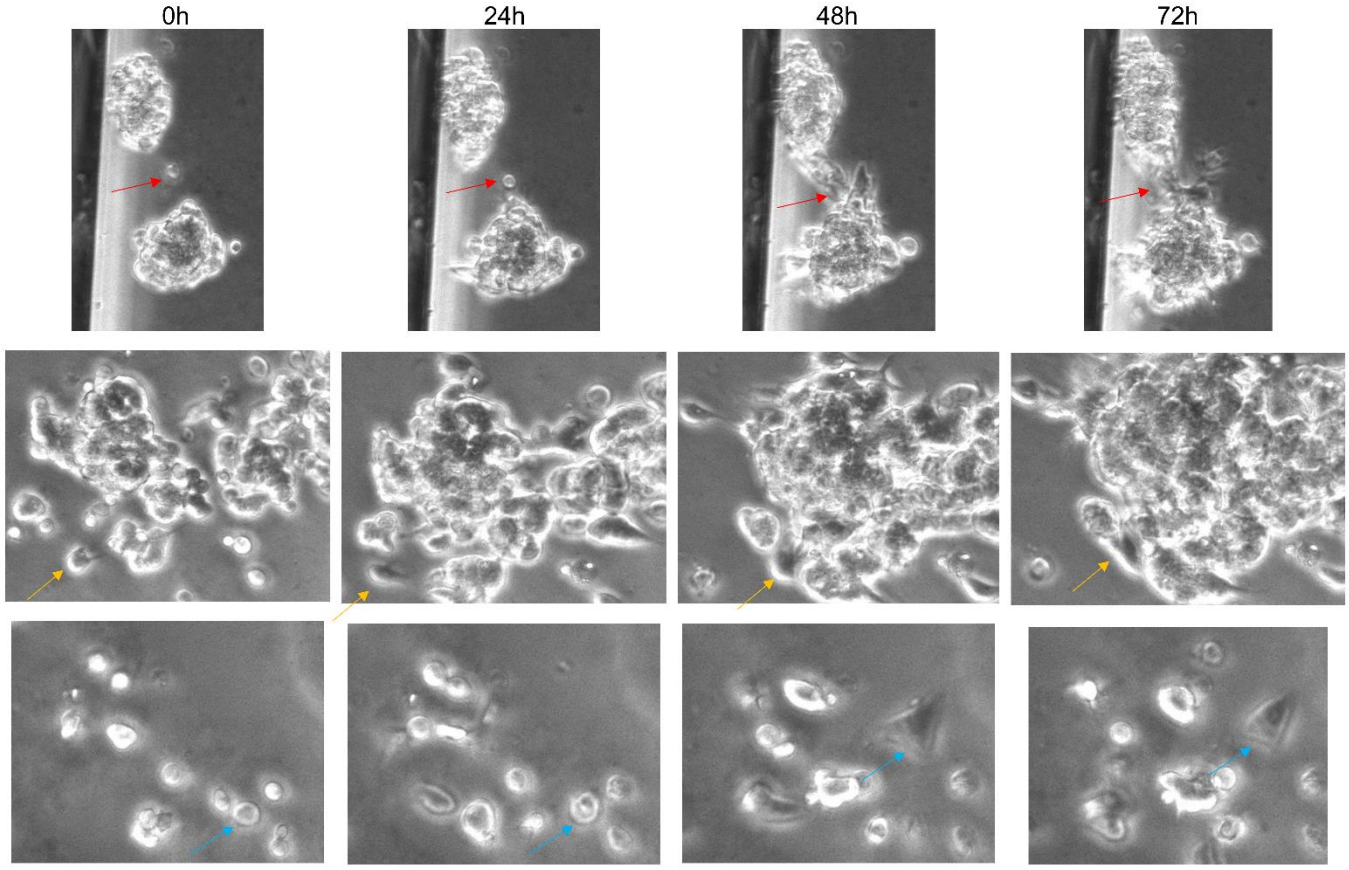


Figure 3.9 continued. A digital magnification of some of the cell behaviours observed when CHLA-01R-MED cells were cultured in BME at high-gelling concentration (10 mg/mL) in a chamber slide. n=1

Summary of sections 3.1 and 3.2

The results presented in sections 3.1 and 3.2 represent the initial stages of this PhD project. The aim of these experiments was to adapt the 3D culture conditions previously developed in our lab by Aishah Nasir (A, Nasir 2016) in order to define consistent BME culture condition for Group 3 and Group 4 medulloblastoma cell lines.

The hypothesis that medulloblastoma cells would migrate when cultured in a 3D matrix composed of basement membrane components could not be significantly proven or disproven, because of the single or low numbers of replicates presented. The data was therefore presented as observations, and led to a better understanding of the cell lines being used and the requirements of an *in vitro* culture model that would enable the capture of migrating cells for molecular analyses.

3.3 A trans-well migration assay to model the basement membrane

Culturing medulloblastoma cells in BME as described in sections 3.1 and 3.2 did not allow the isolation of populations of cells from different stages of migration in the current well-plate assay setup. Therefore, an assay format was needed that would both induce directional cell migration and allow the isolation of migrating cells, as well as obtaining high quality RNA from these cells. The modified Boyden chamber trans-well assay was selected in order to isolate cells at 3 stages of migration: a) non-migratory suspension cells, b) pre-migratory adherent cells and c) migrating and migrated cells (Figure 3.10).

Cells were seeded in the upper compartment, and migrated through a coated membrane to a receiver plate, resulting in three compartments. Cells that did not adhere to the membrane or migrate across it represent the suspension compartment, cells that adhered to the basement membrane coating but remained in the top of the insert represented the pre-migratory adherent compartment, and cells on the underside of the insert represent the migratory compartment.

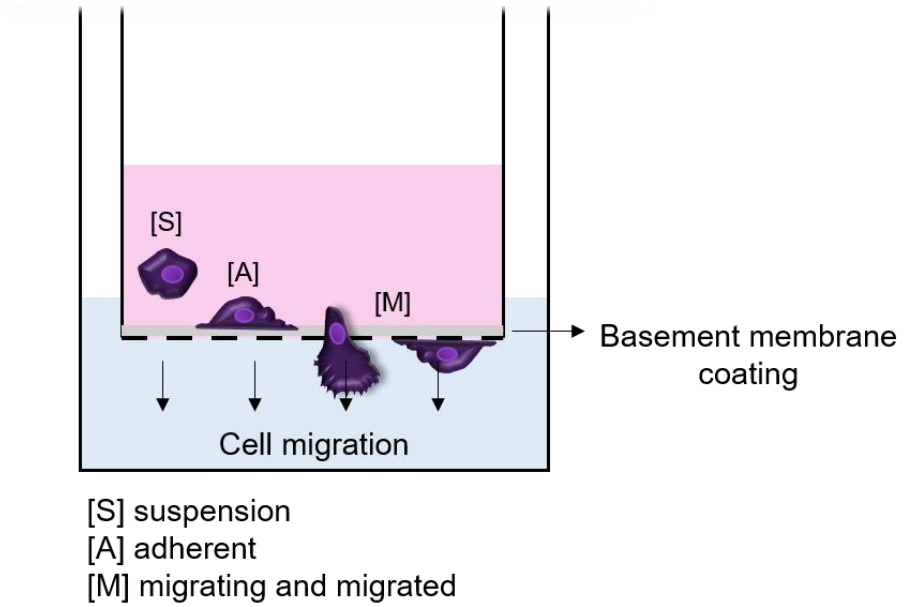


Figure 3.10 A modified Boyden chamber migration assay to capture cells from three compartments.

3.3.1 BME as a basement membrane coating

In order to optimise coating a trans-well insert with BME to induce cell migration and collect migrating cells, BME was compared to an uncoated insert and an insert coated with only collagen IV. In order to determine migration, the membrane at the bottom of the insert was fixed and stained with eosin and haematoxylin after 72 hours of migration. The membrane was then cut off the insert and affixed to a microscope slide for imaging. The breast cancer cell line MDA-MB-231 was used as a control since it is a widely studied metastatic cell line which has been demonstrated to invade through BME (Tang et al., 2019, Lim et al., 2016a) . Collagen IV is one of the two main components of all basement membranes, and essential for the structure and function of the basement membrane. (Pöschl et al., 2004). BME was compared to collagen IV in order to assess whether the cells would migrate through one ECM component. MDA-MB-231 cells migrated in response to 10% FBS through the uncoated well, and through the well coated with collagen IV only. No cells migrated through the well coated with BME (Figure 3.11 A).

Cell invasion through BME was also tested with the Group 3 cell line HD-MB03. The chemokine tested was a combination of growth factors and soluble factors based on previous experiments as well as previously published studies. EGF and FGF were components of the medium in the BME embedding experiments where HD-MB03 cells formed clusters (Figure 3.8). HGF has been shown to induce cell invasion through Matrigel® in SHH cell lines DAOY and UW228 (Kumar et al., 2015a, Kumar et al., 2015b). CXCL12 was used as a chemokine for D556-MED and induced cell migration in combination with WIP1 overexpression (Buss et al., 2015). HD-MB03 did not invade through BME in response to a combination of soluble factors EGF, HGF, FGF and CXCL12 (Figure 3.11 B). However, there was some cell migration in response to this combination of chemokines through an uncoated well or a collagen IV coated well. 10% FBS used as a chemokine also induced cell migration (Figure 3.11 C).

The Group 4 cell lines CHLA-01-MED and CHLA-01R-MED were seeded onto uncoated wells or wells with collagen IV. Migration in response to the combination of chemokines described above or FBS were compared. The following preliminary observations were made from one replicate of the experiment. CHLA-01-MED cells did not migrate in response to no chemoattractant or the combination of chemokines. In a separate experiment, CHLA-01-MED cells migrated only at the edge of the wells in response to 10% FBS. Some of the few instances of cell staining for each experimental condition are shown (Figure 3.12 A and B). CHLA-01R-MED appeared to migrate equally in response to the combination of chemokines and no chemokine, however this was difficult to quantify, as individual cells could not be distinguished in the images. In contrast, CHLA-01R-MED did not migrate at all in response to 10% FBS (Figure 3.12 C). As the preliminary results suggested that neither medulloblastoma cell lines nor the invasive breast cancer cell line control could invade across the BME, this experiment was not repeated, and therefore different concentrations of soluble factors were not tested.

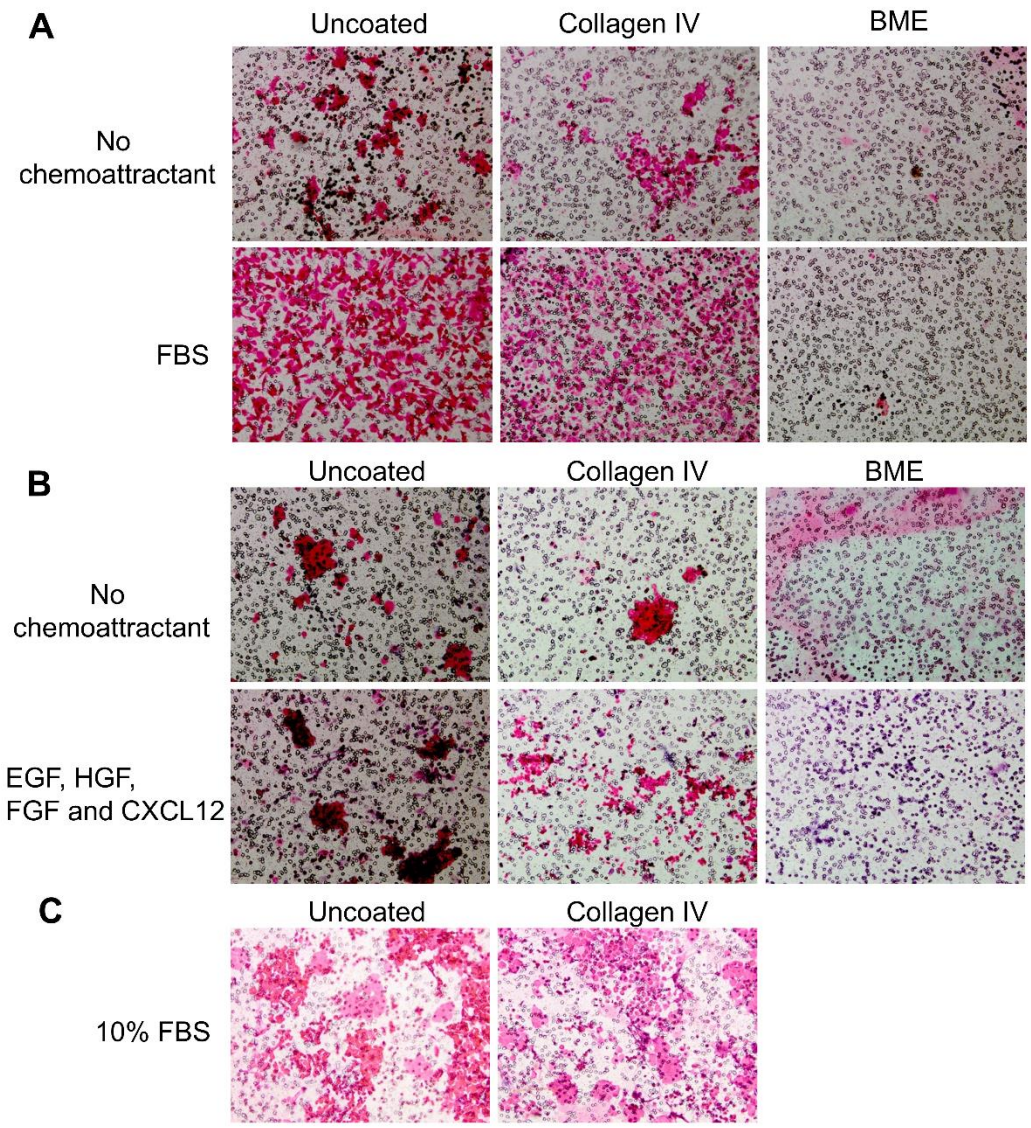


Figure 3.11 Collagen IV, but not BME, allows migration of cells through the migration model.

The cells on the bottom side of the trans-well membrane were fixed and stained with eosin and haematoxylin after 72h. In the micrographs, pink shapes are cells or cell clusters and circles are the pores in the membrane. **A)** MDA-MB-231 was used as a control cell line to optimise a basement membrane coating for the model, however using BME (10 mg/mL) as a coating did not allow cell migration through the trans-well, while cells migrated through an uncoated trans-well and collagen IV (10µg/well) coated trans-well. n=1 **B)** Group 3 cell line HD-MB03 seeded on uncoated trans-wells, collagen IV (10 µg/mL) coated or BME (10mg/mL) coated trans-wells with a combination of chemokines (20 ng/mL EGF, 20 ng/mL FGF, 20 ng/mL HGF, 1 µg/mL CXCL12), n=1. **C)** In a separate experiment, HD-MB03 cells seeded on uncoated trans-wells or trans-wells coated with collagen IV, with 10%FBS as a chemokine. Fpr each, n=1.

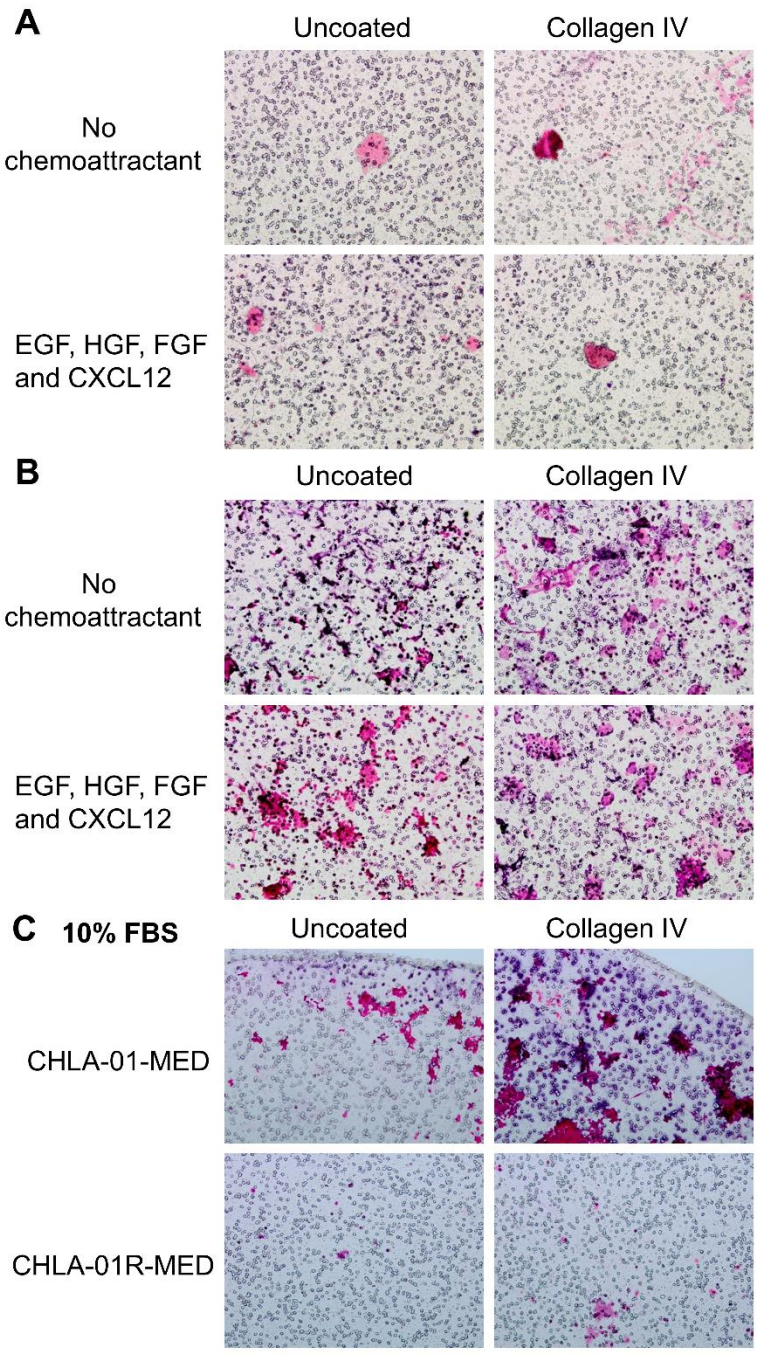


Figure 3.12 Collagen IV coating permits modest migration of Group 4 cell lines.

The cells on the bottom side of the trans-well membrane were fixed and stained with eosin and haematoxylin after 72h. In the micrographs, pink shapes are cells or cell clusters and circles are the pores in the membrane. **A)** CHLA-01-MED cell migration through an uncoated trans-well or a well coated with Collagen IV (10µg/well) in response to 10% FBS or a combination of chemokines (20 ng/mL EGF, 20 ng/mL FGF, 20 ng/mL HGF, 1 µg/mL CXCL12). The only instances of cell staining are shown for all conditions, n=1. **B)** CHLA-01R-MED had some cell migration through an uncoated trans-well or a well coated with Collagen IV (10µg/well) in response to a combination of chemokines (20 ng/mL EGF, 20 ng/mL FGF, 20 ng/mL HGF, 1 µg/mL CXCL12), n=1. **C)** In a separate experiment, CHLA-01-MED and CHLA-01R-MED cells seeded on uncoated trans-wells or trans-wells coated with collagen IV, with 10% FBS as a chemokine. For each, n=1.

The observations made and preliminary results obtained in section 3.3.1 led to 4 points of discussion regarding the method used.

1) A variable in the experiment was not optimal for cells to invade across BME, and the coating therefore had to be further optimised. This may be due to BME being rich in growth factors and masking the gradient of chemokine in the receiver plate, or the variation in ECM components and growth factor concentrations in different batches of BME. A solution to this challenge could be to use reduced growth factor BME or the individual components of BME at known concentrations in order to make the model more reproducible. BME with reduced growth factors was considered, but the decision was made to try individual ECM components instead. There was concern over the concentrations of BME components being variable between batches, and that the range of possible growth factor concentrations in reduced growth factor BME provided by the manufacturer overlapped with the concentrations of growth factors in regular BME.

2) It was observed that cells migrated across collagen IV although this did not always appear different to an uncoated well. These preliminary results suggest that the coating must be optimised if individual BME components are to be used.

3) The combination of chemokines used for HD-MB03 and CHLA-01R-MED cells induced some cell migration, but these results are preliminary and this could likely be improved. In this chapter, only one concentration of each soluble factor was tested based on previously published concentrations, and as the experiment was not repeated, further concentrations were not tested.

4) Imaging the trans-well at the end of the assay gives a qualitative assessment of cell migration. A more quantifiable method would need to be tested to enable robust and accurate assessment of migration.

3.3.2 Optimising a chemokine gradient to induce cell migration

In order to isolate cells for molecular analysis, experiments were performed to identify the chemokine that would induce the highest number of cells to migrate. 10% FBS is commonly used as a chemokine for a variety of cancer types, and was therefore compared to 2% FBS and medium devoid of FBS in our model. Collagen IV only as a coating was used to represent the basement membrane ECM for this section of the optimisation work due to the difficulties presented by BME described in section 3.3.1. A new method of estimating the number of migrated cells was also tested by dissociating migrated cells from the bottom of the trans-well inserts and using a metabolic activity assay to quantify the number of cells (see Chapter 2 for details).

The Group 3 cell lines HD-MB03 and D283-MED had high numbers of migrating cells in response to both concentrations of FBS across uncoated inserts as well as inserts coated with collagen IV, but in HD-MB03 cells, 10% FBS induced a significantly higher number of migrating cells compared to 2% FBS or no chemokine (n=3, ****p<0.0001) (Figure 3.13 A and B). D283-MED had the highest overall migration, with an average of 1.7×10^4 cells, 36% of the cells seeded, migrating in response to 10% FBS (Table 3.2). Migration was not significantly different between the wells coated with collagen IV or the uncoated wells. HD-MB03 had the next highest number of migrating cells with an average of 9.9×10^3 cells, 18% of the cells seeded, migrating in response to 10% FBS. This may have been slightly reduced by the collagen IV coating, although this difference is not significant. D458-MED showed the lowest amount of migration (Figure 3.13 C) with an average of 3.4×10^3, 8% of the cells seeded, migrating, but no significant difference between 10% FBS and 2% FBS or the collagen IV coated or uncoated wells. D283-MED and D458-MED cells did not remain viable in the no chemokine control and therefore could not be quantified.

From the HD-MB03 results, it was concluded that 10% FBS is the optimal chemokine to induce a high number of migrating cells, although a coating made of collagen IV alone may not be sufficient to mimic the basement membrane as it did not affect the number of migrating cells when compared to the uncoated control in any of the cell

lines tested. It is also unclear which components of FBS are inducing the cell migration. Therefore, further experiments were required to determine whether individual soluble factors could also induce migration.

Following these preliminary results, it was decided to compare the cell migrating in response to 10% FBS or individual soluble factors.

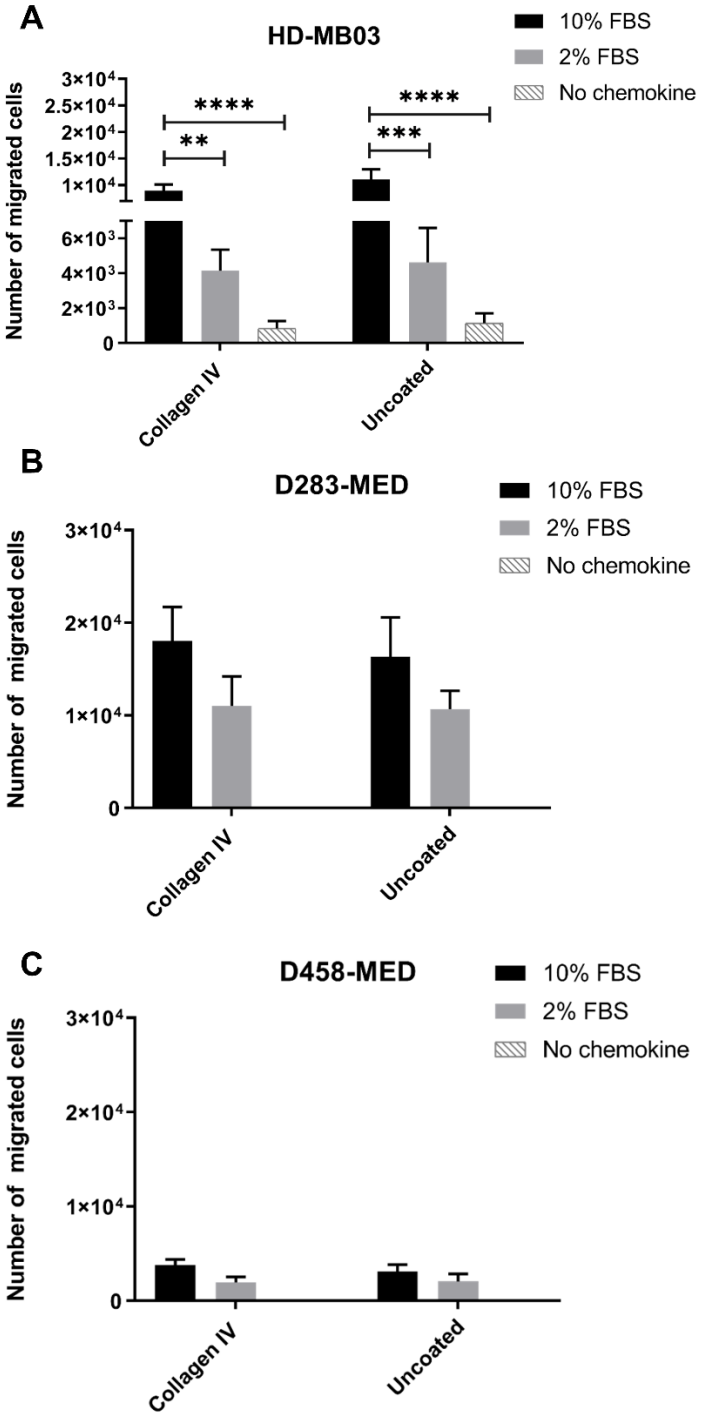


Figure 3.13 Medium supplemented with 10% FBS induced the highest number of migrating cells across three Group 3 cell lines.

The number of **A)** HDMB03, **B)** D283-MED, or **C)** D458-MED migrated cells at 72h across trans-wells coated with collagen IV only towards either medium supplemented with 10%FBS, medium supplemented with 2% FBS or medium without any supplement. Metabolic activity assay results for each condition were plotted against a standard curve of known cell numbers in order to derive the exact number of migrated cells. D283-MED cells did not survive in the “No chemokine” condition, and could not be measured, and D458-MED cells were not exposed to “No chemokine.” Results are shown as the mean number of migrated cells per chemokine (n=3). Statistical significance was calculated using one-way ANOVA with Tukey’s multiple comparisons. (**P=0.0041, ***P=0.0003, ****P<0.0001). Error bars represent SEM.

Table 3.2 Summary table showing the percent (% of seeded cell number) of Group 3 cells that migrated in response to each chemokine in Figure 3.14.

These values represent cells seeded into collagen IV coated wells (10µg/well).

Chemokine	**HD-MB03**	**D283-MED**	**D458-MED**
0% FBS	2	0	n/a
2% FBS	8	22	4
10% FBS	18	36	8

IGF1, Netrin-1 and Shh were selected as experimental chemokines based on previously published studies on medulloblastoma migration. IGF1 has been shown to induce cell migration in D425-MED and CHLA-01-MED cells (Svalina et al., 2016). Netrin-1 has been shown to induce cell invasion across Matrigel in D283-MED, D435-MED, D458-MED and D556-MED cells (Akino et al., 2014). Shh was selected as a chemokine candidate due to its importance in a variety of cancer cell functions in the medulloblastoma subgroup of the same name. Only one concentration of each soluble was tested based on the results from the published studies. It would have been useful to test a range of concentrations, but due to time constraints the decision was made to select the chemokine that led to the highest number of migration cells in this experiment.

The soluble factors were tested individually in medium with 2% serum to maintain viability compared to no chemokine (2% FBS only) across the Group 3 and Group 4 cell lines. The following preliminary observations were based on 1 biological replicate, and are therefore not statistically significant conclusions. Neither IGF1 nor Netrin-1 increased the cell migration compared to the no chemokine condition in HD-MB03 (Figure 3.14 A). IGF-1 and Netrin-1 were also tested as a treatment in the top of the insert, but this did not induce more migration compared to the control condition. There was no cell migration at all in CHLA-01-MED (see Appendix 1 Supp. Fig. 1). CHLA-01R-MED had the highest overall cell migration (Figure 3.14 C), but this was not increased by the inclusion of IGF-1 or Netrin-1. In three Group 3 cell lines, supplementing 2% FBS with Shh made no significant difference to the number of migrating cells (Figure 3.14 B, D, and E). IGF1 and Netrin-1 as chemokines were also tested in D283-MED cells using the image assessment method, but neither chemokine increased cell migration compared to 2% FBS only (see Appendix 1 Supp. Fig. 2).

The observations made and preliminary results obtained in section 3.3.2 led to the following discussion points:

- Based on the statistically significant migration in the HD-MB03 cell line, 10% FBS induced the highest numbers of cells to migrate across uncoated and collagen IV coated trans-well inserts (n=3, ****p<0.0001). Single soluble factors were also tested as chemokines, but as only 1 replicate was completed, these comparisons are not significant.

In addition, the following discussion point was raised regarding the Group 4 cell lines:

- CHLA-01R-MED and CHLA-01-MED had some cell migration in some of the conditions tested, but not in response to the same chemokines. So as not to include only one cell line from the matched pair to represent Group 4, and to keep the experiment conditions consistent across all cell lines, the next set of optimisation experiments and sequencing project were focused on Group 3 cells only.

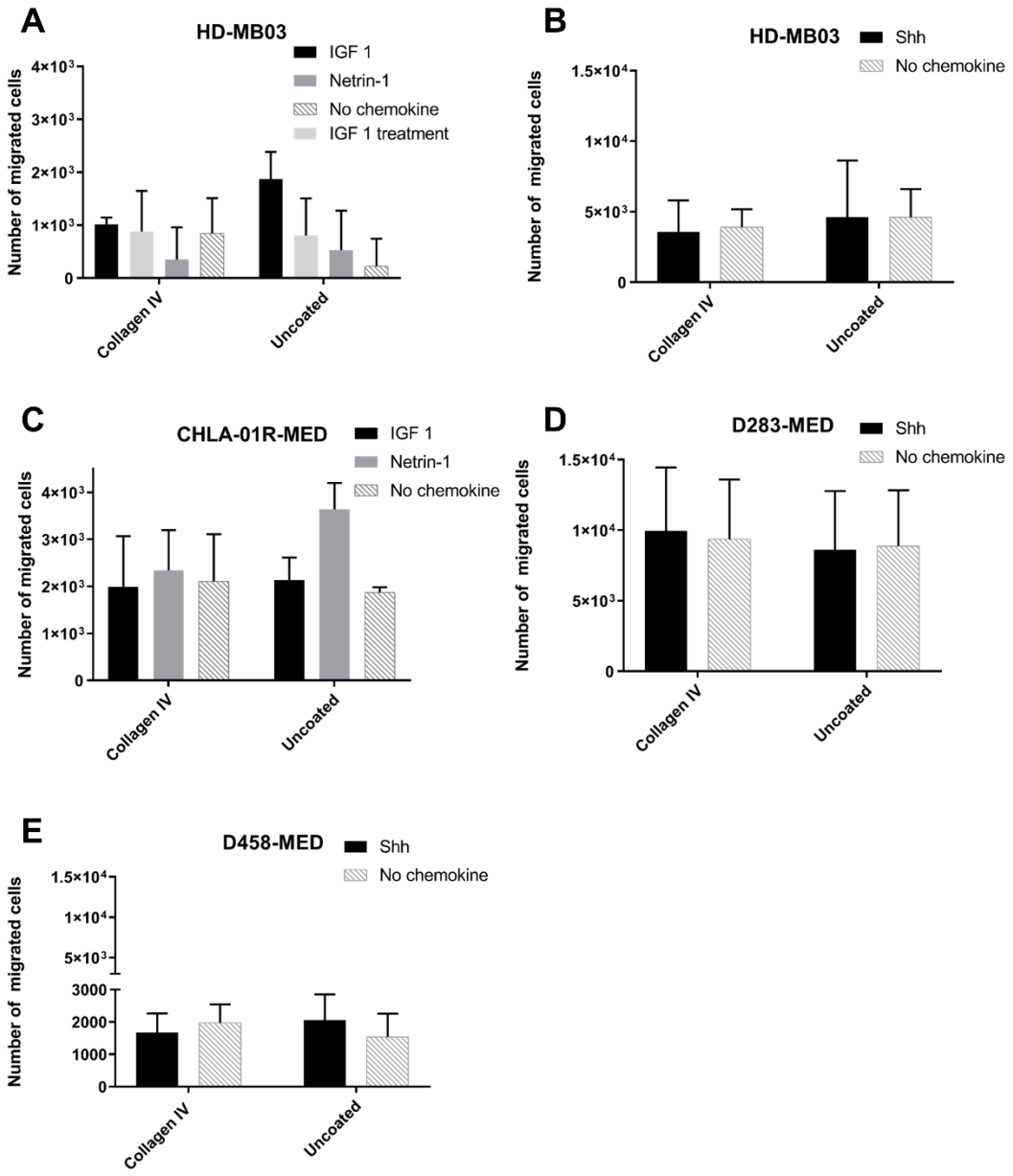


Figure 3.14 Individual soluble factors do not induce migration.

Cells migrated for 72h in a trans-well assay coated with 10 µg collagen IV. The number of migrated cells was quantified by calcein AM metabolic activity assay on only the migrated cells, and the fluorescence values from cells in each condition was plotted against a standard curve of known cell numbers to determine the number of migrated cells. **A)** HD-MB03 cells exposed to either medium supplemented with 2% FBS and 100 ng/mL IGF1 or 2% FBS and 800 ng/mL Netrin-1, or towards 2% FBS only. HD-MB03 cells were also exposed to 100 ng/mL IGF-1 in the top of the trans-well as a treatment. **B)** HDMB03 cells exposed to 2% FBS only or 2% FBS+ 10 nM Shh as a chemokine in the receiver plate. **C)** CHLA-01R-MED cells exposed to either medium supplemented with 2% FBS and 100 ng/mL IGF1 or 2% FBS and 800 ng/mL Netrin-1, or 2% FBS only. **D)** D283-MED cells exposed to 2% FBS only or 2% FBS+ 10 nM Shh as a chemokine in the receiver plate and **E)** D458-MED cells exposed to medium supplemented with 2% FBS only or 2% FBS + 10 nM Shh (for all chemokines n=1). In all graphs, error bars represent SD.

Table 3.3 Summary table showing percentage migration increase (%) from Figure 3.15, in the presence of one soluble chemokine in 2% FBS, compared to 2% FBS as a baseline.

Chemokine	**HD-MB03**	**D283-MED**	**D458-MED**	**CHLA-01R-MED**
100 ng/mL IGF 1	0	n/t	n/t	0
100 ng/mL IGF 1 treatment	0	n/t	n/t	n/t
800 ng/mL Netrin-1	0	n/t	n/t	+1
10 nM Shh	-1	+1	-1	n/t

n/t = not tested

In order to make this simple model more representative of the brain-CSF interface, artificial cerebrospinal fluid (aCSF) was tested to replace the medium component in our assay. The compositions of two commercially-available CSF replacement solutions were compared. Elliotts B® Solution is a buffered intrathecal electrolyte/dextrose injection used as a diluent for intrathecal administration of methotrexate sodium and cytarabine in the clinic (Geiser et al., 1975). TOCRIS aCSF is a commercially available aCSF which closely matches the electrolyte concentrations of CSF, used when sampling from brain interstitial fluid. The composition of both solutions is similar, and resembles the electrolyte composition of CSF (Table 3.4). As only TOCRIS aCSF was available in the United Kingdom, it could not be compared to Elliotts B®. The key difference between the two was the absence of glucose from TOCRIS aCSF, therefore aCSF was supplemented with sterile glucose to 0.8 mg/mL in order to better mimic CSF.

Cells remained viable but did not proliferate when incubated in aCSF containing 10% FBS for 72 hours. HD-MB03 cells did not remain viable in aCSF devoid of serum, and remained viable for 24 hours only in aCSF supplemented with 2% FBS (Figure 3.15 A). In the aCSF with 10% FBS, the cells would migrate without proliferation. This was confirmed by comparing the number of cells on the bottom of the insert after incubation for 48 hours in aCSF with 10% FBS or medium with 10% FBS (Figure 3.15 B). The number of cells in medium with 10% FBS compared to aCSF with 10% FBS, suggesting that migrated cells were proliferating on the underside of the trans-well insert. ACSF with 10% FBS was selected as a more brain-specific condition to induce sufficient cell migration for the isolation of genetic material.

Table 3.4 Comparing the composition of two aCSF solutions to CSF.

The electrolyte composition and pH of Elliotts B Solution and TOCRIS aCSF are compared to CSF. Values for CSF and Elliotts B® Solution were obtained from Elliotts B® Solution data sheets. Values for TOCRIS aCSF were obtained from TOCRIS data sheets.

Solution	Na^+	K^+	Ca^{2+}	Mg	HCO_3^-	Cl^-	pH	Pi	Glc
CSF	117-137	2.3-4.6	2.2	2.2	22.9	113-127	7.31	1.2-2.1	45-80
Elliotts B Solution	149	4.0	2.7	2.4	22.6	132	6.0-7.5	2.3	80
TOCRIS aCSF	150	3.0	2.8	1.6	n/a	155	7.19	3.0	n/i

All ions are in mEQ/L and other solutes in mg/dL; Pi – phosphorus, Glc – glucose.

n/i = not included in formula (Glucose was added to the TOCRIS aCSF for the migration experiments.

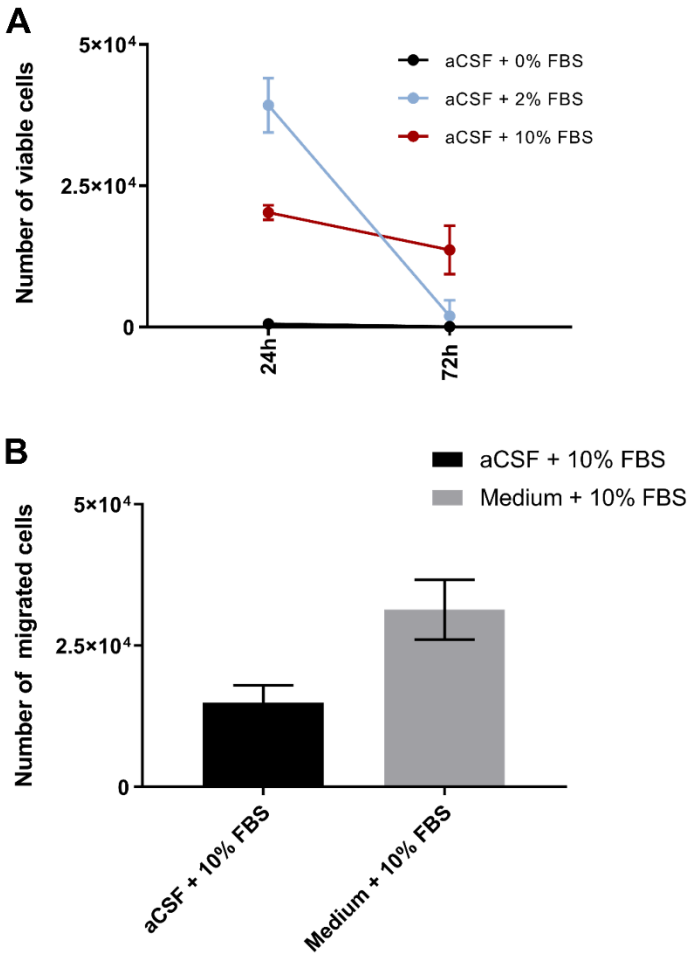


Figure 3.15 aCSF enables migration to be separated from proliferation.

A) HD-MB03 cells were cultured in 96-well culture plates for 72h in aCSF with added 0.8 mg/mL glucose supplemented with either 2% FBS, 10% FBS or no supplement. The metabolic activity of the cells was assayed using PrestoBlue cell viability reagent. The cells in aCSF with 2% FBS or without supplement did not remain viable, however the cells in aCSF with 10% FBS remained viable after 72 hours but did not proliferate (n=1). **B)** HD-MB03 migrated for 72h in a trans-well assay coated with 10 µg collagen IV and 5 µg laminin 111 in response to either aCSF supplemented with 10% FBS or medium supplemented with 10% FBS. The number of migrated cells was quantified by calcein AM metabolic activity assay on only the migrated cells, and the fluorescence values from cells in each condition was plotted against a standard curve of known cell numbers to determine the number of migrated cells. Cell migration was higher in medium supplemented with 10% FBS than in aCSF supplemented with 10% FBS (n=1). In all graphs, error bars represent SD.

3.3.3 Using a combination of collagen IV and Laminin as a basement membrane coating

The second experimental variable optimised was the coating of ECM components to represent the basement membrane. Networks of collagen IV and laminin form the base structure of the basement membrane ECM. The two networks are linked by other ECM proteins including Nidogens and HSPGs, and associate with surrounding cells (Pozzi et al., 2017, Jayadev and Sherwood, 2017). In order to represent the basement membrane *in vitro* in a simple and reproducible manner, the two primary components, collagen IV and laminin were selected. Although these would likely not form the organised networks present in the body without associated proteins and other cell types, the aim was to provide medulloblastoma cells with some interactions to ECM components that may be present at the basement membrane. Basement membranes provide barriers between tissue compartments, and only cells able to activate specific migration and invasion pathways should be able to cross it. Ideally, the basement membrane coating would provide a barrier to cells that had not activated the invasion pathways.

Migration experiments from this point on were performed using collagen IV from human placenta rather than collagen IV from mouse origin due to the higher starting concentration of the human collagen IV (see Appendix 1 Supp. Fig. 3). A range of collagen IV concentrations was tested : 10 µg, 20 µg or 50 µg per insert. There was no significant difference in the number of migrating cells between the three concentrations (Figure 3.16 A). Laminin 111 was combined with the lowest collagen IV concentration, but while there appeared to be an increase in the number of migrating cells compared to the uncoated wells, this difference was not significant.

There was no significant difference between 10 µg, 20 µg or 50 µg of collagen IV or between 5 µg and 50 µg of laminin, therefore the lower concentration was selected for each.

3.3.4 Optimising the time point at which to isolate cell samples

Finally, the last experimental variable to be optimised was the best time point at which to isolate cells from the three compartments. 24, 36, 48 and 72 hours were tested. The exact number of migrated cells collected at each time point differed in each biological replicate, but there was a trend demonstrating that cell numbers continued to increase until 48 hours. It was concluded that 48 hours is the optimal time point to capture cells as they are still migrating across the trans-well insert, while allowing the maximum number of cells possible to cross the membrane for collection.

The seeding density at the start of the experiment does not have a significant impact on the number of cells isolated in the migrated compartment. This was demonstrated by seeding 5 x 10^4 cells per well, as well as double (1 x 10^5) and quadruple (2 x 10^5) this number under the chemokine and basement membrane coating conditions selected (see Appendix 1 Supp. Fig. 4).

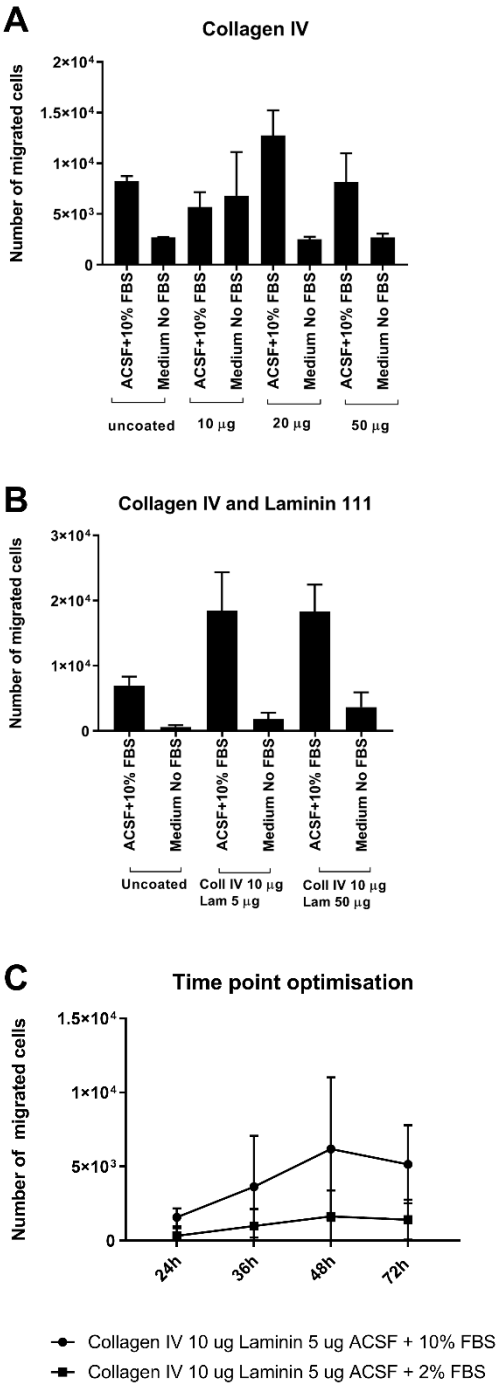


Figure 3.16 Combination of collagen IV and Laminin 111 results in optimisation of a trans-well migration model.

A) HD-MB03 cells migrated for 72 hours through trans-wells coated with 10 µg, 20µg or 50µg of collagen IV from human placenta compared to uncoated wells (n=1). **B)** HD-MB03 cells migrated for 72 hours through trans-wells coated with 10ug collagen IV in combination with 5µg or 50µg Laminin (n=1). **C)** HD-MB03 cells migrated for 24h, 36h, 48h or 72h through trans-wells coated with 10µg collagen IV and 5µg Laminin (n=2). In all graphs, error bars represent SD.

3.3.5 Isolating cells from three compartments for molecular analysis

The optimised trans-well assay conditions were as follows:

First, cells were starved in reduced serum (2% FBS). The collagen IV coating (10 µg) was applied and dried 24 hours prior to seeding. The laminin 111 coating (5 µg) was applied 1 hour before the start of the experiment. 5 x 10^4 cells were seeded in the top of a trans-well insert suspended in medium devoid of serum. aCSF supplemented with 0.8 mg/mL glucose and 10% FBS was added to the receiver plate, creating a chemokine gradient to induce cell migration. After 48 hours of incubation at 37ºC, cells were collected from each of the three compartments (Figure 3.10, see Chapter 2 for full details). All cell lines migrated through the optimised migration assay, however the effect of the basement membrane coating was cell-line dependent (Figure 3.17) and (Table 3.5). HD-MB03 cell migration was slightly increased by the basement membrane coating. D283-MED migration was not affected by the basement membrane coating. D458-MED cell migration was reduced by the basement membrane coating.

The isolation of true biological replicates was controlled by recovering a cryo vial of cells for each migration experiment. Each experiment was performed two times from each cryo vial in order to yield two sets of pellets (A and B). The RNA was isolated in batches based on the date the samples were frozen on, and a selection of samples were quality controlled (QC) using a Bioanalyzer before sending to QIAGEN to make sure there was sufficient RNA for sequencing. 3 or 4 samples from the migrated (M) compartment were measured based on the assumption that they would have the lowest RNA concentration. The concentration of M samples from each of 3 Group 3 call lines ranged from 0.122 ng/µL to 6.089 ng/µL and had a RIN range of 2.4-9.1 (see Appendix 1 Supp. Figure 5). QIAGEN then performed QC on all samples, library prep, and 3’ UPX sequencing, which will be presented in the next chapter.

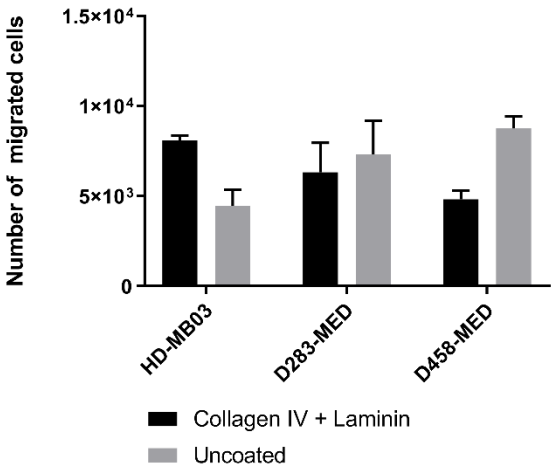


Figure 3.17 Group 3 cells migrated through the optimised brain-CSF migration model.

Results are shown as the mean number of migrated cells per cell line (n=3). Significant differences between each condition and cell line were calculated using one-way ANOVA with Tukey's multiple comparisons. None of the differences are significant. Error bars represent SEM.

Table 3.5 Summary table showing migration increase (%) through the optimised migration model compared to 5 x 10^4 cells as a baseline.

	HD-MB03	D283-MED	D458-MED
Collagen IV + Laminin	16	13	10
Uncoated	9	15	18

3.4 Summary

In order to model migration and sequence the transcriptome of migrating cells, an *in vitro* model was developed and optimised to mimic the interface between the brain and the cerebrospinal fluid.

The first approach taken was using BME in order to model the basement membrane matrix. This approach was chosen following previous work in our lab which had concluded that BME culture allowed the observation of different cell phenotypes between low risk and metastatic medulloblastoma cell lines. Phenotypic differences were observed between the 2D suspension and 3D BME culture of Group 4 cell lines CHLA-01-MED, CHLA-01R-MED, and Group 3 cell lines HD-MB03 and D283-MED when they were cultured in BME, and some of the cell behaviours suggested migration may have been occurring in 3D. Time-lapse microscopy confirmed that CHLA-01R-MED cells migrate within the BME matrix. However, embedding cells in BME did not allow for the isolation of RNA from different stages of cell migration, and a trans-well assay setup was therefore selected.

The trans-well assay setup was used to separate cells from three compartments: [S] non-metastatic suspension cells, [A] early metastatic adherent cells, and [M] metastatic migrated cells. The trans-well format required the replacement of BME with another form of ECM coating as BME proved inhibitory to directional cell migration. This was resolved by coating the trans-well inserts in collagen IV and laminin 111 to mimic a basic composition of the basement membrane. Inclusion of aCSF supplemented with 10% FBS in place of standard culture medium eliminated cell proliferation from the model, in order to isolate the expression of genes inducing migration. Finally, 48 hours was selected as the best time to isolate cells as they were in the process of migration in order to capture sufficient migrating cells before the expression of migration-inducing genes was turned down (Figure 3.18).

In conclusion, a simple *in vitro* model was developed, representing domr features of the interface between the brain and the CSF to enable the capture of migrating cells

from three compartments for molecular analysis. The differences in expression from these three compartments will be compared in order to identify candidate genes for migration and metastasis.

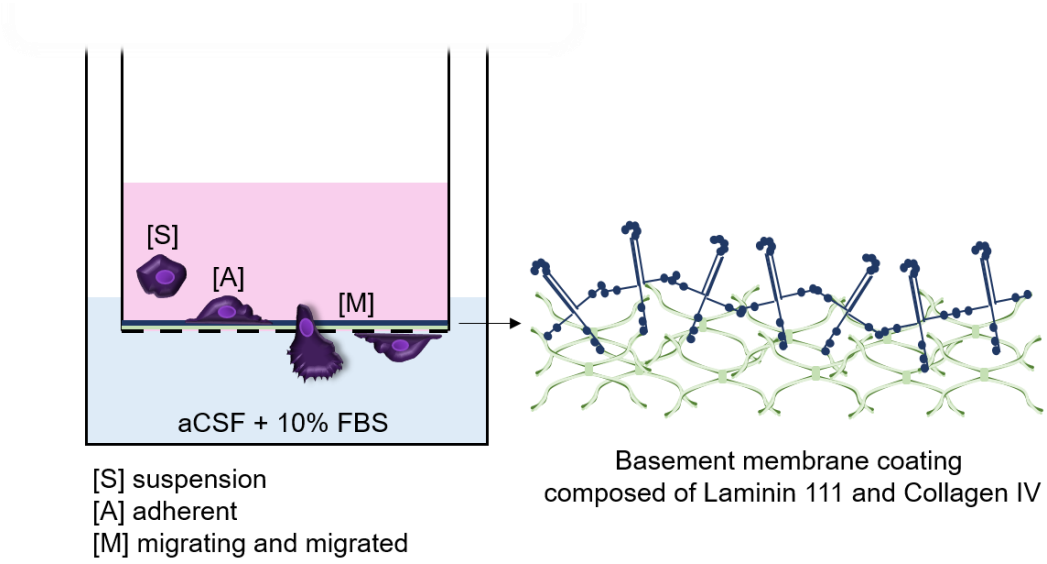


Figure 3.18 Summary schematic of the optimised brain-CSF migration model.

The migration assay setup is shown for one well. The basement membrane coating schematic describes the predicted interaction between Laminin (blue) and collagen IV (green) networks

Chapter 4 Identifying new markers of migration and metastasis through analysis of transcriptomic differences between cells from an optimised *in vitro* model

4.1 Introduction

Aim 2: Identify new markers of migration and metastasis in medulloblastoma by sequencing the transcriptome of migrating cells in the *in vitro* model developed in Chapter 3.

The cell's transcriptome represents the transcripts and a relative measure of their quantity under a particular physiological condition. Over the last 30 years, several methods have been developed to allow researchers to investigate and identify elements of the genome contributing to a specific cell function. Low throughput methods such as qPCR only measure single transcripts, and are therefore suited to the study of known targets but do not allow the analysis of all the genes expressed in a cell. The first high-throughput transcriptomic method to be used was hybridisation-based microarray (Schena et al., 1995). Microarrays are a useful method if there is prior knowledge of the sequences being studied, but do not offer accurate quantification of very low or very high expression (Casneuf et al., 2007, Shendure, 2008). Sequence-based approaches such as Sanger sequencing (Adams et al., 1991, Adams et al., 1995, Kouichi et al., 1994) allow the determination of a transcript's sequence, however this method does not quantify the transcripts. Tag-based methods were later developed to quantify the number of mRNA transcripts (Velculescu et al., 1995, Shiraki et al., 2003). However, these methods require a high input of RNA. The next generation sequencing (NGS) method RNA-seq is a high-throughput, deep-sequencing approach to measure the levels of transcripts and their isoforms. This method was first published in 2008 in studies sequencing the transcriptome of yeast (Nagalakshmi et al., 2008, Wilhelm et al., 2008), plant (Lister et al., 2008), mouse (Mortazavi et al., 2008, Cloonan et al., 2008), and human cells

(Marioni et al., 2008). The use of RNA-seq has become widespread in the last decade and has allowed researchers to elucidate the transcriptome in specific physiological conditions and pathologies (Kukurba and Montgomery, 2015).

In order to observe the gene expression changes that occur during cell migration and identify target genes linked to medulloblastoma metastasis, this project analysed the transcriptome of three Group 3 cell lines from the *in vitro* model of cell migration developed in Chapter 3 through 3′ UPX RNA-Seq on cells from three compartments: suspensions (S), adherent (A) and migrated (M). 3′ UPX RNA-Seq is an RNA-Seq method developed for low input and single cell samples, which sequences libraries only from the 3′ end. This method converts a population of polyadenylated RNAs to a library of cDNA fragments with adaptors attached to one or both ends. These adaptors are used to sequence each cDNA molecule from one or both ends. After sequencing, the reads are aligned to a reference genome to build a transcription map.

The QIAseq 3′ UPX Trancriptome Kit (Qiagen) enables library construction and analysis of purified RNA from 10 pg to 10 ng using only the polyadenylated RNAs. Each RNA molecule is tagged with a unique molecular index (UMI). These unique barcodes (BC) are accomplished by a BC primer mix containing 1) molecular tags (MTs) consisting of 12 random bases, so 4^{12} (16,777,216) unique MTs for each BC primer, 2) gene-specific sequences and 3) common universal primer sequence. Statistically, this will result in each cDNA molecule in the sample receiving a unique MT sequence. Following barcoding, the cDNA molecules are then amplified by PCR, after which the number of unique molecular barcodes in the reads is counted. Library quality control is then performed, and library pools are created in equimolar ratios. The library pools are quantified by qPCR, and then sequenced on a NextSeq500 sequencing instrument, producing the raw sequencing data. The advantage of 3′ UPX RNA-Seq is that only molecules with a poly-A tail are sequenced, which almost guarantees that the RNA sequenced will translate to a protein, enabling quick protein expression validation. The 3′ UPX RNA-Seq workflow is summarised in Figure 1.

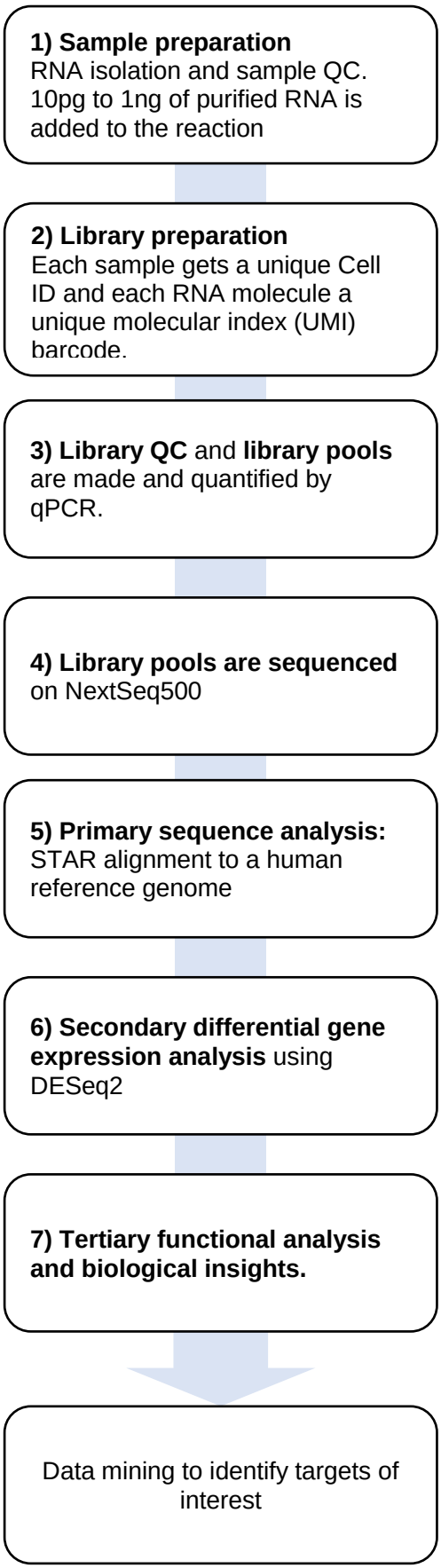


Figure 4.1 3′ UPX RNA-Seq workflow

4.2 Sample preparation

RNA was extracted from three compartments of migrating cells (see the model optimisation in Chapter 3) for cell lines HD-MB03, D283-MED and D458-MED. The migration assays were set up as described in Chapter 3, section 3.3.5. Briefly, 5.0 x 10^4 cells in serum-free medium were seeded onto a coating of 10 µg collagen IV and 5 µg laminin 111. Artificial CSF supplemented with 0.8 mg/mL glucose and 10% FBS was added to the receiver plate to create a chemokine gradient. After 48h of incubation at 37°C, cells were collected and snap-frozen before RNA isolation (see Chapter 2, section 2.6.2). Three independent replicates of each sample were isolated and sent to QIAGEN for sequencing, a total of 27 samples. Preliminary quality control (QC) was performed in order to confirm that the concentration and quality of samples would be suitable for 3′ UPX RNA-Seq (see Appendix 1 Supp. Figure 5). Sample quality was defined by a measure of RNA degradation using the RNA integrity number (RIN) algorithm (Schroeder et al., 2006). A RIN number is between 1 and 10, where 10 is the highest possible RNA quality.

QIAGEN performed additional QC on all the samples sent. The first round of QC performed by QIAGEN showed that several samples had less than 1.4 ng/µL of RNA and therefore may be at a low concentration for 3′ UPX RNA-seq. We requested that these samples be evaporated and the concentration measurement repeated, as (1) the 3′ UPX technique only requires 10 ng of RNA total, and 30 µl of sample had been provided, and (2) 4 of the samples excluded based on the QIAGEN QC had been previously measured in our lab and all had a RIN number ≥7. The samples described in Table 4.1 were selected for 3′ UPX RNA-seq. Samples were selected for sequencing if all samples in one set, one sample from each compartment, suspension (S), adherent (A), and migrated (M), had sufficient RNA concentration for 10 ng and a RIN ≥7. Due to these selection criteria, only two D283-MED independent replicate samples and only one D458-MED sample were considered suitable for further analysis.

Table 4.1 The RNA samples selected for the RNA-Seq study.

The sample numbers are listed, and the cell line and migration compartment that each sample belongs to are detailed. RNA concentration and quality was measured at Qiagen (RNA conc and RIN), and the total RNA yield per sample based on these measurements is detailed (RNA yield). Samples that had a concentration <1.4 ng/µL were measured a second time after evaporation (RNA conc 2).

Sample number	Cell line	Migration compartment	RNA conc (ng/µL)	RIN	RNA yield (ng)	RNA conc 2 (ng/µL)
618A	HDMB03	S	42	10	1,260	
619A		A	31.9	9.9	957	
620A		M	9.2	8.7	257.6	
621B		S	14.4	7.4	432	
622B		A	13.5	9.6	405	
623B		M	24.6	10	738	
624A		S	29.5	9.7	291	
625A		A	11.5	9.2	276	
626A		M	13.3	9.7	291	
606A	D283-MED	S	47.8	10	1,434	
607A		A	21.8	10	654	
608A		M	<1.4	n/a	14.45	1.7
606B		S	78.2	9.7	2,346	
607B		A	24	9.5	720	
608B		M	<1.4	n/a	13.6	1.6
615B	D458-MED	S	45.4	10	1,365	
616B		A	6.4	n/a	192	
617B		M	<1.4	n/a	14.45	1.7

n/a = not detected

4.3 Analysis

Raw data analysis was performed by bioinformaticians at QIAGEN. First, the raw sequencing data FASTQ files were uploaded to the QIAGEN GeneGlobe bioinformatics tool (https://www.qiagen.com/us/geneglobe/). Cells were de-multiplexed using the unique cell IDs. The 3′ poly-A region was then trimmed off and reads were aligned to the human reference genome GRCh38 (RefSeq accession number GCF_000001405.39) using STAR splice aware aligner (Dobin et al., 2013).

4.3.1 Mapping the sequencing data

The aligned reads were annotated to gene regions, and the UMIs were counted for each gene. External RNA Controls Consortium (ERCC) spike ins were used as a standard. The spike ins are used to derive standard calibration curves and relate the read count to RNA concentration in the sample (Jiang et al., 2011). Typically, 30% of each collection of total reads could be aligned to the genome, and 16% of total reads could be related to the standards. The number of UMIs in each sample was on average 10% of all reads, leading to the identification of between 12,670 and 26,359 detected transcripts (Table 4.2).

The sample with the highest number of reads was D283-MED suspension (S) sample 606B, which also had the highest RNA concentration and a RIN of 9.7. The sample with the lowest number of reads was D458-MED adherent (A) sample 616B, which had a low RNA concentration (although not the lowest,) and did not receive a RIN score (Table 4.1). The low number of reads may be due to lower sample quality rather than the concentration of RNA.

The experimental set with the highest number of detected genes was D283-MED samples 606B (S), 607B (A) and 608B (M), followed by D458-MED sample 617B (M). Two samples in this top four had RNA concentrations just over 1.4 ng/μL and were almost excluded from the project at the RNA QC stage. This demonstrates that while a highly concentrated initial RNA sample can lead to a high number of reads (samples 606B and 607B,) a comparable number of reads can be obtained from

samples with low initial concentration (608B, 617B). The RIN may be more indicative of the number of possible reads, as the sample with the lowest RIN had the lowest number of reads (616B).

Table 4.2 Overarching analysis of UPX sequencing data.

The total reads, reads aligned to the reference genome, reads aligned to the standards, total UMI count, and total number of transcripts detected per sample are shown.

Sample #	Cell line	Migration compartment	Total reads	% reads aligned to genome	% reads aligned to standards	% reads identified as UMIs	Detected transcripts
618A	HDMB03	S	10,066,840	29	17	10	19,938
619A		A	6,357,817	31	13	10	18,256
620A		M	2,458,018	29	23	11	13,352
621B		S	9,548,394	31	11	10	20,716
622B		A	7,614,142	29	19	10	19,363
623B		M	9,968,708	32	16	10	20,083
624A		S	6,684,359	32	17	10	18,022
625A		A	3,758,183	27	23	10	15,621
626A		M	6,149,597	30	21	11	17,166
606A	D283-MED	S	9,533,448	30	19	10	19,754
607A		A	6,767,136	27	22	10	18,542
608A		M	6,770,363	24	25	10	18,820
606B		S	26,494,979	32	8	10	26,359
607B		A	16,876,339	30	12	9	24,037
608B		M	14,084,688	28	16	10	23,579
615B	D458-MED	S	11,000,297	30	14	10	20,756
616B		A	1,818,192	26	25	11	12,670
617B		M	16,964,068	32	17	10	23,258
Mean for all samples			**9,6060,420**	**30**	**16**	**10**	**19,461**

4.3.2 Differential expression analysis

The R package DESeq2 software (Love et al., 2014) was used for differential analysis of count data. DESeq2 is a statistical framework which allows the ranking of genes and the testing of their differential expression between biological groups based on thresholds of biological significance. First, the programme normalizes the raw read counts by calculating size factors using the “median of ratios” method. Normalization is essential in differential gene expression analysis, because it allows accurate comparisons between different samples. Normalization takes into account the sequencing depth, length of genes and the composition of the RNA in the samples. DESeq2’s “median of ratios” method creates an artificial reference sample by taking the geometric means of counts from all genes. The software then divides the raw counts by the corresponding normalization factor of that sample.

The dispersion (measure of variability in the data) is estimated using “shrinkage”. A curve is fitted to the dispersion estimate for each gene, and gene-wise dispersion is then shrunk towards the curve. This shrinkage allows the identification of differentially expressed genes to be more accurate in a small sample size, and reduces the chances of false positives. As this project had small numbers of replicates for each group, DESeq2 was chosen in order to accurately estimate the variation of each gene based on mean gene expression level. The DESeq2 method enables a quantitative analysis focused on the significant fold change rather than the presence of differential expression. DESeq2 analysis assumes that genes are not differentially expressed, and therefore assigns a ratio of 1 to genes that are not differentially expressed.

In our analysis, expression from each cell compartment was compared to the gene expression in each of the two other compartments in every combination possible. The differential expression was given as logarithm base 2 (log2) fold change, the log-ratio of expression between two compartments. Log2 fold change was chosen as a significant difference because it treats upregulated and downregulated genes the same way on a continuous spectrum, meaning that the log2 of an upregulated gene

in sample A would be the additive inverse in sample B. Based on the log2 fold change and significance, we could determine whether a particular gene was upregulated (> 1.0), downregulated (< -1.0), or unchanged (≤ 1.0) between two compartments.

4.3.3 Sample classes

In order to determine whether the broad patterns of gene expression related to the biology of the cells, principal component analysis (PCA) was used to reduce and flatten the dimensions of the data. The basis of PCA analysis is transformation of the original large set of variables in the data into a smaller set of variables. The principal components (PC) are constructed from linear combinations of the initial variables, and are used as axes to plot the data in a way in which the differences are easily visualized. PC1 accounts for the largest possible variance in the dataset, PC2 the maximum remaining information, and so on. If the biological differences between the samples are pronounced, this will describe the primary components of the variation in the data. This leads to the separation of samples in different regions of a PCA plot corresponding to their biology. However, if other factors such as sample quality introduce more hidden variation in the data, the samples may not cluster according to the biology.

In the PCA plot (Figure 4.2), samples clustered by cell line, and within each cell line, by their migration compartment. PC1 carried 54% of the data, and PC2 carried 20% of the data. In combination, these explained 74% of the data, meaning that 74% of the variables from the original dataset were represented in the PCA plot. Looking at the cell lines with two or three replicates, the adherent compartment (A) and suspension compartment (S) appear more similar to each other than to the migration compartment (M), and there is some overlap. This may be due to some suspension cells being collected after the suspension cells were washed off. The samples from the migrated compartment clearly grouped together in both HD-MB03 and D283-MED. While it was possible to conclude that D458-MED samples clustered close together, as they originated from the same cell line, the lack of any replicates meant

that the variance between samples from the same compartment could not be compared.

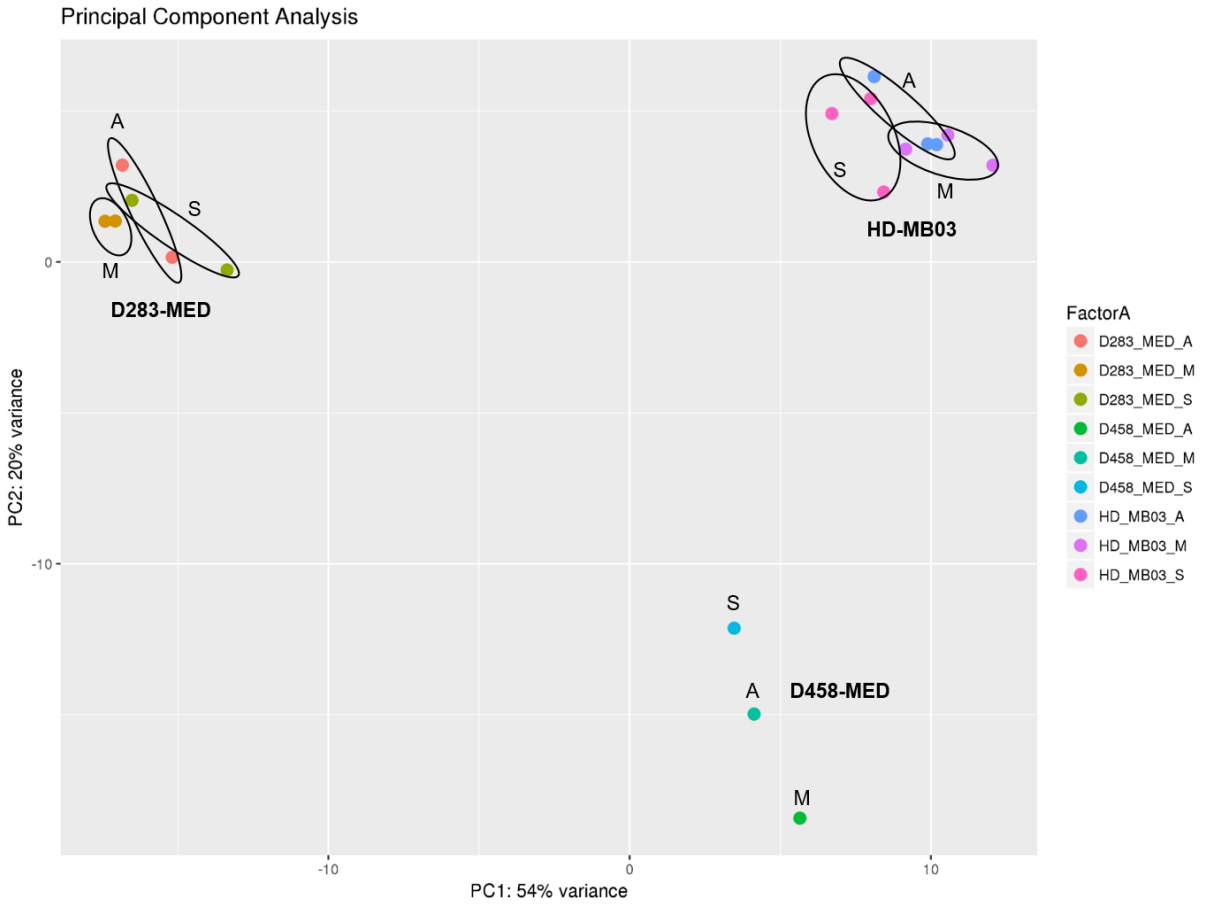


Figure 4.2 Principal Component Analysis (PCA) plot for all samples.

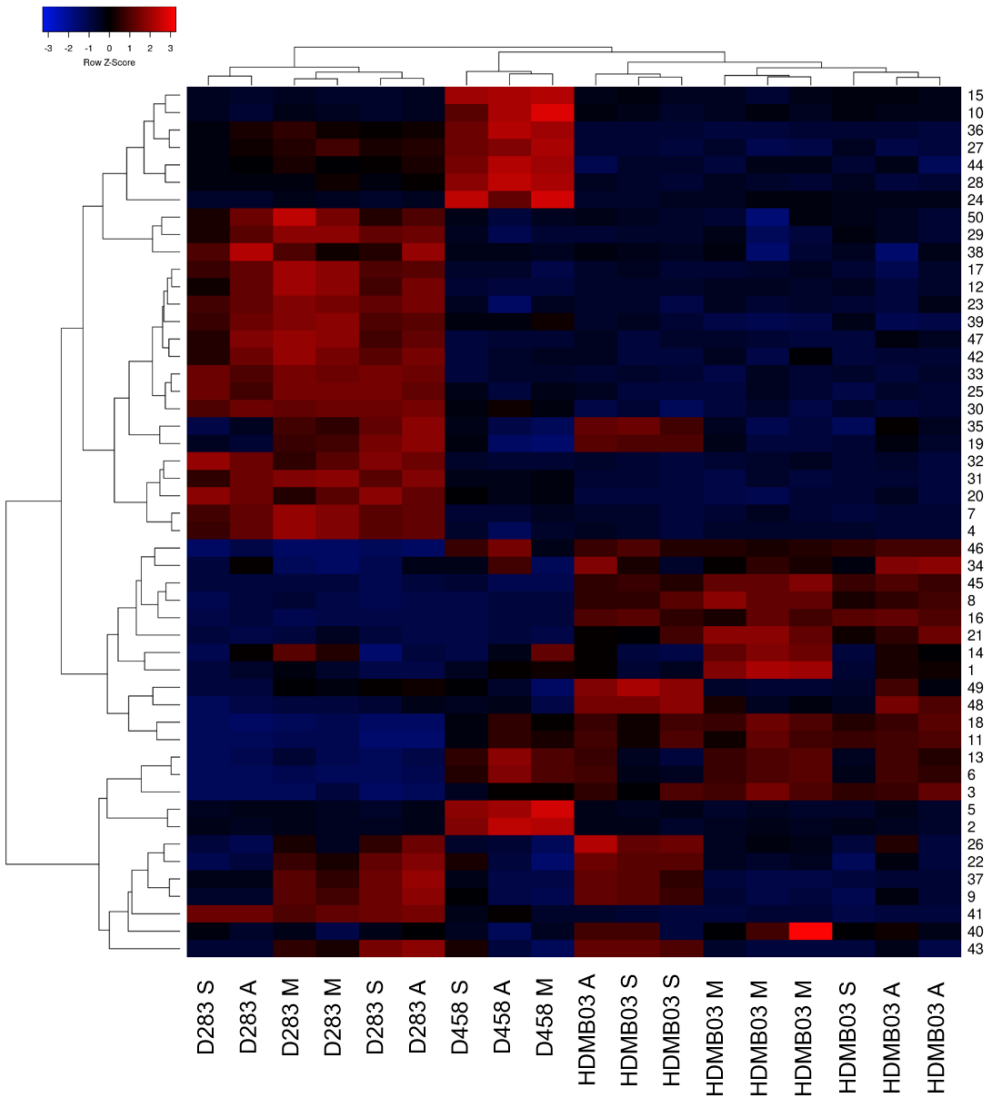
The PCA was performed on all samples using the DESeq2 transformed counts (using variance stabilizing transformation) of all the genes identified in the dataset. The principal components PC1 and PC2 both combined explains 74 % of the variance. This means that 74% of the variables in the original dataset are represented in this PCA plot, showing a decent separation between the different groups

4.3.4 Visualization of genes with large magnitude changes

Unsupervised clustering was performed for all samples based on the top 50 genes with the largest variance across all samples. The gene counts were transformed using DESeq2 variance stabilizing transformation (vst) method. The VST method allows stabilization of the count data to minimize the noise that would result from taking the logarithm of small counts and inflating their variance. This is presented as a heat map generated using the online Heatmapper tool (heatmapper.ca/expression/) (Babicki et al., 2016). The top 50 genes with largest variance resulting from this analysis across all samples (Figure 4.3) corroborated the conclusions drawn from the PCA. Samples clustered based on cell line, and within each cell line the samples from the migrated compartment were most similar. There was some overlap between the samples from the suspension and adherent compartments.

To allow for a quick visual identification of the genes displaying large-magnitude changes which are also statistically significant, volcano plots were constructed. There are two regions of interest in the plot: those points that are found towards the top of the plot (high statistical significance) and the extreme left or right (strongly down and upregulated respectively). The top 10 significant genes, if any, for each comparison are shown in Figure 4.4.

When comparing the transcriptomes of all 3 cell lines in the migrated compartment to the suspension compartment, 7 genes were significantly overexpressed in M compared to S, while 2 genes were significantly overexpressed in S compared to M. Three of the same genes were significantly overexpressed in M compared to A: *SORCS2*, *GCNT1* and *RN7SK*, while 5 genes were overexpressed in A compared to M although none overlap with the previous comparison. Ten genes were significantly overexpressed in A compared to S, and 2 of these overlaped with the genes overexpressed in M: *SORCS2* and *GCNT1*. This data was used to begin building lists of genes that follow different patterns of expression as the cells move through the three migration compartments.



1	*RN7SK*	11	*KCNIP4*	21	*AFF3*	31	*DISC1*	41	*PIP4K2A*
2	*LINC00824*	12	*NEAT1*	22	*EPB41*	32	*MAB21L2*	42	*KCNMA1*
3	*SLC35F4*	13	*PCAT1*	23	*CNTNAP5*	33	*L1TD1*	43	*LRRC75A*
4	*DPYD*	14	*SORCS2*	24	*FDCSP*	34	*CORO2B*	44	*LINC01483*
5	*PVT1*	15	*TTN*	25	*NEFM*	35	*AL590867.1*	45	*IGFBP2*
6	*CASC8*	16	*ZFAT*	26	*GPS2*	36	*SLC35F3*	46	*BCL11A*
7	*SORBS2*	17	*UNC5C*	27	*AC015522.1*	37	*CALR*	47	*RGS6*
8	*CYP1B1*	18	*AC019197.1*	28	*AL354809.1*	38	*HAS2-AS1*	48	*B4GALT1*
9	*AC092069.1*	19	*GOLGA3*	29	*MIR137HG*	39	*GRAMD1B*	49	*CRLF1*
10	*CCDC26*	20	*TMSB4X*	30	*CADPS*	40	*MT-TW*	50	*LINC01435*

Figure 4.3 Heatmap and unsupervised clustering for all samples.

Unsupervised clustering was performed using DESeq2 transformed counts (using variance stabilizing transformation) of the top 50 genes with the largest variance across all samples. Clustering was done based on the Euclidean distance and complete linkage

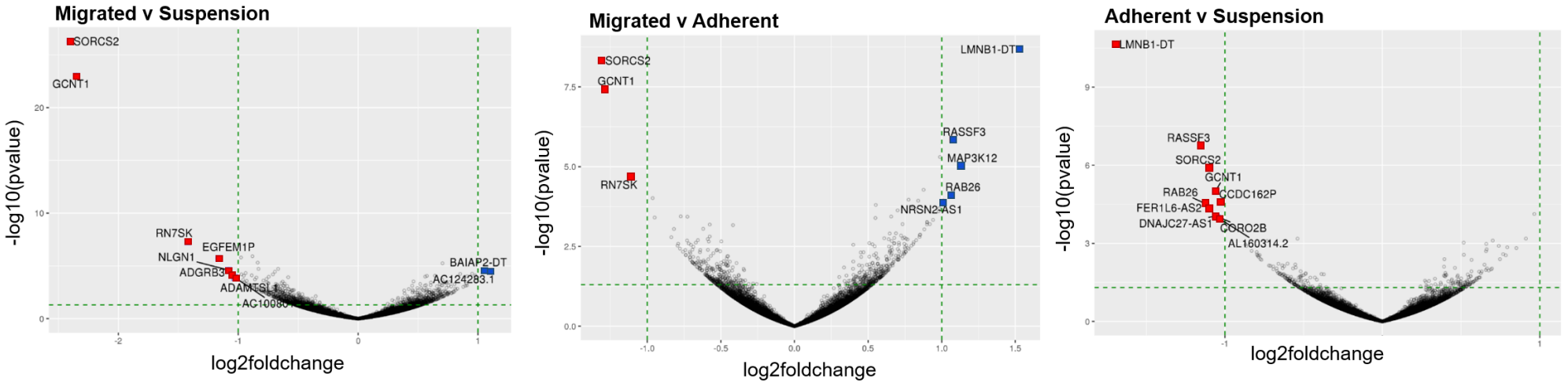


Figure 4.4 Volcano plots to visualize the results of differential expression analysis.

Top 10 significant genes (if any) with the most significant p-value were labelled in the plot. The genes above the p-value threshold (0.05) and log2 fold change threshold (≥1 & ≥-1) were coloured red (upregulated), blue (downregulated). Coloured squares correspond to a false discovery rate (FDR) p-value less than 0.05. The horizontal and vertical dashed green lines represent fold change and significance threshold respectively.

4.3.5 Differentially expressed genes between cell compartments

The mean of normalized counts was calculated for replicate samples, and the cell compartments were each compared within each of the 3 cell lines. The results of differential expression analysis were filtered using the log2 fold change threshold of ≥+/-1, the p-value <0.05, and the mean normalized count >10. Genes were classed as either upregulated, downregulated or unchanged. The top 25 genes for each comparison within each cell line are detailed Appendix 2 Tables 1-18.

With such a complex set of data presented in Appendix 2 Tables 1-18, it was decided to undertake Gene Set Enrichment Analysis (https://www.gsea-msigdb.org/gsea/index.jsp) (Subramanian et al., 2005, Mootha et al., 2003) to determine whether differentially expressed genes between cell compartments overlapped with annotated gene sets in the Molecular Signatures Database (MSigDB) (Subramanian et al., 2005, Liberzon et al., 2011). See Chapter 2 section 2.10 for the method.

Table 4.3 and Table 4.4 summarise the GO terms that that best describe the function of genes showing differential expression between the migrated compartment (M) and the adherent compartment (A; Table 4.3) or between M and the suspension compartment (S; Table 4.4). The genes overexpressed in the M compartment compared to both the A and S compartment were described by GO terms including cell projection organization (GO:0030030), cellular macromolecule localization (GO:0070727) and cytoskeleton organization (GO:0007010). The overlaps with cell projection organization and cytoskeleton organization are particularly interesting, as these are two events that occur in the process of migration. Inspection of the GO terms best defining the genes overexpressed in the A and S compartments (See Appendix 2 Tables 19-22) did not identify these migration-related processes, further supporting the validity of GO analysis.

As none of the genes overlapping with the GO cell projection organization dataset were found in more than one cell line, the genes expressed in HD-MB03 cells were

investigated further, as this was the cell line with three experimental replicates. The genes described by the GO term cell projection organisation included *ADGRB3* which encodes a brain-specific angiogenesis inhibitor, *NRCAM* which encodes a neuronal cell adhesion molecule, and *SEMA3A* which encodes semaphorin 3A and is known to function as a chemo-attractive agent that stimulates the growth of dendrites.

The GO terms that most significantly describe genes from the A compartment are listed in Appendix 2 Tables 19 and 20. The genes overexpressed in the A compartment compared to both the S compartment and M compartment are described by the GO terms for processes that are linked to energy production in the cell and gene expression changes. These genes related to normal cell processes were also expressed in the S and M compartments, but seemed enhanced in the A compartment. This suggested that while the cells were not migratory, they may have been undergoing changes necessary to prepare for migration.

The GO terms that significantly describe the genes from the S compartment are listed in Appendix 2 Tables 21 and 22.The genes are described by GO terms for energy production, cell cycle regulation, RNA and protein modifications, and other normal cell processes necessary to maintaining cell viability and proliferation in a non-migratory state, and did not differ from gene functions found in the A and M compartments.

This GO analysis led to the conclusion that only the cells in the M compartment appeared different to the other cell compartments based on the function of genes expressed. This correlated with the strong clustering of genes from the migrated compartment in the PCA analysis (**Error! Reference source not found.**) and heat m ap (Figure 4.3). This also supported that the *in vitro* model developed in Chapter 3 allowed the separation of migrated cells from the bulk of non-migratory cells.

Table 4.3 GSEA Migrated > Adherent across 3 cell lines.

Gene set enrichment analysis (GSEA) was used to identify the top 21 Gene Ontology (GO) gene sets that significantly overlapped with the genes upregulated in the migrated compartment compared to the adherent compartment (M>A). Significance was defined based on a non-adjusted p-value and a p-value adjusted using the Benjamini-Hochberg false Discovery Rate (FDR) method (FDR q-value).

Gene set	Gene #	p-value	FDR q-value
GO Intracellular Transport (GO:0046907)	50	7.39 e-12	4.16e-8
GO Cellular Macromolecular Localization (GO:0070727)	51	8.82e-12	4.16e-8
GO ATPASE Activity (GO:0016887)	23	4.41e-11	1.39e-7
GO Drug binding (GO:0008144)	46	1.36e-10	3.2e-7
GO Adenyl Nucleotide Binding (GO:0030554)	42	4.88e-10	9.21e-7
Go Ribonucleotide Binding (GO:0032553)	46	2.51e-9	3.95e-6
GO Intracellular Protein Transport (GO:0006886)	34	4.54e-9	6.11e-6
GO Cellular Response To DNA Damage Stimulus (GO:0006974)	28	7.96e-9	9.38e-6
GO Chromosome Organization (GO:0051276)	33	3.73e-8	3.91e-5
GO Cell Projection Organization (GO:0030030)	37	9e-8	8.02e-5
GO RNA Binding (GO:0003723)	43	9.36e-8	8.02e-5
GO Positive Regulation of Gene Expression (GO:0010628)	43	1.94e-7	1.48e-4
GO Hydrolase Activity Acting on Acid AD Anhydrides (GO:0016817)	27	2.04e-7	1.48e-4
GO Cell Cycle (GO:0007049)	41	2.35e-7	1.58e-4
GO Recombinational Repair (GO:0000725)	10	3.24e-7	2.04e-4
GO Double Strand Break Repair (GO:0006302)	13	4.27e-7	2.38e-4
GO Regulation of Cellular Response to Stress (GO:0080135)	23	4.3e-7	2.38e-4
GO Protein Containing Complex Localization (GO:0031503)	14	4.64e-7	2.43e-4
GO Peptidyl Amino Acid Modification (GO:0018193)	31	5.79e-7	2.87e-4
GO DNA Templated Transcription Initiation (GO:0006352)	13	6.79e-7	3.2e-4
GO Cytoskeleton Organization (GO:0007010)	30	4.92e-6	1.49e-3

Table 4.4 GSEA Migrated > Suspension across 3 cell lines.

Gene set enrichment analysis (GSEA) was used to identify the top 20 Gene Ontology (GO) gene sets that significantly overlapped with the genes upregulated in the migrated compartment compared to the suspension compartment (M>S). Significance was defined based on a non-adjusted p-value and a p-value adjusted using the Benjamini-Hochberg false Discovery Rate (FDR) method (FDR q-value).

Gene set	Gene #	p-value	FDR q-value
GO Adenyl Nucleotide Binding (GO:0030554)	59	2.05 e-14	1.88 e-10
GO Ribonucleotide Binding (GO:0032553)	64	3.86 e-13	1.77 e-9
GO Drug Binding (GO:0008144)	60	7.34 e-13	2.25 e-9
GO Neurogenesis (GO:0022008)	56	3.54 e-12	7.32 e-9
GO Regulation of Intracellular Signal Transduction (GO:1902531)	61	3.98 e-12	7.32 e-9
GO Protein Phosphorylation (GO:0006468)	63	6.38 e-12	9.72 e-9
GO Neuron Differentiation (GO:0030182)	50	7.4 e-12	9.72 e-9
GO Animal Organ Morphogenesis (GO:0009887)	41	8.83 e-11	1.01 e-7
GO Cell projection organization (GO:0030030)	51	1.33 e-10	1.36 e-7
GO Kinase Activity (GO:0016301)	34	1.75 e-10	1.61 e-7
GO Cytoskeleton Organization (GO:0007010)	46	2.39 e-10	1.72 e-7
GO Enzyme Regulator Activity (GO:0030234)	40	2.42 e-10	1.72 e-7
GO Circulatory System Development (GO:0072359)	43	2.5 e-10	1.72 e-7
GO GTPase Regulator Activity (GO:0030695)	21	2.62 e-10	1.72 e-7
GO Positive Regulation of Molecular Function (GO:0044093)	55	3.62 e-10	2.22 e-7
GO Tube Development (GO:0035295)	41	6.34 e-10	3.64 e-7
GO Cellular Macromolecule Localization (GO:0070727)	57	7.8 e-10	4.21 e-7
GO Cellular Component Morphogenesis (GO:0032989)	41	8.24 e-10	4.21 e-7
GO Positive Regulation of Catalytic Activity (GO:0043085)	47	1.07 e-9	5.16 e-7
GO Transferase Activity Transferring Phosphorus Containing Groups (GO:0016772)	36	1.39 e-9	6.37 e-7

4.4 Identifying patterns of gene expression

4.4.1 Patterns of gene expression across cell lines

While the GO analysis identified interesting biological processes consistent with the experimental model, the power of RNA-seq analysis comes from the ability to investigate individual genes. In order to narrow down the gene lists and identify targets playing a possible role in cell migration, the gene lists for each cell compartment were compared across the 3 cell lines using Gene List Venn Diagram (http://genevenn.sourceforge.net/) and the results are presented in Figure 4.5-4.7. See Chapter 2 section 2.11 for the method.

The genes that were differentially expressed between compartments in all 3 cell lines, or in the two cell lines HD-MB03 and D283-MED were separated from genes differentially expressed in only one cell line. As described in section 4.2, only one sample was sequenced for each compartment from cell line D458-MED. As the significance of differential expression was not corrected by any replicates, D458-MED gene expression was used to strengthen the selection of genes also expressed in both HD-MB03 and D283-MED, but not genes expressed in D458-MED only or D458-MED and one other cell line. An example of this strategy is shown in Figure 4.5 B where the 12 genes overlapping between HD-MB03 and D458-MED are not considered further, but the 5 genes that are shown to be differentially expressed in D283-MED and HD-MB03 (overlap between blue and green in the Venn diagram) are included.

Following these criteria, the gene sortilin related VPS10 domain containing receptor 2 (*SORCS2*) was upregulated in the migrated compartment compared to the adherent compartment (M>A) in all three cell lines. A further 2 genes, glucosaminyl (N-acetyl) transferase 1 (*GCNT1*) and *FRAS1*-related extracellular matrix 2 (FREM2), were upregulated in HD-MB03 and D283-MED (Figure 4.5 A). 6 genes were upregulated in migrated compartment compared to suspension compartment (M>S) in all three cell lines, and a further 5 in two cell lines (Figure 4.5 B). 5 genes were upregulated in adherent compartment compared to migrated compartment (A>M) in three cell lines

and a further 3 genes in two cell lines (Figure 4.6 A). 2 genes were upregulated in adherent compartment compared to suspension compartment (A>S) in three cell lines, and a further 5 genes in two cell lines (Figure 4.6 B). In the suspension compartment, 2 genes were upregulated compared to migrated compartment (S>M) in two cell lines (Figure 4.7 A), and 2 genes were upregulated compared to the adherent compartment (S>A) (Figure 4.7 B). The divergent transcript for BAR/IMD domain containing adaptor protein 2 (*BAIAP2-DT*) was upregulated in the suspension compartment compared to both the migrated and adherent compartments in both HD-MB03 and D283-MED.

All genes upregulated or downregulated in one cell compartment compared to another across at least two cell lines (HD-MB03 and D283-MED) or three cell lines are summarised in (Table 4.5).

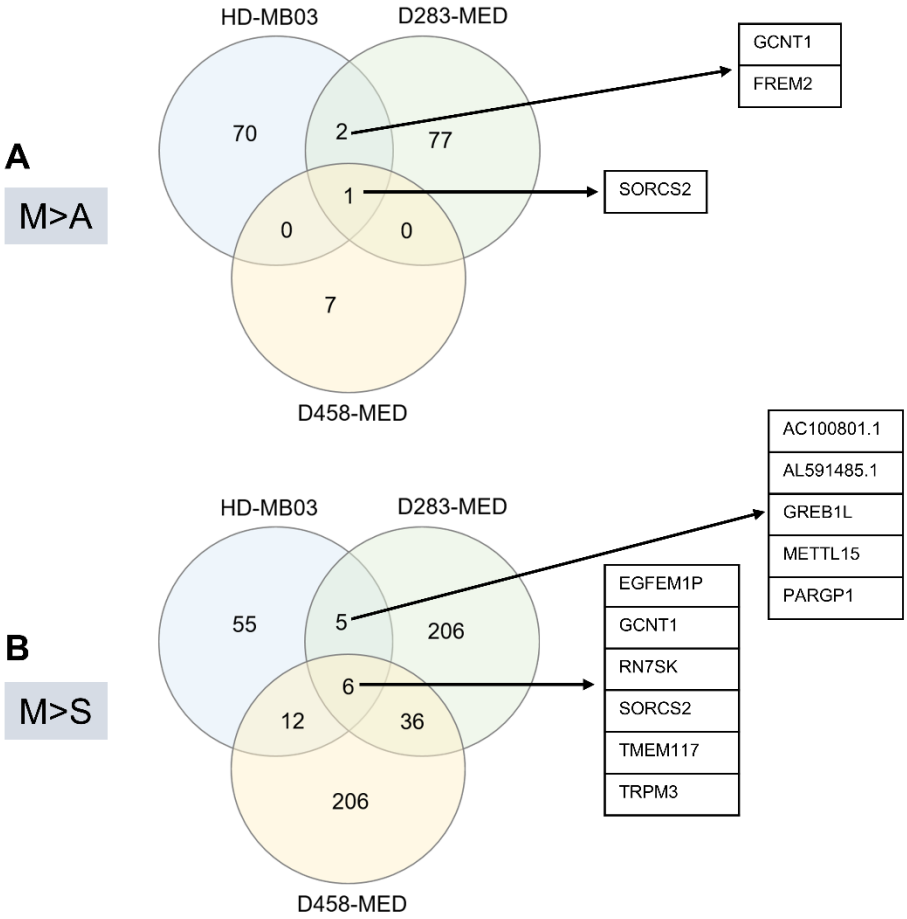


Figure 4.5 Genes overexpressed in the migrated compartment.

Gene lists were compared across the three cell lines using Gene List Venn Diagram. Genes that were found in all three cell lines, or the two cell lines HD-MB03 and D283-MED are shown.

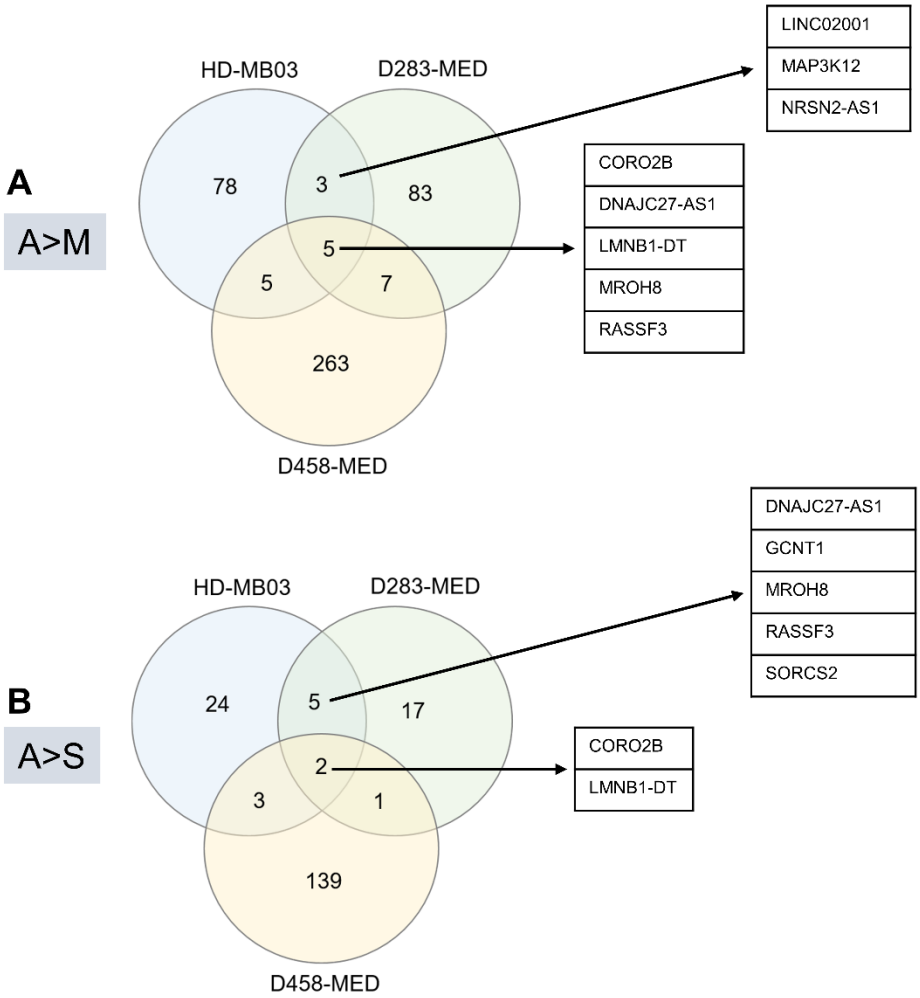


Figure 4.6 Genes overexpressed in the Adherent compartment.

Gene lists were compared across the three cell lines using Gene List Venn Diagram. Genes that were found in all three cell lines, or the two cell lines HD-MB03 and D283-MED are shown.

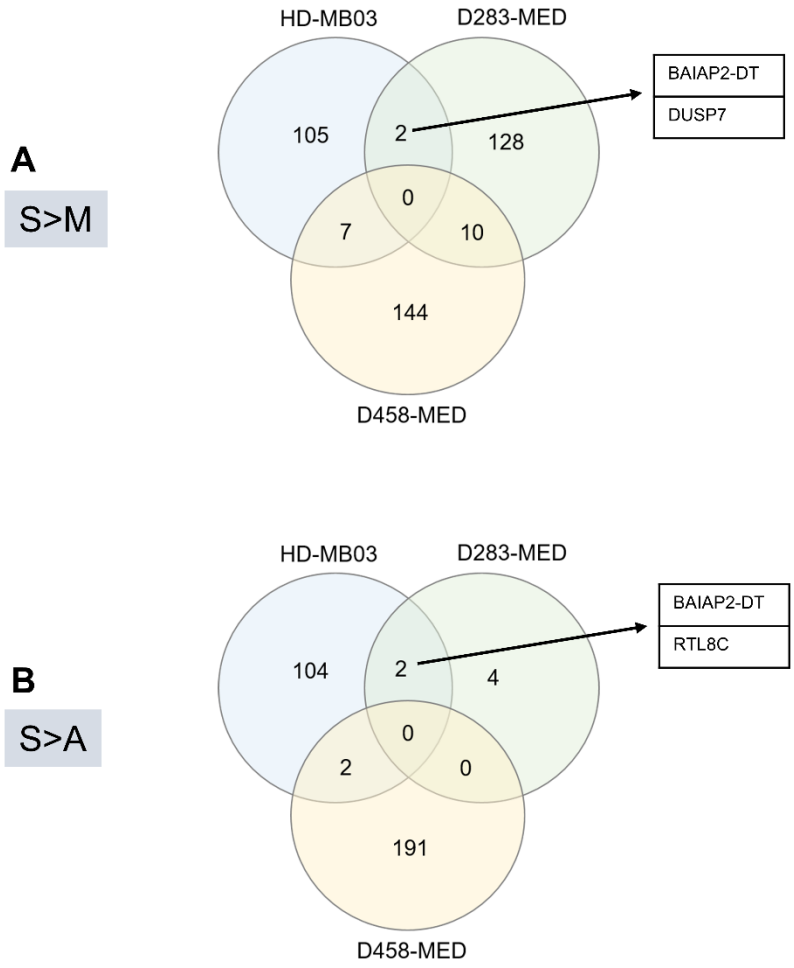


Figure 4.7 Genes overexpressed in the suspension compartment.

Gene lists were compared across the three cell lines using Gene List Venn Diagram. Genes that were found in all three cell lines, or the two cell lines HD-MB03 and D283-MED are shown.

Table 4.5 List of upregulated and downregulated genes

All the genes from Figure 4.5, Figure 4.6 and Figure 4.7 are shown.

		Upregulated in S	Upregulated in A	Upregulated in M
Downregulated in	S	/	*CORO2B* *DNAJC27-AS1* *GCNT1** *LMNB1-DT* *MROH8* *RASSF3* *SORCS2**	*AC100801.1* *AL591485.1* *EGFEM1P* *GCNT1** *GREB1L* *METTL15* *PARGP1* *RN7SK* *SORCS2** *TMEM117* *TRPM3*
	A	*BAIAP2-DT* *RTL8C*	/	*FREM2* *GCNT1** *SORCS2**
	M	*BAIAP2-DT* *DUSP7*	*CORO2B* *DNAJC27-AS1* *LINC02001* *LMNB1-DT* *MAP3K12* *MROH8* *NRSN2-AS1* *RASSF3*	/

* Genes were overexpressed in both the adherent and migrated compartments.

4.4.2 Patterns of gene expression across cell compartments

Up until this point, differential expression has been studied between two cell compartments only. The *in vitro* cell migration model designed allowed for the transition of cells through three compartments, it was therefore investigated whether any genes followed a pattern of expression across all three compartments. Four possible patterns of expression to study were defined.

In the first pattern, gene expression increases as cells transition from the suspension compartment to the adherent compartment, and increases further as cells transition to the migration compartment (S<A<M). In the HD-MB03 cell line, three genes followed this pattern. Two of these same genes followed this pattern in the cell line D283-MED (Figure 4.8), *SORCS2* and *GCNT1*. These genes may be involved in cell processes that enable adhesion to and migration through a basement membrane.

Another possible pattern is an upregulation in gene expression as cells transition from the suspension compartment to the adherent compartment, and downregulation from the adherent compartment to the migrated compartment (S<A>M). Only one transcript followed this pattern in the HD-MB03 cell line, and none in D283-MED or D458-MED (Figure 4.9). Lamin B1 divergent transcript (*LMNB1-DT*) was increased in the adherent compartment compared to the suspension compartment (A>S) and the migrated compartment (A>M) in both HD-MB03 and D283-MED. *LMNB1-DT* may be involved in cell processes allowing adhesion to the basement membrane.

A third possible pattern of expression is an upregulation as cells transition from suspension to adherent, followed by no change in gene expression between adherent and migrated (S<(A=M)). Genes following this pattern may enable cells to transition from suspension to adherent and are maintained in migrating cells. Over 10,000 genes were not significantly changed between adherent and migrated compartments in all three cell lines. Although several genes seemed to follow this pattern of expression, there were no overlaps between the three cell lines (Figure 4.10). It has been shown earlier that the gene poly(ADP-ribose) glycohydrolase

pseudogene 1 (*PARGP1*) was upregulated in the migrated compartment compared to the suspension compartment in both HD-MB03 and D283-MED (Figure 4.5 B).

Finally, genes that were overexpressed in suspension cells and downregulated as the cells transitioned into the adherent compartment and then the migrated compartment (S>A>M) were investigated. However, no genes followed this pattern (Figure 4.11).

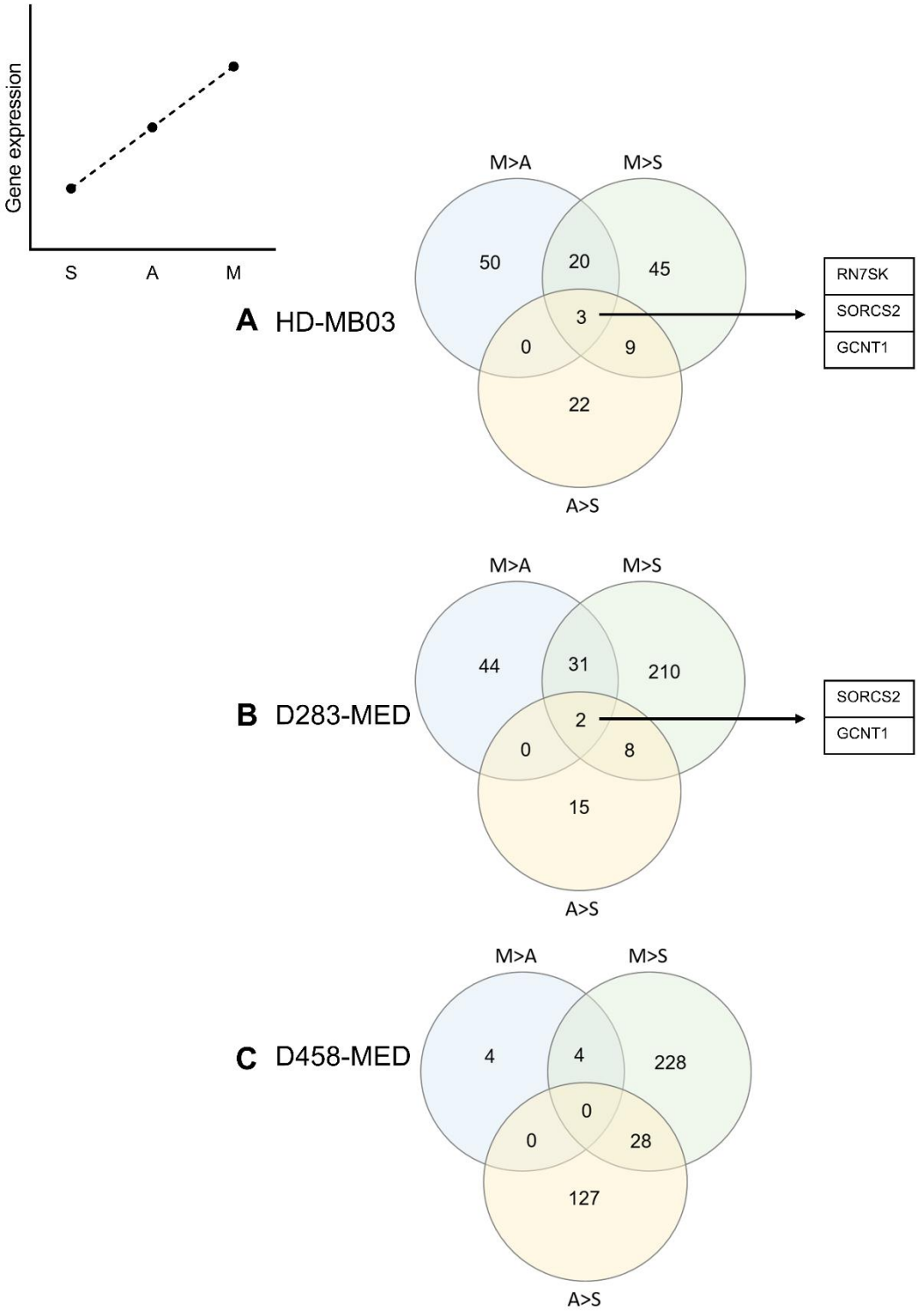


Figure 4.8 Genes following the pattern S<A<M

Gene lists were compared across the three cell lines using Gene List Venn Diagram.

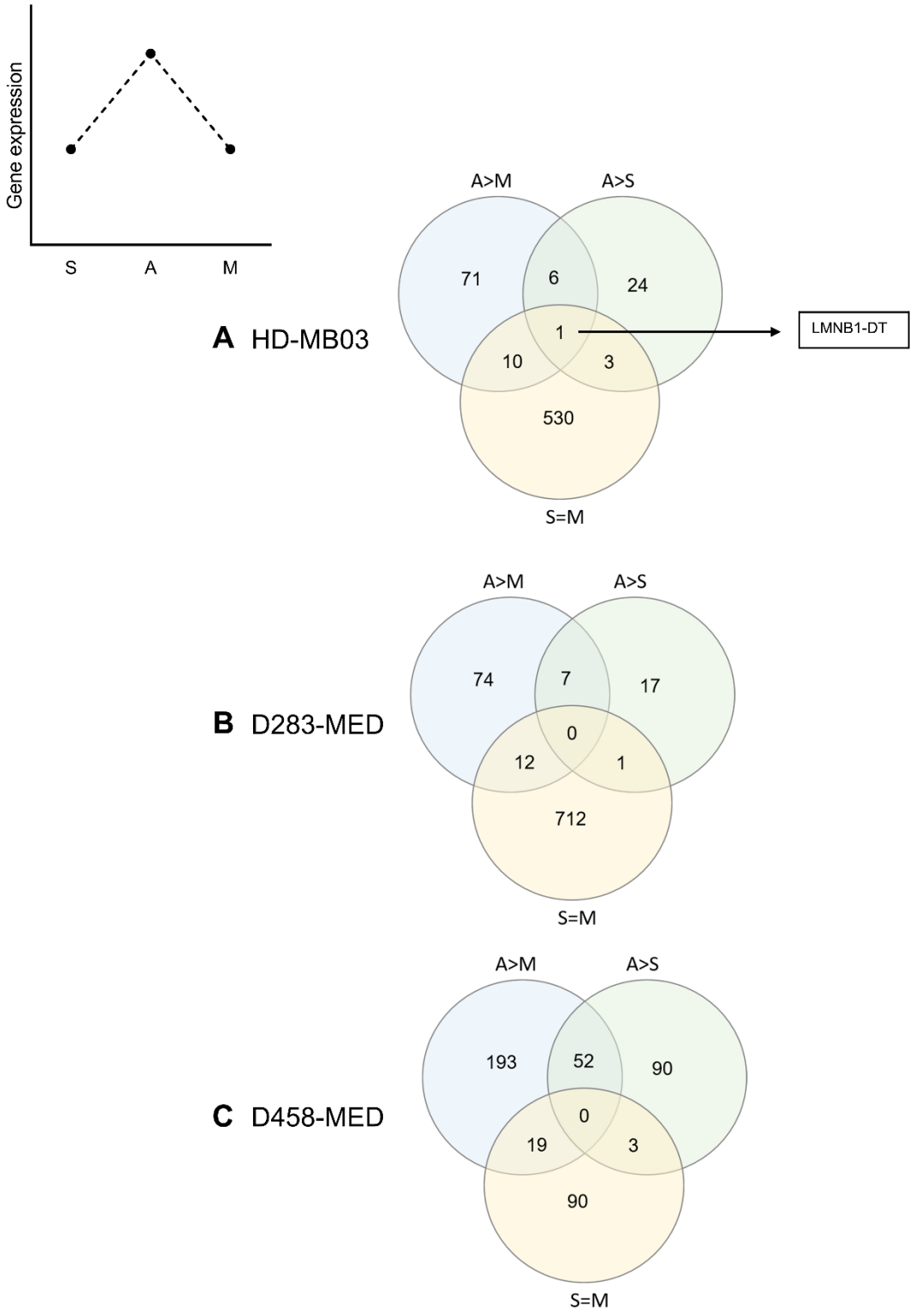


Figure 4.9 Genes following the pattern S<A>M

Gene lists were compared across the three cell lines using Gene List Venn Diagram.

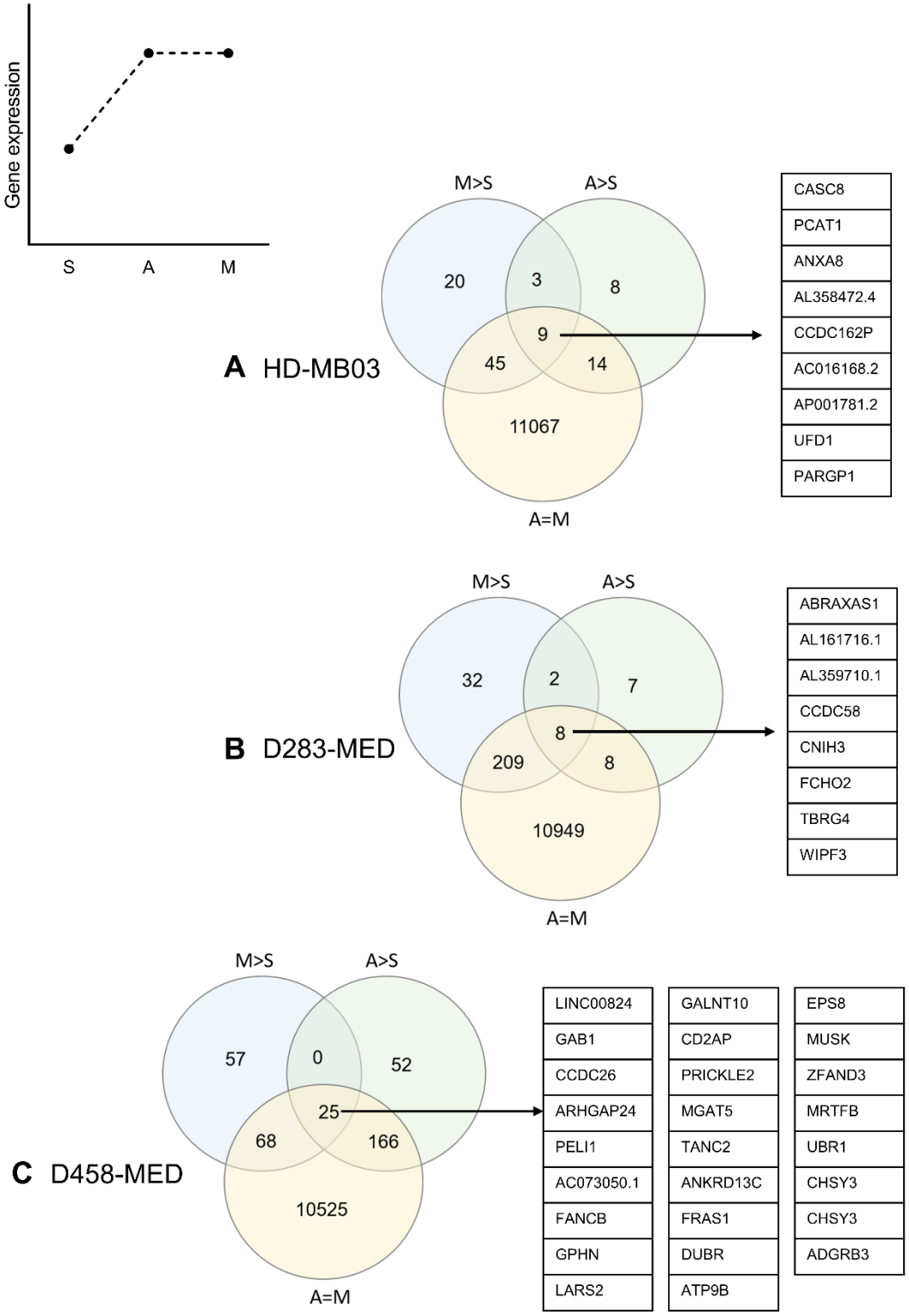


Figure 4.10 Genes following the pattern S<(A=M)

Gene lists were compared across the three cell lines using Gene List Venn Diagram.

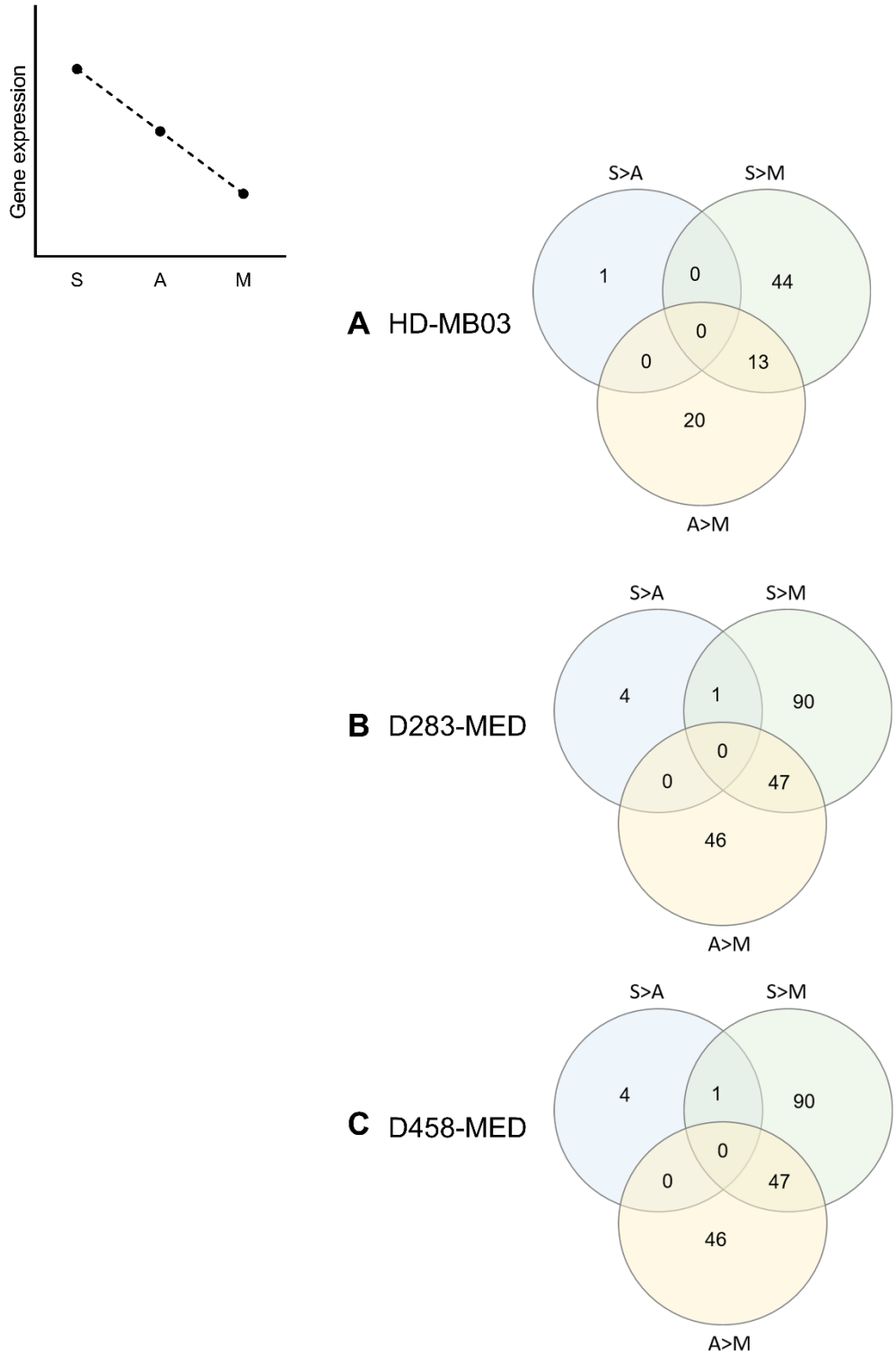


Figure 4.11 Genes following the pattern S>A>M

Gene lists were compared across the three cell lines using Gene List Venn Diagram.

4.5 Identifying target genes involved in migration and metastasis

The gene expression data from this study offers a breadth of information which could be interpreted in many different ways. To remain in line with the aims to identify and validate novel target genes that play a role in migration and metastasis, the gene lists that followed the pattern S<A<M (Figure 4.8) and genes that were upregulated in part of this pattern: A>S (Figure 4.6 B) or M>A (Figure 4.5 A) or M>S (Figure 4.5 B) were investigated further. It was hypothesized that these genes play a role in cell processes that lead to either the adhesion of cells to a basement membrane matrix and/or the migration of cells through the basement membrane towards CSF. In order to select one or more genes for functional validation experiments, the expression of these genes was analysed in publicly available medulloblastoma patient datasets.

The transcripts were categorised based on whether they were upregulated in:

- The adherent compartment (A): *CORO2B, LMNB1-DT, RASSF3, DNAJC27-DT*
- The migrated compartment (M): *GREB1L, METTL15, PARGP1, RN7SK, TMEM117, TRPM3, FREM2*
- Both the A and M compartments: *SORCS2*, *GCNT1*

All of these transcripts and their known functions are described in Table 4.6 and Table 4.7.

Table 4.6 Genes upregulated in the migrated compartment.

The genes upregulated in the migrated compartment compared to the adherent and suspension compartments (M>A and M>S) are shown along with their full names and general function if known.

Gene symbol	Gene name	Function
*GCNT1**	glucosaminyl (N-acetyl) transferase 1	Essential to the formation of Gal beta 1-3(GlcNAc beta 1-6)GalNAc structures and the core 2 O-glycan branch.
*SORCS2**	sortilin related VPS10 domain containing receptor 2	Receptor for the precursor forms of NGF (proNGF) and BDNF (proBDNF) as a heterodimer with $P75^{NTR}$ (NGFR).
FREM2	FRAS1 related extracellular matrix 2	Localizes to the basement membrane, forming a ternary complex that plays a role in epidermal-dermal interactions.
GREB1L	GREB1 like retinoic acid receptor coactivator	Plays a major role in development of early metanephros and genitals.
METTL15	methyltransferase like 15	Probable S-adenosyl-L-methionine-dependent methyltransferase.
PARGP1	poly(ADP-ribose) glycohydrolase pseudogene 1	PARG is the major enzyme responsible for the catabolism of poly(ADP-ribose), a reversible covalent-modifier of chromosomal proteins.
RN7SK	RNA component of 7SK nuclear ribonucleoprotein	Small nuclear non-coding RNA present in small nuclear ribonucleoproteins, negatively regulates genes through P-TEFb activity.
TMEM117	Transmembrane protein 117	Involved in endoplasmic reticulum (ER) stress-induced cell death pathway.
TRPM3	transient receptor potential cation channel subfamily M member 3	Cation-selective channels important for cellular calcium signalling and homeostasis.

* Genes were overexpressed in both the adherent and migrated compartments.

Table 4.7 Genes upregulated in the adherent compartment.

The genes upregulated in the adherent compartment compared to the suspension compartment (A>S) are shown along with their full names and general function if known.

Gene symbol	Gene name	Function
CORO2B	Coronin, actin binding protein, 2B	May play a role in the reorganization of neuronal actin structure.
LMNB1-DT	lncRNA, a divergent transcript of lamin B1	The complement sequence of LMNB1. LMNB1 is one of the two B-type lamin proteins, a component of the nuclear lamina.
RASSF3	Ras association domain family member 3	Plasma membrane GTP-binding protein that modulates intracellular signal transduction pathways.
DNAJC27-AS1	DnaJ heat shock protein family (Hsp40) member C27, antisense RNA	Antisense RNA of DNAJC27. DNAJC27 is a GTPase which can activate the MEK/ERK pathway and induce cell transformation when overexpressed.

4.5.1 Gene expression in patients by subgroup

The expression of genes in medulloblastoma patients was assessed by analysis of a large medulloblastoma patient dataset (Cavalli et al., 2017) using the R2 Genomics Analysis and Visualization Platform (r2platform.com). See Chapter 2 section 2.12 for method. The Cavalli dataset consists of 763 samples representing 4 molecular subgroups. The metastatic status of patients (either M0 or M+) was also known for some patients. Principal component analysis on the patient data showed that patients were clearly grouped into the 4 molecular subgroups of medulloblastoma (see Appendix 2 Supp. Figure 1). Significant differences in gene expression between the 4 subgroups were calculated between groups using the one-way ANOVA with Tukey's multiple comparisons to compare each group to every other group. It was hypothesized that a gene which plays a role in migration and metastasis would be most highly expressed in the most metastatic subgroup, Group 3. *LMNB1-DT* and *DNAJC27-AS1* were not present in the patient dataset, therefore the coding genes for these divergent transcripts were examined as surrogates.

Among the genes upregulated in the migrated compartment *CORO2B* ($p<0.0001$) and *LMNB1* ($p<0.0001$) were most highly expressed in Group 3 medulloblastoma patients (Figure 4.12 A and B). *RASSF3* ($p<0.0001$) and *DNAJC27* ($p<0.0219$) were most highly expressed in the WNT subgroup (Figure 4.12 C and D). WNT is the rarest medulloblastoma subgroup, and also has the lowest incidence of metastasis and best prognosis (Northcott et al., 2012a).

Among the genes upregulated in the adherent compartment, *GREB1L* ($p<0.0001$) and *METTL15* ($p<0.0001$) were most highly expressed in patients with SHH tumours (Figure 4.13 A and B). The expression of *PARG* ($p=0.0003$) and *RN7SK* ($p<0.0001$, $p=0.0004$, $p=0.0124$) was highest in patients with Group 4 tumours (Figure 4.13 C and D). The expression of *PARG* pseudogene 1 (*PARGP1*) was not available in the dataset, therefore the expression of *PARG* was investigated. The small nuclear non-coding RNA *RN7SK* was the most highly expressed transcript out of all the genes studied. The expression of *TMEM117* ($p<0.0001$) was highest in patients with Group

4 and expression of *TRPM3* ($p<0.0001$) was highest in WNT tumours (Figure 4.13 E and F). *FREM2* ($p<0.0001$) was most highly expressed in the WNT subgroup, followed by patients with Group 3 tumours (Figure 4.13 G).

Finally, the genes upregulated in both the migrated and adherent compartments were investigated. In medulloblastoma patients, GCNT1 expression was highest in the WNT subgroup ($p<0.0001$). *SORCS2* expression was highest in the WNT subgroup and Group 3 subgroups (Figure 4.14 A and B). For the gene *SORCS2*, the differences in gene expression were all significant ($p<0.0001$) except the difference between Group 3 and WNT which was not significant.

Based on the analysis of gene expression between subgroups, *LMNB1*, *CORO2B*, *FREM2* or *SORCS2* are of interest for further investigation as these genes were significantly overexpressed in Group 3 compared to at least 2 other subgroups.

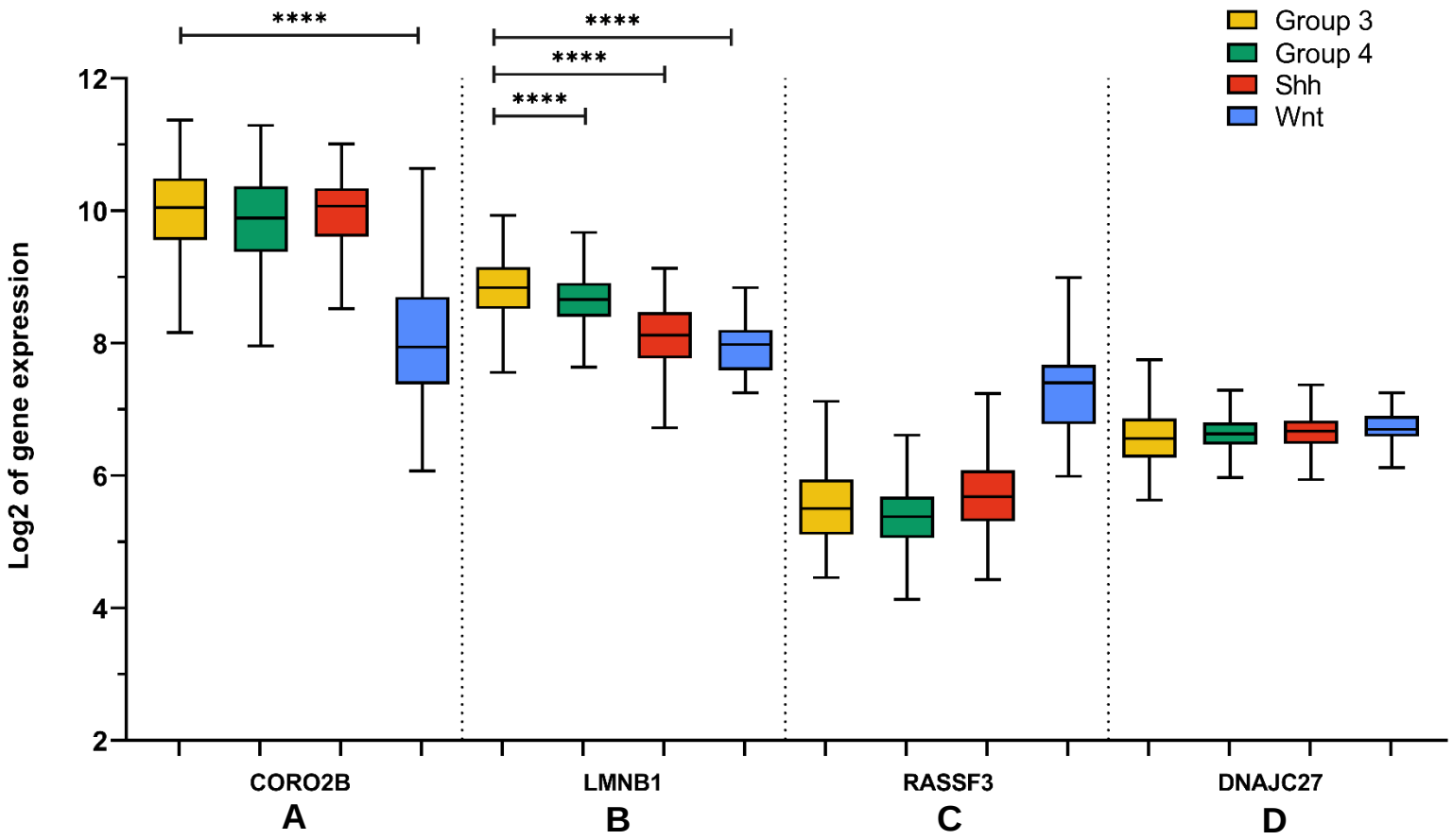


Figure 4.12 CORO2B and LMNB1 are associated with Group 3 subgroup. RASSF3 and DNAJC27 are associated with WNT subgroup.

Gene expression (log2) of genes was assessed using the R2 Genomics Analysis and Visualization Platform using the Cavalli dataset. Group 3 = 144, Group 4= 326, Shh = 223, Wnt = 70. Significant differences in expression between each group were calculated using one-way ANOVA with Tukey's multiple comparisons. Only significant upregulations in Group 3 compared to other groups are shown (**** p<0.0001).

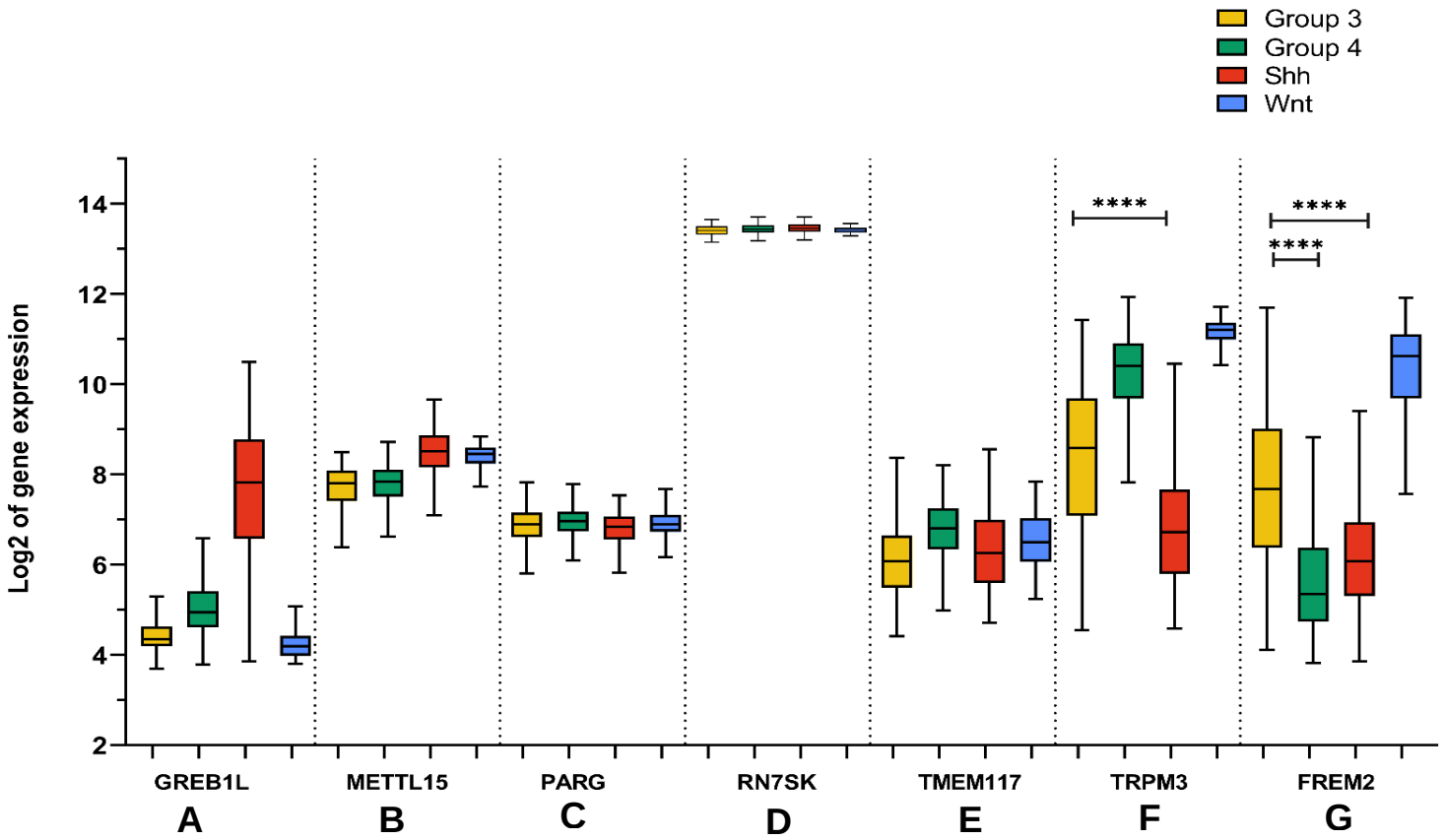


Figure 4.13 GREB1L and METTL15 are associated with SHH. PARG, RN7SK and TMEM117 are associated with Group 4. TRPM3 and FREM2 are associated with WNT.

Gene expression (log2) of genes was assessed using the R2 Genomics Analysis and Visualization Platform using the Cavalli dataset. Group 3 = 144, Group 4= 326, Shh = 223, Wnt = 70. Significant differences in expression between each group were calculated using one-way ANOVA with Tukey's multiple comparisons. Only significant upregulations in Group 3 compared to other groups are shown (**** $p<0.0001$).

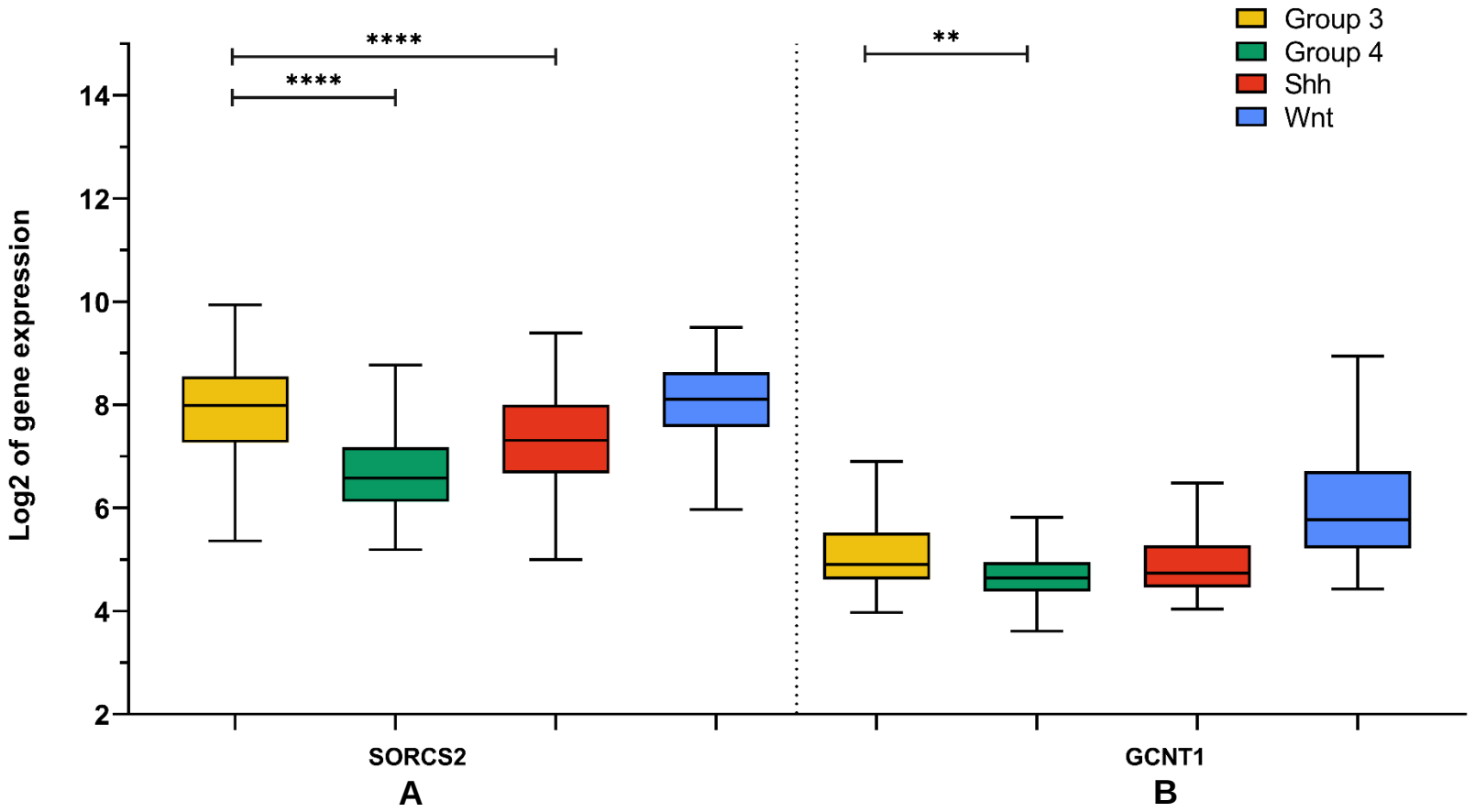


Figure 4.14 Genes expressed in both the adherent and migrated compartments are differentially expressed in medulloblastoma subgroups.

Gene expression (log2) of genes was assessed using the R2 Genomics Analysis and Visualization Platform using the Cavalli dataset. Group 3 = 144, Group 4= 326, Shh = 223, Wnt = 70. Significant differences in expression between each group were calculated using one-way ANOVA with Tukey's multiple comparisons. Only significant upregulations in Group 3 compared to other groups are shown (**** $p<0.0001$, ** $p=0.0013$).

4.5.2 Gene expression in patients by metastatic status

While there are common differences in the occurrence of metastasis between subgroups, metastasis is not restricted to one subgroup. Therefore, the expression of the same genes was investigated between non metastatic (M0) and metastatic (M+) tumours in medulloblastoma patients from the *Cavalli et al*., dataset. Principal component analysis on the patient data showed that patients did not group as clearly based on metastatic status as they did based on subgroup (see Appendix 2 Supp. Figure 2).

In the adherent compartment (A), the expression of genes *CORO2B* ($p=0.0127$) and *LMNB1* ($p<0.0001$) was significantly more expressed in M+ patients compared to M0 patients. In contrast, the genes *RASSF3* and *DNAJC27* were not significantly different between non-metastatic and metastatic tumours (Figure 4.15).

In the migrated compartment (M), the genes *GREB1L* ($p<0.0001$) and *METTL15* ($p<0.0001$) were more highly expressed in non-metastatic tumours compared to metastatic tumours. The rest of the genes, including *FREM2* which had shown a significantly higher expression in Group 3 patients, were not significantly different between patients with M0 and M+ tumours (Figure 4.16).

In both the A and M compartments, *SORCS2* expression showed no significant difference between non-metastatic and metastatic tumours while *GCNT1* ($p=0.0139$) was more highly expressed in non-metastatic tumours (Figure 4.17).

Based on the analysis of expression between non-metastatic and metastatic patients, the genes *CORO2B* and *LMNB1* may play a role in medulloblastoma metastasis. Taken with the conclusion from section 4.5.1, *LMNB1* is the only gene that is overexpressed in Group 3 compared to the other medulloblastoma subgroups as well as in metastatic tumours of all subgroups compared to non-metastatic tumours from all subgroups. These differences in expression between M0 and M+ may also vary within each of the 4 medulloblastoma subgroups.

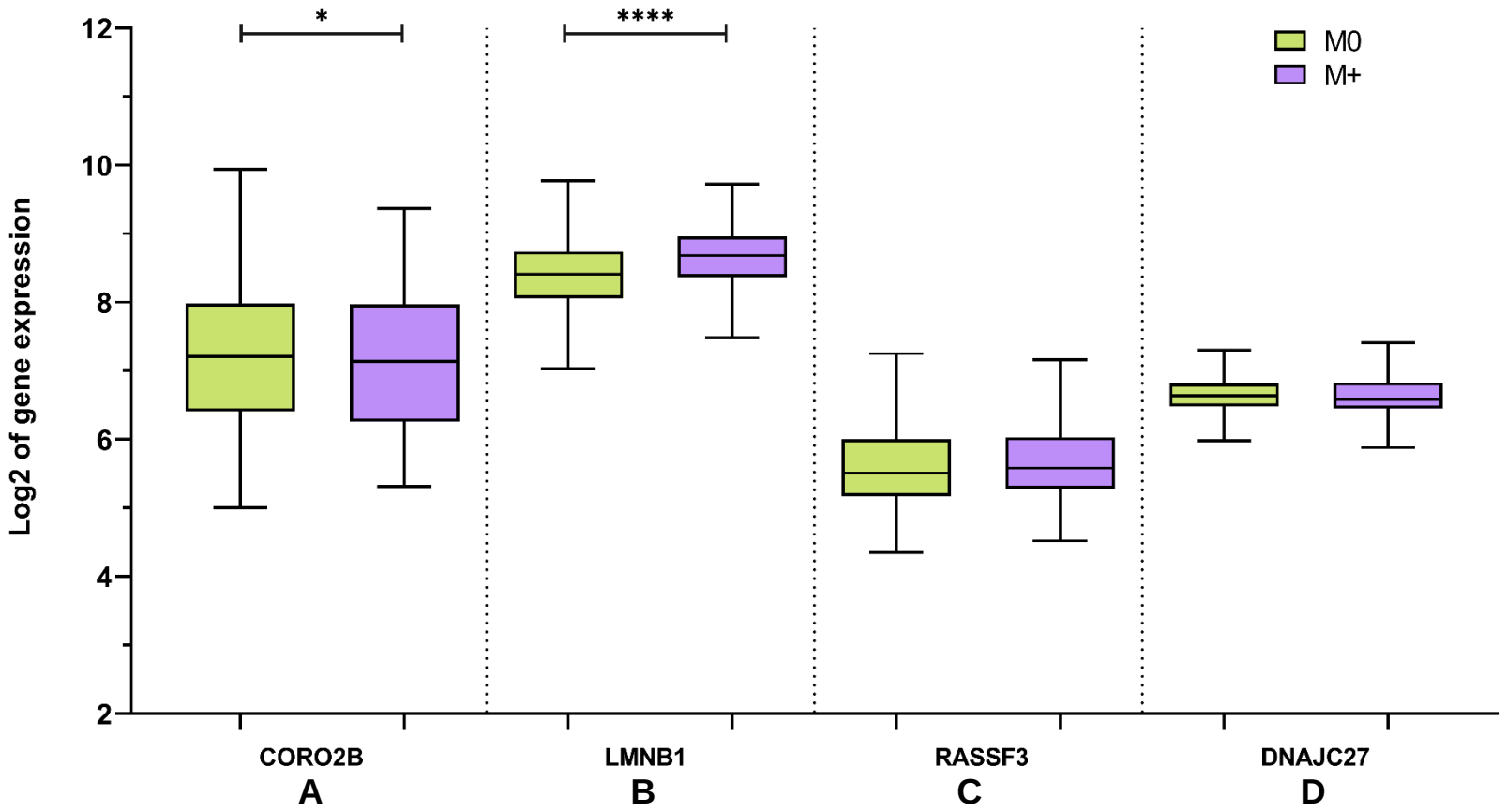


Figure 4.15 Expression of CORO2B and LMNB1 are associated with metastatic tumours.

Gene expression (log2) of genes was assessed using the R2 Genomics Analysis and Visualization Platform using the Cavalli dataset. M0 = 66, M+ = 43. Significant differences in expression between each group were calculated with an unpaired t-test using SEM (**** p<0.0001,* p=0.0127).

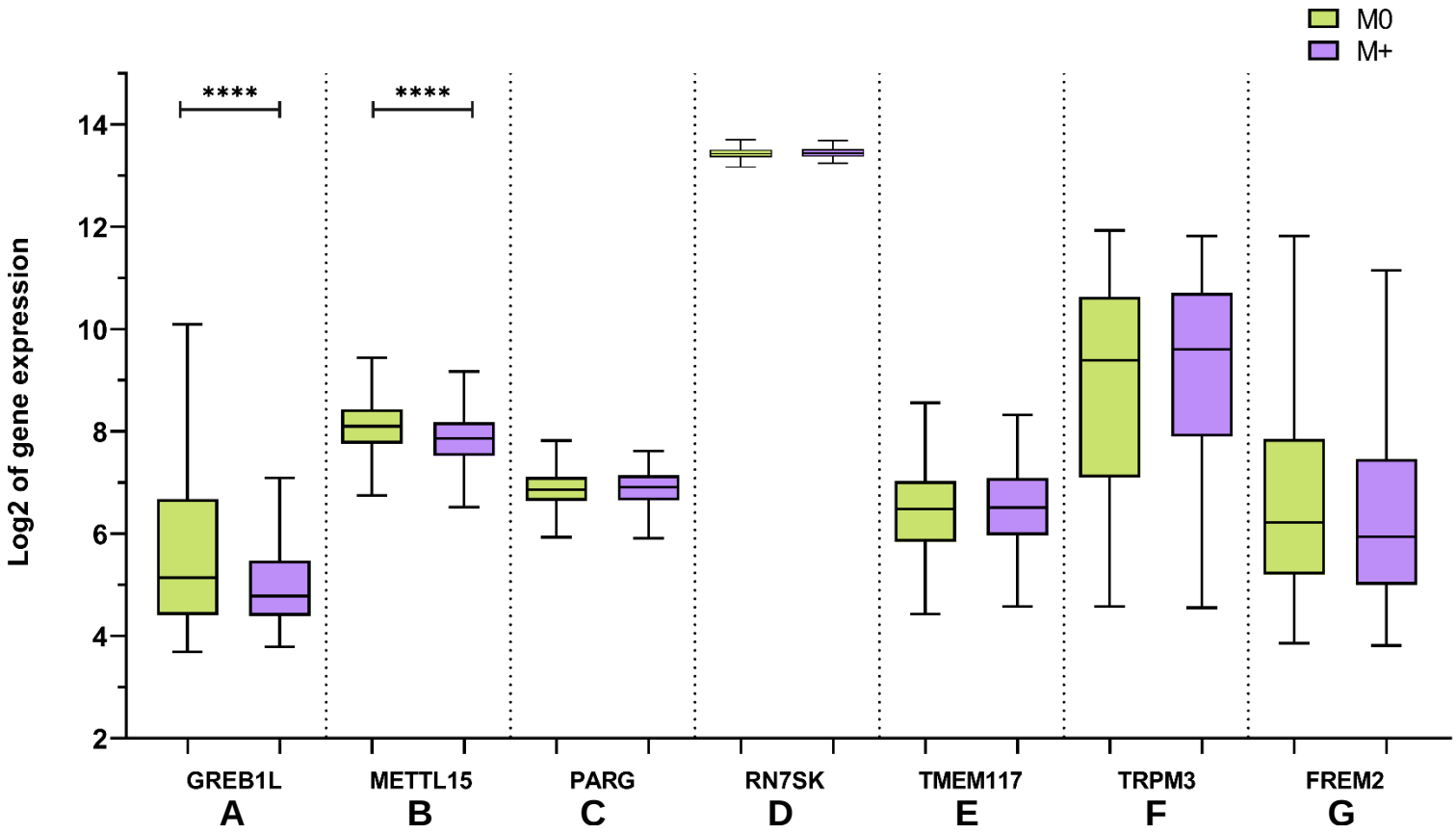


Figure 4.16 Expression of the genes GREB1L and METTL15 in the migrated compartment are associated with non-metastatic tumours.

Gene expression (log2) of genes was assessed using the R2 Genomics Analysis and Visualization Platform using the Cavalli dataset. M0 = 66, M+ = 43. Significant differences in expression between each group were calculated with an unpaired t-test using SEM (**** p<0.0001).

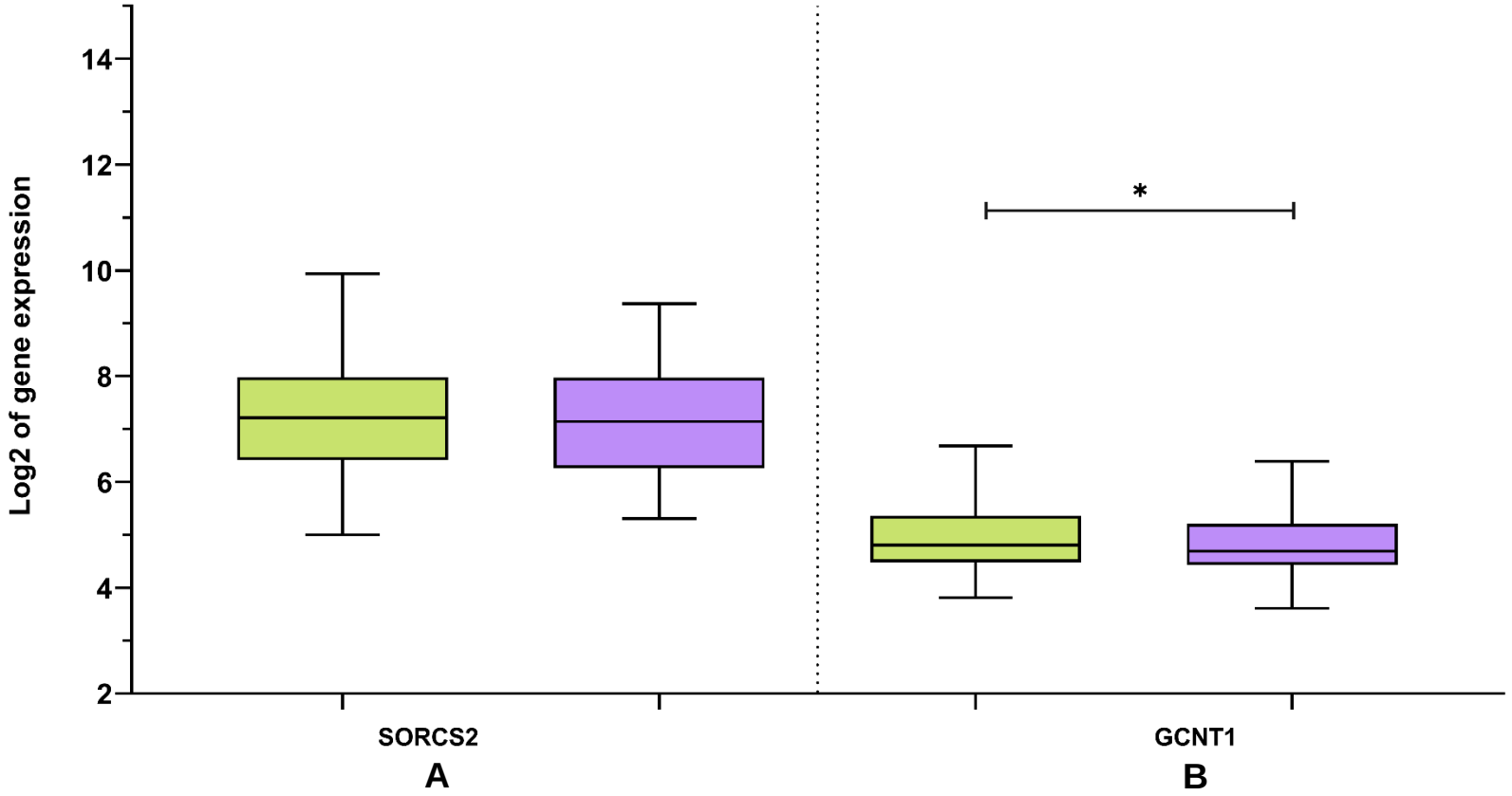


Figure 4.17 Expression of the gene GCNT1 is associated with non-metastatic tumours.

Gene expression (log2) of genes was assessed using the R2 Genomics Analysis and Visualization Platform using the Cavalli dataset. M0 = 66, M+ = 43. Significant differences in expression between each group were calculated with an unpaired t-test using SEM (* p=0.0139).

4.5.3 Patient survival

Kaplan Meier curves are visual representations showing the probability of survival. The survival of medulloblastoma patients based on high or low expression of one gene was assessed by analysis of a large medulloblastoma patient dataset (Cavalli et al., 2017) using the R2 Genomics Analysis and Visualization Platform (r2platform.com). Metastasis is associated with poor survival in medulloblastoma, and it was therefore investigated whether the expression of genes overexpressed in the adherent compartment, migrated compartment, or both, had an effect on patient survival.

In the adherent compartment (A), in patients with high gene expression of *LMNB1* (p=0.057) and *RASSF3* (p=0.013), survival was worst. In contrast, patients with low expression of *DNAJC27* followed a poorer survival trend. The only significant difference in survival between low and high expression was *RASSF3* (Figure 4.18).

In the migrated compartment (M), patients with high expression of *GREB1L*, *METTL15*, *PARG*, *RN7SK*, *TMEM117* and *TRPM3* to be followed a better prognosis trend, but this only reached significance for *TRPM3*. High expression of *FREM2*, however, was associated with a poor prognosis trend (Figure 4.19 and Figure 4.20).

Patients with high expression of *SORCS2* and *GCNT1* appeared to be follow a poor survival trend (Figure 4.21). Although neither of these comparisons was significant, the Kaplan-Meier plot for *SORCS2* showed a steep drop in patient survival within the first 12 months. Medulloblastoma tumours recur within the first 2 years from diagnosis (12 to 20 months) (Ramaswamy et al., 2013), and this may be linked to the patient death within the first year.

Based on the high gene expression in medulloblastoma patients with poor survival, the genes *CORO2B, LMNB1, RASSF3, SORCS2* and *GCNT1* are of interest. In order to correlate this decrease in survival with metastasis, we would have to investigate patient survival filtered by both gene expression and metastatic status. Taken with the results from 4.5.1 and 4.5.2, the gene *LMNB1* was highly expressed

in metastatic tumours, most highly expressed in Group 3 tumours, and high expression of *LMNB1* was found in patients with low survival. The gene *CORO2B* was associated with metastatic tumours, and high expression was also found in patients with poor survival. Finally, the gene *SORCS2* was most highly expressed in Group 3 tumours compared to two other medulloblastoma molecular subgroups, and high expression of *SORCS2* was observed in patients with poor survival during the first 12 months.

Taken together, these observations led to the selection of candidates of interest which met the following criteria: upregulated in patients with either Group 3 tumours, M+ tumours, and highly expressed in patients following a trend of poor survival. The aim was to narrow the list of genes in order to select specific targets for functional validation. Genes upregulated in the conditions listed may have been upregulated to allow cells to migrate, and were therefore of interest in this study. These genes were *SORCS2*, *LMNB1* and *CORO2B*. Future project could also be designed to investigate the downregulated genes and their possible roles in cell migration. When comparing back to the early analyses across all samples sequenced in the study in Section 4.3, *SORCS2* and *CORO2B* were in the top 50 genes with largest variance (Figure 4.3), while *SORCS2* and *LMNB1* were in the top 10 genes with the largest magnitude changes and significance (Figure 4.4). *LMNB1*, *CORO2B* and *SORCS2* were therefore selected for further validation.

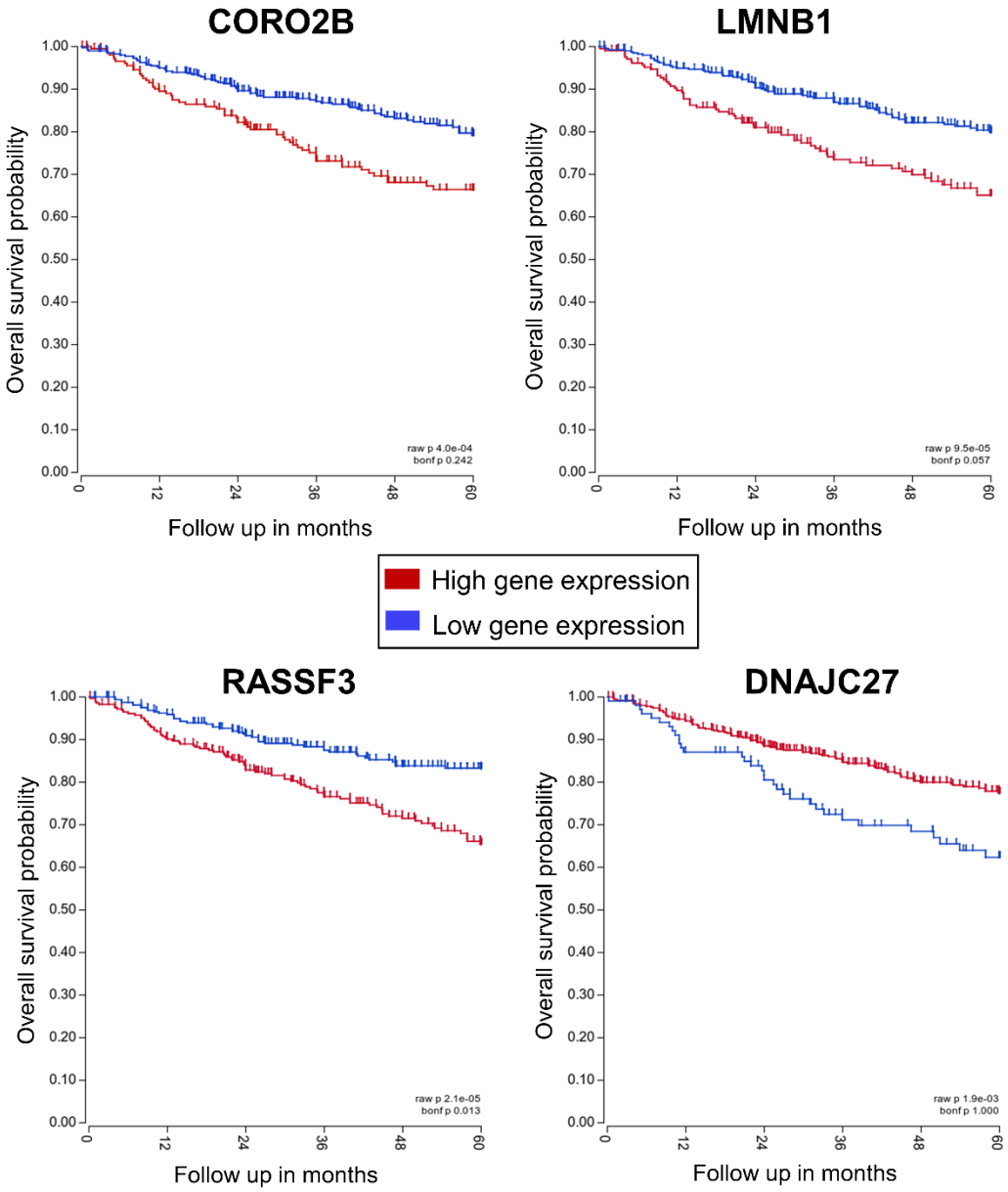


Figure 4.18 Patients with high expression of CORO2B and LMNB1 followed a negative survival trend, although this was not significant. Patients with high expression of RASSF3 had worst survival than patients with low expression. Patients with low expression of DNAJC27 followed a negative survival trend, although this was not significant.

The survival of medulloblastoma patients based on high or low expression of one gene in the Cavalli *et al.* 2017 dataset using the R2 Genomics Analysis and Visualization Platform. CORO2B p=0.242, LMNB1 p=0.057, RASSF3 p=0.013, DNAJC27 p=1.000.

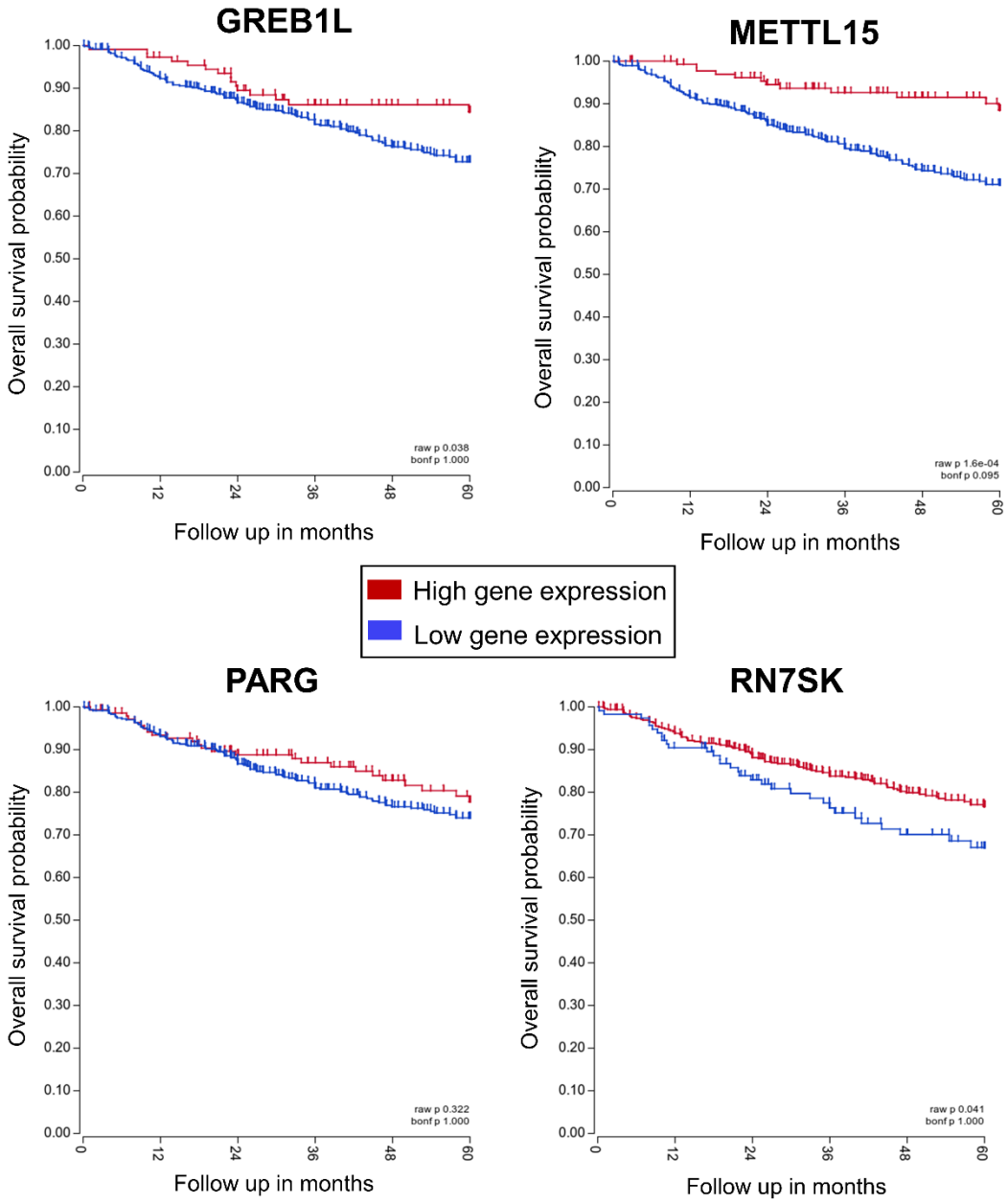


Figure 4.19 Patients with high expression of GREB1l, METTL15, PARG and RN7SK followed a positive survival trend, although this was not significant.

The survival of medulloblastoma patients based on high or low expression of one gene in the Cavalli *et al*. 2017 dataset using the R2 Genomics Analysis and Visualization Platform. For all genes studied, p=ns.

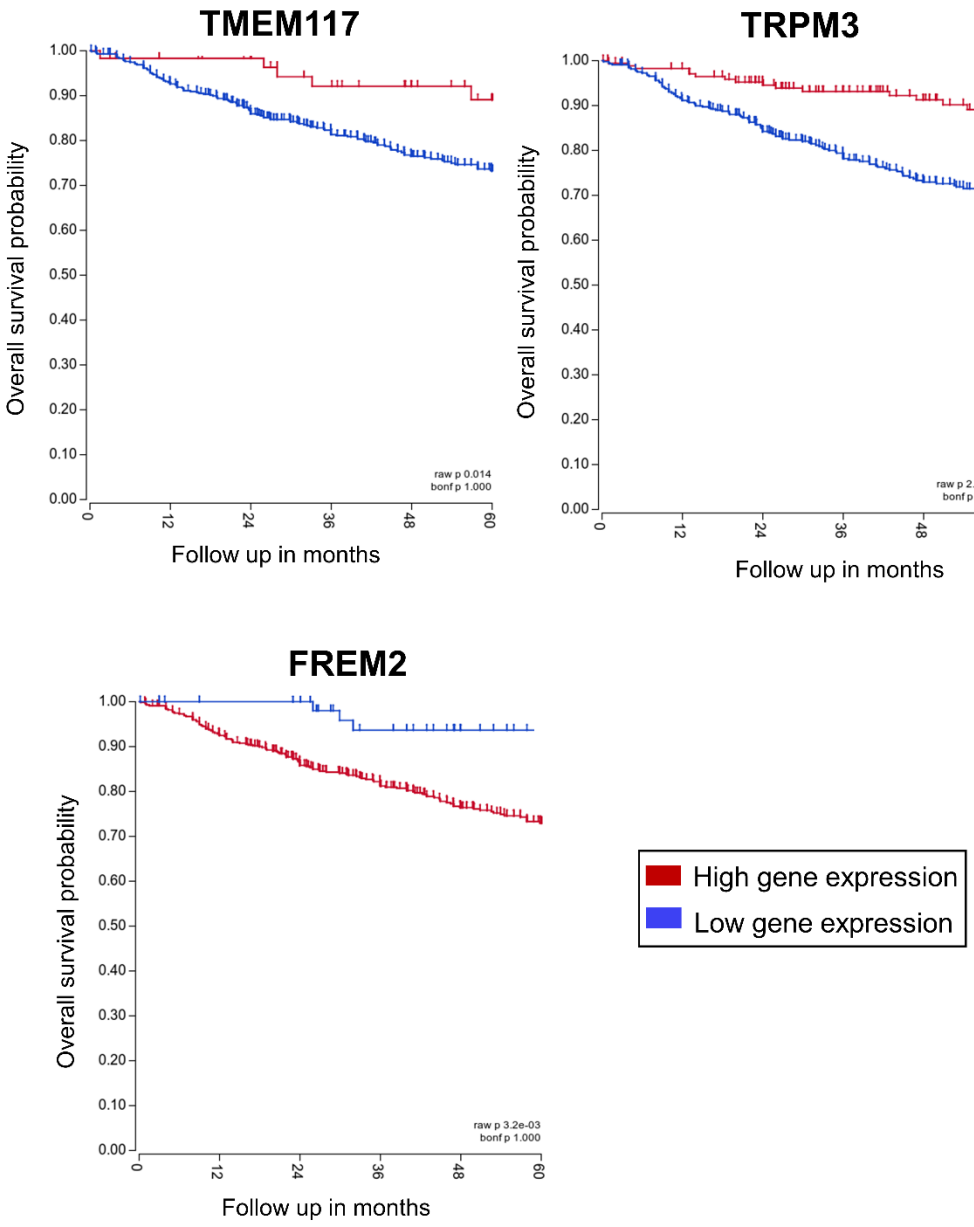


Figure 4.20 Patients with high expression of TMEM117 followed a positive survival trend, although this was not significant. Patients with high expression of TRPM3 had significantly better survival than patients with low expression. Patients with high expression of FREM2 followed a negative survival trend, although this was not significant.

The survival of medulloblastoma patients based on high or low expression of one gene in the Cavalli *et al.* 2017 dataset using the R2 Genomics Analysis and Visualization Platform. TMEM117 p=ns, TRPM3 p<0.05, FREM2 p=ns.

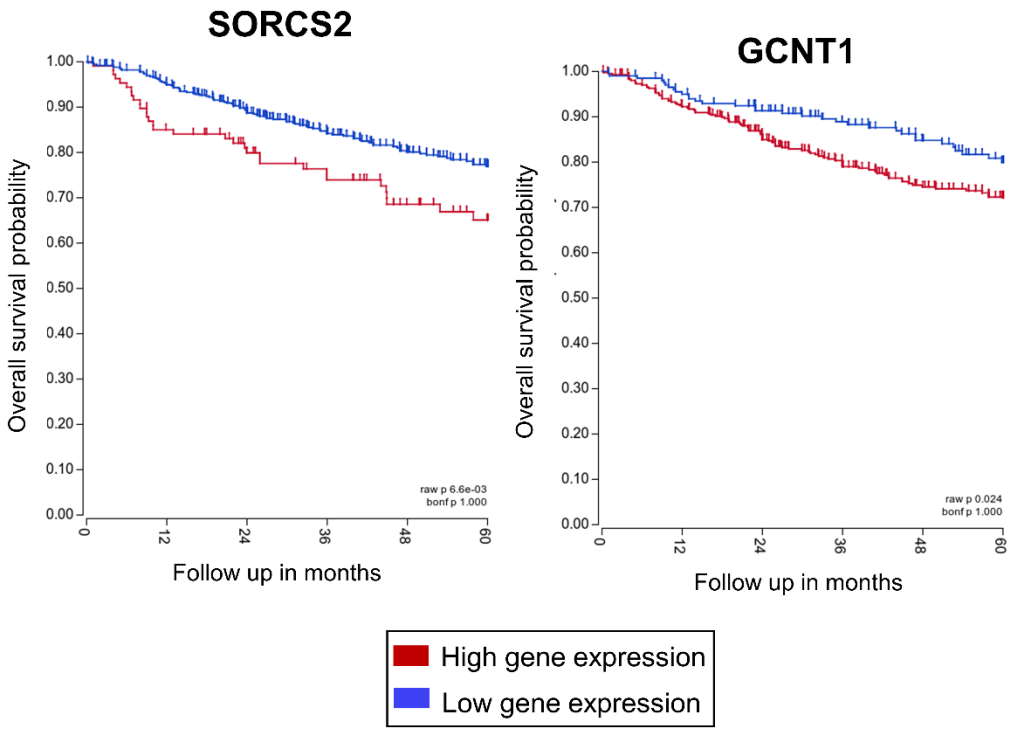


Figure 4.21 Patients with high expression of SORCS2 or GCNT1 followed a worst survival trend, although this was no significant.

The survival of medulloblastoma patients based on high or low expression of one gene in the Cavalli *et al.* 2017 dataset using the R2 Genomics Analysis and Visualization Platform. SORCS2 p=1.000, GCNT1 p=1.000.

4.6 Summary

In order to observe the gene expression changes that occur during cell migration and identify target genes linked to medulloblastoma metastasis, the transcriptomes of three Group 3 cell lines were analysed by 3′ UPX RNA-Seq following separation of cells into three compartments: suspension (S), adherent (A) and migrated (M). After RNA sample quality control, three experimental replicates were sequenced for each compartment from the HD-MB03 cell line, two experimental replicates from the D283-MED cell line, and only one experimental replicate from the D458-MED cell line. The primary component of the variation between samples was cell line, and within each cell line, the migration compartments. Principal component analysis and Gene Ontology analysis validated the separation of migrating cells in the migrated compartment (M) from non-migrating cells in the adherent (A) and suspension (S) compartments.

Patterns of gene expression were observed between cell lines, and between migration compartments. The pattern of expression S<A<M was further investigated in order to identify possible gene targets involved in cell migration that may play a role in metastasis. The expression of genes of interest was assessed in medulloblastoma patient datasets based on molecular subgroup classification and metastatic status of tumours, as well as the effect of low or high gene expression on patient survival outcome.

Based on the analysis of gene expression between subgroups, the transcripts *LMNB1-DT, FREM2 or SORCS2* may be of interest in Group 3 tumours. Based on the analysis of expression between non-metastatic and metastatic patients, the transcripts *CORO2B* and *LMNB1-DT* may be of interest in medulloblastoma metastasis. *CORO2B, LMNB1-DT, RASSF3, SORCS2* and *GCNT1* were highly expressed in patients with poor prognosis. From these candidates, *SORCS2, CORO2B and LMNB1-DT* were selected for further investigation in the context of this project.

Chapter 5 Proposing a novel role for SORCS2 in medulloblastoma migration and metastasis

Aim 3: Validate the expression and function of candidates of interest in medulloblastoma patients and *in vitro*.

5.1 Introduction

In Chapter 4, genes that are likely to be linked to cell migration and medulloblastoma metastasis were identified by comparing the transcriptomes of cells from 3 compartments of migration. From the lists of transcripts differentially expressed in the migrated or adherent cell compartments, *SORCS2, LMNB1-DT,* and *CORO2B* were selected for further investigation based on high expression in patients with Group 3 tumours or metastatic tumours, and high expression resulting in a negative survival trend.

The gene *SORCS2* was one of the top 50 genes with the highest differential expression across all the samples sequenced, and was the most significantly upregulated gene in the migrated compartment compared to both the adherent and suspension compartments. *LMNB1-DT*, a divergent transcript of the gene for lamin B1, and *CORO2B*, encoding the actin binding protein coronin 2B, were among the most significantly upregulated genes in the adherent compartment compared to the suspension compartment. When patient survival was analysed in a large patient dataset, high expression of all 3 genes appeared to be associated with reduce 5-year survival when collectively examining all the medulloblastoma subgroups. Additionally, in patients with high expression of *SORCS2*, a marked drop in survival was observed within the first 12 months, which could be associated with tumour relapse.

SORCS2 is an extracellular receptor for pro-neurotrophins (proNTs) known to play a role in synaptic plasticity. Synaptic plasticity is the modification of strength of signal transmission at a synapse, and is central to brain functions such as memory formation (Citri and Malenka, 2008). The pathophysiology of mood disorders is driven

by impairments in synaptic plasticity, and treatments for these, such as antidepressant drugs and lithium, increase signalling by neurotrophic (NT) factors including SORCS2 ligands. VPS10p receptors bind and sort a diverse array of ligands for secretion, internalization, and sorting by endosomes or lysosomes (Deinhardt et al., 2011, Glerup et al., 2014, Glerup et al., 2016). The ligands pro-nerve growth factor (proNGF) and pro-brain derived neurotrophic factor (proBDNF) can trigger neuronal apoptosis, growth cone retraction, and regulate neuronal plasticity through receptor complexes that include VPS10p members SORCS2 or Sortilin (SORT1).

Variations in the *SORCS2* gene have been shown to occur more frequently in the context of neuronal function, implicating it in neurodegenerative diseases or mood disorders. For example, single nucleotide polymorphisms (SNPs) in SORCS2 confer a risk for bipolar disorder and schizophrenia (Baum et al., 2008, Ollila et al., 2009, Christoforou et al., 2011). A literature search revealed that upregulated *SORCS2* gene expression had been reported in colorectal cancer patients with poor survival (Aziz et al., 2016), and tongue carcinoma patients with lymphatic metastasis (Watanabe et al., 2008). SNPs in *SORCS2* have also been identified in advanced non-small cell lung cancer (NSCLC) patients with poor survival (Wu et al., 2011). To date, only one sequencing study further investigated the function for SORCS2 in cancer, reporting that it is involved in migratory activity in basal-like breast carcinoma cells (Shkurnikov et al., 2019).

LMNB1-DT is an anti-sense long non-coding RNA (lncRNA) of the protein coding gene for LMNB1. While lncRNAs do not code for proteins, they can interact with nucleic acids or proteins and can subsequently regulate their transcription and translation (Fernandes et al., 2019). There is currently no evidence in the literature reporting whether *LMNB1-DT* interacts with the *LMNB1* coding gene or protein. However, as *LMNB1-DT* was not present in the medulloblastoma patient datasets analysed, the expression of the *LMNB1* coding gene was examined as a surrogate in order to gain some insights into the possible impact of the transcript in

medulloblastoma patients. *LMNB1* encodes a member of the family of Lamins, intermediate filament proteins that make up the nuclear lamina. Lamin B1 and B2 have essential roles in cell growth and viability (Lammerding et al., 2006). *LMNB1* duplication has been found to cause autosomal dominant leukodystrophy, often mistaken for multiple sclerosis (Padiath et al., 2006). *LMNB1* has also been identified as a circulating biomarker in liver cancer (Sun et al., 2010) and a therapeutic target in pancreatic cancer (Li et al., 2013) among other cancer-related roles.

CORO2B encodes a coronin actin binding protein family member. The family is divided into 3 groups by sequence similarity, with *CORO2A* and *CORO2B* belonging to the Type II subtype. Type II coronins are only found in vertebrates, and CORO2B is found enriched in the brain and kidneys (Nakamura et al., 1999, Rogg et al., 2017). CORO2B is best studied in glomerular podocyte cells, where it recruits the protein CFL1, an actin de-polymerization factor, to focal adhesions and actin stress fibres. Its exact function at focal adhesions is still under investigation, but studies have concluded that CORO2B may contribute to the pathogenesis of glomerular diseases such as diabetic nephropathy (Rogg et al., 2017, Schwarz et al., 2019). At this time, there have been no published studies reporting a function for CORO2B in cancer. However, upregulation of family-member *CORO1C* has been reported in malignant glioblastoma where its knockdown resulted in reduced cell motility and invasion (Thal et al., 2008).

In order to further investigate a possible role for *SORCS*2, *LMNB1* and *CORO2B* in medulloblastoma metastasis, the expression of these genes was further studied in medulloblastoma patients.

5.2 Expression of genes of interest in patients

5.2.1 SORCS2, LMNB1 and CORO2B RNA is expressed in medulloblastoma patients

The expression of *SORCS2, LMNB1* and *CORO2B* was assessed by analysis of a large medulloblastoma patient dataset (Cavalli et al., 2017) using the R2 Genomics Analysis and Visualization Platform (r2platform.com). The Cavalli dataset consists of gene expression data from 763 medulloblastoma patients with good representation of the 4 histological subgroups and 4 molecular subgroups. The study by Cavalli *et al*., defined 12 molecular subtypes of medulloblastoma based on an integrated study of genomic expression and methylation data. The metastatic status of patients (either M0 or M+) was also known for most patients. The dataset by Cavalli *et al*., did not include normal control tissue, and the comparison between medulloblastoma samples and normal cerebellum will therefore not be shown in the following results.

Pairwise comparison demonstrated a significant difference in *SORCS2* expression between all 4 subgroups. The expression of *SORCS2* was highest in WNT patients, followed by Group 3 patients when compared to Group 4 and SHH (all comparisons $p<0.0001$) (Figure 5.1 A). This was a surprising finding, as WNT has the lowest occurrence of metastasis and the best survival. The *LMNB1* gene was significantly more expressed in Group 3 tumours compared to the other 3 subgroups (compared to SHH and WNT $p<0.0001$, compared to Group 4 $p<0.001$) (Figure 5.1 B). *CORO2B* expression was highest in Group 3 tumours, but this was only significant compared to WNT tumours ($p<0.0001$) (Figure 5.1 C). The expression of genes was also assessed the medulloblastoma subtypes in two additional datasets (Northcott et al., 2012b, Northcott et al., 2017) (Appendix 2 Supp. Fig. 2, 3 and 4), and these supported the patterns of expression observed in the Cavalli *et al*., dataset. High expression of all 3 genes in Group 3, the subgroup with highest rate of metastasis, supports a possible link to metastasis.

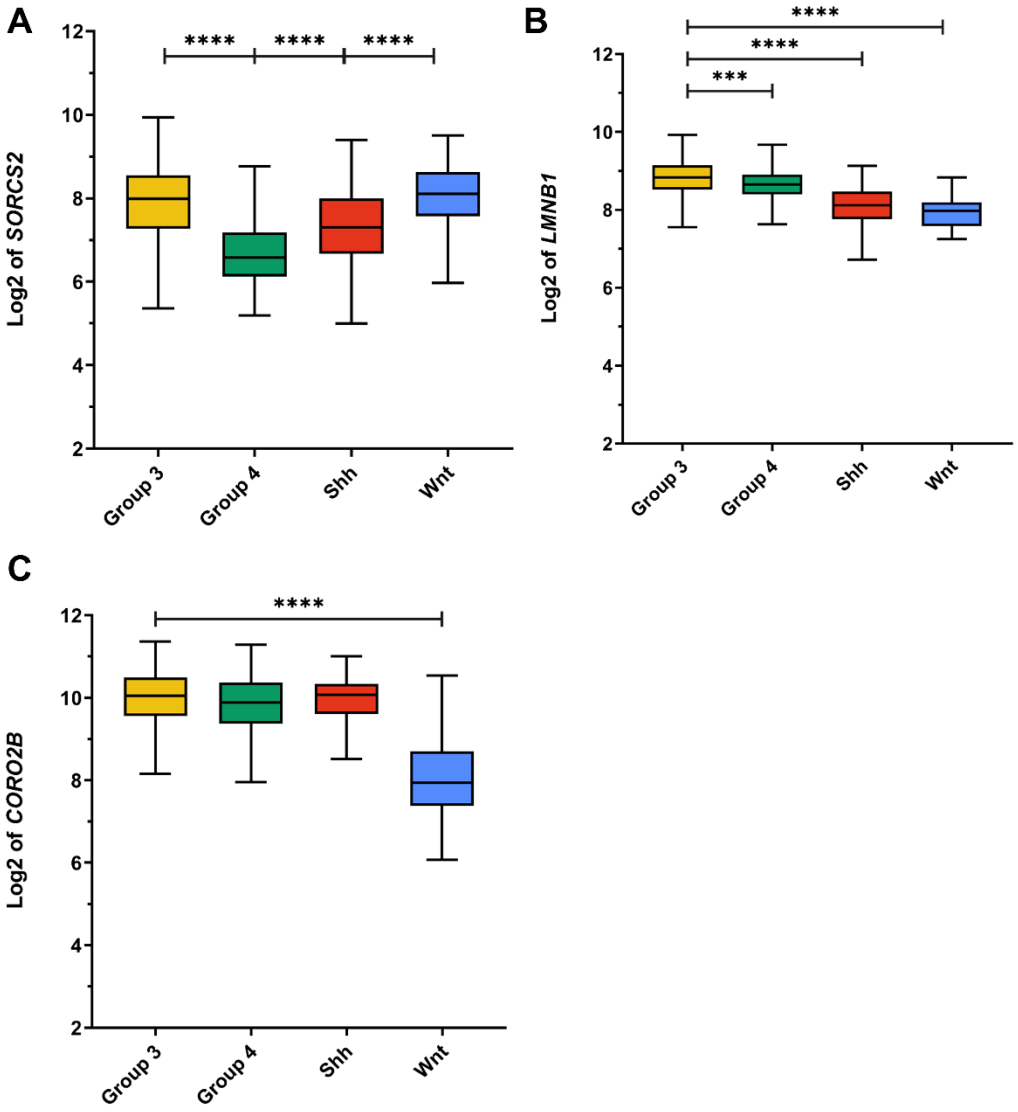


Figure 5.1 Gene expression across medulloblastoma molecular subgroups.

Gene expression (Log2) was assessed using the R2 Genomics Analysis and Visualization Platform using the Cavalli dataset in the four histological subgroups of medulloblastoma (Group 3 = 144, Group 4= 326, Shh = 223, Wnt = 70). **A)** *SORCS2* expression **B)** *LMNB1* expression, **C)** *CORO2B* expression. Significant differences in expression between each group were calculated using one-way ANOVA with Tukey's multiple comparisons (***p<0.001, **** p<0.0001). The full results for significant differences in expression can be found in Appendix 3 (Supp. Fig. 1).

The Group 3 subtypes are distinct in their prognosis and occurrence of metastasis. Group 3α and 3γ have similar frequency of metastasis, and 3γ also has the worst prognosis. Group 3β has a more favourable prognosis compared to Group 3γ, and is infrequently metastatic (Cavalli et al., 2017). In order to further examine subgroup-specific gene expression and investigate why the expression of SORCS2 was highest in WNT tumours, the expression of all 3 genes in the 12 medulloblastoma molecular subtypes was examined. This revealed that *SORCS2* expression is significantly higher in Group 3 alpha (α) and gamma (γ) subtypes compared to Group 3 beta (β), and WNTα (for all comparisons $p<0.0001$). The lower expression in Group 3β explains why the expression of SORCS2 in Group 3 overall was lower than WNT (Figure 5.2). *LMNB1* gene was not significantly different between the Group 3 subtypes (Figure 5.3). *CORO2B* expression was highest is the Group 3α tumours compared to Group 3β and Group 3γ, which may also relate it to metastasis in these patients (Figure 5.4).

In conclusion, *SORCS2, LMNB1* and *CORO2B* expression correlated not only with Group 3 expression, but were highest in the Group 3 subtypes with the highest occurrence of metastasis and the worst prognosis.

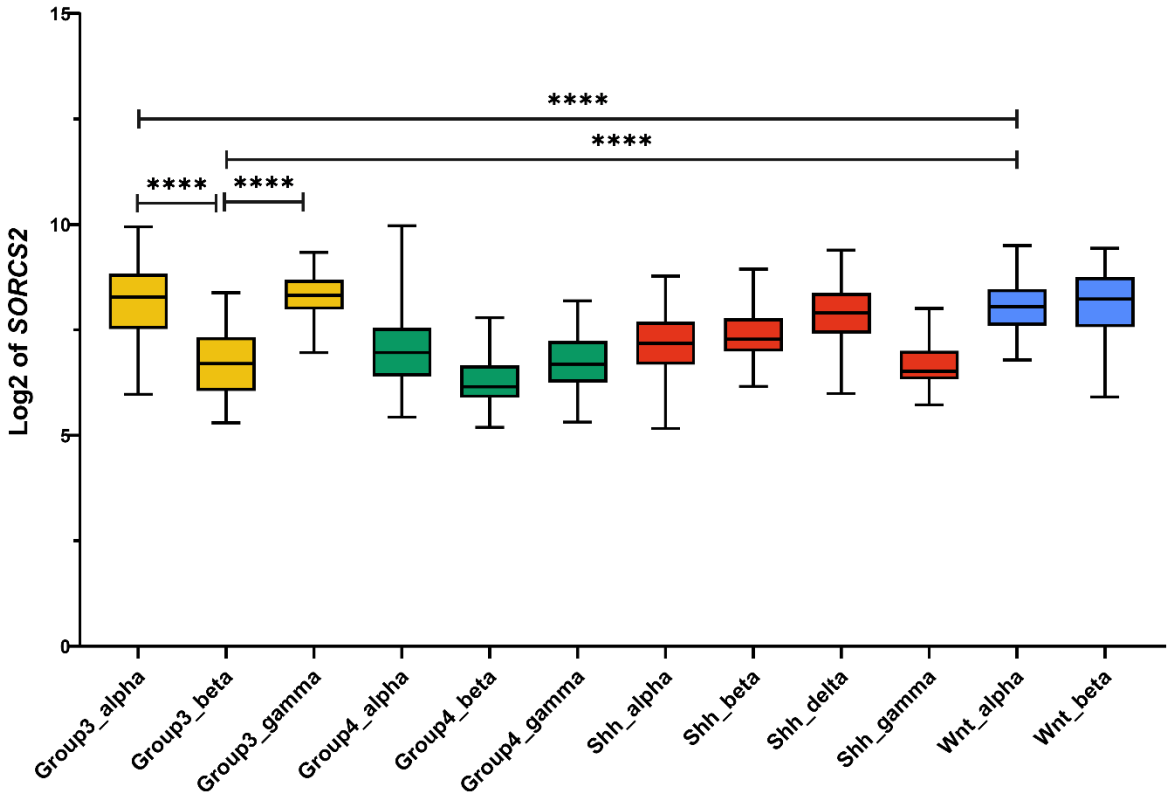


Figure 5.2 SORCS2 expression in 12 medulloblastoma subtypes.

Gene expression (Log2) of SORCS2 was assessed using the R2 Genomics Analysis and Visualization Platform using the Cavalli dataset. Significant differences in expression between each group were calculated using one-way ANOVA with Tukey's multiple comparisons (**** $p<0.0001$). Only significant differences between Group 3 subtypes are shown. The full results for significant differences in expression between the 12 molecular subtypes can be found in Appendix 3 (Supp. Fig. 5).

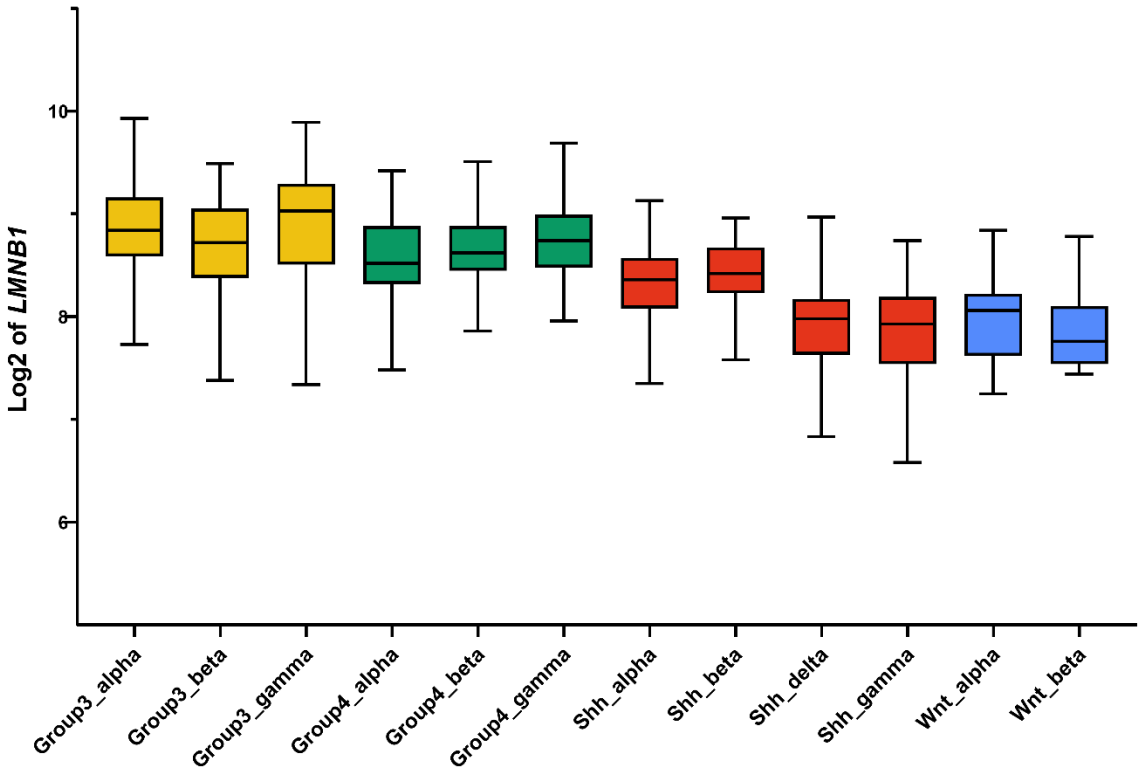


Figure 5.3 LMNB1 expression in 12 medulloblastoma subtypes.

Gene expression (Log2) of LMNB1 was assessed using the R2 Genomics Analysis and Visualization Platform using the Cavalli dataset. Significant differences in expression between each group were calculated using one-way ANOVA with Tukey's multiple comparisons (**p<0.01, **** p<0.0001). Only significant differences between Group 3 subtypes are shown. The full results for significant differences in expression between the 12 molecular subtypes can be found in Appendix 3 (Supp. Fig. 6).

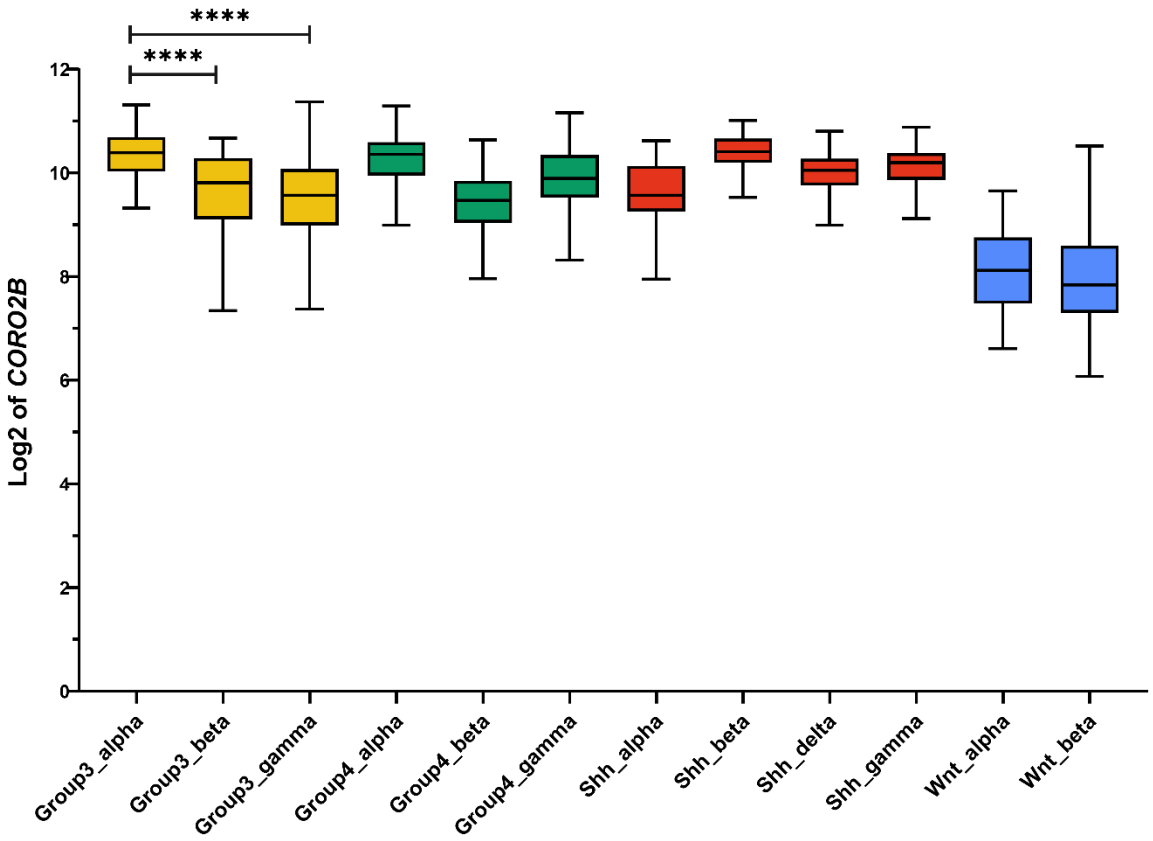


Figure 5.4 CORO2B expression in 12 medulloblastoma subtypes.

Gene expression (Log2) of CORo2B was assessed using the R2 Genomics Analysis and Visualization Platform using the Cavalli dataset. Significant differences in expression between each group were calculated using one-way ANOVA with Tukey's multiple comparisons (**p<0.01, **** p<0.0001). Only significant differences between Group 3 subtypes are shown. The full results for significant differences in expression between the 12 molecular subtypes can be found in Appendix 3 (Supp. Fig. 7).

While Group 3 is the most highly metastatic subgroup, genes driving metastatic processes may also act in a subgroup-independent manner. The expression of the 3 genes of interest was therefore analysed in all patients with metastatic tumours, compared to Group 3 patients with metastatic tumours. In the dataset by Cavalli et al, metastatic status is defined as non-metastatic (M0) or metastatic (M1 through M4). There was no significant difference in *SORCS2* expression between non-metastatic patients and metastatic patients when examining all the subgroups in combination. However, this did not take into account differences in the molecular subgroups or patient survival. When only the Group 3 tumours were analysed (Figure 5.5), *SORCS2* and *CORO2B* expression was significantly higher in the patients with metastatic tumours compared to the non-metastatic tumours. *LMNB1* expression followed the opposite pattern; the gene expression was significantly higher in M+ patients compared to M0 patients when the subgroups were examined collectively. However, this difference was not significant in the Group 3 patients alone. This further links the 3 genes of interest to medulloblastoma metastasis, and in the case of *SORCS2*, this is specific to the Group 3 subgroup.

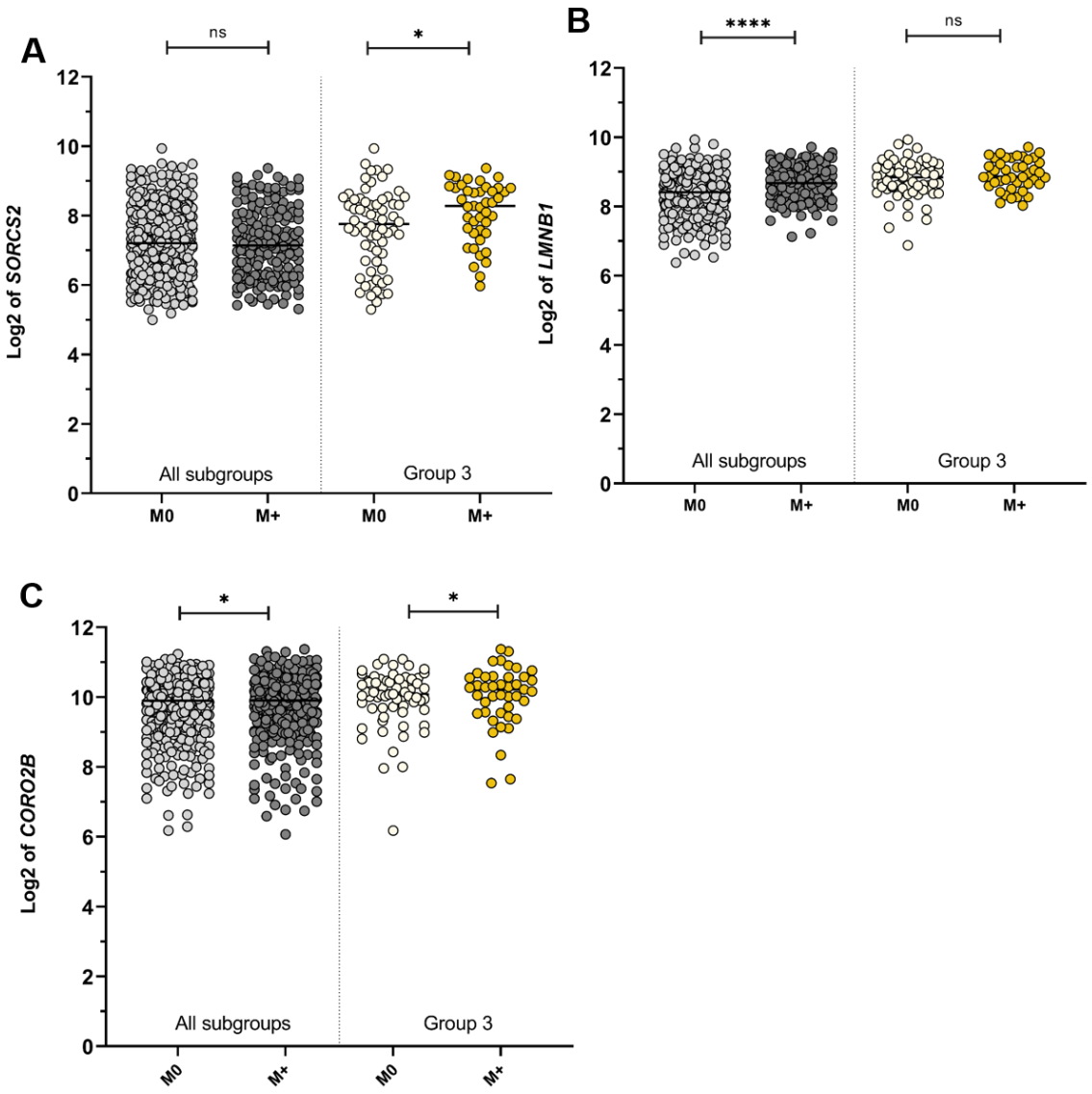


Figure 5.5 Variation in gene expression were observed in Group 3 tumours in patients with non-metastatic (M0) or metastatic (M+) tumours.

Gene expression was analysed in patients with tumours from all molecular subgroups (M0 = 397, M+ = 176) or patients with Group 3 tumours only (M0 = 66, M+ = 43). **A)** *SORCS2* expression, **B)** *LMNB1* expression, C) *CORO2B* expression. Significant differences in expression between each group were calculated using an unpaired T-test, *p<0.05, ****p<0.0001.

5.2.2 Gene expression in metastatic tumours may be associated with poor patient outcome

It has previously been shown that patient survival followed a negative trend in patients with high *SORCS2* expression compared to patients with low *SORCS2* expression (see Chapter 4 Figure 4.21), although this difference was not significant when patient data from all molecular subgroups was examined collectively. Notably there was a sharp drop off in patient survival in the first 12-18 months, which corresponds to the time to recurrence for most medulloblastoma tumours (Ramaswamy et al., 2013). When *SORCS2, LMNB1* and *CORO2B* gene expression was investigated in Group 3 patients over 5 years, the differences between patients with high gene expression and low gene expression were not significant. Patients with high *SORCS2* or *CORO2B* expression followed a poorer survival trend, including a steep decline in survival within the first 12 months in patients with high *SORCS2* (Figure 5.6 A and C). However, none of the differences observed were significant, and conclusions could therefore not be drawn from this data.

In order to correlate gene expression with metastasis and survival, patients were grouped according to gene expression (high or low) and metastatic status (M0 or M+). The most significant expression cut-off was calculated using the KaplanScan feature on the R2 platform, which uses a logrank test to create 2 groups. The numbers of patients in the “high” and “low” expression groups differed between genes as the most significant cut-off was calculated separately for each gene. This analysis revealed a significantly poorer outcome for patients with both metastatic disease and high SORCS2 expression compared to the other groups of patients (Figure 5.7 A). The survival of this patient population decreased sharply within the typical recurrence window of 12 months and had the worst survival rate overall. Patients with M+ tumours expressing high *LMNB1* or *CORO2B* also had the poorest survival, while patients with M0 tumours and low *LMNB1* or *CORO2B* had the best survival (Figure 5.7 B and C). The effect of high gene expression on survival was more significant in the patients with high *CORO2B* than high *LMNB1*. Although

significant, the impact of LMNB1 on metastatic medulloblastoma patients was not as clear as that of *SORCS2* and *CORO2B*. The divergent transcript *LMNB1-DT* identified in this sequencing study may not be functioning through the *LMNB1* gene, and this warrants further investigation into the role of lncRNAs in medulloblastoma.

These results demonstrated a strong link between high expression of *SORCS2* or *CORO2B*, metastasis, and patient death. The most striking effect on survival was high *SORCS2* expression correlating with a sharp decline within the first 12 months, and suggesting a link to early recurrence. Following these results, *SORCS2* was selected for further validation in order to elucidate its function in metastatic medulloblastoma.

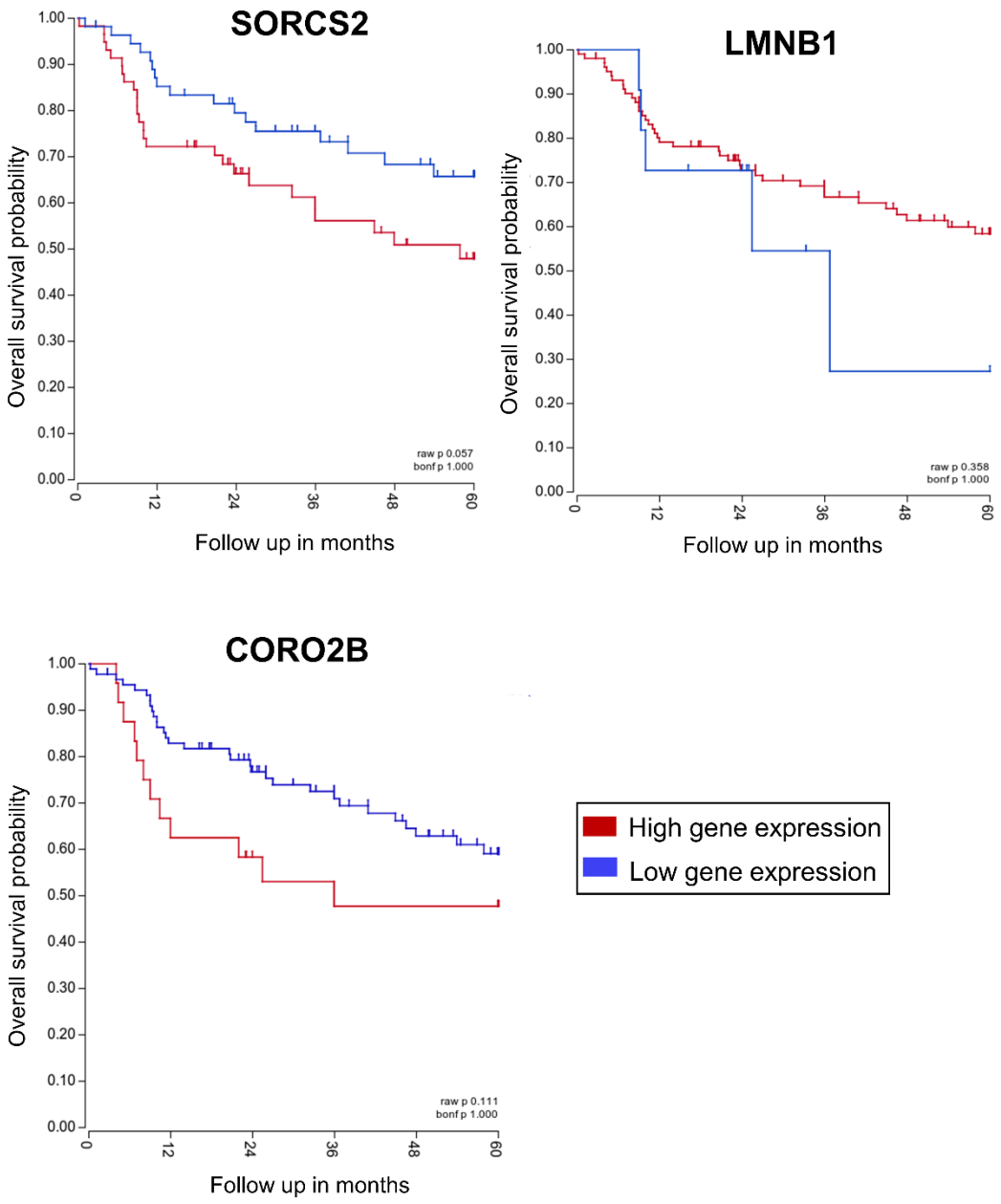


Figure 5.6 Patients with high SORCS2 and CORO2B followed poor survival trends in Group 3 patients.

The survival of medulloblastoma patients with Group 3 tumours based on high or low expression of *SORCS2* in the Cavalli *et al.* 2017 dataset using the R2 Genomics Analysis and Visualization Platform. SORCS2 p=ns, LMNB1 p=ns, CORO2B p=ns.

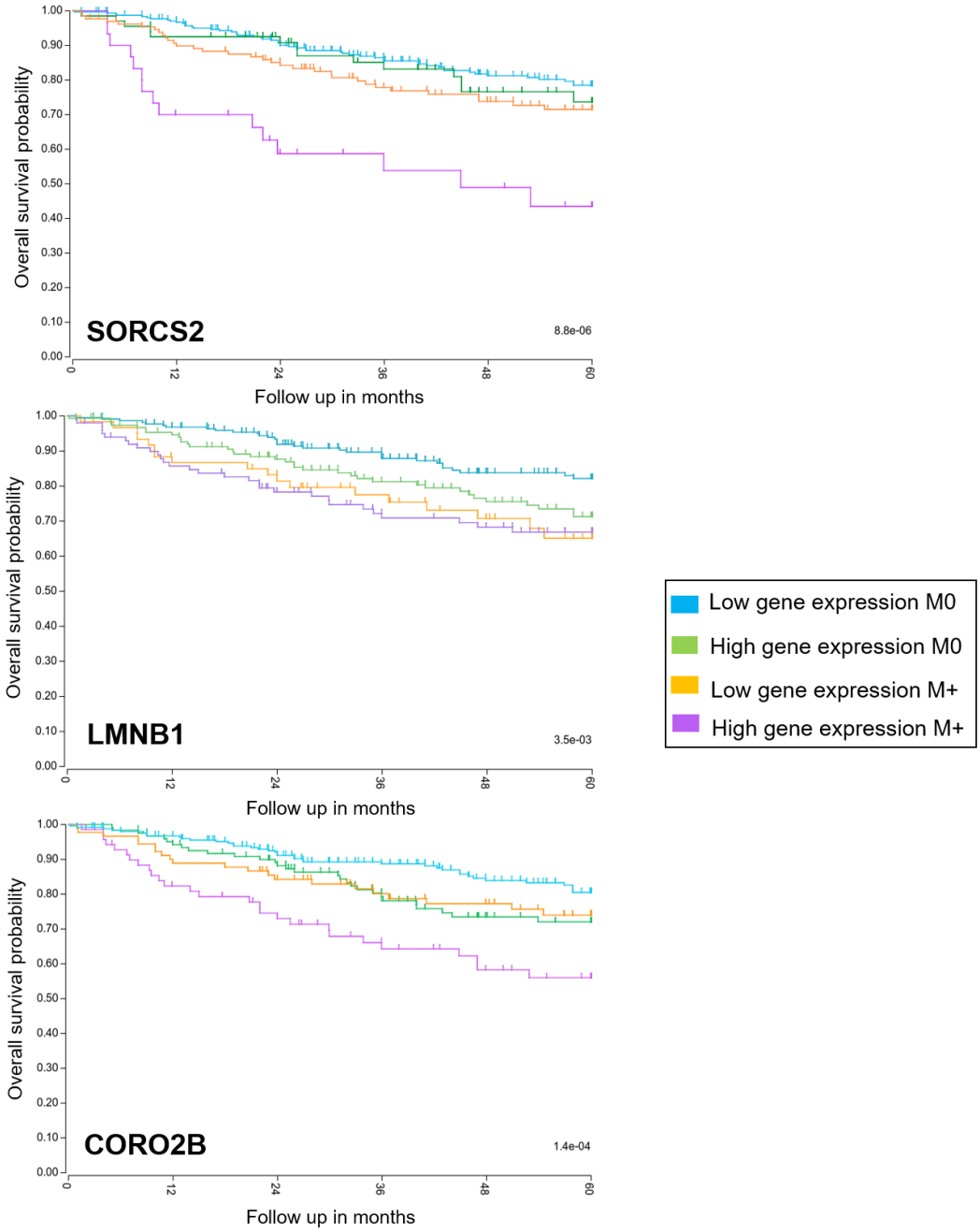


Figure 5.7 Patients with high expression of SORCS2 and metastatic tumours had the worst outcome.

The survival of medulloblastoma patients was analysed based on high or low expression of *SORCS2, LMNB1* or *CORO2B* and metastatic status in the Cavalli *et al.* 2017 dataset using the R2 Genomics Analysis and Visualization Platform. *SORCS2* $p=8.8e^{-06}$, *LMNB1* $p=3.5e^{-03}$, *CORO2B* $p=1.4^{-04}$. *SORCS2* high M0 n=67, *SORCS2* high M+ n=30, SORCS2 low M0 n=310, SORCS2 low M+ n=131. LMNB1 high M0 n=154, *LMNB1* high M+ n=100, *LMNB1* low M0 n=223, *LMNB1* low M+ n=61. *CORO2B* high M0 n=123, *CORO2B* high M+ n=71, *CORO2B* low M0 n=254, *CORO2B* low M+ n=90.

5.2.3 SORCS2 protein is expressed in medulloblastoma patient tissue

With the aim of determining whether high SORCS2 protein expression correlated with metastatic medulloblastoma tumours, tumour microarrays (TMAs) were stained by immunohistochemistry (IHC) for SORCS2 expression. Normal hippocampus tissue was used as a positive control, and the same tissue stained only with the secondary antibody was used as a negative control. In the negative control, no staining was observed in any cell types. In the positive control, there was some SORCS2 cytoplasmic staining in the pyramid cells (see Appendix 3 Supp. Fig. 6) as well as the white matter, glia, and cortical neurons. This was consistent with previously-published studies showing SORCS2 expression in these cell types (Mori et al., 2015, Malik et al., 2019). Based on the positive control, SORCS2 staining in the tumour cores was expected to be cytoplasmic.

The expression of SORCS2 protein was scored on a scale of 0 to 3 (Table 5.1 and Figure 5.8) based on qualitative observation of the images of 6 TMAs without knowledge of the clinical information associated with each tumour core. Tumour cores without any SORCS2 staining in tumour cells received a score of 0. Tumour cores with SORCS2 staining in a few cells and up to 10% of the tumour cells in the core received a score of 1. Tumour cores with SORCS2 staining in up to 50% of the core received a score of 2. Finally, tumour cores with strong SORCS2 staining in over 50% of the core received a score of 3. The cores were independently scored by two blinded observers after a meeting with a pathologist who pointed out the areas of non-tumour or non-specific staining. In order to score the tumour cores most accurately, the pathologist defined the areas of staining that would not contribute to the staining score. Normal CNS parenchyma was stained in several cores (Figure 5.9 A). This presented as areas of tissue completely stained brown, with few, small, round nuclei that were not stained. Although this staining may be SORCS2-specific, it was not counted in the scoring as it was not tumour tissue. In some samples, tumour cells had infiltrated normal CNS parenchyma, and there was background staining from the normal brain tissue (Figure 5.9 B). In these cases, only specific areas where

tumour cells expressed SORCS2 were scored. Some of the tumours had haemorrhaged, which resulted in an abundance of erythrocytes making the sample appear light brown (Figure 5.9 C), and these were not included in the SORCS2 score. Some of the tumours had been damaged by crushing, likely during surgery or due to handling before they were fixed, and these areas appeared as dense, dark blue (Figure 5.9 D). If a tumour had been crushed to an extent that prevented the identification or recognisable cell structures (Figure 5.9 E), the core was not scored at all. If a tumour core had become partially detached or scratched on the slide, some false positive staining was observed, and these areas were not included in the SORCS2 score (Figure 5.9 F).

In total, cores from 71 patients were scored. The scores assigned by the two observers were largely consistent, only 2 cores differed by 1 point. The SORCS2 expression score was averaged for each core, and then for each patient tumour. Only then was the clinical data examined for each patient (see Appendix 3 Tables 1 and 2). In addition to the false-positive staining, some interesting tissue organization or structures were observed. One core was taken from the leptomeninges, and had strong SORCS2 staining (Figure 5.10 A). Sometimes, a more intensely stained area was observed due to necrosis (Figure 5.10 B). Conversely, blood vessels and fibrous tissue were negative for SORCS2 staining (Figure 5.10 C), although erythrocytes stained light brown (Figure 5.10 C, arrow).

Table 5.1 The scoring guide followed in order to quantify SORCS2 staining.

Score	Characteristics
0	No SORCS2-specific staining in tumour cells
1	SORCS2 staining in a few tumour cells, up to ~10% of the core
2	SORCS2 staining in ~10-50% of tumour cells in the core
3	SORCS2 staining in tumour cells in ~ >50% of the core

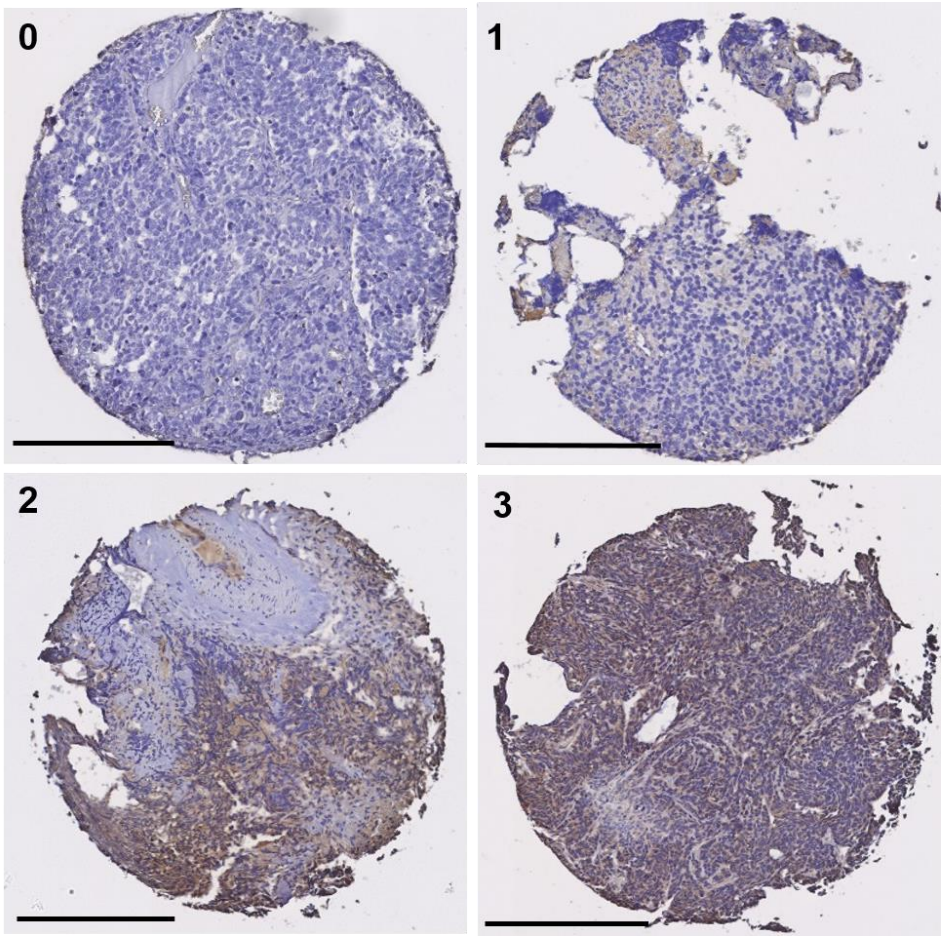


Figure 5.8 Examples of SORCS2 protein expression scores following the guide in Table 5.1.

6 patients tumour microarrays were stained for SORCS2 protein and imaged on a Nanozoomer instrument. Images of tumour cores at 40X magnification are shown, representing the SORCS2 scores 0 through 3. Scale bars represent 250 μm.

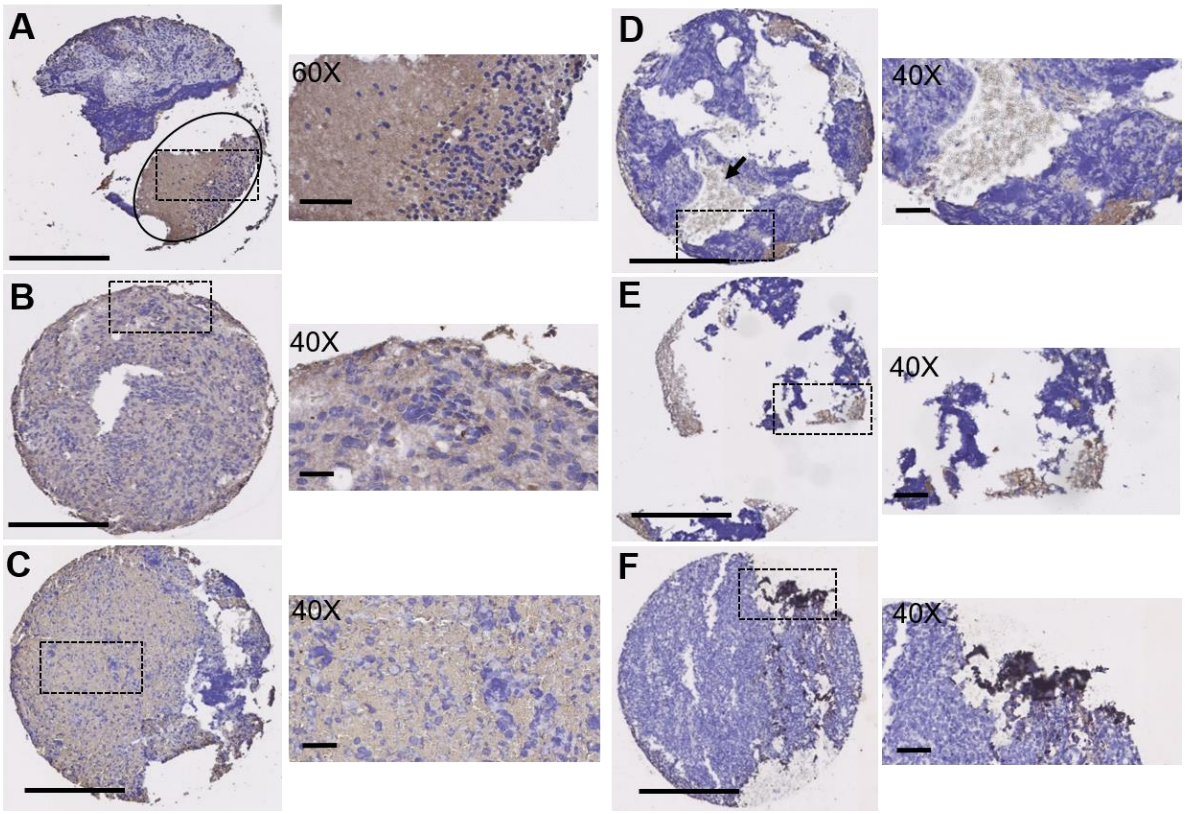


Figure 5.9. Areas of SORCS2 staining that were not scored.

Whole section images were taken at 15X magnification (scale bars represent 250 μm). For each the box shows a section at 40X or 60X magnification, as annotated (scale bars represent 50 μm). **A)** Normal CNS tissue with SORCS2 staining (circled). **B)** Tumour cells infiltrated into normal CNS tissue with a background of SORCS2 staining. **C)** Haemorrhage in the tumour. **D)** An area of erythrocytes (arrow) in surrounding crushed tissue. **E)** A core unrecognisable due to crushing damage and depletion. **F)** False dark staining at the edge of a core.

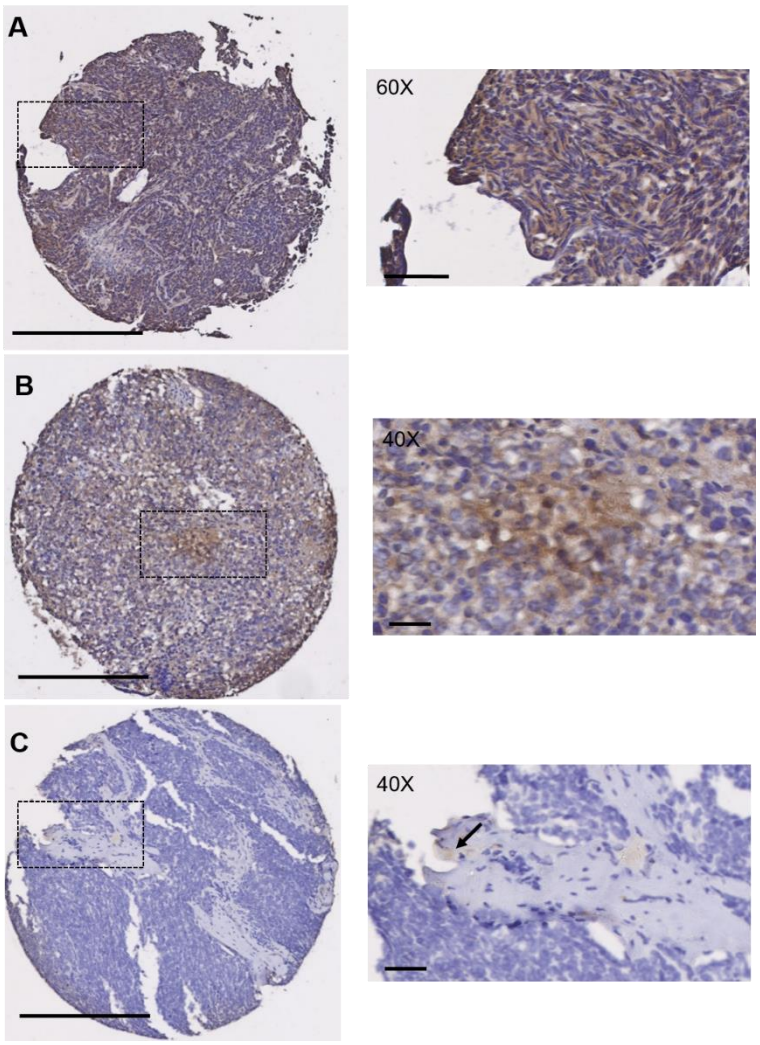


Figure 5.10 Interesting types of tissue in the TMAs.

Whole section images were taken at 15X magnification (scale bars represent 250 μm). For each the box shows a section at 40X or 60X magnification (scale bars represent 50 μm), as annotated. **A)** Positive SORCS2 staining in tumour cells infiltrated in the leptomeninges. **B)** An area of necrosis with amplified staining (magnified image). **C)** Blood vessels with areas of erythrocytes (arrow).

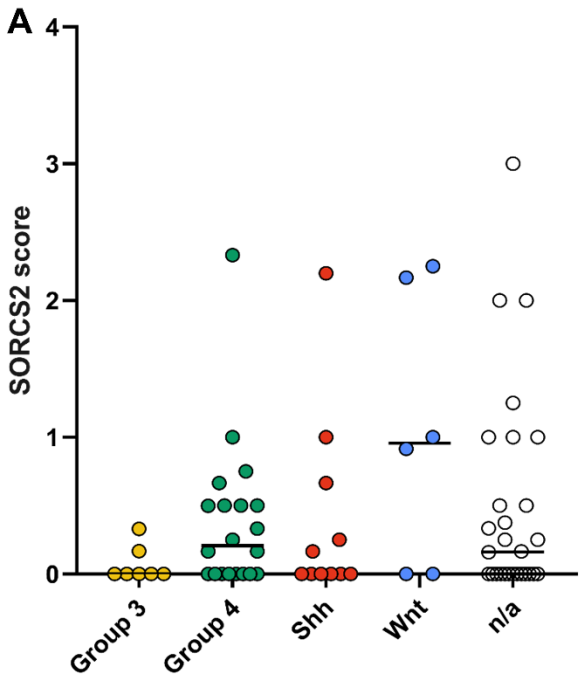
The clinical data from the patients whose tissue was part of the TMAs was correlated with the SORCS2 scores to determine whether there was a correlation between clinical characteristics and SORCS2 expression. The SORCS2 protein was most highly expressed in the WNT tumours, followed by the SHH and Group 4 tumours, while the Group 3 tumours had the lowest expression (Figure 5.11 A). However, none of these differences were significant. The expression of SORCS2 in WNT tumours agreed with the gene expression data (Figure 5.1). The lack of metastatic Group 3 tumours may be a reason why Group 3 cores had the lowest SORCS2 expression, and do not support the gene expression data presented in section 5.2.

Chang's staging system is widely used to define the metastatic stage of medulloblastoma tumours (Table 1.3) (Chang et al., 1969), ranking tumours on a scale of 0 to 4. The clinical information for the patients whose tissue was used in this analysis were divided into Groups based on their metastatic stage (M0-M4) or into the group "n/a" if the metastatic staging was unknown. There was no significant increase in SORCS2 expression with increasing Chang's metastatic status (Figure 5.11 B). The patients were also grouped into metastatic (M+) and non-metastatic (M0) categories, where M1 through M4 were combined into the M+ group, but there was no significant difference in SORCS2 protein expression (Appendix 3 Supp. Fig. 8).

There was no significant difference in survival between patients with or without SORCS2 protein expression (Figure 5.12). When patients were grouped based on positive or negative SORCS2 expression and metastatic status (M0 or M+), a worst survival trend was observed for M+ patients. In the M0 and M+ groups, survival was not significantly different between patients with positive or negative SORCS2 (Figure 5.12 B). The sample size used for this analysis was limited, and SORCS2 expression was low overall. Of the 71 cores analysed, 38 had SORCS2 staining (54%), and within these, 14 had a SORCS2 score above 1.0 (37%). 33 cores did not have any SORCS2 expression (46%). Although details of metastasis and recurrence events were not available for every patient, these occurred in patients whose tumour cores

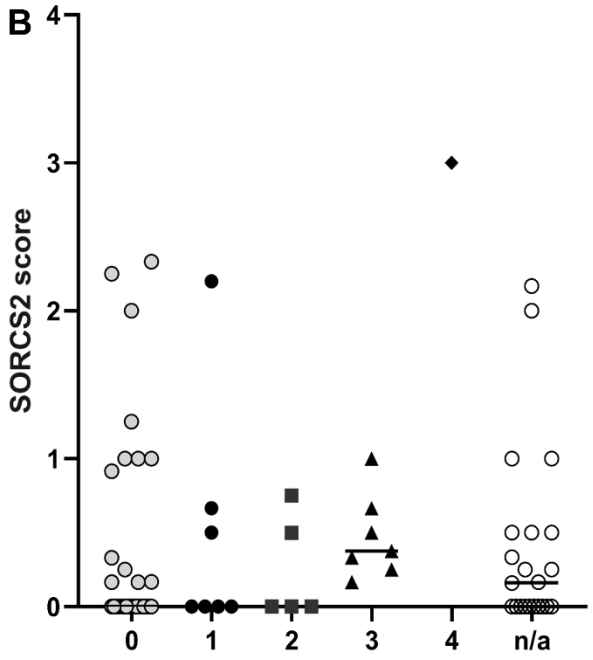
had SORCS2 staining as well as those that did not. A full list of clinical information on the patients whose tumours were included in the analysis can be found in Appendix 3.

It is also important to note that tumour cores used in the TMAs were obtained from the primary tumour and may not reflect the protein expression at the invasive edge of the tumour, or the metastatic recurrences. Further analysis could be performed in collaboration with a pathologist on the samples that represent the tumour's invasive edge and compare these results with samples from the tumour's core. It is also possible that the hypothesis that SORCS2 is involved in metastatic medulloblastoma is wrong.



Subgroup	#	Mean
Group 3	7	0.07095
Group 4	20	0.3830
Shh	11	0.3891
Wnt	6	1.055
n/a	28	0.4923

n/a = information not available



Met status (Chang)	#	Mean
M0	30	0.4275
M1	7	0.4807
M2	5	0.2497
M3	7	0.4698
M4	1	3
n/a	22	0.4012

n/a = information not available

Figure 5.11 SORCS2 expression was not significantly correlated with patient clinical characteristics.

A) The molecular classification and mean of SORCS2 score for each tumour core examined. **B)** The Chang's metastatic group and mean of SORCS2 score for each tumour core examined. Significant differences in expression between each group were calculated using one-way ANOVA with Tukey's multiple comparisons. The full results for significant differences in expression between the 12 molecular subtypes can be found in Appendix 3 (Supp. Fig. 7).

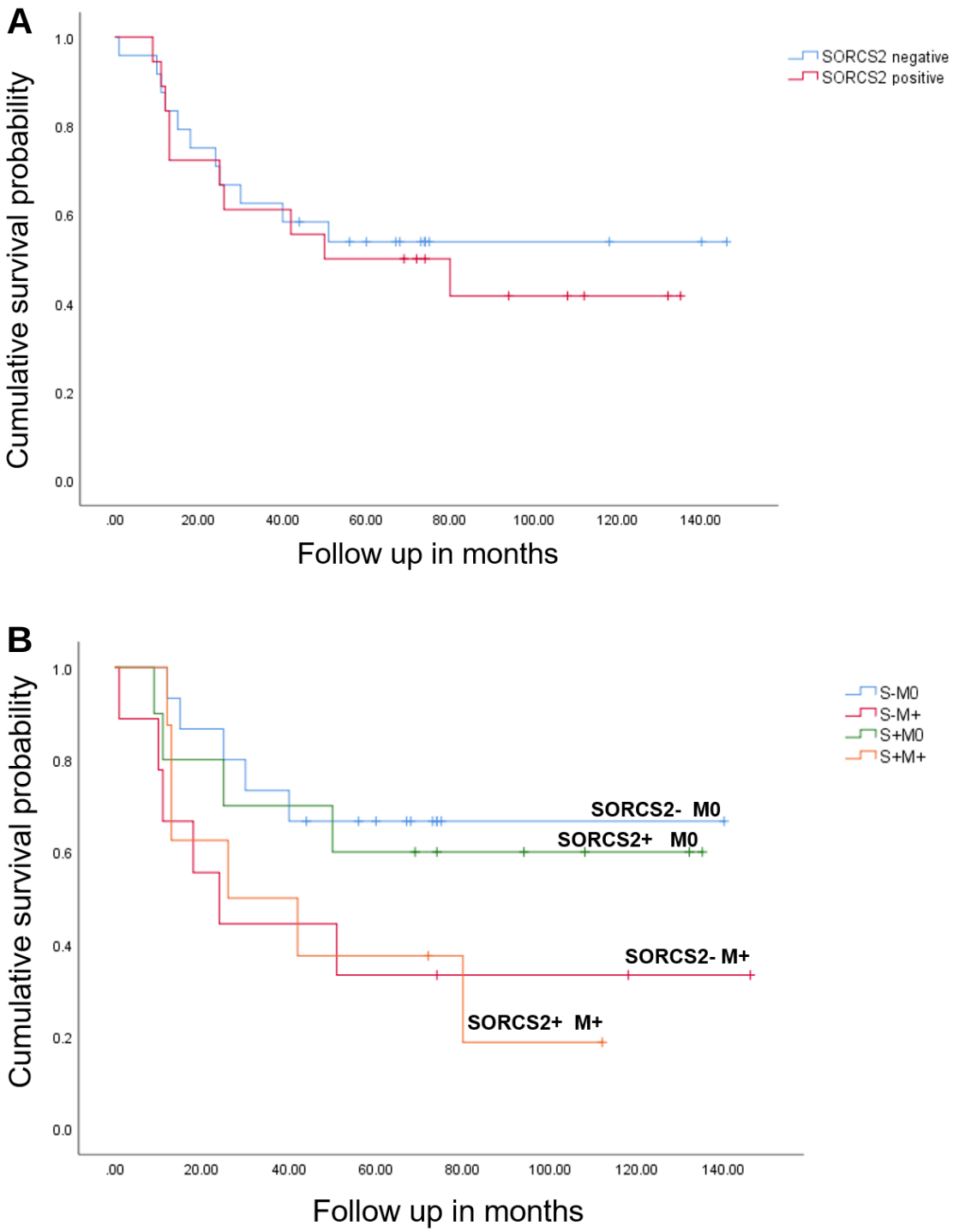


Figure 5.12 Survival of patients included in the TMA analysis.

A) The clinical data available for some of the medulloblastoma patients whose tumours were included in the TMA analysis was analysed. Kaplan Meier survival curves were generated using IBM SPSS® Statistics based on positive or negative expression of SORCS2. SORCS2 negative n=24; SORCS2 positive n=18; p=ns. **B)** The patients were grouped according to SORCS2 expression (high or low) and metastatic status; non-metastatic patients (M0) or metastatic patients (M+ includes M1-4 combined). SORCS2 negative M0 n=15; SORCS2 negative M+ n=9; SORCS2 positive M0 n=10; SORCS2 positive M+ n=8; p=ns. None of the differences were significant.

5.3 SORCS2 is expressed in Group 3 and group 4 medulloblastoma cell lines

SORCS2 expression has not been previously reported in medulloblastoma. The gene and protein expression of SORCS2 was therefore quantified in a range of established medulloblastoma cell lines representing 3 molecular subgroups (Group 3, Group 4 and SHH). *SORCS2* gene expression was quantified by qRT-PCR in medulloblastoma cell lines grown in standard culture conditions. RNA expression was highest in the Group 3 cell line HD-MB03, followed by the Group 4 cell line CHLA-01-MED. *SORCS2* RNA expression was also high in Group 3 cell lines D283-MED and D458-MED. CHLA-01R-MED had expression of *SORCS2* although lower than CHLA-01-MED and the Group 3 cell lines. Expression was barely detectable in SHH cell lines DAOY and ONS76 (Figure 5.13). These results do not completely correlate with gene expression in patients (Figure 5.1), based on which lowest expression would have been expected in Group 4 cell lines. However, the Group 4 cell lines CHLA-01-MED and CHLA-01R-MED cell lines are from a highly aggressive and metastatic tumour and recurrence. While SHH cell line DAOY is a cell line derived from a non-metastatic primary tumour and may not have expressed genes needed for cell migration, the ONS76 line was derived from a SHH tumour at stage M2.

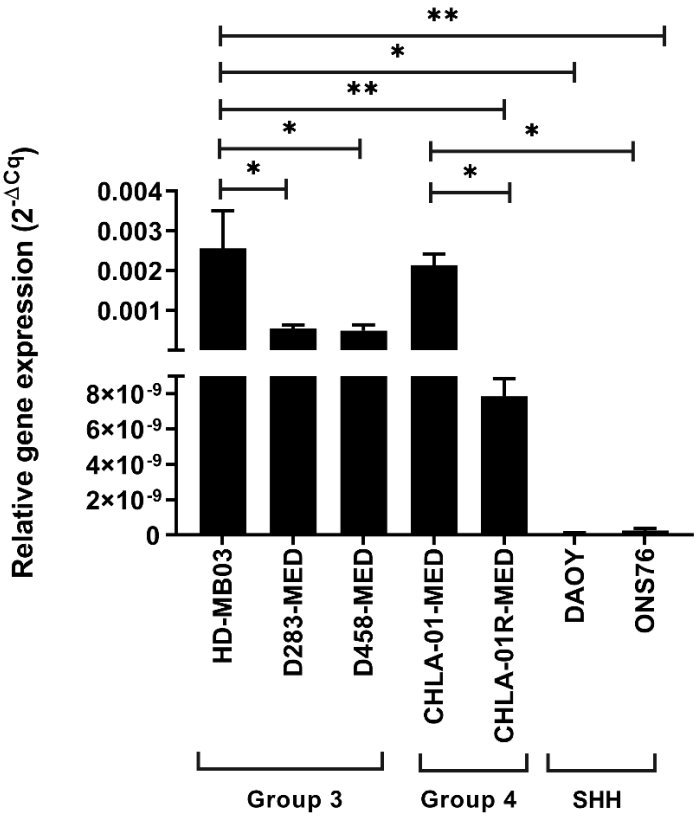


Figure 5.13 SORCS2 gene expression in medulloblastoma cell lines.

Mean RNA expression quantified by qRT-PCR (n=3 except DAOY n=2). Significant differences in means between each group were calculated using one-way ANOVA with Tukey's multiple comparisons. (*p<0.05, **p<0.01). Error bars represent SEM.

SORCS2 exists as a proform of around 130kDa, which can then be cleaved into a 122kDa single-chain receptor or a double-chain receptor of 104kDa and 18kDa. Both single-chain and double-chain isoforms can interact with SORCS2 ligands and co-receptors (Glerup et al., 2014).

In order to explore the expression of SORCS2 protein in medulloblastoma cell lines, the protein from at least 2 lines representing 3 medulloblastoma subgroups was assayed by western blot. The protein bands from 3 or 4 separate blots were quantified by area measurements using ImageJ image analysis software. The highest protein expression was found in CHLA-01-MED and CHLA-01R-MED, followed by HD-MB03 and D283-MED (Figure 5.14). The protein was hardly detectable in D458-MED, DAOY and ONS76 cell lines. The 18kDa product was not detectable on the blots from 8% gels, and was assumed to have run off in all the replicates. All Group 3 and Group 4 cell lines expressed single-chain and double-chain receptors at comparable levels (Figure 5.14 B), with the exception of CHLA-01R-MED which expressed more single-chain than double-chain receptors.

Only the SHH cell lines DAOY and ONS76 had a band at 130kDa, which may represent the uncleaved SORCS2 proform. However, the RNA expression of SORCS2 was extremely low in both DAOY and ONS76, while the expression of protein at 130kDa was strong. This discrepancy between RNA and protein expression may suggest that the protein seen around 130kDa is an unspecific signal.

Conversely, D458-MED had high SORCS2 RNA expression but low SORCS2 protein expression. This suggests that SORCS2 RNA may not be translated into protein in this cell line. It is important to keep in mind that these samples were cultured in standard conditions and are not migrating cells. A proteomics analysis on migrating cells would allow for a correlation between the RNA-Seq data presented in Chapter 4 and the expression of protein in migrating cells. For this to be possible, the scale of the migration assay would need to be increased in order to isolate a greater number of migrating cells.

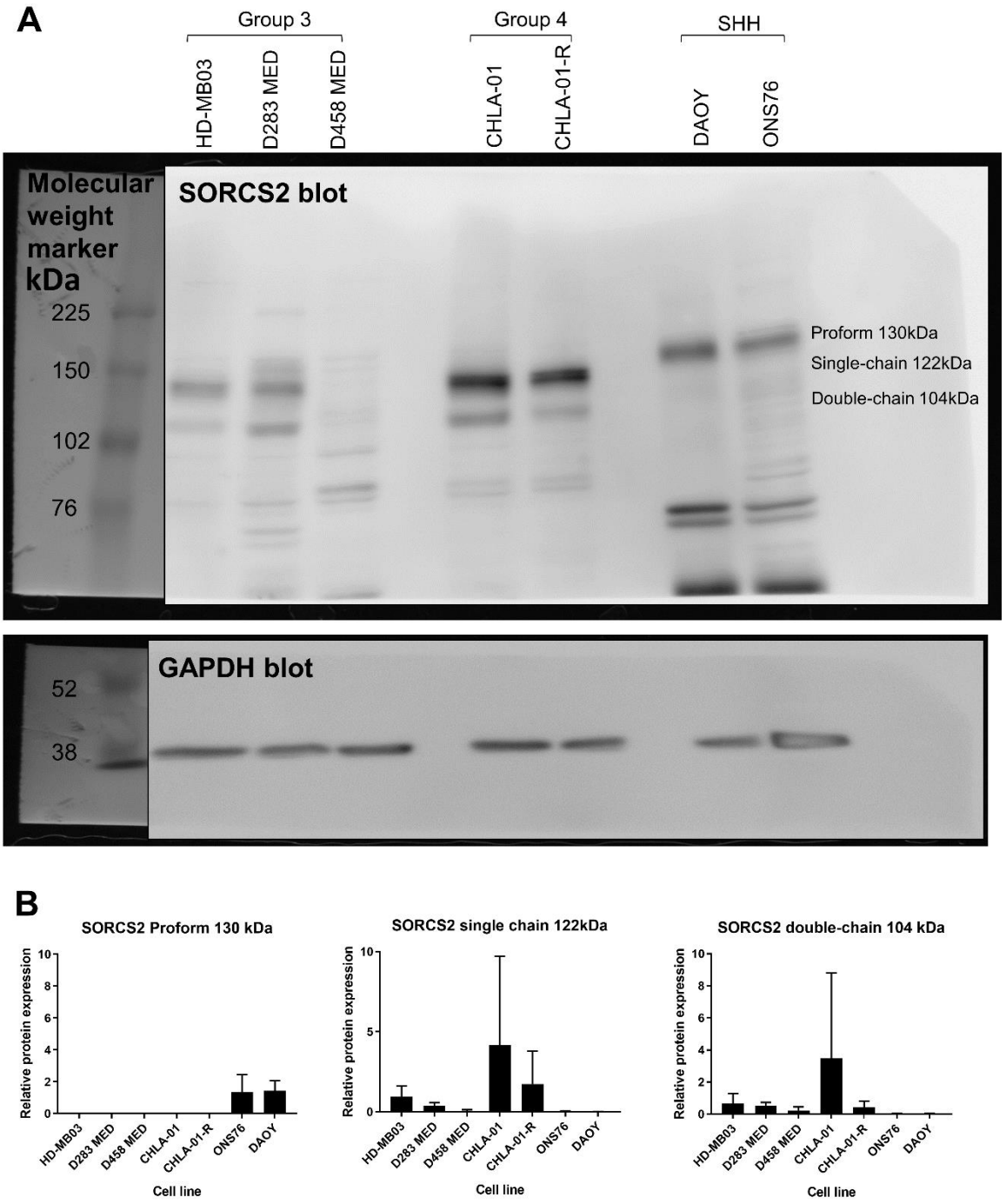


Figure 5.14 SORCS2 protein expression in medulloblastoma cell lines.

SORCS2 protein was quantified using Western Blot. Protein samples from 7 medulloblastoma cell lines were run on an 8% gel and transferred onto a PVDF membrane. The blot was cut between the 76 and 52 kDa markers. **A)** A representative Western Blot (one of 3 or 4, depending on the cell line) showing protein expression of SORCS2 and housekeeping protein GAPDH in medulloblastoma cell lines. A light image of the molecular weight marker is shown alongside each blot. **B)** 3 or 4 independent western blot replicates were quantified by area measurements using ImageJ image analysis software, and this data was used to calculate SORCS2 expression relative to housekeeping protein GAPDH in medulloblastoma cell lines (HD-MB03 and D283-MED n=4, CHLA01-MED, CHLA-01R-MED, ONS76 and DAOY n=3). Significant differences in means between each group were calculated using one-way ANOVA with Tukey's multiple comparisons, none of the differences were significant.

5.4 Optimising transfection and knockdown in Group 3 cell lines

5.4.1 Optimising transient transfection and siRNA knockdown of SORCS2

With the aim of knocking down *SORCS2* expression in Group 3 cell lines using siRNA, a method of transient transfection was optimised in HD-MB03 cells. Nucleofection with GFP resulted in 65-70% transfection efficiency, which was sustained over 96 hours (see Appendix 3 Supp. Fig. 9). A control experiment was done to determine that the combination of nucleofection (without siRNA) and overnight starvation did not have an impact on cell migration (see Appendix Supp. Fig. 10).

Nucleofected cells were used to seed three experiments: 1) the migration assay, 2) a parallel viability assay, 3) collection of cells every 24 hours to quantify knockdown efficiency through qRT-PCR. Figure 5.15 is a schematic summary of the optimised protocol. Cells were nucleofected, then allowed to settle for at least 5 hours before the medium was replaced with reduced serum (2% FBS) overnight. At 24 hours post-nucleofection, cells were counted and seeded into the migration assay and viability assay. A cell viability measurement and a cell pellet to quantify the knockdown efficiency were taken every 24 hours. Cells were allowed to migrate for 48 hours before the end of the assay, when the number of migrated cells was then quantified.

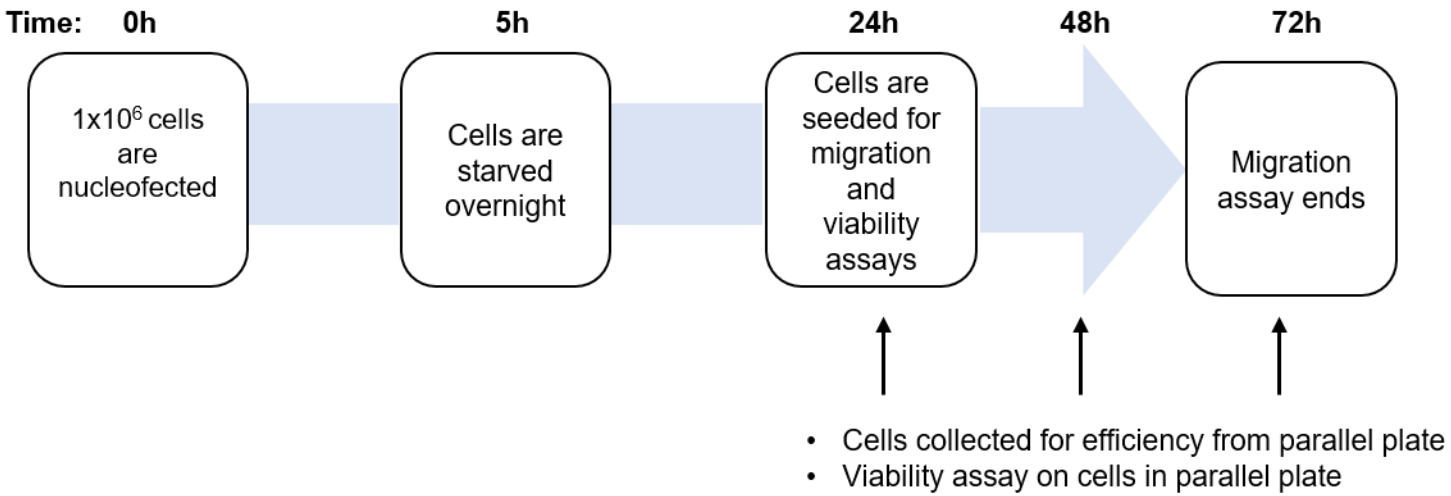


Figure 5.15 Summary of the optimised transfection and migration/viability assay setup.

After optimising the transfection method, the transient knockdown of *SORCS2* gene was optimised before beginning the migration assays. The ON-TARGET Plus SMARTpool siRNA for human SORCS2 was selected as it contains 4 siRNA sequences in one reagent. This siRNA pool or a control non-targeting siRNA were nucleofected into HD-MB03 cells. The manufacturer recommends using 30-300nM siRNA per nucleofection reaction. Two concentrations at the higher end of the scale were tested, 200nM and 300nM. The efficiency of knockdown was quantified by qRT-PCR every 24 hours over the course of 74 hours.

Although the knockdown efficiency of 200nM siRNA on RNA expression was not significant, SORCS2 protein was reduced over the course of 72 hours (Figure 5.16 A). 300nM siRNA seemed to only reduce RNA expression at 72h, although the RNA concentration was too low to conduct qRT-PCR at 24h (Figure 5.16 B). It is possible that the highest siRNA concentration may have been damaging to the cells. However, a viability assay was not done at this stage so this effect could not be quantified. Protein knockdown was seen at 24h and 48h of both single-strand and double-strand cleaved SORCS2, and at 72h for single-strand cleaved SORCS2 (Figure 5.17). 200nM siRNA was selected as the maximum concentration of siRNA to use for knockdown experiments.

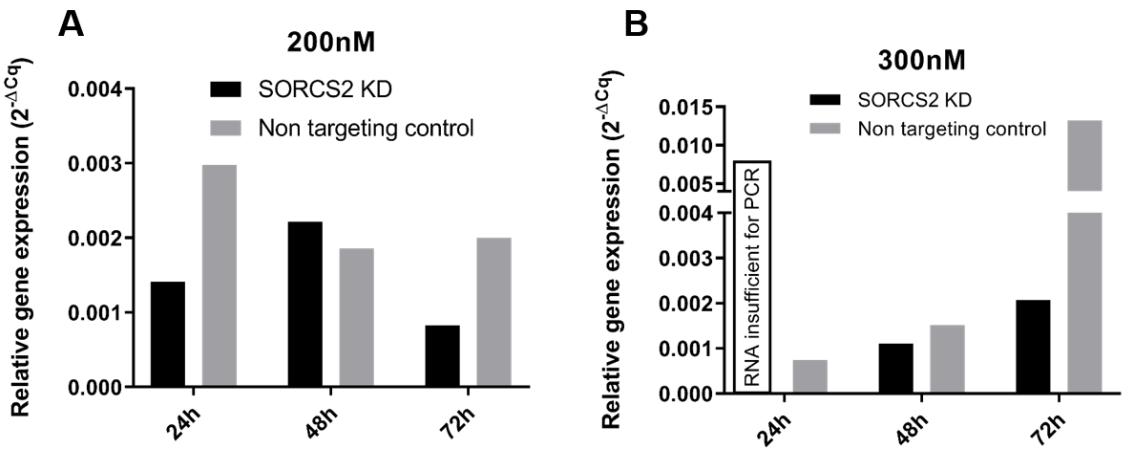


Figure 5.16 siRNA reduces SORCS2 RNA expression with varying efficiency in HD-MB03 cells .

SORCS2 RNA expression was quantified by qRT-PCR and normalised with housekeeping gene GAPDH in cells treated with **A)** 200 nM or **B)** 300nM SORCS2 siRNA or 200 nM or 300nM of a non-targeting control (n=1 for each graph).

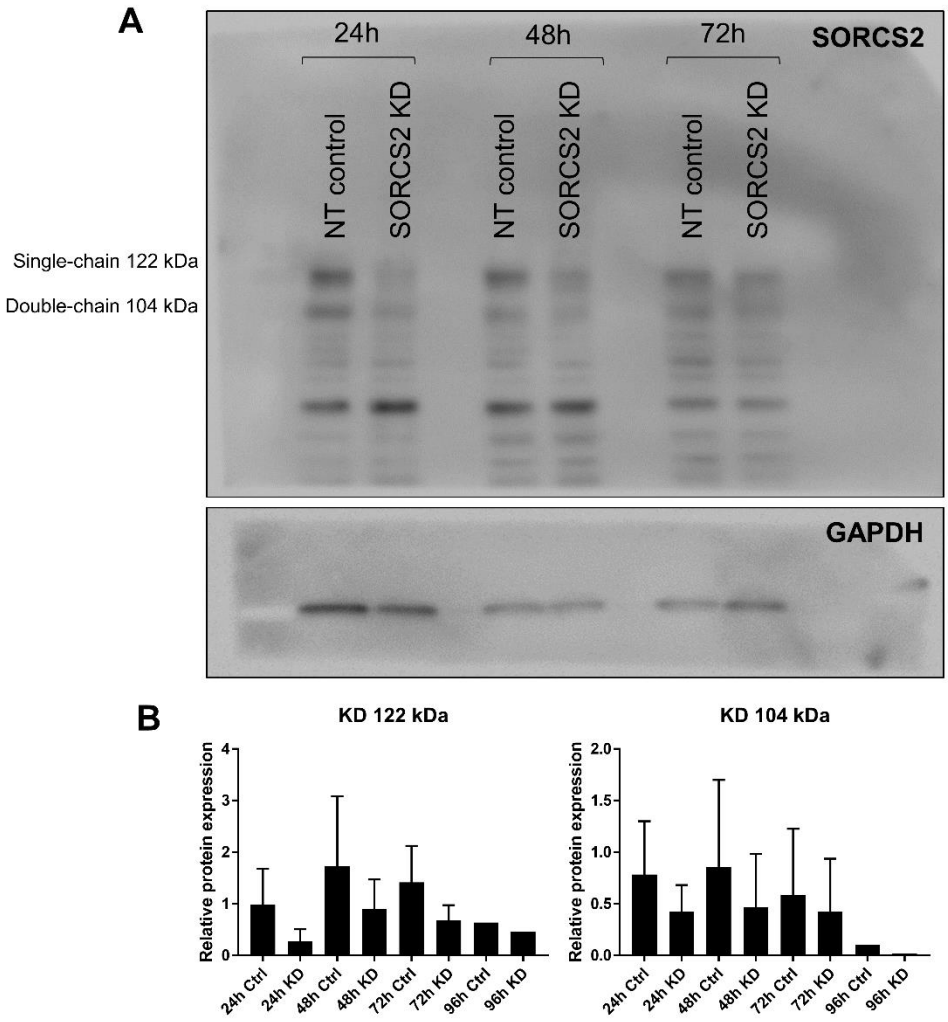


Figure 5.17 SORCS2 protein expression is decreased by siRNA in HD-MB03 cells.

SORCS2 protein expression was quantified by western blot following siRNA knockdown in HD-MB03 cells, but no migration assay was performed using these cells. Protein samples were run on an 8% gel and transferred onto a PVDF membrane. The molecular weight marker image for this blot was misplaced, but bands were identified based on previous SORCS2 blots (Figure 5.14) and based on which bands decreased in the knockdown samples. **A)** A representative western blot showing SORCS2 and GAPDH expression after SORCS2 siRNA (SORCS2 KD) or non-targeting control siRNA (NT control) in HD-MB03 cells **B)** 2 independent western blot replicates were quantified by area measurements using ImageJ image analysis software, and this data was used to calculate SORCS2 expression relative to housekeeping protein GAPDH. Error bars represent SEM (n=2).

5.5 Knockdown of SORCS2 seems to reduce cell migration, but not cell viability in Group 3 cell lines

Next, the transfected cells were assayed for their ability to migrate through coated trans-wells using the migration assay optimised in Chapter 3 in order to test the effect of transiently knocking down *SORCS2* on migration and viability.

The HD-MB03 cells treated with *SORCS2* siRNA seemed to follow a trend of reduced migration, although the difference with the control was not significant. Knocking down *SORCS2* did not reduce cell viability over 96 hours. Gene expression knockdown was quantified by qRT-PCR on RNA collected at 24h-96h after electroporation. A reduction in *SORCS2* expression was seen at every time point in control cells, although this did not go below 32% knockdown. However, there was no significant correlation between recorded gene expression knockdown and difference in cell migration (see Appendix 3 Supp. Fig 11).

In order to determine whether the siRNA knockdown had an impact on SORCS2 protein in the HD-MB03 cell line, protein was quantified by western blot following one of three migration experiments. The expression of SORCS2 protein was reduced compared to the non-targeting control at 24h and 48h, before returning at 72h and 96h. The RNA expression for this experiment did not show the same pattern, with *SORCS2* RNA only being reduced at 24h and seemingly recovering at 48h and 72h before drastically dropping at 96h (see Appendix 3 Supp. Fig. 12). Unfortunately, while protein expression may be a more robust method to correlate knockdown efficiency with functional effects, protein extraction was not successful for the other sample replicates and could therefore not be used to quantify knockdown efficiency across the experiments. These results suggested that there was some protein knockdown as a result of siRNA, although this would need to be repeated in order to draw any conclusions.

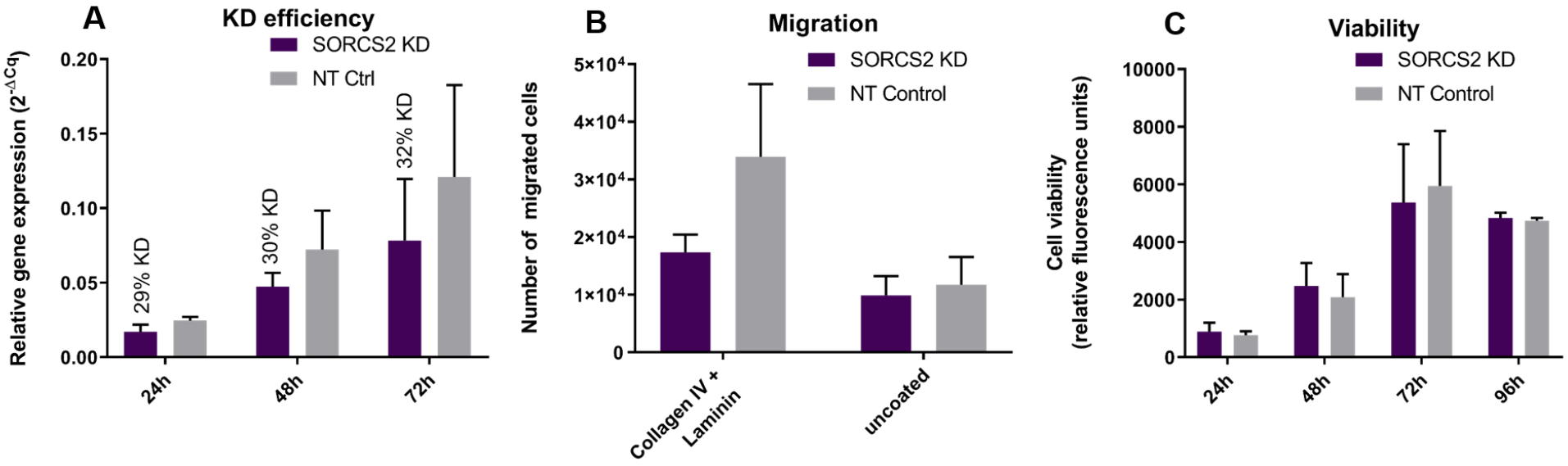


Figure 5.18 A decrease in SORCS2 expression decreased cell migration but did not impact cell viability in HD-MB03.

A) The mean of RNA expression in HD-MB03 cells treated with SORCS2 siRNA (SORCS2 KD) or a non-targeting control (NT control) siRNA was quantified by qRT-PCR and normalised with housekeeping gene HPRT. **B)** Cells migrated for 48h across inserts coated with 5 µg laminin and 10 µg collagen IV towards aCSF supplemented with 10% FBS. The number of migrated cells treated with SORCS2 siRNA or a non-targeting control siRNA were quantified by calcein AM metabolic activity assay. Fluorescence readings for each condition were plotted against a standard curve of known cell numbers in order to derive the exact number of migrated cells. **C)** The metabolic activity of cells in 96 well plates over 96 hours was assayed using PrestoBlue cell viability reagent. Significant differences in means between SORCS2 KD and NT control were calculated using one-way ANOVA with Tukey's multiple comparisons. None of the differences are significant. Error bars represent SEM (n=3).

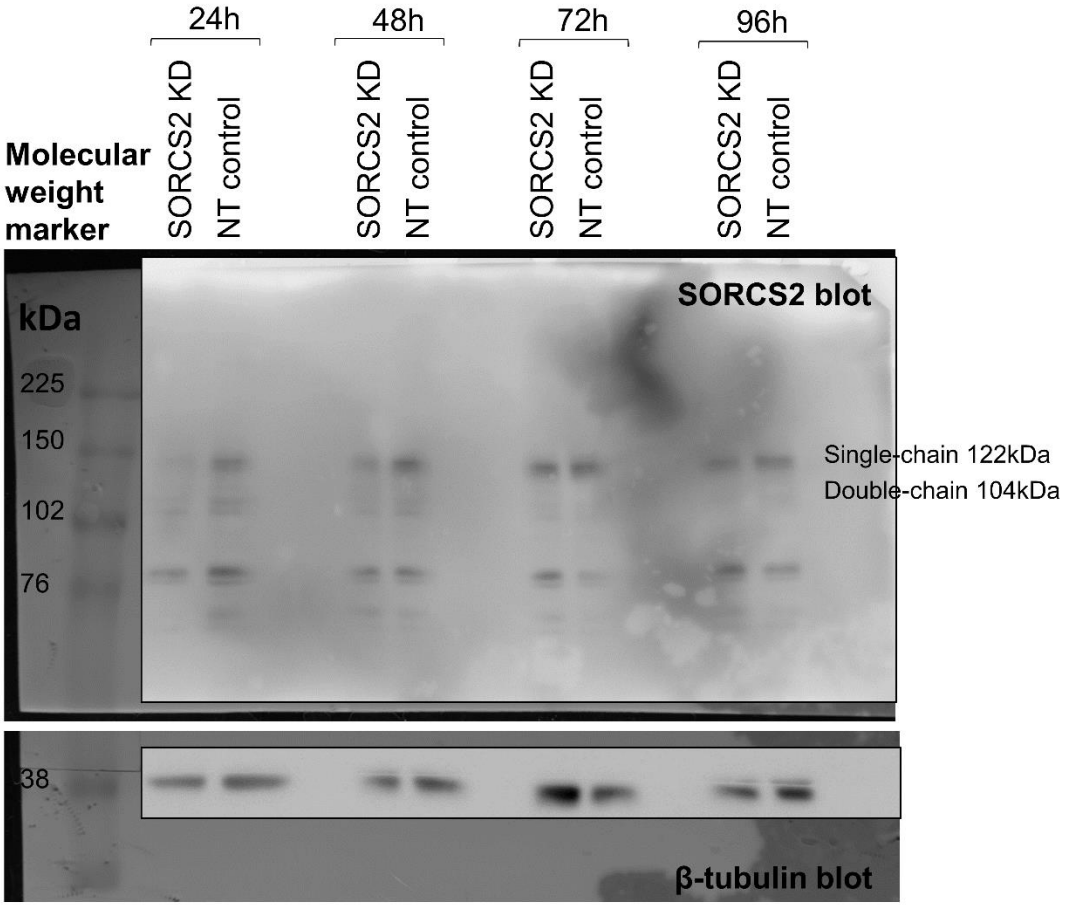


Figure 5.19 SORCS2 protein decreases after siRNA knockdown.

SORCS2 protein expression was quantified by western blot following siRNA knockdown in HD-MB03 cells. Protein samples were run on an 8% gel and transferred onto a PVDF membrane. A light image of the molecular weight marker is shown alongside each blot. The blot was cut at the 52 kDa marker. The Western Blot showing SORCS2 and housekeeping protein β-tubulin expression in HD-MB03 cells with SORCS2 siRNA (SORCS2 KD) or a non-targeting control siRNA (NT control) is shown (n=1).These values represent one of the migration assay experimental replicates in Figure 5.17.

SORCS2 knockdown also seemed to reduce D283-MED cell migration, although this was not significant when compared to the control. While the RNA expression knockdown was of 53% at 24h and 44% at 72h, there was a 9% increase in expression in the knockdown compared to the control at 48h. This cannot be explained biologically, as gene expression would not decrease again after an increase in expression. However, this increase at 48h was seen in 2 samples out of the 3, and the third sample only showed a 7% decrease in expression compared to the control at 48h. Interestingly, *SORCS2* knockdown also seemed to increase cell viability. This confirms that the reduction in migrated cells observed was not due to a reduction of cell viability, and suggests further work into SORCS2's role in cell viability in a cell line-dependent manner. Protein extraction was unsuccessful on the D283-MED cell line, and an siRNA effect on protein expression could therefore not be investigated.

The results from these experiments may not allow the drawing of significant conclusions relating to SORCS2 function in migration, however they offer preliminary data encouraging further investigation. While problems with the method may have affected the absence of a significant effect on cell function, these results may also indicate that SORCS2 does not play a direct role in cell migration. This null hypothesis is supported by the IHC analysis of patient TMAs presented in section 5.2.3. In order to definitively prove or disprove the hypothesis that SORCS2 has a function in medulloblastoma metastasis relating to cell motility and invasion, more robust data is needed.

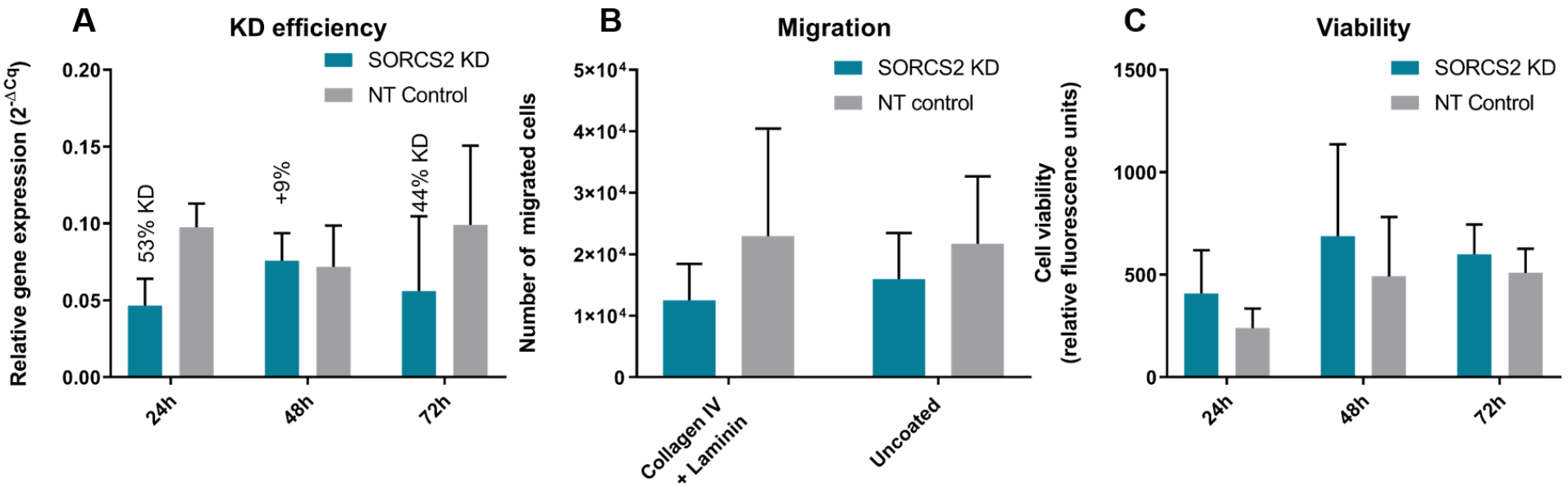


Figure 5.20 A decrease in SORCS2 expression decreased cell migration and increased cell viability in D283-MED.

A) The mean of RNA expression in D283-MED cells treated with SORCS2 siRNA (SORCS2 KD) or a non-targeting control (NT control) siRNA was quantified by qRT-PCR and normalised with housekeeping gene HPRT. **B)** Cells migrated for 48h across inserts coated with 5 µg laminin and 10 µg collagen IV towards aCSF supplemented with 10% FBS. The number of migrated cells treated with SORCS2 siRNA or a non-targeting control siRNA were quantified by calcein AM metabolic activity assay. Fluorescence readings for each condition were plotted against a standard curve of known cell numbers in order to derive the exact number of migrated cells. **C)** The metabolic activity of cells in 96 well plates over 96 hours was assayed using PrestoBlue cell viability reagent. Significant differences in means between SORCS2 KD and NT control were calculated using one-way ANOVA with Tukey's multiple comparisons. None of the differences are significant. Error bars represent SEM (n=3).

5.6 Summary

The expression of genes of interest *SORCS2, LMNB1* and *CORO2B* in medulloblastoma patients was investigated in this chapter. Although *SORCS2* expression was highest in the WNT subgroup overall, analysing expression in the 12 molecular subtypes demonstrated that SORCS2 expression was highest in Group 3α and Group 3γ, the two most metastatic subtypes with the poorest patient survival. In addition, *SORCS2* was more highly expressed in metastatic Group 3 patients compared to the non-metastatic patients of the same subgroup. Patients with the poorest survival had metastatic tumours and high *SORCS2* expression. These patients' survival dramatically decreased within the first 12-18 months in the presence of both high SORCS2 and metastasis, suggesting a possible link between SORCS2, metastasis, and tumour recurrence.

CORO2B and *LMNB1* were most highly expressed in Group 3 tumours, and the patient data also suggested a possible link between their gene expression to metastasis and survival. High *CORO2B* expression was also found in patients with metastatic tumours and poor survival. In the case of *LMNB1-DT*, further investigation is needed into how lncRNAs such as this one may regulate genes and proteins in order to affect medulloblastoma phenotypes. *LMNB1-DT* and *CORO2B* remain targets of interest for further investigation, although due to time constraints the end of this project was focused on investigating the expression and possible function of only one gene, *SORCS2*, in medulloblastoma tissue and cell lines.

Although the analysis of patient gene expression and survival suggested a link between *SORCS2*, metastasis, early recurrence and poor survival, protein expression in patient TMAs did not corroborate this hypothesis. Analysis by IHC showed that SORCS2 expression was found in tumour cells in just over half of the cores studied. SORCS2 expression was strongest in WNT tumour cores, in agreement with the patient gene expression in the Cavalli *et al.* dataset. However, protein expression was not significantly present in tumour cores representing Group 3 or metastasis, and SORCS2 was not significantly higher in the patients with poorer

prognosis. This did not support a function for SORCS2 in malignant medulloblastoma tumours. The sampling size may have been insufficient to make significant conclusions about the tumour characteristics that correlate with higher SORCS2 expression. Further protein expression analyses on an individual cell level, and on samples of the invasive edge of the tumour may be needed to make any conclusions. This also brought to light a possible challenge in investigating SORCS2 in brain tumours, since SORCS2 was highly expressed in normal CNS tissue in the tumour cores.

The expression of *SORCS2* RNA and protein was confirmed in 7 established medulloblastoma *in vitro* cell lines. In order to test the hypothesis proposing a role for SORCS2 in cell migration, the migration assay developed in Chapter 3 was used to quantify cell migration after *SORCS2* knockdown by siRNA. *SORCS2* knockdown did not have a significant effect on cell migration *in vitro*. Further testing is needed to conclude whether a more robust and stable knockdown cell line would have reduced motility and invasion capacity, or whether *SORCS2* may not have a function in cell migration after all.

Based on the results shown in Chapter 4 and Chapter 5, further investigation into the function of SORCS2 was proposed in order to confirm or disprove the hypothesis that this gene and encoded protein have a function in metastatic medulloblastoma.

Chapter 6 Discussion

6.1 Main Findings

A simple *in vitro* model representing key features of the interface between the brain and the CSF was developed to enable the capture of migrating cells from three compartments: suspension, adherent, and migrated, for molecular analysis.

In order to observe the gene expression changes that occur during cell migration and identify target genes linked to medulloblastoma metastasis, the transcriptomic changes of Group 3 cell lines were analysed using 3′ UPX RNA-Seq as they progressed through the three compartments of the *in vitro* model. The analyses yielded a list of genes of interest that may play a role in cell processes that lead to either the adhesion of cells to a basement membrane matrix and/or the migration of cells through the basement membrane towards CSF. The candidates *SORCS2, CORO2B* and *LMNB1-DT* were selected for further investigation in the context of this project.

The expression of these genes of interest in medulloblastoma patients was investigated, with *SORCS2* emerging as the strongest candidate. In patients with high *SORCS2* and metastatic tumours, there was a drop in survival within the first 12-18 months, suggesting a strong link between SORCS2, metastasis, and tumour recurrence. However, preliminary functional experiments did not support this hypothesis. This thesis proposes further investigation into the possible function of SORCS2 in metastatic medulloblastoma. The published functions of SORCS2 will be reviewed, and suggested future works will be discussed in this chapter.

6.2 Developing an *in vitro* model of medulloblastoma

6.2.1 Addressing the need to identify the subset of clones that drives metastatic dissemination

One of the 10 “hallmarks of cancer” as defined by Hanahan and Weinberg is tumour cells “activating invasion and metastasis” (Weinberg and Hanahan, 2000, Hanahan and Weinberg, 2011). Since the publication of the hallmarks of cancer framework, researchers have defined an invasion-metastasis cascade whereby metastatic cells invade their local tissue, enter the blood or lymphatic system and remain in transit until they exit into their secondary site to form micro-metastases, and finally, grow into macroscopic tumours that colonize the secondary site (Fidler, 2003, Welch and Hurst, 2019). Tumours are made up of multiple clones, and metastatic disease is understood to stem from a small subset of clones in the primary tumour (Talmadge and Fidler, 1982, Yamamoto et al., 2003, Navin et al., 2011).

In medulloblastoma, clonal selection was demonstrated in metastasis using the *Sleeping Beauty* transposon system (Ivics et al., 1997) in a SHH mouse model (Wu et al., 2012). This random mutagenic approach has been used to identify genes which are assumed to be altered to confer a survival benefit. The genetic makeup of primary and metastatic tumours in the model of SHH medulloblastoma demonstrated that >10% of common insertion site events overlapped between the two compartments. The same model also showed that the genetic characteristics of metastatic deposits were found in small sub-clone populations of the primary tumour, and that different metastatic deposits were heterogeneous (Wu et al., 2012). Based on this understanding, it is unlikely that research will identify one overarching signalling pathway to control and inhibit metastasis, particularly one that applied to all 4 subgroups. This is made more difficult as most of the available medulloblastoma tissue and cell lines are derived from primary tumours, and may not represent the key characteristics of metastatic cells.

Metastatic tissue is rare and difficult to obtain, and if available, is often insufficient to address the growing number of research questions. One way to answer pre-clinical

research questions in order to identify biomarkers and therapeutic targets is the use of patient derive xenograft (PDX), orthotopic mouse models, and relevant transgenic animal models. Another method is replicating the TME *in vitro* to induce gene expression and protein function that cells would employ *in situ* to metastasise. Currently, all *in vivo* models of Group 3 medulloblastoma rely on *MYC* amplification, which only accounts for 17% of the patient population, and there is a lack of any *in vivo* models that represent the Group 4 subgroup. Increasingly sophisticated *in vitro* models may be the answer to better informed *in vivo* studies and allowing optimal use of precious tissue samples in validation studies.

In the context of this project, creating a model whereby cells transitioned through 3 compartments representing stages of basement membrane invasion, aimed to isolate the subset of cells with the ability to metastasise and disseminate. The pros and cons of the model will be discussed in section 6.2.3.

6.2.2 Addressing the need to investigate the poorly understood TME of leptomeningeal metastasis

In order to better target metastatic and disseminated medulloblastoma tumours, there is a need to understand the genomics and functions of cells that are unique to the metastatic niche. Primary medulloblastoma tumours occur in an environment that includes various cell types such as neurons, astrocytes and immune cells, as well as non-cellular components that make up the extracellular matrix (ECM). The primary tumour niche in the brain is rich in growth factors, nutrients, and interactions with the cellular and non-cellular components of the TME. In contrast, the tumour cells that disseminate to secondary sites to form metastases are exposed to a vastly different TME in the subarachnoid space (Figure 6.1). This leptomeningeal niche is made up of basement membrane lamina and CSF which has dramatically lower concentrations of growth factors and nutrients than those found in the brain parenchyma niche (Van Ommeren et al., 2019). In the field of medulloblastoma research, there is a need to investigate the poorly understood TME of leptomeningeal metastasis in order to identify therapeutic strategies to inhibit and treat dissemination.

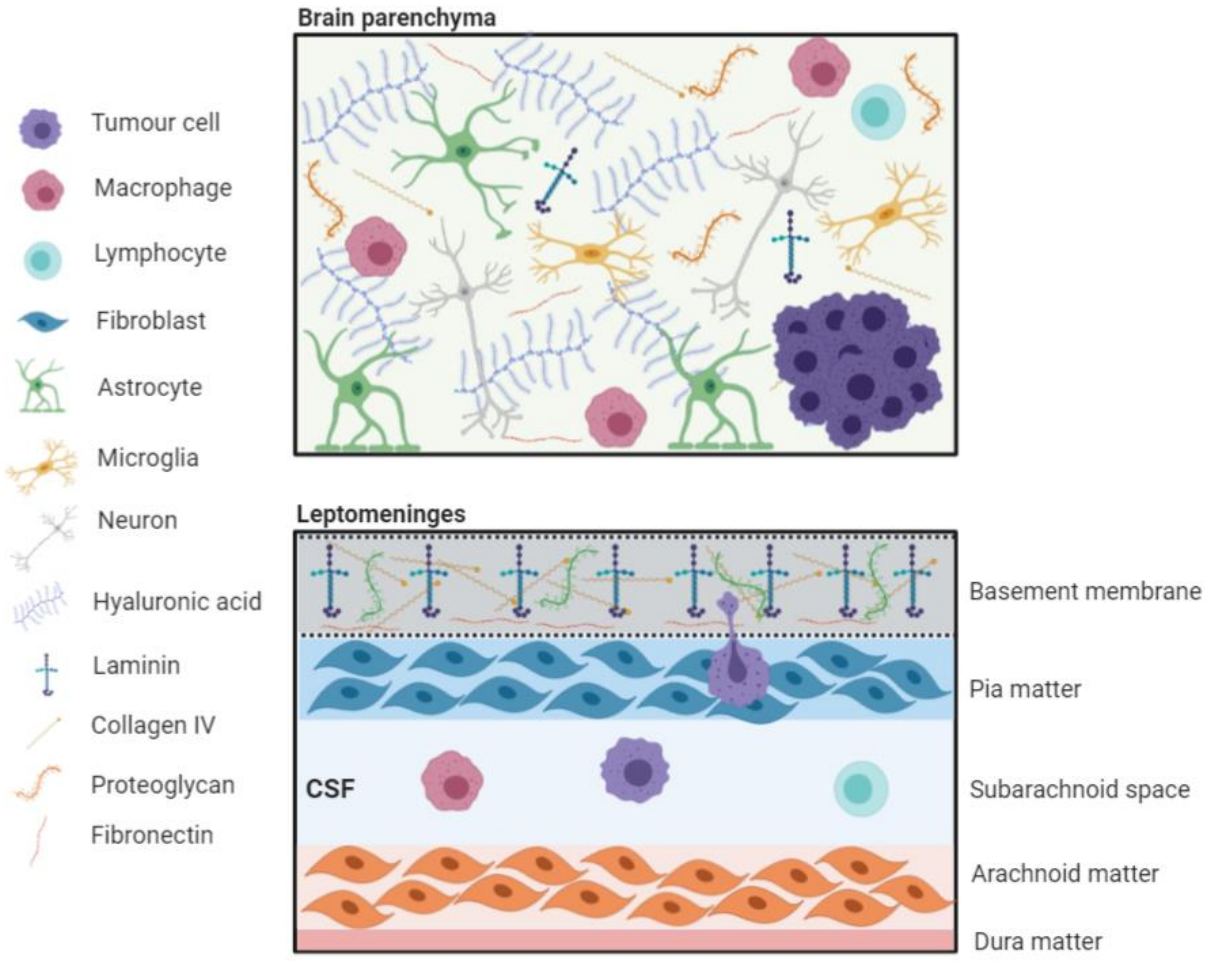


Figure 6.1 The primary tumour niche in the brain parenchyma and metastatic niche in the leptomeninges differ in composition and structure.

The primary tumour niche is in the brain is rich with signals from ECM and various neural and immune cell types. In comparison, the cerebrospinal fluid in the subarachnoid space is a sparse environment that tumour cells invade into. A better understanding of the signals that drive metastatic invasion, encourage tumour cell survival, and lead to the colonization of the leptomeninges are key to better targeting metastatic medulloblastoma. This schematic was adapted from Sofroniew, M.V., 2015 and Van Ommeren *et al*., 2019 using “app.biorender.com”.

The TME also differs according the medulloblastoma tumour subgroup, for example it is known that Group 3 and Group 4 tumours have more cytotoxic lymphocytes and endothelial cells than the other medulloblastoma subgroups (Bockmayr et al., 2018). It is also known that Group 3 and Group 4 tumours most commonly occur in the 4th ventricle, but that Group 3 tumours have the smallest primary tumours (Zapotocky et al., 2018). This suggests that the most highly metastatic subgroup, Group 3, may rely on invasion into the CSF system through the 4th ventricle rather than growing in size to reach the CSF niche. In order to address this particular metastatic event, the project presented in this thesis aimed to model the interface between the primary tumour niche and leptomeningeal metastatic niche that Group 3 cells invade across. This aim was not entirely achieved, because the migration assay did not recapitulate many elements of the tissue environment including a 3D matrix and different stromal cell types. The benefits and caveats of this migration assay will be discussed in the following section.

As described in Chapter 3, the classic migration assay was adapted in order to represent certain features of the leptomeningeal niche in a simple and reproducible manner, in a format that would allow routine cell assays to be performed, as well as the isolation of cells for molecular analyses. The approach taken was to coat the trans-well insert membrane with two ECM components of the basement membrane and artificial CSF to represent the subarachnoid space. Although the artificial CSF has the same base composition as human CSF (Table 3.4), this did not contain proteins and cell types that would be present in the leptomeninges. This will be discussed further in section 6.2.3.2 below. Cell-based assays are performed routinely in most research laboratories, but often in vastly different conditions from *in vivo* experiments and the *in situ* tissue environment that is being investigated. In this project, the *in vitro* model in question was used to isolate cells at three different stages of migration that likely occur as cells invade the 4th ventricle, and the same model was used to begin validating the function of identified candidate of interest SORCS2 in cell migration.

6.2.3 Pros and cons of the model

6.2.3.1 Pros:

- Cells are separated into different compartments based on behaviour, which allows precise quantification of migrating cells.
- Standard cell assays can be performed, and cells can be isolated for molecular analysis.
- Simple, made up of a few specific components, and therefore easily reproducible.

The modified Boyden chamber assay was selected rather than a scratch wound assay or spheroid invasion assay as it enables the separation of cells into compartments based on their migratory behaviour. In this project, the separation of cell compartments through the assay was exploited in order to sequence their differential transcriptomes. Modifying an existing migration assay allows the application of standard cell assays including migration and proliferation assays while the cells are cultured in the model. Separating the migrating cells from non-migrating cells also has the advantage of accurately quantifying the migrating cells.

The tendency of Group 3 and Group 4 medulloblastoma cells to grow in suspension or semi-adherently means spheroids are difficult to form. Most of the cell lines used in this project could not be induced to form spheroids. Consequently, culturing cells in their standard culture conditions on top of or encapsulated in matrix was selected for this project. Later work in our lab demonstrated that some cell lines can form tight aggregates when cultured in neurosphere medium containing methylcellulose (Roper, S.J., 2019; Roper et al., 2020 unpublished data currently under review). The modified trans-well format was best suited for the particular research aim of isolating migrating cells. Reproducible Group 3 and Group 4 spheroids could be used as a model in future projects, possible in conjunction with the application of laser-capture microdissection (LCM) to isolate of the invasive edge of spheroids cultured in a hydrogel matrix for analysis (Espina et al., 2006).

Another advantage of the modified trans-well model presented in this thesis is its simple composition which makes it cost effective, easily reproducible and adaptable for other research projects. The two major components of the basement membrane, collagen IV and laminin (Rowe and Weiss, 2008), were used to coat the trans-well insert, and commercially-available aCSF was used in the receiver plate. Collagen IV was selected as it makes up 50% of all basement membrane components, and laminin as it is the most abundant glycoprotein in basement membranes (LeBleu et al., 2007, Mak and Mei, 2017). Other proteins such as Nidogens and HSPGs also contribute to basement membrane protein composition, but at lower levels. Laminin isoform 111 was chosen as it is a specific component of the parenchymal basement membrane along with laminin 211, whereas laminin isoforms 411 and 511 are more specific to the endothelial basement membrane (Thomsen et al., 2017). The parenchymal basement membrane is a collective name for the meningeal, epithelial and astroglial basement membranes which separate the brain parenchyma from the Pia matter (Sofroniew, 2015), and would likely be crossed by cells invading from the brain to the CSF. Different isoforms of laminin could be compared in a future study to determine whether they have varying effects on cell migration.

In Chapter 3, the steps taken to compare collagen IV and laminin with BME were described. BME contains high concentrations of many components commonly found in basement membranes and has been used in the past as the main *in vitro* invasion assay to identify the PDGFRA-Akt-ERK pathway (Abouantoun and MacDonald, 2009), GLI2 and ARNT (Jenkins et al., 2014), and NICD1, the active form of NOTCH1, (Kahn et al., 2018) as drivers of medulloblastoma metastasis. While it has been successfully used by other researchers to model invasion of medulloblastoma cells and other solid tumour types (Sun et al., 2015, Lim et al., 2016a, Tang et al., 2019, Wang et al., 2019), BME was not conducive to the migration of cell lines in my hands. In addition, the batch variability of BME and the lack of information regarding the applied BME concentration of several publications impede reproducibility between labs (Hughes et al., 2010). A simpler basement membrane composition was therefore selected for the model in this thesis.

Other studies have reported methods that allow the recapitulation of native cerebellum composition and structure *in vitro*. Medulloblastoma spheroids implanted onto ex-vivo organotypic cerebellum slice culture (OCSC) cultivated on inserts has been reported to conserve cellular and structural components of the primary brain tissue (Neve et al., 2017). By immunofluorescence labelling of cells, Neve et al observed cell growth and infiltration into the organ slice. Organotypic tissue slice culture could be seen as an intermediate between *in vitro* cultures designed and assembled by researchers, and *in vivo* models. A similar model would be more complex to replicate due to the need for a supply of *in vivo* tissue, and may also be impacted by variability in animals. Additionally, the isolation of implanted cells from the organotypic slice culture was not reported, and would need to be optimised in order to derive molecular information about the invasive cells. A combination of different methods and techniques may be the future of developing more complex 3D cultures that are representative of native tissue.

6.2.3.2 Cons:

- Most of the model optimisation work lacks appropriate number of replicates to draw significant conclusions.
- The absence of other components of the TME.
- "Contamination" from cells at different stages of migration in each compartment.
- Cells cannot be imaged while migrating.
- FBS is likely not an accurate model for signals in CSF
- The upper compartment does not represent the 3D brain environment.

The model presented was developed in line with the aim of this project to isolate and sequence migrating cells. The format does however have caveats that could be resolved by further adapting the conditions of the current model or selecting a different *in vitro* model based on the requirements of the project.

First, it is important to address the lack of biological replicates in most of the optimisation work presented in Chapter 3. The development of the migration assay

took much longer than anticipated for several reason. First, cells were embedded in BME with the aim of replicating work previously done in our lab demonstrating that there were differences in migration patterns between low risk and metastatic medulloblastoma cell lines (A. Nasir, unpublished data). The main observation from these experiments was that it could not be concluded whether cell migration occurred based on imaging alone, and migrating cells could not be specifically isolated. While several experiments were performed with cells embedded in BME, the parameters of the culture (concentration of BME, culture medium, cell seeding density) were changed after 1 or 2 replicates, which prevented significant conclusions from being drawn from most of the experiments. The trans-well assay approach was then selected as it would allow quantification of migrating cell numbers. A trans-well assay can be done without a coating, which is referred to as a migration assay, or the membrane can be coating with an ECM which acts as a barrier overcome by invasive cells, referred to as an invasion assay. In this thesis, the use of BME as a coating did not allow cell migration in certain cell lines, and only minimal cell migration in others. After the initial invasion assay experiment was performed, the decision was made to change the coating to individual components of the basement membrane (collagen IV and laminin 111) rather than continue with BME from a different batch.

Another key detail is that the BME used in this thesis was not growth factor reduced. This is likely the main reason that cells did not migrate across the BME, as the presence of growth factors may have masked the chemokine in the receiver plate. The standard invasion assays in most published studies use growth factor reduced BME, and the two types of BME should have been compared before moving forward with collagen IV and laminin 111 only. Another caveat of these experiments is that few concentrations of collagen IV and laminin 111 were tested, and only 1 or 2 replicates were performed for each. The concentrations were selected based on a published study that optimised ECM coating for migration assays (Brenner et al., 2000), but a wider range of concentrations should have been tested several more times in order to make significant conclusions about the effect of concentration on migrating cell number. As the collagen IV and laminin coating was not compared to

growth factor reduced BME, and their combination did not seem to act as a barrier to the cell line, this cannot be called an invasion assay. The final conditions used in the migration assay (laminin 111 5 µg, collagen IV 10 µg, aCSF supplemented with 10% FBS and 0.8 mg/mL glucose and 48h) were repeated at least 3 times and the number of migrating cells was deemed sufficient to extract RNA for sequencing.

Another caveat of the model presented in this thesis is that it relied on only two components, collagen IV and laminin 111, to represent the basement membrane. While this gives the assay the advantage of being cost-effective and reproducible, it may be more representative of the *in situ* basement membrane to include other components such as fibronectin, nidogens, and HSPGs such as perlecan (Fox et al., 1991, Yurchenco and Cheng, 1993, Timpl, 1996). The Group 3 cell lines used in this project responded differently to the collagen IV / laminin coating. D283-MED was derived from metastatic cells in the patient's ascetic fluid, but the number of migrating cells was not influenced by the basement membrane coating. D458-MED was derived from metastatic cells in the patient's CSF, and the cell line's migration appeared reduced by the basement membrane coating. HD-MB03 was derived from the patient's primary tumour after surgical resection, and the cell line's migration appeared slightly increased by the basement membrane coating. A more complex 3D culture model would be useful to test whether different cell lines can display a consistent migration pattern, or whether the behaviours observed have biological relevance.

While the model format allowed separation of cells into compartments based on their behaviour, there may still have been some uncontrolled overlap. For example, some cells in the suspension compartment may have upregulated adhesion-related genes while preparing to adhere to the membrane. Furthermore, some cells in the migrated compartment may have lost the gene expression changes that allowed them to migrate. Such "contamination" could have led to gene expression changes in specific cell types (suspension, adherent, migrated) being missed. Alternatively, it is possible that the differential expression of the gene targets selected is in reality more

significant than was reported. Imaging the cell migrated process in the assay and quantifying the proportion of each type of cell behaviour in each compartment would be a possible method to control the occurrence of such overlaps.

Another disadvantage of the trans-well assay format is that cells could not be imaged while migrating as the membrane and pores make it difficult to differentiate between cells in the upper compartment and cells on the bottom of the insert. Images of cell migration at different time points could be used to ensure migrating cells were captured at the right time to detect the transcriptomic changes being investigated. Additionally, live cell imaging would provide key insights into the types of cell behaviours in the migration model. This may be resolved by testing more sophisticated imaging methods, or by using other assay formats. For example, the ibidi chemotaxis chamber slide (Zengel et al., 2011) used in Chapter 3 enables culture and live-imaging of cells embedded in a 3D matrix. However, this method does not allow the isolation of migrating cells from the chamber slide. The spheroid invasion assay mentioned in the previous section can also be used in conjunction with an automatic cell motility analysis platform to quantify cell spread and distance in a 3D matrix. Such an assay has been validated in SHH medulloblastoma cell lines (Kumar et al., 2015a). As 3D culture models continue to evolve, improved methods for imaging as well as cell isolation may become available.

There is little understanding of the signals that attract metastatic cells to the CSF, and most of our understanding comes from the study of non-CNS solid tumours that also metastasize to the brain. It has been shown that breast cancer cell lines can prepare the leptomeningeal niche in the subarachnoid space to support growth of metastases by secreting complement protein C3 (Boire et al., 2017). The modified trans-well model presented in this thesis incorporates aCSF to represent the sparse environment cells are exposed to in the leptomeninges, but it likely does not recapitulate the specific signals produced by leptomeningeal cells that may guide and/or support the tumour cells in the metastatic niche. In order to improve this, a co-culture model could be developed with cell types that may be producing migratory

cues for tumour cells in the body such as neurons, astrocytes, arachnoid cells, pial cells, immune cells and endothelial cells.

Finally, in order to deem this model a true representation of the interface between solid brain parenchyma and the CSF in the leptomeninges, essential characteristics of the primary tumour environment would need to be incorporated into the model. An approach to accomplish this in the trans-well format presented is inclusion of a 3D brain-like matrix in the top compartment. The culture environment affects gene expression profiles, which in turn impacts cell phenotype and behaviour *in vitro*. This was recently demonstrated in a study by Sood and colleagues. Primary patient ependymoma and glioblastoma multiforme (GBM) cells were cultured in 3D tissue models, and differential expression was observed between models containing brain ECM components and models with non-brain-derived ECM. The study was also the first to report lipid droplet production by GBM cells cultured *in vitro*, a feature that had previously only been seen in *in vivo* models of high grade GBM (Sood et al., 2019). This supports the importance of developing *in vitro* models that accurately incorporate the complex ECM microenvironment in order to recreate key tumour cell phenotypes only observed *in vivo*.

Looking back at the optimisation work, it may have been beneficial to spend more time on the basement membrane coating. This includes a comparison between growth factor reduced BME, standard BME and the combination of collagen IV laminin. The concentrations of collagen IV and laminin could have been further optimised with more replicates and different concentrations to obtain statistically significant differences in migrating cells when comparing different coatings. While the model used in this thesis accomplished the aim of separating cells into different stages of migration, it does not accurately model the basement membrane and this is an aspect that would be important to develop in the future in a more complex 3D *in vitro* model.

6.2.4 Future directions

The development of more sophisticated and representative *in vitro* models may be the key to accelerating preclinical research of novel biomarkers and druggable targets for translation into the clinic. Ongoing work in our research group is aimed at developing more accurate 3D culture models in order to study metastatic medulloblastoma cell functions. This includes the development of a 3D *in vitro* brain model using the semi-synthetic hyaluronan-based hydrogel (Linke et al., 2018)(F. Linke, unpublished data). In order to select this hydrogel model, we have compared the hyaluronan hydrogel, BME, and a PEG/dextran-based gel for short and long-term culture of medulloblastoma cells.

The brain matrix is unique and characterized by glycosaminoglycans such as hyaluronic acid (HA) and the presence of several brain-specific proteins and link protein (Spicer et al., 2003). We concluded that the sarcoma-derived BME poorly represented this specific brain matrix composition, and therefore may enable cell interactions with matrix components that are rarely present in the brain while failing to support crucial interactions e.g. with HA. Another consideration was the adaptability of matrix stiffness, as cells embedded in a 3D matrix will use different strategies for movement compared to those growing in 2D (Liu et al., 2006). As a consequence, the global gene expression differs between cells cultured in 2D compared to 3D, and different 3D environments. BME alone provided a very soft hydrogel (~100 Pa), which is not brain-specific (Abbott, 2003, Chaudhuri et al., 2014, Asthana and Kisaalita, 2013). The stiffness of the hyaluronan-based hydrogel, however, can be customised to resemble that of the brain (1-2 kPa). The composition of the hyaluronan hydrogel is also customisable by adding more brain specific matrix components.

This work is the next step towards developing more accurate models of the distinct TMEs encountered by medulloblastoma cells in the tumour niche and the leptomeningeal metastasis niche. The modified trans-well basement membrane assay presented in this thesis could be combined with the hyaluronan hydrogel

model, and other cell types introduced to create a co-culture environment (Figure 6.2). This could form the basis of a more complex model combining a brain ECM-like 3D environment, a basement membrane barrier, and stromal cell types found in the medulloblastoma niche.

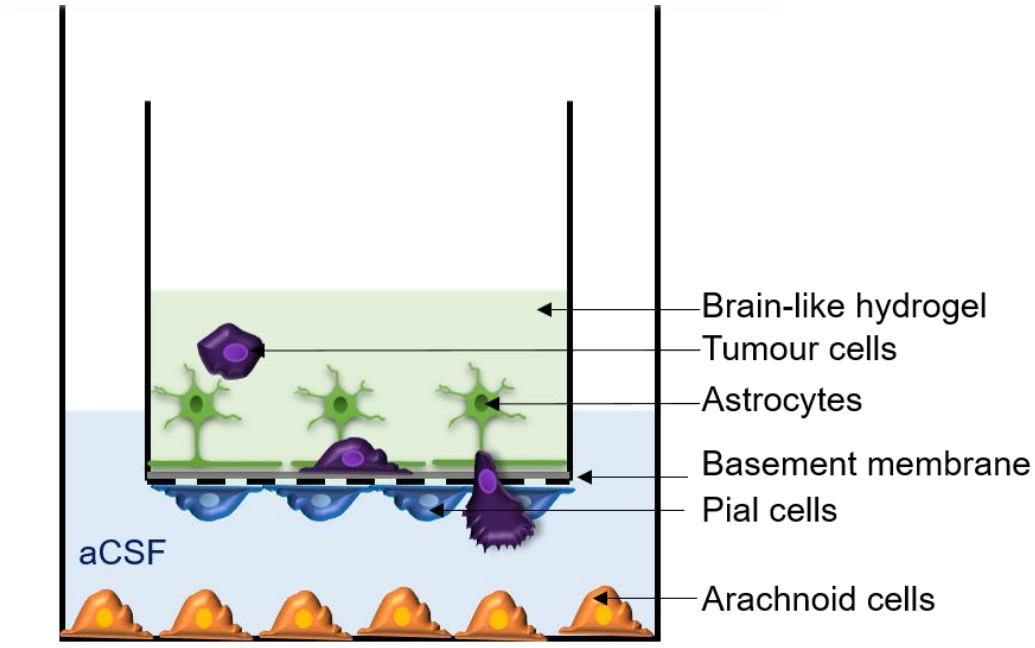


Figure 6.2 Summary of a possible complex 3D culture model representing the brain-leptomeninges interface.

A summary of the 3D culture model with key features of the primary tumour niche and metastatic niche in the leptomeninges. The astrocyte end feet and pial cell layers would contribute to the basement membrane barrier between the two niches. Pial cells and arachnoid cells may secret signals into the aCSF to induce invasion. This base model could be further adapted to represent subgroup-specific features such as neuronal and immune cells in the brain ECM-like hydrogel.

6.2.4.1 Conclusions

In summary, Chapter 3 of this thesis presented an approach to adapt the established trans-well migration assay format in order to make it more representative of the tissue niche studied. The work presented also suggested two possible uses of the simple *in vitro* migration format: performing standard cell culture assays to investigate cell migration, and the isolation of cells from any of the 3 compartments for molecular analysis. While trans-well assays are commonly used to investigate the migrational and invasive capabilities of cells, this project may be one of the first to demonstrate its use for isolating cells. The modified Boyden chamber model presented in reproducible and accessible, as all components are commercially available. It has since been successfully applied to other Group 3 and Group 4 cell lines in the context of the ongoing projects within our research group. Data from these experiments can be used as a starting point towards addressing two key challenges in medulloblastoma research: dissemination between a primary and metastatic niche, and identifying characteristics of sub-clones that drive dissemination.

6.3 Identifying novel markers of migration and metastasis using NGS

The genomic landscape of medulloblastoma has been the focus of several studies (Northcott et al., 2012a, Northcott et al., 2012b, Robinson et al., 2012, Jones et al., 2012, Rausch et al., 2012, Ramaswamy et al., 2013, Northcott et al., 2014, Morrissy et al., 2016). A common goal of these informatics studies was to identify the differences and similarities between the distinct medulloblastoma entities in order to discover novel therapeutic approaches.

Whatever the type of data (genomic, proteomic, methylation), large-scale studies often collectively look at global expression in a large cohort. Methods that allow a more precise focus on individual cells and molecules are also needed in order to fully understand the biology of particular genes, proteins, and their pathways. The following sections discuss the advantages and disadvantages of the transcriptomic sequencing study in this thesis.

6.3.1 Advantages of the study

- 3′ UPX RNA-seq allows the sequencing of small samples.
- Target identification studies could help filter the vast amounts of data obtained from large-scale ‘omics studies.

It is crucial to relate data discovered *in vitro* with its clinical relevance, but this is challenging without the availability of large amounts of relevant tissue samples. As discussed in section 6.2, the lack of availability of metastatic material from patients for use in research necessitates the development of relevant *in vitro* and *in vivo* models in order to identify individual molecules that contribute to cellular processes. An advantage of the approach presented in this thesis is that it was model-led rather than target-led, and identified possible drivers of cell migration in small numbers of cells. New NGS techniques such as 3′ UPX RNA seq allow the power of RNA-seq to be applied to small-scale *in vitro* projects investigating small numbers of cells. Conclusions drawn from transcriptomic changes identified in our *in vitro* model relied on the assumption that processes employed by the cells adhering to basement-

membrane like surface and migrating through the membrane are representative of the cell phenotypes that lead to migration and metastasis *in situ*.

The method presented cannot replace the information gained from large scale sequencing studies on patient tissue to elucidate the drivers of disease. However, target identification studies such as this one can help filter the vast amounts of information from large-scale 'omics studies and shed light on previously disregarded genes. For example, patients from the study by Cavalli et al (Cavalli et al., 2017) with high expression of *SORCS2* in metastatic tumours had poor survival, but this would not have been identified were it not for the guidance provided by our focused dataset. The use of single cell RNA-seq (scRNA-seq) has recently elucidated the elusive cellular lineage of medulloblastoma subgroups. Studies employing scRNA-seq reported the likely cells of origin for Group 3 and Group 4 medulloblastoma (Hovestadt et al., 2019b, Vladoiu et al., 2019). Expanding the use of precise genomic methods such as scRNA-seq will facilitate our ability to relate genomic data between *in vitro* models, *in vivo* models, and bulk tumour sequencing studies.

6.3.2 Disadvantages of the study

- Data derived from 3′ UPX RNA-seq does not inform on post-transcriptional and modifications and epigenetic control of target genes.
- Protein expression validation or proteomic studies are needed to investigate the function of gene candidates.

The key pathways and the mutations within these that drive the WNT and SHH subgroups were the most straightforward to identify, while the drivers of Group 3 and Group 4 subgroups remain elusive. This is because defining gene alterations have not been found in Group 3 and Group 4 at such a high frequency as SHH and WNT tumours. One possible explanation for this is that most studies to date have focused on bulk genomic sequencing. The expression of driver genes may be altered at several levels: transcription, post-transcription, and during translation into protein. Therefore, the future of medulloblastoma profiling likely lies in the integration of gene

data with non-gene-based data as well as the union of large scale studies with relevant pre-clinical *in vivo* and *in vitro* studies.

The 3′ UPX RNA-seq method does not provide data relating to DNA methylation, which may be significantly influencing the transcription and translation of the genes studied. Methylation is one of the most common RNA modifications, which results in gene silencing by acting on the structure of the chromatin, post-transcriptional mRNA, and translation into proteins (Greenberg and Bourc'his, 2019). The importance of integrating gene data with non-gene-based data has been demonstrated by recent large-scale medulloblastoma studies. A key example of how methylation data has enhanced understanding up medulloblastoma is the application of similarity network fusion (SNF) to integrate gene expression data with DNA methylation data by Cavalli *et al*. This led to the definition of 12 clinically and biologically relevant medulloblastoma subtypes within the 4 known subgroups. While previous studies focusing on gene expression could not delineate the overlap between Group 3 and Group 4, the integrated approach supported their categorisation into two different biological entities (Cavalli et al., 2017). The dataset created by Cavalli *et al* was used to validate the transcriptomic changes identified in this thesis.

While the cell's gene expression is most commonly investigated, it is the proteins that ultimately influence different cell phenotypes. Integrating proteomic profiling with other forms of data may be another way to get a more complete view of what drives cancer. While this thesis has identified candidates of interest, protein validation work or a proteomic study is needed in order to investigate the function of these candidates in medulloblastoma. A recent study examined the proteomic, phospho-proteomic and protein acetylation data for 45 medulloblastoma tissue samples. Most of the samples had pre-existing genome sequencing, RNA-seq or methylation profiling and thus the researchers concluded that the proteomic profiles corresponded to the 4 medulloblastoma consensus subgroups (Archer et al., 2018). A similar study by Rivero-Hinojosa and colleagues also reported that proteomic

classification of medulloblastoma tumours validated the 4 molecular subgroups. However, they demonstrated that clustering tumours based on the genes that encode the proteins used for their proteomic classification did not result in the 4 medulloblastoma subgroups (Rivero-Hinojosa et al., 2018).

These studies revealed that while the medulloblastoma classification based on genomic and methylation data is valid and useful, investigating the proteome offers a new opportunity to identify molecules that contribute to the phenotype. These publications also reported certain molecular mechanisms that had not been found through transcriptomic or genomic data. Finally, the studies found that Group 3 and Group 4 tumours had the lowest correlation between mRNA and protein expression, suggesting that mRNA abundance may not be an accurate predictor of protein expression and function. This further highlighted the need to validate findings from genomic studies at the protein level, particularly in Group 3 and Group 4 tumours. The WNT and SHH subgroups are characterised by mutations in key elements of the signalling pathways after which they are named, but the two other subgroups do not have mutations at the same frequency and it has therefore been more difficult to characterise them. Subdividing medulloblastoma into groups based on their genomic characteristics has led to a better understanding of their differences, but a better understanding of the proteomic profiled of these tumours is needed for more translational clinical diagnostic and therapeutic tools. For example, a focus on proteomics could help to prioritise which genomic differences influence the cell phenotype.

In this thesis, IHC analysis of patient TMAs was performed to investigate the expression of SORCS2 protein in medulloblastoma. Histopathological analysis requires a large sample size with sufficient representation from molecular and metastatic groups as well as tumour regions (edge versus core) in order to effectively investigate protein expression in patients. Tissue banks for rare tumours such as medulloblastoma take decades to build, and the TMAs and tissue samples for genomic or proteomic analysis are a precious yet finite resource needed to answer a

disproportionately high number of research questions. The creation of a large proteomics database similar to the R2 platform could allow data generated from patient tissue to be used most efficiently by researchers around the world.

6.3.3 Candidates of interest identified by the analysis of 3′ RNA-seq data

In order to select the most probable drivers of migration in medulloblastoma, the lists of genes identified in the 3′ UPX RNA-seq study were investigated in gene expression datasets from a large patient cohort (Cavalli et al., 2017). The dataset by Cavalli et al provided valuable insights into details of metastatic status, patient survival, and the most up to date medulloblastoma subtype classification. Analysis against the Cavalli patient dataset led to the selection of *SORCS2, LMNB1-DT* and *CORO2B* as transcripts likely linked to metastasis and poor survival. *SORCS2* was selected for preliminary functional validation as part of this project, and will be discussed in detail in the following section. While there was insufficient time in this project to investigate *CORO2B* and *LMNB1-DT* further, both remain targets of interest and warrant future study.

6.3.3.1 CORO2B

Coronins are a family of actin binding proteins consisting of 3 subgroups. Type I coronins (*CORO1A, CORO1B* and *CORO1C*) are the most investigated subtype, known to bind to F-actin filaments. They are important for cellular processes related to actin dynamics including cell motility and endocytosis (De Hostos et al., 1993, Mishima and Nishida, 1999). *CORO1C* regulates F-actin turnover during cell migration and neurite growth in the brain, and is overexpressed in certain brain tumours including glioblastoma. However, expression of *CORO1C* has not been detected in medulloblastoma (Thal et al., 2008, Roadcap et al., 2008).

CORO2B was first identified in neural cell types (Nakamura 1999), but has attracted less interest that its Type I family members. The function of Type 2 coronins (*CORO2A* and *CORO2B*) has only recently come to light in studies reporting its role

at the focal adhesions of podocytes. Podocytes are a specialised type of cell found in the glomerulus where their function is essential for renal filtration. Actin dynamics is central to podocytes wrapping their foot processes around capillaries to enable blood filtration (Reiser and Altintas, 2016). However, exactly how *CORO2B* affects actin dynamics in podocytes is still under investigation. It is possible that there is a yet-unexplored function for *CORO2B* in the brain, and its identification in this thesis suggests a role in medulloblastoma cells. The known function of *CORO2B* in cytoskeleton dynamics makes it an interesting candidate for cell migration, and demands further study.

6.3.3.2 LMNB1

The divergent transcript of *LMNB1* (*LMNB1-DT*) was identified as the most upregulated gene in cells adhered to the basement membrane in the *in vitro* migration model. This divergent transcript is a long non-coding RNA (lncRNA), the reverse transcript of gene for lamin b1, a component of the nuclear lamina. lncRNAs can regulate the up- or down-regulation of neighbouring protein-coding genes on many levels. lncRNAs can contribute to chromatic organization, the transcriptional process, mRNA processing, translation and posttranslational processing (Kopp and Mendell, 2018). lncRNAs can be found in the nucleus, nucleolus, cytoplasm, and mitochondria (Cabili et al., 2015). lncRNAs can also be secreted into extracellular vesicles, which can impact the cell's environment (Hewson et al., 2016). Although the *LMNB1* protein-coding transcript was not upregulated in this study, it is possible that the lncRNA may have an effect on the translation of the *LMNB1* gene into protein. It is also possible that *LMNB1-DT* has a function entirely separate to *LMNB1* through one of the many lncRNA mechanisms mentioned. Exploring these hypotheses could be the basis of a future project focused on the role of lncRNAs in medulloblastoma.

Further patient data and *in vitro* experimental data is needed to investigate a function for *CORO2B, LMNB1-DT* or other identified transcripts in medulloblastoma. In order to investigate a function for candidates in cell processes including proliferation,

migration and stemness, knockdown and overexpression studies could be performed. Future work could also include inhibition of genes of interest through the identification of drug molecules or targeting transcription factors that regulate gene expression. A suggested experimental design will be described in section 6.4.5 for *SORCS2*, which could also be applied to other target genes. In the case of lncRNAs, the experiment design would be more complex, but would adapt similar principles to investigate transcripts and the proteins that they may associate with. For example, specialised siRNAs exist to knockdown different lncRNAs, and techniques such as ribonucleoprotein (RNP) immunoprecipitation-microarray (RIP-Chip) are designed to identify RNAs that associate with RNA binding proteins complexes (Keene et al., 2006).

6.3.3.3 Conclusions

In conclusion, integrating different types of data from large-scale studies on patient cohorts will help paint a better picture of complex medulloblastoma processes such as metastasis. Data from these studies can then be used to inform smaller-scale studies employing *in vivo* models or relevant *in vitro* models. It is also important for insights gained from *in vivo* or *in vitro* studies to be validated using integrated patient datasets. In this project, cell migration into the cerebrospinal fluid was recreated *in vitro* to identify target genes of interest. The approach taken was using a trans-well assay format to separate cells into non-migration suspension cells, cells adhering to a membrane coated with the two main components of the basement membrane (collagen IV and laminin) and cells that migrated through these ECM components. In addition, artificial CSF was used instead of culture medium to mimic a liquid environment sparse in signalling molecules such as the one in the CSF. The advantages and disadvantages of this model have been discussed in section 6.2. The transcriptomic targets identified through analysis of the 3′ RNA-seq data were then validated using the Cavalli et al 2017 dataset, which integrates genomic and methylation data for detailed risk-stratification of medulloblastoma tumours. Future

work on the targets identified should include further investigation in large ‘omics datasets, as well as *in vitro* and *in vivo* experiments.

6.4 Investigating a novel role for SORCS2 in brain tumour cell migration

6.4.1 SORCS2 function in neural cells

SORCS2 is a little studied gene, encoding a family member of the vacuolar protein sorting 10 protein domain (Vps10p-D) family of type-1 membrane receptors, named after their N-terminal domain homologous to the yeast vacuolar sorting protein. There are 5 Vps10p-D proteins; sortilin (Petersen et al., 1997, Mazella et al., 1998), sorLA (Jacobsen et al., 1996, Yamazaki et al., 1996, Hampe et al., 1999), and SORCS1-3 (Hermey et al., 1999, Rezgaoui et al., 2001, Hermey et al., 2004), all containing an N-terminal Vps10p-D and a short C-terminal cytoplasmic domain. The cytoplasmic domain encodes signals for internalization and sorting, and several of the receptors have been functionally defined as sorting proteins (Jacobsen et al., 2001, Nielsen et al., 2001, Hermey et al., 2003). The receptors are most highly expressed in developing and adult brains (Rezgaoui et al., 2001, Hermey et al., 2004, Boggild et al., 2016, Boggild et al., 2018), and have been studied primarily in the context of neuronal function and neurodegenerative diseases. Recent studies reviewed by Heine and colleagues have highlighted that functions of neuronal cell may also be of interest in the field of cancer metastasis, and encouraged the comparison of these two cell types (Heine et al., 2015).

SorCS2 was the fourth Vps10p-D receptor identified in *Mus musculus* (Rezgaoui et al., 2001). SORCS2 single nucleotide polymorphisms (SNPs) are associated with risk of bipolar disorder (Christoforou et al., 2011, Ollila et al., 2009, Baum et al., 2008), schizophrenia (Christoforou et al., 2011), and attention-deficit/hyperactivity disorder (ADHD) (Alemany et al., 2015). Upregulation of *Sorcs2* was identified in a mouse model of temporal lobe epilepsy (Malik et al., 2019), and *Sorcs2* expression was induced in astrocytes following ischemic stroke (Malik et al., 2020). SORCS2's role in brain pathologies and mood disorders has been linked to its functions as a component of the intracellular trafficking apparatus (Malik et al., 2019, Malik et al., 2020) and as a pro-neurotrophin (pro-NT) receptor (Glerup et al., 2014). The pathophysiology of mood disorders is driven by impairments in synaptic plasticity,

and treatments for these, such as antidepressant drugs and lithium, increase signalling by NT factors including SORCS2 ligands nerve growth factor (NGF) and brain derived neurotrophic factor (BDNF). SORCS2 is known to form a co-receptor with $p75^{NTR}$ that mediates the postsynaptic response to NGF and BDNF as well as their precursor proteins, and therefore, controls synaptic plasticity (Deinhardt et al., 2011, Pedersen et al., 2017).

6.4.2 SORCS2 in growth cone motility

One way in which SORCS2 controls synaptic plasticity is through its function at the tip of an extending dendrite, termed the growth cone. Growth cones are rich in actin structures including filopodia and lamellipodia whose extension and retraction is regulated by Rho family GTPases. Neuronal networks are formed when attractive and repulsive guidance cues, including semaphorins, neurotrophins and pro-neurotrophins, direct axons and dendrites by influencing growth cone motility. The NGF precursor, proNGF, is responsible for initiating the collapse of the neuron growth cone when it binds to the receptor complex formed by SORCS2, $p75^{NTR}$ and Trio, and subsequently decreases Rac activation at the leading edge of the extending dendrite (Figure 6.3). The collapse of actin-based protrusions at the growth cone results from the phosphorylation and subsequent inactivation of the protein fascin. (Deinhardt et al., 2011). Characteristics such as dynamic cytoskeletal changes are shared between neuronal and cancer cells, and may be used by both cell types for similar migratory functions (Heine et al., 2015). For example, fascin has also been reported to have a key function in filopodia and invadopodia formation of highly invasive cancer cells (Li et al., 2010, Machesky and Li, 2010). In addition, there is an interesting overlap in function for signal molecules that guide axons and dendrites during development and nerve regeneration, and which induce cell motility in metastatic migration of cancers.

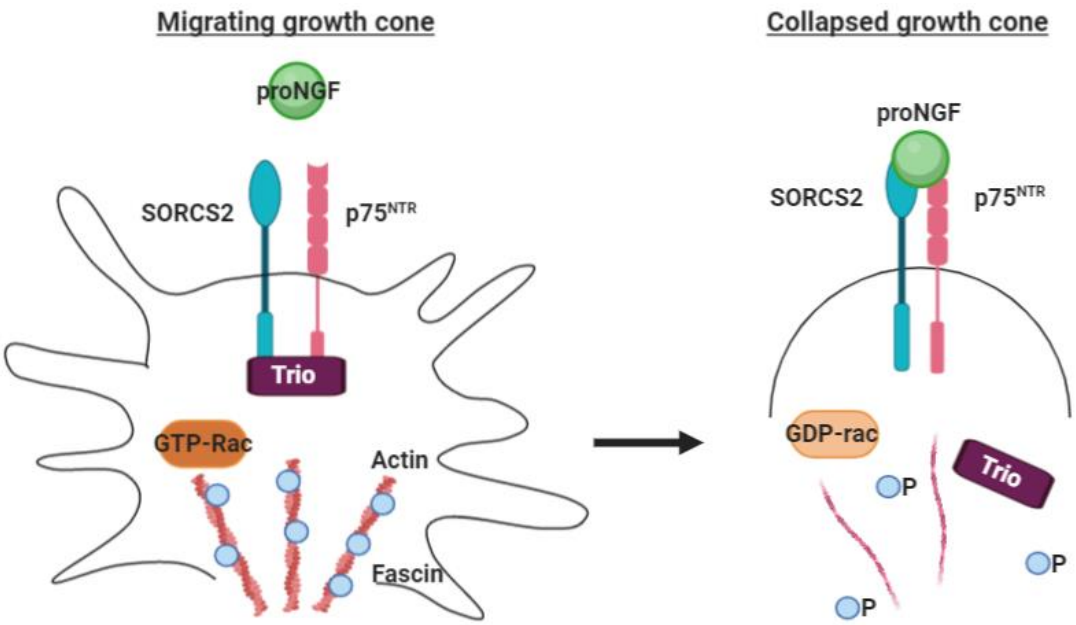


Figure 6.3 SORCS2 forms a receptor complex that binds proNGF and causes growth cone collapse.

The association of SORCS2 and P75NTR with Trio localizes Rac activity to the dynamic growth cone. Binding of proNGF to the receptor complex of SORCS2/p75NTR/Trio causes dissociation of Trio, Rac inactivation, PKC inactivation, and fascin phosphorylation. Fascin is responsible for actin bundling, and becomes inactivated when phosphorylated. This results in actin filament collapse and impaired filopodia formation. This figure was adapted from Deinhardt *et al*., 2011 using “app.biorender.com”.

SorcS2 expression in the brain during development has been extensively studied in mice. Its expression was reported as most prominent at the floor plate, which produces an array of molecules responsible for influencing axon guidance include Netrin-1, semaphorins and Shh (Boggild et al., 2018). The researchers who identified the marked expression of SorcS2 at the floor plate speculated that SorcS2 may influence the expression or effect of any of these molecules through its function as a sorting receptor. SEMA3A has been reported to act as a chemo-attractive signal inducing glioma cell migration (Nasarre et al., 2009). Netrin-1 has been shown to induce cell invasion in medulloblastoma cell lines (Akino et al., 2014), and was tested as a chemoattractant for the *in vitro* model in this thesis. In Chapter 3 section 3.3.2, HD-MB03 (Group 3) and CHLA-01R-MED (Group 4) cells migrated in response to medium containing Netrin-1, but this was not significantly different to migration in response to the control (medium with 2% FBS). This experiment could be repeated

with SORCS2-KD cell lines to determine whether Netrin-1 and SORCS2 function together in medulloblastoma cell migration. Although this has not yet been reported, SORCS2's influence on neuron motility may also overlap with a function in cancer cell migration.

Finally, it would be interesting to investigate whether the expression of *SORCS2* identified in this study was a result of the ECM coating that cells were exposed to in the migration assay. Although there is currently no evidence for a direct interaction between SORCS2 and laminin or collagen, one study reported that immobilized laminin and the SORCS2 ligand NGF on a glass surface resulted in neurite extensions (Achyuta et al., 2009). These authors' aim was to investigate the combined effect of adhesion proteins (laminin) and growth factors (NGF) on neurite outgrowth *in vitro*. They concluded that the combination of proteins had a synergistic impact on neurite growth. While this is not a direct connection to SORCS2 or to cancer cell motility, it would be interesting to study the relationship between ECM components and growth factors in the context of migration, and determine whether the expression and function of SORCS2 is affected by these. NGF was not added to the experiments presented in this thesis, but it is possible that it was present in the FBS at unknown concentrations. Future work on SORCS2's function in cancer should take into account the possible indirect regulation of the receptor through its known ligands, including NGF.

6.4.3 SORCS2 in cellular trafficking

Another role for SORCS2's in brain pathologies relates to its function in neuronal protein sorting. SORCS2 has been shown to control trafficking of protein receptors between the intracellular compartment and the cell surface in hippocampal nerves (Malik et al., 2019, Yang et al., 2020) and astrocytes (Malik et al., 2020). In the context of temporal lobe epilepsy, SORCS2 has a function in trafficking the glutamate and cysteine transporter EAAT3 to the cell surface in Rab11+ intracellular vesicles, thereby protecting neurons from oxidative stress during seizures (Figure 6.4) (Malik et al., 2019). While SORCS2's functions have been predominantly studied in

hippocampal neurons, recent studies have also implicated it in non-neuronal cell types.

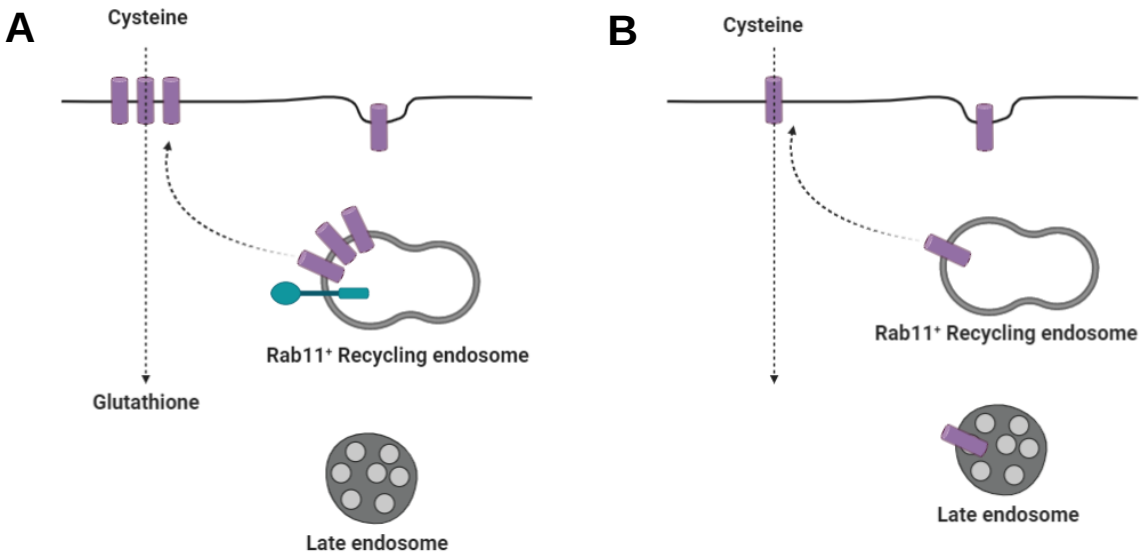


Figure 6.4 SORCS2 function in EAAT3 transporter sorting.

A) SORCS2 is responsible for targeting EAAT3 to Rab11⁺ recycling vesicles, leading to a sustained pool of EAAT3 that can mobilize to the cell surface and facilitate the uptake of cysteine. **B)** In the absence of SORCS2, EAAT3 is targeted to the late endosomes for degradation, reducing the amounts of EAAT3 molecules at the neuronal cell surface. Figure adapted from Malik *et al*., 2019 using "app.biorender.com".

In the context of ischemic stroke, SORCS2 expression in astrocytes was induced by TGF-β, and resulted in a SORCS2-dependent secretion of IGFBP3 and endostatin (Malik et al., 2020). Endostatin results from the cleavage of collagen XVIII by cathepsin L and metalloproteinase (MMP-3,-7,-9,-13 and -20) (Felbor et al., 2000, Heljasvaara et al., 2005), and is known to inhibit angiogenesis in tumour models (O'Reilly et al., 1997). Recombinant human endostatin has been used in many clinical trials as an anti-angiogenesis and anti-lymphangiogenesis treatment (Li et al., 2018). IGFBP3 has been reported to have a context-dependent effect on tumours, both as a pro-apoptotic tumour suppressor (Rajah et al., 1997, Jogie-Brahim et al., 2009) and, in contrast, as a facilitator of tumour growth in a hypoxic tumour microenvironment (Natsuizaka et al., 2014). SORCS2 functions have been described

in situations tied to oxidative stress damage in both epilepsy and ischemic stroke. Oxidative stress conditions are also found in the tumour microenvironment, which raises the question of whether the pathways linking SORCS2 function to oxidative stress response may also contribute to a role in cancer cells. Given its role as a sorting protein influencing the exposure of proteins on the cell surface or the secretion of proteins into the ECM, SORCS2 could be involved in signalling pathways leading to the secretion factors such as IGFBP3, endostatin, or others in the context of tumour growth or metastasis.

A recently published study suggested a function for *SORCS2* in breast cancer. The research showed that an IGFBP6 gene knockdown resulted in cell migration inhibition and an increase in proliferation in the breast cancer cell line MDA-MB-231. The study traced secondary and tertiary regulatory interactions of this knockdown to *LAMA4*, its regulation by miRNA (miR-4274) and the miRNA's host gene, *SORCS2* (Shkurnikov et al., 2019). miRNAs are a class of non-coding RNAs, and over half of these occur within introns of protein-coding transcription units. The transcription of miRNAs and their host transcript can occur in parallel (Rodriguez et al., 2004), and miRNAs regulate genes with complementary sequences by targeting them for translational inhibition (Liu et al., 2019). Shkurnikov et al also identified a negative correlation between expression levels of *SORCS2* and *LAMA4* in basal-like breast cancer samples (Shkurnikov et al., 2019). This supports the need for detailed investigations into the molecular networks that underlie cancer-related functions of proteins. While this thesis has suggested a possible role for *SORCS2* in a specific subset of medulloblastoma patients, it is likely this effect is the result of molecular changes and protein networks unexplored in the current study.

Upregulated *SORCS2* gene expression has also been linked to poor survival in colorectal cancer patients (Aziz et al., 2016) and lymphatic metastasis as a consequence of advanced tongue carcinoma (Watanabe et al., 2008). In addition, SNPs in *SORCS2* have been identified in patients with advanced non-small cell lung cancer (NSCLC) and poor survival (Wu et al., 2011), although none have led to

functionality studies at this time. While sequencing studies such as our own and the aforementioned published works support the need for further investigation into the function of SORCS2 in these tumours, the existing literature on SORCS2 protein function shows us that differential gene expression does not give the full picture of the role SORCS2 may be playing. As a receptor that influences the localization of proteins, clues about the pathways SORCS2 is involved in are likely lost by focusing on gene expression data alone. Despite this caveat, the gene expression dataset produced by this project and others could be used as a starting point to guide more protein-focused projects that elucidate a function for SORCS2 in cancer cells.

6.4.4 Functional overlap with Sortilin

SORCS2's family member sortilin (SORT1) is better studied in the field of oncology. SORCS2 and SORT1 expression does not often overlap in the CNS (Glerup et al., 2014, Boggild et al., 2016), but there is some overlap in their functions including the transmission of pro-BDNF and pro-NGF signals when in complex with $p75^{NTR}$. This suggests that the two genes may compensate for each other, and it would be interesting to determine whether other functions of SORT1 are also performed by SORCS2.

6.4.4.1 Therapeutic targeting of SORT1 and SORCS2

SORT1 has been reported to promote invasion in the brain tumour glioblastoma by promoting epithelial to mesenchymal transition (EMT) through the GSK-3β/β-catenin/Twist pathway. The study demonstrated that a sortilin inhibitor repressed this sortilin-mediated invasion (Yang et al., 2019). If a function for SORCS2 in medulloblastoma is confirmed in the future, inhibitors of VPS10P receptor family members could be tested to repress cell invasion.

It has also been demonstrated that SORT1 is more highly expressed by ovarian carcinoma tissue than in non-malignant ovarian epithelium (Donninger et al., 2004, Ghaemimanesh et al., 2014). A novel peptide conjugation platform to target sortilin

has recently been developed where doxorubicin and docetaxel were conjugated to a sortilin-binding peptide to selectively target ovarian cancer cell lines *in vi*tro and *in vivo* (Annabi et al., 2019). Conjugating existing drug agents to a peptide that selectively target tumour biomarkers is a strategy that could improve drug delivery into cancer cells by exploiting differences between the tumour and the stroma. If SORCS2 is confirmed as a biomarker of metastatic medulloblastoma cells, a similar method could be investigated as a therapeutic strategy.

There is an existing patent for drug modulation of VPS10P-D receptors for the treatment of mental and behavioural disorders (Pedersen et al., 2017), and an inhibitor of sortilin has been reported (Schrøder et al., 2014). Identifying a significant link between SORCS2 and cancer could offer a new incentive to develop and screen targeted inhibitors.

6.4.4.2 A function for SORT1 and SORCS2 in extracellular vesicles

SORT1 has been identified in the exosomes released by a variety of cancer cells including GBM (Choi et al., 2018). It has also been shown that SORT1 forms a complex with tropomyosin-related kinase B (TrkB) and epidermal growth factor receptor (EGFR) which is essential for exosome release as well as activation and migration of endothelial cells in the context of non-small cell lung cancer (NSCLC)(Wilson et al., 2014). Interestingly, BDNF signalling through TrkB promoted cell invasion in NSCLC cells (Zhang et al., 2010). SORCS2 has also been identified in exosomes derived from ovarian cancer cell lines (Liang et al., 2013). The role of exosomes in oncology is a fast-growing field, and research from our lab is investigating extracellular vesicles as potential diagnostic biomarkers in metastatic medulloblastoma (Jackson, H.K., 2017) (Jackson et al., 2018). It would be interesting to investigate whether SORCS2 also forms a complex with TrkB in order to implicate it in exosome release that mediates changes in the metastatic niche, or to induce cell invasion in response to BDNF signalling.

6.4.5 Future Directions

The results presented in this thesis may not allow significant conclusions relating to SORCS2 function in cell migration to be drawn; however, they offer promising preliminary data encouraging further investigation. Following the transient knockdown experiments presented in Chapter 5 section 5.5, a cell line with stable knockdown of *SORCS2* may offer a more reliable model to test the function of SORCS2 and other candidates in cell migration. The cell lines HD-MB03 and D283-MED could not be successfully transduced during the timeframe of this project. The following is therefore a proposed experiment plan that could lead to validating the SORCS2 function in migration.

- A cell line with stable knockdown of *SORCS2* could be used in the *in vitro* model of migration, as well as assays to quantify its effect on proliferation and stemness. This would offer a more robust model than transient transfection of siRNA as the knockdown effect on gene and protein expression would be maintained throughout the experiments.
- Knockdown efficiency should be assessed by quantifying both RNA and protein expression.
- Should the *SORCS2* knockdown correlate with significant decrease in cell migration, the knockdown cell lines could be used in an *in vivo* tumour growth experiment in order to conclude whether the lack of *SORCS2* significantly impacts the spread of tumour and occurrence of leptomeningeal metastasis around the brain and spine.

6.4.5.1 Defining SORCS2 localization in migrating cells

Defining the localization of SORCS2 in medulloblastoma tumours would also yield valuable insights into its function. The IHC staining presented in this thesis demonstrated that SORCS2 was cytoplasmic in medulloblastoma tumour sections, but this finding could be expanded by examining SORCS2 expression on an individual cell basis and in samples from the invasive edge of the tumour. Further

work could also include immunofluorescent (IF) labelling of SORCS2 in cells and tissue samples. As SORCS2 is commonly expressed in the brain, *in vitro* models could be used to eliminate the background expression found in patient or animal tissue. For example, labelling fixed migrating cells could confirm whether SORCS2 localizes to the cell membrane at the leading edge as it does during growth cone collapse.

6.4.5.2 Inhibiting SORCS2 expression and function in vitro and in vivo

Small molecule inhibition of SORCS2 may also be possible if pharmacological inhibitors of the Vps10p-D family of proteins are developed. Both knockdown cell lines and small molecule inhibitors would be useful tools to investigate SORCS2 function *in vitro* an *in vivo* model by developing a xenograft model. As discussed earlier, the existing SORT1 inhibitor could be tested to investigate its effects on SORCS2 functions. Another *in vitro* method to explore could be inhibiting SORCS2 protein through the use of antibodies. In a published study, SORCS2 was blocked by an antibody to prevent its ability to bind to its ligand proNGF, and this subsequently inhibited the induction of nerve growth cone collapse (Deinhardt et al., 2011). There are currently no reported transcription factors that regulate SORCS2's expression. The identification of such regulatory factor would be another opportunity to test the effect of downregulating SORCS2, and would shed some light on the larger signalling networks SORCS2 may contribute to.

6.4.5.3 Investigating SORCS2 pathways in cell migration

Due to the restricted amount of published data on SORCS2 functions and its molecular networks, it may be useful to mine large published datasets to identify possible signalling pathway connections. In order to identify links to known signalling pathways, Pearson's correlation analysis was applied to the medulloblastoma dataset by Cavalli *et al*., (Cavalli et al., 2017) to analyse the correlation between the expression of *SORCS*2 and other genes previously reported as biomarkers in medulloblastoma. The absolute value of r 0.4-0.59 is regarded as moderate

correlation (Swinscow and Campbell, 2002), and was used to filter the results. The most interesting finding was a significant inverse correlation between *SORCS2* and the gene for synuclein-α interacting protein (*SNCAIP*) in medulloblastoma patients (r -0.508, p<0.0001), particularly those with Group 3 tumours (r -0.569, p<0.0001) (Appendix 3 Supp. Fig 13). *SNCAIP* has been previously identified by a large medulloblastoma genomic study as a regulator of enhancer hijacking (Northcott et al., 2017). Northcott *et al*., reported that the gene *PRDM6* was up-regulated in Group 4 tumours as a result of enhancer hijacking associated with a duplication of *SNCAIP*. Another study focusing on α-synuclein (*SNCA)*, which encodes a protein known to interact with *SNCAIP*, reported that an *SNCA* gene knockdown *in vitro* increased the invasion ability of medulloblastoma cells (Li et al., 2018). The correlation between *SORCS2* and *SNCA* expression was also investigated in medulloblastoma patients. Although the r value was just below 0.4, the inverse correlation between the two genes was significant in patients overall (r -0.383, p<0.0001), and in Group 3 patients only (r -0.391, p<0.0001). There was also a significant correlation between *SNCAIP* and *SNCA* gene expression in medulloblastoma patients (r 0.475, p<0.0001), and Group 3 patients only (r 0.3678, p<0.0001). Taken together, these correlation analyses encourage the investigation of a molecular network within which high expression of *SORCS2* may be linked to decreased expression of *SNCAIP* and *SNCA*. If confirmed, it would be interesting to investigate signalling or interactions between the proteins, and whether upregulated *SORCS2* along with downregulated *SNCAIP* and *SNCA* has an effect on cell motility and invasion. This connection with data from a previous large-scale genomics study suggests a promising starting point for the identification of signalling pathways involving SORCS2. Identifying molecular networks that control cell migration would open up new therapeutic strategies for targeting metastatic cells.

Finally, the published works on *SORCS2* presented in this discussion chapter suggest that a possible function for SORCS2 in migration may be through the trafficking of other proteins, or the transmission of signals as a cell membrane receptor. These are functions that cannot be fully explored based on genomic data

only, and protein-based assays would therefore be needed. Co-immunoprecipitation assays could determine whether SORCS2 directly interacts with other receptors in medulloblastoma cells, such as $p75^{NTR}$ or TRkB. This method could also be used to confirm whether SORCS2 interacts with other molecules identified through correlation analysis of gene expression. However, a direct interaction is not necessary for different molecules to function in the same pathway, and imaging their co-localizations may therefore offer valuable insights. IF labelling could be used to image the co-localization of SORCS2 with proteins of correlated genes such as SNCAIP.

6.5 Conclusion

To conclude, transcriptomic studies such as the one presented in this thesis open doors to countless downstream studies of increasing specificity. The identification of *SORCS2* and *CORO2B* as genes/proteins of interest and *LMNB1-DT* as a lncRNA of interest could form the basis of several future projects in our research group and others. As discussed in this chapter, it is important to consider the complex, multi-layered nature of cancer phenotype, and incorporate wet lab and bioinformatics approaches that compare and integrate different approaches and types of data. Additionally, the *in vitro* migration model developed in this project offers a reproducible method to assay cell migration for the continued study of medulloblastoma metastasis. Several possible avenues of future research into a possible function of SORCS2 in cell migration have been discussed, which may lead to the confirmation of SORCS2 as a therapeutic target or biomarker in medulloblastoma.

Publications

- Data and conclusions from the experiments described in Chapter 3 were included in the manuscript by Linke *et al*., *Comparative study of medulloblastoma 3D hydrogel models*, currently in preparation (Linke et al., 2020).
- Conference abstract published in Neuro-Oncology in 2018 : Aldighieri, Macha, *et al*. "MBRS-44. MODELLING THE BRAIN/CSF INTERFACE IN MEDULLOBLASTOMA." Neuro-Oncology 20.Suppl 2 (2018): i137.

Conferences & meetings

Oral presentations

- December 2019: Children's Brain Tumour Research Centre Research Day (Nottingham, UK)
- November 2018: Sue Watson School of Medicine Postgraduate Research Forum (Nottingham, UK)- prize winner
- April 2018: Children's Brain Tumour Research Centre Research Day (Nottingham, UK)

Poster presentations

- September 2019: Poster at the Cancer Research Nottingham symposium (Nottingham, UK)- prize winner
- September 2018: Poster at the Cancer Research Nottingham symposium (Nottingham, UK)
- September 2018: Poster at EACR Goodbye Flat Biology (Berlin, Germany)
- July 2018: Poster at International Symposium on Pediatric Neuro-Oncology (Denver, USA)

Prizes and awards

- September 2019: 1st place 3rd year prize at the Cancer Research Nottingham symposium for a poster.
- November 2018: 1st place judges' prize and 1st place students' choice prize at the Sue Watson Oral Presentation Event for an oral presentation.
- June 2018: Received the Graduate School Travel Prize (£600) and the School of Medicine DPC funding (£600) to attend the International Symposium on Pediatric Neuro-Oncology conference in Denver, USA.

References

<Brenner et al., 2000 Coll Iv and Laminin invasion renal carcinoma.pdf>.

ABBOTT, A. 2003. Biology's new dimension. Nature Publishing Group.

ABOUANTOUN, T. J. & MACDONALD, T. J. 2009. Imatinib blocks migration and invasion of medulloblastoma cells by concurrently inhibiting activation of platelet-derived growth factor receptor and transactivation of epidermal growth factor receptor. *Molecular cancer therapeutics,* 8**,** 1137-1147.

ABOUNADER, R. & LATERRA, J. 2005. Scatter factor/hepatocyte growth factor in brain tumor growth and angiogenesis. *Neuro-oncology,* 7**,** 436-451.

ACHYUTA, A. K. H., CIERI, R., UNGER, K. & MURTHY, S. K. 2009. Synergistic effect of immobilized laminin and nerve growth factor on PC12 neurite outgrowth. *Biotechnology progress,* 25.

ADAMS, M. D., KELLEY, J. M., GOCAYNE, J. D., DUBNICK, M., POLYMEROPOULOS, M. H., XIAO, H., MERRIL, C. R., WU, A., OLDE, B. & MORENO, R. F. 1991. Complementary DNA sequencing: expressed sequence tags and human genome project. *Science,* 252**,** 1651-1656.

ADAMS, M. D., KERLAVAGE, A. R., FLEISCHMANN, R. D., FULDNER, R. A., BULT, C. J., LEE, N. H., KIRKNESS, E. F., WEINSTOCK, K. G., GOCAYNE, J. D. & WHITE, O. 1995. Initial assessment of human gene diversity and expression patterns based upon 83 million nucleotides of cDNA sequence. *Nature,* 377**,** 3-174.

AKINO, T., HAN, X., NAKAYAMA, H., MCNEISH, B., ZURAKOWSKI, D., MAMMOTO, A., KLAGSBRUN, M. & SMITH, E. 2014. Netrin-1 promotes medulloblastoma cell invasiveness and angiogenesis, and demonstrates elevated expression in tumor tissue and urine of patients with pediatric medulloblastoma. *Cancer research,* 74**,** 3716-3726.

ALBINI, A., BENELLI, R., NOONAN, D. M. & BRIGATI, C. 2004. The" chemoinvasion assay": a tool to study tumor and endothelial cell invasion of basement membranes. *International Journal of Developmental Biology,* 48**,** 563-571.

ALBINI, A., IWAMOTO, Y., KLEINMAN, H., MARTIN, G., AARONSON, S., KOZLOWSKI, J. & MCEWAN, R. 1987. A rapid in vitro assay for quantitating the invasive potential of tumor cells. *Cancer research,* 47**,** 3239-3245.

ALEMANY, S., RIBASÉS, M., VILOR‐TEJEDOR, N., BUSTAMANTE, M., SÁNCHEZ‐MORA, C., BOSCH, R., RICHARTE, V., CORMAND, B., CASAS, M. & RAMOS‐QUIROGA, J. A. 2015. New suggestive genetic loci and biological pathways for attention function in adult attention‐deficit/hyperactivity disorder. *American Journal of Medical Genetics Part B: Neuropsychiatric Genetics,* 168**,** 459-470.

ANNABI, B., DEMEULE, M., CURRIE, J.-C., LAROCQUE, A., CHARFI, C. & BÉLIVEAU, R. 2019. Increasing potency and safety of anticancer drugs through sortilin receptor-mediated cancer therapy: A new targeted approach for the treatment of ovarian cancer. American Society of Clinical Oncology.

ARCHER, T. C., EHRENBERGER, T., MUNDT, F., GOLD, M. P., KRUG, K., MAH, C. K., MAHONEY, E. L., DANIEL, C. J., LENAIL, A. & RAMAMOORTHY, D. 2018. Proteomics, post-translational modifications, and integrative analyses reveal

molecular heterogeneity within medulloblastoma subgroups. *Cancer cell,* 34**,** 396-410. e8.

ASHBURNER, M., BALL, C. A., BLAKE, J. A., BOTSTEIN, D., BUTLER, H., CHERRY, J. M., DAVIS, A. P., DOLINSKI, K., DWIGHT, S. S. & EPPIG, J. T. 2000. Gene ontology: tool for the unification of biology. *Nature genetics,* 25**,** 25-29.

ASTHANA, A. & KISAALITA, W. S. 2013. Biophysical microenvironment and 3D culture physiological relevance. *Drug discovery today,* 18**,** 533-540.

AZIZ, N. A. A., MOKHTAR, N. M., HARUN, R., MOLLAH, M. M. H., ROSE, I. M., SAGAP, I., TAMIL, A. M., NGAH, W. Z. W. & JAMAL, R. 2016. A 19-Gene expression signature as a predictor of survival in colorectal cancer. *BMC medical genomics,* 9**,** 58.

BABICKI, S., ARNDT, D., MARCU, A., LIANG, Y., GRANT, J. R., MACIEJEWSKI, A. & WISHART, D. S. 2016. Heatmapper: web-enabled heat mapping for all. *Nucleic acids research,* 44**,** W147-W153.

BARSHES, N., DEMOPOULOS, A. & ENGELHARD, H. H. 2005. Anatomy and physiology of the leptomeninges and CSF space. *Leptomeningeal Metastases.* Springer.

BAUM, A., AKULA, N., CABANERO, M., CARDONA, I., CORONA, W., KLEMENS, B., SCHULZE, T., CICHON, S., RIETSCHEL, M. & NÖTHEN, M. 2008. A genome-wide association study implicates diacylglycerol kinase eta (DGKH) and several other genes in the etiology of bipolar disorder. *Molecular psychiatry,* 13**,** 197-207.

BEIN, A., SHIN, W., JALILI-FIROOZINEZHAD, S., PARK, M. H., SONTHEIMER-PHELPS, A., TOVAGLIERI, A., CHALKIADAKI, A., KIM, H. J. & INGBER, D. E. 2018. Microfluidic organ-on-a-chip models of human intestine. *Cellular and molecular gastroenterology and hepatology,* 5**,** 659-668.

BHATIA, S. N. & INGBER, D. E. 2014. Microfluidic organs-on-chips. *Nature biotechnology,* 32**,** 760.

BINNING, M. J., NIAZI, T., PEDONE, C. A., LAL, B., EBERHART, C. G., KIM, K. J., LATERRA, J. & FULTS, D. W. 2008. Hepatocyte growth factor and sonic Hedgehog expression in cerebellar neural progenitor cells costimulate medulloblastoma initiation and growth. *Cancer research,* 68**,** 7838-7845.

BIRCHMEIER, C., BIRCHMEIER, W., GHERARDI, E. & WOUDE, G. F. V. 2003. Met, metastasis, motility and more. *Nature reviews Molecular cell biology,* 4**,** 915-925.

BOCKMAYR, M., MOHME, M., KLAUSCHEN, F., WINKLER, B., BUDCZIES, J., RUTKOWSKI, S. & SCHÜLLER, U. 2018. Subgroup-specific immune and stromal microenvironment in medulloblastoma. *Oncoimmunology,* 7**,** e1462430.

BOGGILD, S., MOLGAARD, S., GLERUP, S. & NYENGAARD, J. R. 2016. Spatiotemporal patterns of sortilin and SorCS2 localization during organ development. *BMC cell biology,* 17**,** 8.

BOGGILD, S., MOLGAARD, S., GLERUP, S. & NYENGAARD, J. R. 2018. Highly segregated localization of the functionally related vps10p receptors sortilin and SorCS2 during neurodevelopment. *Journal of Comparative Neurology,* 526**,** 1267-1286.

BOIRE, A., ZOU, Y., SHIEH, J., MACALINAO, D. G., PENTSOVA, E. & MASSAGUÉ, J. 2017. Complement component 3 adapts the cerebrospinal fluid for leptomeningeal metastasis. *Cell,* 168**,** 1101-1113. e13.

BOYDEN, S. 1962. The chemotactic effect of mixtures of antibody and antigen on polymorphonuclear leucocytes. *The Journal of experimental medicine,* 115**,** 453-466.

BRENNER, W., GROß, S., STEINBACH, F., HORN, S., HOHENFELLNER, R. & THÜROFF, J. W. 2000. Differential inhibition of renal cancer cell invasion mediated by fibronectin, collagen IV and laminin. *Cancer letters,* 155**,** 199-205.

BROWN, H. G., KEPNER, J. L., PERLMAN, E. J., FRIEDMAN, H. S., STROTHER, D. R., DUFFNER, P. K., KUN, L. E., GOLDTHWAITE, P. T. & BURGER, P. C. 2000. "Large cell/anaplastic" medulloblastomas: a pediatric oncology group study. *Journal of Neuropathology & Experimental Neurology,* 59**,** 857-865.

BUDDAY, S., NAY, R., DE ROOIJ, R., STEINMANN, P., WYROBEK, T., OVAERT, T. C. & KUHL, E. 2015. Mechanical properties of gray and white matter brain tissue by indentation. *Journal of the mechanical behavior of biomedical materials,* 46**,** 318-330.

BURGER, J. A. & KIPPS, T. J. 2006. CXCR4: a key receptor in the crosstalk between tumor cells and their microenvironment. *Blood,* 107**,** 1761-1767.

BUSS, M. C., READ, T.-A., SCHNIEDERJAN, M. J., GANDHI, K. & CASTELLINO, R. C. 2012. HDM2 promotes WIP1-mediated medulloblastoma growth. *Neuro-oncology,* 14**,** 440-458.

BUSS, M. C., REMKE, M., LEE, J., GANDHI, K., SCHNIEDERJAN, M. J., KOOL, M., NORTHCOTT, P. A., PFISTER, S. M., TAYLOR, M. D. & CASTELLINO, R. C. 2015. The WIP1 oncogene promotes progression and invasion of aggressive medulloblastoma variants. *Oncogene,* 34**,** 1126-1140.

BUTTS, T., GREEN, M. J. & WINGATE, R. J. 2014. Development of the cerebellum: simple steps to make a 'little brain'. *Development,* 141**,** 4031-4041.

BYRNE, J., FEARS, T. R., MILLS, J. L., ZELTZER, L. K., SKLAR, C., MEADOWS, A. T., REAMAN, G. H. & ROBISON, L. L. 2004. Fertility of long‐term male survivors of acute lymphoblastic leukemia diagnosed during childhood. *Pediatric blood & cancer,* 42**,** 364-372.

CABILI, M. N., DUNAGIN, M. C., MCCLANAHAN, P. D., BIAESCH, A., PADOVAN-MERHAR, O., REGEV, A., RINN, J. L. & RAJ, A. 2015. Localization and abundance analysis of human lncRNAs at single-cell and single-molecule resolution. *Genome biology,* 16**,** 20.

CASNEUF, T., VAN DE PEER, Y. & HUBER, W. 2007. In situ analysis of cross-hybridisation on microarrays and the inference of expression correlation. *BMC bioinformatics,* 8**,** 461.

CAVALLI, F. M. G., REMKE, M., RAMPASEK, L., PEACOCK, J., SHIH, D. J. H., LUU, B., GARZIA, L., TORCHIA, J., NOR, C., MORRISSY, A. S., AGNIHOTRI, S., THOMPSON, Y. Y., KUZAN-FISCHER, C. M., FAROOQ, H., ISAEV, K., DANIELS, C., CHO, B. K., KIM, S. K., WANG, K. C., LEE, J. Y., GRAJKOWSKA, W. A., PEREK-POLNIK, M., VASILJEVIC, A., FAURE-CONTER, C., JOUVET, A., GIANNINI, C., NAGESWARA RAO, A. A., LI, K. K. W., NG, H. K., EBERHART, C. G., POLLACK, I. F., HAMILTON, R. L., GILLESPIE, G. Y., OLSON, J. M., LEARY, S., WEISS, W. A., LACH, B., CHAMBLESS, L. B., THOMPSON, R. C., COOPER, M. K., VIBHAKAR, R., HAUSER, P., VAN VEELEN, M. C., KROS, J. M., FRENCH, P. J., RA, Y. S., KUMABE, T., LOPEZ-AGUILAR, E., ZITTERBART, K., STERBA, J., FINOCCHIARO, G., MASSIMINO, M., VAN MEIR, E. G., OSUKA, S., SHOFUDA, T., KLEKNER, A., ZOLLO, M., LEONARD, J. R., RUBIN, J. B., JABADO, N., ALBRECHT, S., MORA, J., VAN METER, T. E., JUNG, S., MOORE, A. S., HALLAHAN, A. R., CHAN, J. A., TIRAPELLI, D. P. C., CARLOTTI, C. G., FOULADI, M., PIMENTEL, J., FARIA, C.

C., SAAD, A. G., MASSIMI, L., LIAU, L. M., WHEELER, H., NAKAMURA, H., ELBABAA, S. K., PEREZPENA-DIAZCONTI, M., CHICO PONCE DE LEON, F., ROBINSON, S., ZAPOTOCKY, M., LASSALETTA, A., HUANG, A., HAWKINS, C. E., TABORI, U., BOUFFET, E., BARTELS, U., DIRKS, P. B., RUTKA, J. T., BADER, G. D., REIMAND, J., GOLDENBERG, A., RAMASWAMY, V. & TAYLOR, M. D. 2017. Intertumoral Heterogeneity within Medulloblastoma Subgroups. *Cancer Cell,* 31**,** 737-754 e6.

CHADWICK, E. J., YANG, D. P., FILBIN, M. G., MAZZOLA, E., SUN, Y., BEHAR, O., PAZYRA-MURPHY, M. F., GOUMNEROVA, L., LIGON, K. L. & STILES, C. D. 2015. A brain tumor/organotypic slice co-culture system for studying tumor microenvironment and targeted drug therapies. *JoVE (Journal of Visualized Experiments)***,** e53304.

CHANG, C. H., HOUSEPIAN, E. M. & HERBERT, C. 1969. An operative staging system and a megavoltage radiotherapeutic technic for cerebellar medulloblastomas. *Radiology,* 93**,** 1351-1359.

CHAUDHURI, O., KOSHY, S. T., DA CUNHA, C. B., SHIN, J.-W., VERBEKE, C. S., ALLISON, K. H. & MOONEY, D. J. 2014. Extracellular matrix stiffness and composition jointly regulate the induction of malignant phenotypes in mammary epithelium. *Nature materials,* 13**,** 970-978.

CHO, Y.-J., TSHERNIAK, A., TAMAYO, P., SANTAGATA, S., LIGON, A., GREULICH, H., BERHOUKIM, R., AMANI, V., GOUMNEROVA, L. & EBERHART, C. G. 2011. Integrative genomic analysis of medulloblastoma identifies a molecular subgroup that drives poor clinical outcome. *Journal of Clinical Oncology,* 29**,** 1424.

CHOI, D., MONTERMINI, L., KIM, D.-K., MEEHAN, B., ROTH, F. P. & RAK, J. 2018. The impact of oncogenic EGFRvIII on the proteome of extracellular vesicles released from glioblastoma cells. *Molecular & Cellular Proteomics,* 17**,** 1948-1964.

CHRISTOFOROU, A., MCGHEE, K., MORRIS, S., THOMSON, P., ANDERSON, S., MCLEAN, A., TORRANCE, H., LE HELLARD, S., PICKARD, B. & STCLAIR, D. 2011. Convergence of linkage, association and GWAS findings for a candidate region for bipolar disorder and schizophrenia on chromosome 4p. *Molecular psychiatry,* 16**,** 240-242.

CITRI, A. & MALENKA, R. C. 2008. Synaptic plasticity: multiple forms, functions, and mechanisms. *Neuropsychopharmacology,* 33**,** 18-41.

CLAIR, W. S., ADAMS, J., BUES, M., FULLERTON, B., LA SHELL, S., KOOY, H., LOEFFLER, J. & TARBELL, N. 2004. Advantage of protons compared to conventional X-ray or IMRT in the treatment of a pediatric patient with medulloblastoma. *International Journal of Radiation Oncology* Biology* Physics,* 58**,** 727-734.

CLOONAN, N., FORREST, A. R., KOLLE, G., GARDINER, B. B., FAULKNER, G. J., BROWN, M. K., TAYLOR, D. F., STEPTOE, A. L., WANI, S. & BETHEL, G. 2008. Stem cell transcriptome profiling via massive-scale mRNA sequencing. *Nature methods,* 5**,** 613.

COHEN, S. 1982. Familial polyposis coli and its extracolonic manifestations. *Journal of medical genetics,* 19**,** 193-203.

CONSORTIUM, G. O. 2019. The gene ontology resource: 20 years and still GOing strong. *Nucleic acids research,* 47**,** D330-D338.

CUSHING, H. 1925. Cameron lectures. 1. The third circulation and its channels. *Lancet,* 2**,** 851-857.

DE HOSTOS, E. L., REHFUEß, C., BRADTKE, B., WADDELL, D. R., ALBRECHT, R., MURPHY, J. & GERISCH, G. 1993. Dictyostelium mutants lacking the cytoskeletal protein coronin are defective in cytokinesis and cell motility. *The Journal of cell biology,* 120**,** 163-173.

DEINHARDT, K., KIM, T., SPELLMAN, D. S., MAINS, R. E., EIPPER, B. A., NEUBERT, T. A., CHAO, M. V. & HEMPSTEAD, B. L. 2011. Neuronal growth cone retraction relies on proneurotrophin receptor signaling through Rac. *Sci. Signal.,* 4**,** ra82-ra82.

DEUTSCH, M., THOMAS, P. R., KRISCHER, J., BOYETT, J. M., ALBRIGHT, L., ARONIN, P., LANGSTON, J., ALLEN, J. C., PACKER, R. J. & LINGGOOD, R. 1996. Results of a prospective randomized trial comparing standard dose neuraxis irradiation (3,600 cGy/20) with reduced neuraxis irradiation (2,340 cGy/13) in patients with low-stage medulloblastoma. *Pediatric neurosurgery,* 24**,** 167-177.

DOBIN, A., DAVIS, C. A., SCHLESINGER, F., DRENKOW, J., ZALESKI, C., JHA, S., BATUT, P., CHAISSON, M. & GINGERAS, T. R. 2013. STAR: ultrafast universal RNA-seq aligner. *Bioinformatics,* 29**,** 15-21.

DONNINGER, H., BONOME, T., RADONOVICH, M., PISE-MASISON, C. A., BRADY, J., SHIH, J. H., BARRETT, J. C. & BIRRER, M. J. 2004. Whole genome expression profiling of advance stage papillary serous ovarian cancer reveals activated pathways. *Oncogene,* 23**,** 8065-8077.

DUBUC, A. M., REMKE, M., KORSHUNOV, A., NORTHCOTT, P. A., ZHAN, S. H., MENDEZ-LAGO, M., KOOL, M., JONES, D. T., UNTERBERGER, A. & MORRISSY, A. S. 2013. Aberrant patterns of H3K4 and H3K27 histone lysine methylation occur across subgroups in medulloblastoma. *Acta neuropathologica,* 125**,** 373-384.

EAGLE, H. & FOLEY, G. E. 1958. Cytotoxicity in human cell cultures as a primary screen for the detection of anti-tumor agents. *Cancer research,* 18**,** 1017-1025.

EDMONDSON, R., BROGLIE, J. J., ADCOCK, A. F. & YANG, L. 2014. Three-dimensional cell culture systems and their applications in drug discovery and cell-based biosensors. *Assay and drug development technologies,* 12**,** 207-218.

ELLISON, D. W., DALTON, J., KOCAK, M., NICHOLSON, S. L., FRAGA, C., NEALE, G., KENNEY, A. M., BRAT, D. J., PERRY, A. & YONG, W. H. 2011. Medulloblastoma: clinicopathological correlates of SHH, WNT, and non-SHH/WNT molecular subgroups. *Acta neuropathologica,* 121**,** 381-396.

ELLISON, D. W., ONILUDE, O. E., LINDSEY, J. C., LUSHER, M. E., WESTON, C. L., TAYLOR, R. E., PEARSON, A. D. & CLIFFORD, S. C. 2005. β-Catenin status predicts a favorable outcome in childhood medulloblastoma: the United Kingdom Children's Cancer Study Group Brain Tumour Committee. *Journal of Clinical Oncology,* 23**,** 7951-7957.

ESPINA, V., WULFKUHLE, J. D., CALVERT, V. S., VANMETER, A., ZHOU, W., COUKOS, G., GEHO, D. H., PETRICOIN, E. F. & LIOTTA, L. A. 2006. Laser-capture microdissection. *Nature protocols,* 1**,** 586.

FARES, J., FARES, M. Y., KHACHFE, H. H., SALHAB, H. A. & FARES, Y. 2020. Molecular principles of metastasis: a hallmark of cancer revisited. *Signal transduction and targeted therapy,* 5**,** 1-17.

FELBOR, U., DREIER, L., BRYANT, R. A., PLOEGH, H. L., OLSEN, B. R. & MOTHES, W. 2000. Secreted cathepsin L generates endostatin from collagen XVIII. *The EMBO journal,* 19**,** 1187-1194.

FERNANDES, J. C., ACUÑA, S. M., AOKI, J. I., FLOETER-WINTER, L. M. & MUXEL, S. M. 2019. Long non-coding RNAs in the regulation of gene expression: physiology and disease. *Non-coding RNA,* 5**,** 17.

FIDLER, I. J. 2003. The pathogenesis of cancer metastasis: the'seed and soil'hypothesis revisited. *Nature reviews cancer,* 3**,** 453-458.

FOX, J., MAYER, U., NISCHT, R., AUMAILLEY, M., REINHARDT, D., WIEDEMANN, H., MANN, K., TIMPL, R., KRIEG, T. & ENGEL, J. 1991. Recombinant nidogen consists of three globular domains and mediates binding of laminin to collagen type IV. *The EMBO journal,* 10**,** 3137-3146.

FRIEDL, P. & GILMOUR, D. 2009. Collective cell migration in morphogenesis, regeneration and cancer. *Nature reviews Molecular cell biology,* 10**,** 445.

FRIEDRICH, J., SEIDEL, C., EBNER, R. & KUNZ-SCHUGHART, L. A. 2009. Spheroid-based drug screen: considerations and practical approach. *Nature protocols,* 4**,** 309.

FULTS, D. W., TAYLOR, M. D. & GARZIA, L. 2019. Leptomeningeal dissemination: a sinister pattern of medulloblastoma growth. *Journal of Neurosurgery: Pediatrics,* 23**,** 613-621.

GAJJAR, A., CHINTAGUMPALA, M., ASHLEY, D., KELLIE, S., KUN, L. E., MERCHANT, T. E., WOO, S., WHEELER, G., AHERN, V. & KRASIN, M. J. 2006. Risk-adapted craniospinal radiotherapy followed by high-dose chemotherapy and stem-cell rescue in children with newly diagnosed medulloblastoma (St Jude Medulloblastoma-96): long-term results from a prospective, multicentre trial. *The lancet oncology,* 7**,** 813-820.

GARZIA, L., KIJIMA, N., MORRISSY, A. S., DE ANTONELLIS, P., GUERREIRO-STUCKLIN, A., HOLGADO, B. L., WU, X., WANG, X., PARSONS, M. & ZAYNE, K. 2018. A hematogenous route for medulloblastoma leptomeningeal metastases. *Cell,* 172**,** 1050-1062. e14.

GAYNON, P. S., ANGIOLILLO, A. L., CARROLL, W. L., NACHMAN, J. B., TRIGG, M. E., SATHER, H. N., HUNGER, S. P. & DEVIDAS, M. 2010. Long-term results of the children's cancer group studies for childhood acute lymphoblastic leukemia 1983–2002: a Children's Oncology Group Report. *Leukemia,* 24**,** 285-297.

GEISER, C., BISHOP, Y., JAFFE, N., FURMAN, L., TRAGGIS, D. & FREI, E. D. 1975. Adverse effects of intrathecal methotrexate in children with acute leukemia in remission. *Blood,* 45**,** 189-195.

GHAEMIMANESH, F., AHMADIAN, G., TALEBI, S., ZARNANI, A.-H., BEHMANESH, M., HEMMATI, S., HADAVI, R., JEDDI-TEHRANI, M., FARZI, M. & AKHONDI, M. M. 2014. The effect of sortilin silencing on ovarian carcinoma cells. *Avicenna journal of medical biotechnology,* 6**,** 169.

GIANGASPERO, F., RIGOBELLO, L., BADIALI, M., LODA, M., ANDREINI, L., BASSO, G., ZORZI, F. & MONTALDI, A. 1992. Large-cell medulloblastomas: a distinct variant with highly aggressive behavior. *The American journal of surgical pathology,* 16**,** 687-693.

GIBSON, P., TONG, Y., ROBINSON, G., THOMPSON, M. C., CURRLE, D. S., EDEN, C., KRANENBURG, T. A., HOGG, T., POPPLETON, H., MARTIN, J., FINKELSTEIN, D., POUNDS, S., WEISS, A., PATAY, Z., SCOGGINS, M., OGG, R., PEI, Y., YANG, Z. J., BRUN, S., LEE, Y., ZINDY, F., LINDSEY, J. C., TAKETO, M. M., BOOP, F. A., SANFORD, R. A., GAJJAR, A., CLIFFORD, S. C., ROUSSEL, M. F., MCKINNON, P. J., GUTMANN, D. H., ELLISON, D. W., WECHSLER-REYA, R. & GILBERTSON, R. J. 2010. Subtypes of medulloblastoma have distinct developmental origins. *Nature,* 468**,** 1095-9.

GIORDANA, M. T., D'AGOSTINO, C., POLLO, B., SILVANI, A., FERRACINI, R., PAIOLO, A., GHIGLIONE, P. & CHIÒ, A. 2005. Anaplasia is rare and does not influence prognosis in adult medulloblastoma. *Journal of Neuropathology & Experimental Neurology,* 64**,** 869-874.

GLERUP, S., BOLCHO, U., MØLGAARD, S., BØGGILD, S., VAEGTER, C., SMITH, A., NIETO-GONZALEZ, J., OVESEN, P., PEDERSEN, L. & FJORBACK, A. 2016. SorCS2 is required for BDNF-dependent plasticity in the hippocampus. *Molecular psychiatry,* 21**,** 1740-1751.

GLERUP, S., OLSEN, D., VAEGTER, C. B., GUSTAFSEN, C., SJOEGAARD, S. S., HERMEY, G., KJOLBY, M., MOLGAARD, S., ULRICHSEN, M. & BOGGILD, S. 2014. SorCS2 regulates dopaminergic wiring and is processed into an apoptotic two-chain receptor in peripheral glia. *Neuron,* 82**,** 1074-1087.

GREENBERG, M. V. & BOURC'HIS, D. 2019. The diverse roles of DNA methylation in mammalian development and disease. *Nature reviews Molecular cell biology***,** 1-18.

GUDRUNARDOTTIR, T., MORGAN, A. T., LUX, A. L., WALKER, D. A., WALSH, K. S., WELLS, E. M., WISOFF, J. H., JUHLER, M., SCHMAHMANN, J. D. & KEATING, R. F. 2016. Consensus paper on post-operative pediatric cerebellar mutism syndrome: the Iceland Delphi results. *Child's Nervous System,* 32**,** 1195-1203.

GUPTA, M. & AHMAD, M. 2019. Pediatric Medulloblastoma: A Radiation Oncologist Perspective. *Brain and Spinal Tumors-Primary and Secondary.* IntechOpen.

GURNEY, J. G., NESS, K. K., SIBLEY, S. D., O'LEARY, M., DENGEL, D. R., LEE, J. M., YOUNGREN, N. M., GLASSER, S. P. & BAKER, K. S. 2006. Metabolic syndrome and growth hormone deficiency in adult survivors of childhood acute lymphoblastic leukemia. *Cancer,* 107**,** 1303-1312.

HALLMANN, R., HORN, N., SELG, M., WENDLER, O., PAUSCH, F. & SOROKIN, L. M. 2005. Expression and function of laminins in the embryonic and mature vasculature. *Physiological reviews,* 85**,** 979-1000.

HAMPE, W., URNY, J., FRANKE, I., HOFFMEISTER-ULLERICH, S., HERRMANN, D., PETERSEN, C. M., LOHMANN, J. & SCHALLER, H. C. 1999. A head-activator binding protein is present in hydra in a soluble and a membrane-anchored form. *Development,* 126**,** 4077-4086.

HANAHAN, D. & WEINBERG, R. A. 2011. Hallmarks of cancer: the next generation. *cell,* 144**,** 646-674.

HEINE, P., EHRLICHER, A. & KÄS, J. 2015. Neuronal and metastatic cancer cells: unlike brothers. *Biochimica et Biophysica Acta (BBA)-Molecular Cell Research,* 1853**,** 3126-3131.

HELJASVAARA, R., NYBERG, P., LUOSTARINEN, J., PARIKKA, M., HEIKKILÄ, P., REHN, M., SORSA, T., SALO, T. & PIHLAJANIEMI, T. 2005. Generation of biologically active endostatin fragments from human collagen XVIII by distinct matrix metalloproteases. *Experimental cell research,* 307**,** 292-304.

HERMEY, G., KEAT, S. J., MADSEN, P., JACOBSEN, C., PETERSEN, C. M. & GLIEMANN, J. 2003. Characterization of sorCS1, an alternatively spliced receptor with completely different cytoplasmic domains that mediate different trafficking in cells. *Journal of Biological Chemistry,* 278**,** 7390-7396.

HERMEY, G., PLATH, N., HÜBNER, C. A., KUHL, D., SCHALLER, H. C. & HERMANS‐BORGMEYER, I. 2004. The three sorCS genes are differentially expressed and regulated by synaptic activity. *Journal of neurochemistry,* 88**,** 1470-1476.

HERMEY, G., RIEDEL, I. B., HAMPE, W., SCHALLER, H. C. & HERMANS-BORGMEYER, I. 1999. Identification and characterization of SorCS, a third member of a novel receptor family. *Biochemical and biophysical research communications,* 266**,** 347-351.

HEWSON, C., CAPRARO, D., BURDACH, J., WHITAKER, N. & MORRIS, K. V. 2016. Extracellular vesicle associated long non-coding RNAs functionally enhance cell viability. *Non-coding RNA research,* 1**,** 3-11.

HILL, R. M., KUIJPER, S., LINDSEY, J. C., PETRIE, K., SCHWALBE, E. C., BARKER, K., BOULT, J. K., WILLIAMSON, D., AHMAD, Z. & HALLSWORTH, A. 2015. Combined MYC and P53 defects emerge at medulloblastoma relapse and define rapidly progressive, therapeutically targetable disease. *Cancer cell,* 27**,** 72-84.

HIRSCHBERG, E. 1958. Tissue culture in cancer chemotherapy screening. *Cancer research,* 18**,** 869-878.

HOVESTADT, V., AYRAULT, O., SWARTLING, F. J., ROBINSON, G. W., PFISTER, S. M. & NORTHCOTT, P. A. 2019a. Medulloblastomics revisited: biological and clinical insights from thousands of patients. *Nature Reviews Cancer***,** 1-15.

HOVESTADT, V., SMITH, K. S., BIHANNIC, L., FILBIN, M. G., SHAW, M. L., BAUMGARTNER, A., DEWITT, J. C., GROVES, A., MAYR, L. & WEISMAN, H. R. 2019b. Resolving medulloblastoma cellular architecture by single-cell genomics. *Nature,* 572**,** 74-79.

HUA, C., BASS, J. K., KHAN, R., KUN, L. E. & MERCHANT, T. E. 2008. Hearing loss after radiotherapy for pediatric brain tumors: effect of cochlear dose. *International Journal of Radiation Oncology* Biology* Physics,* 72**,** 892-899.

HUGHES, C. S., POSTOVIT, L. M. & LAJOIE, G. A. 2010. Matrigel: a complex protein mixture required for optimal growth of cell culture. *Proteomics,* 10**,** 1886-1890.

HUH, D., MATTHEWS, B. D., MAMMOTO, A., MONTOYA-ZAVALA, M., HSIN, H. Y. & INGBER, D. E. 2010. Reconstituting organ-level lung functions on a chip. *Science,* 328**,** 1662-1668.

INDELICATO, D. J., MERCHANT, T., LAPERRIERE, N., LASSEN, Y., VENNARINI, S., WOLDEN, S., HARTSELL, W., PANKUCH, M., BRANDAL, P. & LAW, C.-C. K. 2016. Consensus report from the Stockholm pediatric proton therapy conference. *International Journal of Radiation Oncology• Biology• Physics,* 96**,** 387-392.

IVANOV, D. P., COYLE, B., WALKER, D. A. & GRABOWSKA, A. M. 2016. In vitro models of medulloblastoma: Choosing the right tool for the job. *J Biotechnol,* 236**,** 10-25.

IVICS, Z., HACKETT, P. B., PLASTERK, R. H. & IZSVÁK, Z. 1997. Molecular reconstruction of Sleeping Beauty, a Tc1-like transposon from fish, and its transposition in human cells. *Cell,* 91**,** 501-510.

JACKSON, H. K., LINKE, F., KERR, I. & COYLE, B. 2018. Extracellular vesicles from metastatic medulloblastoma cell lines carry mRNAs known to correlate with metastatic disease. *Journal of Extracellular Vesicles,* 7**,** 233-233.

JACOBSEN, L., MADSEN, P., JACOBSEN, C., NIELSEN, M. S., GLIEMANN, J. & PETERSEN, C. M. 2001. Activation and functional characterization of the mosaic receptor SorLA/LR11. *Journal of Biological Chemistry,* 276**,** 22788-22796.

JACOBSEN, L., MADSEN, P., MOESTRUP, S. K., LUND, A. H., TOMMERUP, N., NYKJÆR, A., SOTTRUP-JENSEN, L., GLIEMANN, J. & PETERSEN, C. M. 1996. Molecular characterization of a novel human hybrid-type receptor that

binds the α2-macroglobulin receptor-associated protein. *Journal of Biological Chemistry,* 271**,** 31379-31383.

JAKACKI, R. I., BURGER, P. C., ZHOU, T., HOLMES, E. J., KOCAK, M., ONAR, A., GOLDWEIN, J., MEHTA, M., PACKER, R. J. & TARBELL, N. 2012. Outcome of children with metastatic medulloblastoma treated with carboplatin during craniospinal radiotherapy: a Children's Oncology Group Phase I/II study. *Journal of clinical oncology,* 30**,** 2648.

JAYADEV, R. & SHERWOOD, D. R. 2017. Basement membranes. *Current Biology,* 27**,** R207-R211.

JENKINS, N. C., KALRA, R. R., DUBUC, A., SIVAKUMAR, W., PEDONE, C. A., WU, X., TAYLOR, M. D. & FULTS, D. W. 2014. Genetic drivers of metastatic dissemination in sonic hedgehog medulloblastoma. *Acta neuropathologica communications,* 2**,** 85.

JENKINS, N. C., RAO, G., EBERHART, C. G., PEDONE, C. A., DUBUC, A. M. & FULTS, D. W. 2016. Somatic cell transfer of c-Myc and Bcl-2 induces large-cell anaplastic medulloblastomas in mice. *Journal of neuro-oncology,* 126**,** 415-424.

JOGIE-BRAHIM, S., FELDMAN, D. & OH, Y. 2009. Unraveling insulin-like growth factor binding protein-3 actions in human disease. *Endocrine reviews,* 30**,** 417-437.

JONES, D. T., JÄGER, N., KOOL, M., ZICHNER, T., HUTTER, B., SULTAN, M., CHO, Y.-J., PUGH, T. J., HOVESTADT, V. & STÜTZ, A. M. 2012. Dissecting the genomic complexity underlying medulloblastoma. *Nature,* 488**,** 100-105.

KAHN, S. A., WANG, X., NITTA, R. T., GHOLAMIN, S., THERUVATH, J., HUTTER, G., AZAD, T. D., WADI, L., BOLIN, S. & RAMASWAMY, V. 2018. Notch1 regulates the initiation of metastasis and self-renewal of Group 3 medulloblastoma. *Nature communications,* 9**,** 1-9.

KAWAUCHI, D., ROBINSON, G., UZIEL, T., GIBSON, P., REHG, J., GAO, C., FINKELSTEIN, D., QU, C., POUNDS, S., ELLISON, D. W., GILBERTSON, R. J. & ROUSSEL, M. F. 2012. A mouse model of the most aggressive subgroup of human medulloblastoma. *Cancer Cell,* 21**,** 168-80.

KEENE, J. D., KOMISAROW, J. M. & FRIEDERSDORF, M. B. 2006. RIP-Chip: the isolation and identification of mRNAs, microRNAs and protein components of ribonucleoprotein complexes from cell extracts. *Nature protocols,* 1**,** 302.

KIENAST, Y., VON BAUMGARTEN, L., FUHRMANN, M., KLINKERT, W. E., GOLDBRUNNER, R., HERMS, J. & WINKLER, F. 2010. Real-time imaging reveals the single steps of brain metastasis formation. *Nature medicine,* 16**,** 116.

KOOL, M., JONES, D. T., JÄGER, N., NORTHCOTT, P. A., PUGH, T. J., HOVESTADT, V., PIRO, R. M., ESPARZA, L. A., MARKANT, S. L. & REMKE, M. 2014. Genome sequencing of SHH medulloblastoma predicts genotype-related response to smoothened inhibition. *Cancer cell,* 25**,** 393-405.

KOOL, M., KORSHUNOV, A., REMKE, M., JONES, D. T., SCHLANSTEIN, M., NORTHCOTT, P. A., CHO, Y.-J., KOSTER, J., SCHOUTEN-VAN MEETEREN, A. & VAN VUURDEN, D. 2012. Molecular subgroups of medulloblastoma: an international meta-analysis of transcriptome, genetic aberrations, and clinical data of WNT, SHH, Group 3, and Group 4 medulloblastomas. *Acta neuropathologica,* 123**,** 473-484.

KOPP, F. & MENDELL, J. T. 2018. Functional classification and experimental dissection of long noncoding RNAs. *Cell,* 172**,** 393-407.

KOUICHI, I., KENICHI, M. & KOUSAKU, O. 1994. Identification of an active gene by using large-scale cDNA sequencing. *Gene,* 140**,** 295-296.

KUKURBA, K. R. & MONTGOMERY, S. B. 2015. RNA sequencing and analysis. *Cold Spring Harbor Protocols,* 2015**,** pdb. top084970.

KUMAR, K. S., PILLONG, M., KUNZE, J., BURGHARDT, I., WELLER, M., GROTZER, M. A., SCHNEIDER, G. & BAUMGARTNER, M. 2015a. Computer-assisted quantification of motile and invasive capabilities of cancer cells. *Scientific reports,* 5**,** 15338.

KUMAR, K. S., TRIPOLITSIOTI, D., MA, M., GRÄHLERT, J., EGLI, K. B., FIASCHETTI, G., SHALABY, T., GROTZER, M. A. & BAUMGARTNER, M. 2015b. The Ser/Thr kinase MAP4K4 drives c-Met-induced motility and invasiveness in a cell-based model of SHH medulloblastoma. *Springerplus,* 4**,** 19.

LAMMERDING, J., FONG, L. G., JI, J. Y., REUE, K., STEWART, C. L., YOUNG, S. G. & LEE, R. T. 2006. Lamins A and C but not lamin B1 regulate nuclear mechanics. *Journal of Biological Chemistry,* 281**,** 25768-25780.

LEBLEU, V. S., MACDONALD, B. & KALLURI, R. 2007. Structure and function of basement membranes. *Experimental biology and medicine,* 232**,** 1121-1129.

LI, A., DAWSON, J. C., FORERO-VARGAS, M., SPENCE, H. J., YU, X., KÖNIG, I., ANDERSON, K. & MACHESKY, L. M. 2010. The actin-bundling protein fascin stabilizes actin in invadopodia and potentiates protrusive invasion. *Current biology,* 20**,** 339-345.

LI, K., SHI, M. & QIN, S. 2018. Current Status and Study Progress of Recombinant Human Endostatin in Cancer Treatment. *Oncology and Therapy,* 6**,** 21-43.

LI, L., DU, Y., KONG, X., LI, Z., JIA, Z., CUI, J., GAO, J., WANG, G. & XIE, K. 2013. Lamin B1 is a novel therapeutic target of betulinic acid in pancreatic cancer. *Clinical Cancer Research,* 19**,** 4651-4661.

LI, Y., LAL, B., KWON, S., FAN, X., SALDANHA, U., REZNIK, T. E., KUCHNER, E. B., EBERHART, C., LATERRA, J. & ABOUNADER, R. 2005. The scatter factor/hepatocyte growth factor: c-met pathway in human embryonal central nervous system tumor malignancy. *Cancer research,* 65**,** 9355-9362.

LI, Y. X., YU, Z. W., JIANG, T., SHAO, L. W., LIU, Y., LI, N., WU, Y. F., ZHENG, C., WU, X. Y., ZHANG, M. & ZHENG, D. F. 2018 SNCA, a novel biomarker for Group 4 medulloblastomas, can inhibit tumor invasion and induce apoptosis. *Cancer Science,* 109.

LIANG, B., PENG, P., CHEN, S., LI, L., ZHANG, M., CAO, D., YANG, J., LI, H., GUI, T. & LI, X. 2013. Characterization and proteomic analysis of ovarian cancer-derived exosomes. *Journal of proteomics,* 80**,** 171-182.

LIBERZON, A., SUBRAMANIAN, A., PINCHBACK, R., THORVALDSDÓTTIR, H., TAMAYO, P. & MESIROV, J. P. 2011. Molecular signatures database (MSigDB) 3.0. *Bioinformatics,* 27**,** 1739-1740.

LIM, S. K., LU, S. Y., KANG, S.-A., TAN, H. J., LI, Z., WEE, Z. N. A., GUAN, J. S., CHICHILI, V. P. R., SIVARAMAN, J. & PUTTI, T. 2016a. Wnt signaling promotes breast cancer by blocking ITCH-mediated degradation of YAP/TAZ transcriptional coactivator WBP2. *Cancer research,* 76**,** 6278-6289.

LIM, S. Y., YUZHALIN, A. E., GORDON-WEEKS, A. N. & MUSCHEL, R. J. 2016b. Targeting the CCL2-CCR2 signaling axis in cancer metastasis. *Oncotarget,* 7**,** 28697.

LIN, R. Z. & CHANG, H. Y. 2008. Recent advances in three‐dimensional multicellular spheroid culture for biomedical research. *Biotechnology Journal: Healthcare Nutrition Technology,* 3**,** 1172-1184.

LINKE, F., ALDIGHIERI, M., GRABOWSKA, A. M., STOLNIK, S., KERR, I. D., MERRY, C. L. R. & COYLE, B. 2020. Comparative study of group 4 medulloblastoma 3D hydrogel models.

LINKE, F., MERRY, C. L., GRABOWSKA, A. M., STOLNIK-TRENKIC, S., KERR, I. D. & COYLE, B. 2018. MBRS-43. MODELLING MEDULLOBLASTOMA INVASION AND CHEMORESISTANCE IN A 3D HYALURONAN HYDROGEL SYSTEM. *Neuro-Oncology,* 20**,** i137.

LISTER, R., O'MALLEY, R. C., TONTI-FILIPPINI, J., GREGORY, B. D., BERRY, C. C., MILLAR, A. H. & ECKER, J. R. 2008. Highly integrated single-base resolution maps of the epigenome in Arabidopsis. *Cell,* 133**,** 523-536.

LIU, B., SHYR, Y., CAI, J. & LIU, Q. 2019. Interplay between miRNAs and host genes and their role in cancer. *Briefings in functional genomics,* 18**,** 255-266.

LIU, H., LIN, J. & ROY, K. 2006. Effect of 3D scaffold and dynamic culture condition on the global gene expression profile of mouse embryonic stem cells. *Biomaterials,* 27**,** 5978-5989.

LOUIS, D. N., PERRY, A., REIFENBERGER, G., VON DEIMLING, A., FIGARELLA-BRANGER, D., CAVENEE, W. K., OHGAKI, H., WIESTLER, O. D., KLEIHUES, P. & ELLISON, D. W. 2016. The 2016 World Health Organization Classification of Tumors of the Central Nervous System: a summary. *Acta Neuropathol,* 131**,** 803-20.

LOVE, M. I., HUBER, W. & ANDERS, S. 2014. Moderated estimation of fold change and dispersion for RNA-seq data with DESeq2. *Genome biology,* 15**,** 550.

MACHESKY, L. M. & LI, A. 2010. Fascin: Invasive filopodia promoting metastasis. *Communicative & integrative biology,* 3**,** 263-270.

MAK, K. M. & MEI, R. 2017. Basement membrane type IV collagen and laminin: an overview of their biology and value as fibrosis biomarkers of liver disease. *The Anatomical Record,* 300**,** 1371-1390.

MALIK, A. R., LIPS, J., GORNIAK‐WALAS, M., BROEKAART, D. W., ASARO, A., KUFFNER, M. T., HOFFMANN, C. J., KIKHIA, M., DOPATKA, M. & BOEHM‐STURM, P. 2020. SorCS2 facilitates release of endostatin from astrocytes and controls post‐stroke angiogenesis. *Glia*.

MALIK, A. R., SZYDLOWSKA, K., NIZINSKA, K., ASARO, A., VAN VLIET, E. A., POPP, O., DITTMAR, G., FRITSCHE-GUENTHER, R., KIRWAN, J. A., NYKJAER, A., LUKASIUK, K., ARONICA, E. & WILLNOW, T. E. 2019. SorCS2 Controls Functional Expression of Amino Acid Transporter EAAT3 and Protects Neurons from Oxidative Stress and Epilepsy-Induced Pathology. *Cell Rep,* 26**,** 2792-2804 e6.

MANI, S. A., GUO, W., LIAO, M.-J., EATON, E. N., AYYANAN, A., ZHOU, A. Y., BROOKS, M., REINHARD, F., ZHANG, C. C. & SHIPITSIN, M. 2008. The epithelial-mesenchymal transition generates cells with properties of stem cells. *Cell,* 133**,** 704-715.

MARIONI, J. C., MASON, C. E., MANE, S. M., STEPHENS, M. & GILAD, Y. 2008. RNA-seq: an assessment of technical reproducibility and comparison with gene expression arrays. *Genome research,* 18**,** 1509-1517.

MARTIROSIAN, V., CHEN, T. C., LIN, M. & NEMAN, J. 2016. Medulloblastoma initiation and spread: where neurodevelopment, microenvironment and cancer cross pathways. *Journal of neuroscience research,* 94**,** 1511-1519.

MAZELLA, J., ZSÜRGER, N., NAVARRO, V., CHABRY, J., KAGHAD, M., CAPUT, D., FERRARA, P., VITA, N., GULLY, D. & MAFFRAND, J.-P. 1998. The 100-kDa neurotensin receptor is gp95/sortilin, a non-G-protein-coupled receptor. *Journal of Biological Chemistry,* 273**,** 26273-26276.

MCMANAMY, C. S., PEARS, J., WESTON, C. L., HANZELY, Z., IRONSIDE, J. W., TAYLOR, R. E., GRUNDY, R. G., CLIFFORD, S. C., ELLISON, D. W., CLINICAL BRAIN TUMOUR GROUP, C. S. C. & LEUKAEMIA GROUP , U. 2007. Nodule formation and desmoplasia in medulloblastomas—defining the nodular/desmoplastic variant and its biological behavior. *Brain Pathology,* 17**,** 151-164.

MENG, W., GARNETT, M. C., WALKER, D. A. & PARKER, T. L. 2016. Penetration and intracellular uptake of poly (glycerol-adipate) nanoparticles into three-dimensional brain tumour cell culture models. *Experimental Biology and Medicine,* 241**,** 466-477.

MILDE, T., LODRINI, M., SAVELYEVA, L., KORSHUNOV, A., KOOL, M., BRUECKNER, L. M., ANTUNES, A. S., OEHME, I., PEKRUN, A. & PFISTER, S. M. 2012. HD-MB03 is a novel Group 3 medulloblastoma model demonstrating sensitivity to histone deacetylase inhibitor treatment. *Journal of neuro-oncology,* 110**,** 335-348.

MISHIMA, M. & NISHIDA, E. 1999. Coronin localizes to leading edges and is involved in cell spreading and lamellipodium extension in vertebrate cells. *J Cell Sci,* 112**,** 2833-2842.

MOOTHA, V. K., LINDGREN, C. M., ERIKSSON, K.-F., SUBRAMANIAN, A., SIHAG, S., LEHAR, J., PUIGSERVER, P., CARLSSON, E., RIDDERSTRÅLE, M. & LAURILA, E. 2003. PGC-1α-responsive genes involved in oxidative phosphorylation are coordinately downregulated in human diabetes. *Nature genetics,* 34**,** 267-273.

MORI, F., MIKI, Y., TANJI, K., KAKITA, A., TAKAHASHI, H., UTSUMI, J., SASAKI, H. & WAKABAYASHI, K. 2015. Sortilin-related receptor CNS expressed 2 (SorCS2) is localized to Bunina bodies in amyotrophic lateral sclerosis. *Neuroscience letters,* 608**,** 6-11.

MORRIS, A. W., CARARE, R. O., SCHREIBER, S. & HAWKES, C. A. 2014. The cerebrovascular basement membrane: role in the clearance of β-amyloid and cerebral amyloid angiopathy. *Frontiers in aging neuroscience,* 6**,** 251.

MORRISSY, A. S., GARZIA, L., SHIH, D. J., ZUYDERDUYN, S., HUANG, X., SKOWRON, P., REMKE, M., CAVALLI, F. M., RAMASWAMY, V. & LINDSAY, P. E. 2016. Divergent clonal selection dominates medulloblastoma at recurrence. *Nature,* 529**,** 351-357.

MORTAZAVI, A., WILLIAMS, B. A., MCCUE, K., SCHAEFFER, L. & WOLD, B. 2008. Mapping and quantifying mammalian transcriptomes by RNA-Seq. *Nature methods,* 5**,** 621.

MOXON-EMRE, I., BOUFFET, E., TAYLOR, M. D., LAPERRIERE, N., SCANTLEBURY, N., LAW, N., SPIEGLER, B. J., MALKIN, D., JANZEN, L. & MABBOTT, D. 2014. Impact of craniospinal dose, boost volume, and neurologic complications on intellectual outcome in patients with medulloblastoma. *Journal of Clinical Oncology,* 32**,** 1760-1768.

NAGALAKSHMI, U., WANG, Z., WAERN, K., SHOU, C., RAHA, D., GERSTEIN, M. & SNYDER, M. 2008. The transcriptional landscape of the yeast genome defined by RNA sequencing. *Science,* 320**,** 1344-1349.

NAKAMURA, T., TAKEUCHI, K., MURAOKA, S., TAKEZOE, H., TAKAHASHI, N. & MORI, N. 1999. A neurally enriched coronin-like protein, ClipinC, is a novel candidate for an actin cytoskeleton-cortical membrane-linking protein. *Journal of Biological Chemistry,* 274**,** 13322-13327.

NASARRE, C., KONCINA, E., LABOURDETTE, G., CREMEL, G., ROUSSEL, G., AUNIS, D. & BAGNARD, D. 2009. Neuropilin-2 acts as a modulator of Sema3A-dependent glioma cell migration. *Cell adhesion & migration,* 3**,** 383-389.

NATSUIZAKA, M., KINUGASA, H., KAGAWA, S., WHELAN, K. A., NAGANUMA, S., SUBRAMANIAN, H., CHANG, S., NAKAGAWA, K. J., RUSTGI, N. L. & KITA, Y. 2014. IGFBP3 promotes esophageal cancer growth by suppressing oxidative stress in hypoxic tumor microenvironment. *American journal of cancer research,* 4**,** 29.

NAVIN, N., KENDALL, J., TROGE, J., ANDREWS, P., RODGERS, L., MCINDOO, J., COOK, K., STEPANSKY, A., LEVY, D. & ESPOSITO, D. 2011. Tumour evolution inferred by single-cell sequencing. *Nature,* 472**,** 90.

NEVE, A., KUMAR, K. S., TRIPOLITSIOTI, D., GROTZER, M. A. & BAUMGARTNER, M. 2017. Investigation of brain tissue infiltration by medulloblastoma cells in an ex vivo model. *Scientific reports,* 7**,** 1-12.

NIELSEN, M. S., MADSEN, P., CHRISTENSEN, E. I., NYKJÆR, A., GLIEMANN, J., KASPER, D., POHLMANN, R. & PETERSEN, C. M. 2001. The sortilin cytoplasmic tail conveys Golgi–endosome transport and binds the VHS domain of the GGA2 sorting protein. *The EMBO journal,* 20**,** 2180-2190.

NORTHCOTT, P. A., BUCHHALTER, I., MORRISSY, A. S., HOVESTADT, V., WEISCHENFELDT, J., EHRENBERGER, T., GROBNER, S., SEGURA-WANG, M., ZICHNER, T., RUDNEVA, V. A., WARNATZ, H. J., SIDIROPOULOS, N., PHILLIPS, A. H., SCHUMACHER, S., KLEINHEINZ, K., WASZAK, S. M., ERKEK, S., JONES, D. T. W., WORST, B. C., KOOL, M., ZAPATKA, M., JAGER, N., CHAVEZ, L., HUTTER, B., BIEG, M., PARAMASIVAM, N., HEINOLD, M., GU, Z., ISHAQUE, N., JAGER-SCHMIDT, C., IMBUSCH, C. D., JUGOLD, A., HUBSCHMANN, D., RISCH, T., AMSTISLAVSKIY, V., GONZALEZ, F. G. R., WEBER, U. D., WOLF, S., ROBINSON, G. W., ZHOU, X., WU, G., FINKELSTEIN, D., LIU, Y., CAVALLI, F. M. G., LUU, B., RAMASWAMY, V., WU, X., KOSTER, J., RYZHOVA, M., CHO, Y. J., POMEROY, S. L., HEROLD-MENDE, C., SCHUHMANN, M., EBINGER, M., LIAU, L. M., MORA, J., MCLENDON, R. E., JABADO, N., KUMABE, T., CHUAH, E., MA, Y., MOORE, R. A., MUNGALL, A. J., MUNGALL, K. L., THIESSEN, N., TSE, K., WONG, T., JONES, S. J. M., WITT, O., MILDE, T., VON DEIMLING, A., CAPPER, D., KORSHUNOV, A., YASPO, M. L., KRIWACKI, R., GAJJAR, A., ZHANG, J., BEROUKHIM, R., FRAENKEL, E., KORBEL, J. O., BRORS, B., SCHLESNER, M., EILS, R., MARRA, M. A., PFISTER, S. M., TAYLOR, M. D. & LICHTER, P. 2017. The whole-genome landscape of medulloblastoma subtypes. *Nature,* 547**,** 311-317.

NORTHCOTT, P. A., JONES, D. T., KOOL, M., ROBINSON, G. W., GILBERTSON, R. J., CHO, Y. J., POMEROY, S. L., KORSHUNOV, A., LICHTER, P., TAYLOR, M. D. & PFISTER, S. M. 2012a. Medulloblastomics: the end of the beginning. *Nat Rev Cancer,* 12**,** 818-34.

NORTHCOTT, P. A., LEE, C., ZICHNER, T., STÜTZ, A. M., ERKEK, S., KAWAUCHI, D., SHIH, D. J., HOVESTADT, V., ZAPATKA, M. & STURM, D. 2014. Enhancer hijacking activates GFI1 family oncogenes in medulloblastoma. *Nature,* 511**,** 428-434.

NORTHCOTT, P. A., ROBINSON, G. W., KRATZ, C. P., MABBOTT, D. J., POMEROY, S. L., CLIFFORD, S. C., RUTKOWSKI, S., ELLISON, D. W., MALKIN, D. & TAYLOR, M. D. 2019. Medulloblastoma. *Nature Reviews Disease Primers,* 5**,** 1-20.

NORTHCOTT, P. A., SHIH, D. J., PEACOCK, J., GARZIA, L., MORRISSY, A. S., ZICHNER, T., STÜTZ, A. M., KORSHUNOV, A., REIMAND, J. & SCHUMACHER, S. E. 2012b. Subgroup-specific structural variation across 1,000 medulloblastoma genomes. *Nature,* 488**,** 49-56.

O'MEARA, W. P., BORKAER, S. A., STAMBUK, H. E. & LYMBERIS, S. C. 2007. Leptomeningeal Metastasis. *Current Problems in Cancer,* 31**,** 372-424.

O'REILLY, M. S., BOEHM, T., SHING, Y., FUKAI, N., VASIOS, G., LANE, W. S., FLYNN, E., BIRKHEAD, J. R., OLSEN, B. R. & FOLKMAN, J. 1997. Endostatin: an endogenous inhibitor of angiogenesis and tumor growth. *cell,* 88**,** 277-285.

OLLILA, H., SORONEN, P., SILANDER, K., PALO, O., KIESEPPÄ, T., KAUNISTO, M. A., LÖNNQVIST, J., PELTONEN, L., PARTONEN, T. & PAUNIO, T. 2009. Findings from bipolar disorder genome-wide association studies replicate in a Finnish bipolar family-cohort. *Molecular psychiatry,* 14**,** 351-353.

ONION, D., ARGENT, R. H., REECE-SMITH, A. M., CRAZE, M. L., PINEDA, R. G., CLARKE, P. A., RATAN, H. L., PARSONS, S. L., LOBO, D. N. & DUFFY, J. P. 2016. 3-Dimensional patient-derived lung cancer assays reveal resistance to standards-of-care promoted by stromal cells but sensitivity to histone deacetylase inhibitors. *Molecular cancer therapeutics,* 15**,** 753-763.

ORKIN, R., GEHRON, P., MCGOODWIN, E. B., MARTIN, G., VALENTINE, T. & SWARM, R. 1977. A murine tumor producing a matrix of basement membrane. *The journal of experimental medicine,* 145**,** 204-220.

OSTROM, Q. T., GITTLEMAN, H., TRUITT, G., BOSCIA, A., KRUCHKO, C. & BARNHOLTZ-SLOAN, J. S. 2018. CBTRUS statistical report: primary brain and other central nervous system tumors diagnosed in the United States in 2011–2015. *Neuro-oncology,* 20**,** iv1-iv86.

OTHMAN, R. T., KIMISHI, I., BRADSHAW, T. D., STORER, L. C., KORSHUNOV, A., PFISTER, S. M., GRUNDY, R. G., KERR, I. D. & COYLE, B. 2014. Overcoming multiple drug resistance mechanisms in medulloblastoma. *Acta neuropathologica communications,* 2**,** 1.

PADIATH, Q. S., SAIGOH, K., SCHIFFMANN, R., ASAHARA, H., YAMADA, T., KOEPPEN, A., HOGAN, K., PTÁČEK, L. J. & FU, Y.-H. 2006. Lamin B1 duplications cause autosomal dominant leukodystrophy. *Nature genetics,* 38**,** 1114-1123.

PALUCH, E. K. & RAZ, E. 2013. The role and regulation of blebs in cell migration. *Current opinion in cell biology,* 25**,** 582-590.

PATAY, Z., DESAIN, L. A., HWANG, S. N., COAN, A., LI, Y. & ELLISON, D. W. 2015. MR Imaging Characteristics of Wingless-Type-Subgroup Pediatric Medulloblastoma. *AJNR Am J Neuroradiol,* 36**,** 2386-93.

PEDERSEN, S. G., BOLCHO, U., JENSEN, K. & NYKJAER, A. 2017. Modulation of the VPS10p-Domain Receptor Family for the Treatment of Mental and Behavioural Disorders. Google Patents.

PEI, Y., MOORE, C. E., WANG, J., TEWARI, A. K., EROSHKIN, A., CHO, Y. J., WITT, H., KORSHUNOV, A., READ, T. A., SUN, J. L., SCHMITT, E. M., MILLER, C. R., BUCKLEY, A. F., MCLENDON, R. E., WESTBROOK, T. F., NORTHCOTT, P. A., TAYLOR, M. D., PFISTER, S. M., FEBBO, P. G. & WECHSLER-REYA, R. J.

2012. An animal model of MYC-driven medulloblastoma. *Cancer Cell,* 21**,** 155-67.

PERREAULT, S., RAMASWAMY, V., ACHROL, A., CHAO, K., LIU, T., SHIH, D., REMKE, M., SCHUBERT, S., BOUFFET, E. & FISHER, P. 2014. MRI surrogates for molecular subgroups of medulloblastoma. *American Journal of Neuroradiology,* 35**,** 1263-1269.

PETERSEN, C. M., NIELSEN, M. S., NYKJÆR, A., JACOBSEN, L., TOMMERUP, N., RASMUSSEN, H. H., RØIGAARD, H., GLIEMANN, J., MADSEN, P. & MOESTRUP, S. K. 1997. Molecular identification of a novel candidate sorting receptor purified from human brain by receptor-associated protein affinity chromatography. *Journal of Biological Chemistry,* 272**,** 3599-3605.

PÖSCHL, E., SCHLÖTZER-SCHREHARDT, U., BRACHVOGEL, B., SAITO, K., NINOMIYA, Y. & MAYER, U. 2004. Collagen IV is essential for basement membrane stability but dispensable for initiation of its assembly during early development. *Development,* 131**,** 1619-1628.

POZZI, A., YURCHENCO, P. D. & IOZZO, R. V. 2017. The nature and biology of basement membranes. *Matrix Biol,* 57-58**,** 1-11.

PUGH, T. J., WEERARATNE, S. D., ARCHER, T. C., KRUMMEL, D. A. P., AUCLAIR, D., BOCHICCHIO, J., CARNEIRO, M. O., CARTER, S. L., CIBULSKIS, K., ERLICH, R. L. & GREULICH, H. 2012. Medulloblastoma exome sequencing uncovers subtype-specific somatic mutations. *Nature,* 488**,** 106-110.

RAJAH, R., VALENTINIS, B. & COHEN, P. 1997. Insulin-like growth factor (IGF)-binding protein-3 induces apoptosis and mediates the effects of transforming growth factor-β1 on programmed cell death through a p53-and IGF-independent mechanism. *Journal of Biological Chemistry,* 272**,** 12181-12188.

RAMASWAMY, V., REMKE, M., BOUFFET, E., BAILEY, S., CLIFFORD, S. C., DOZ, F., KOOL, M., DUFOUR, C., VASSAL, G., MILDE, T., WITT, O., VON HOFF, K., PIETSCH, T., NORTHCOTT, P. A., GAJJAR, A., ROBINSON, G. W., PADOVANI, L., ANDRE, N., MASSIMINO, M., PIZER, B., PACKER, R., RUTKOWSKI, S., PFISTER, S. M., TAYLOR, M. D. & POMEROY, S. L. 2016. Risk stratification of childhood medulloblastoma in the molecular era: the current consensus. *Acta Neuropathol,* 131**,** 821-31.

RAMASWAMY, V., REMKE, M., BOUFFET, E., FARIA, C. C., PERREAULT, S., CHO, Y. J., SHIH, D. J., LUU, B., DUBUC, A., NORTHCOTT, P. A., SCHULLER, U., GURURANGAN, S., MCLENDON, R. E., BIGNER, D. D., FOULADI, M., LIGON, K. L., POMEROY, S. L., DUNN, S., TRISCOTT, J., JABADO, N., FONTEBASSO, A., JONES, D. T., KOOL, M., KARAJANNIS, M. A., GARDNER, S. L., ZAGZAG, D., NUNES, S., PIMENTAL, J., MORA, J., LIPP, E., WALTER, A. W., RYZHOVA, M., ZHELUDKOVA, O., KUMIROVA, E., ALSHAMI, J., CROUL, S., RUTKA, J. T., HAWKINS, C., TABORI, U., CODISPOTI, K. T., PACKER, R., PFISTER, S. M., KORSHUNOV, A. & TAYLOR, M. D. 2013. Recurrence patterns across medulloblastoma subgroups: an integrated clinical and molecular analysis. *Lancet Oncology,* 14**,** 1200-1207.

RAUSCH, T., JONES, D. T., ZAPATKA, M., STÜTZ, A. M., ZICHNER, T., WEISCHENFELDT, J., JÄGER, N., REMKE, M., SHIH, D. & NORTHCOTT, P. A. 2012. Genome sequencing of pediatric medulloblastoma links catastrophic DNA rearrangements with TP53 mutations. *Cell,* 148**,** 59-71.

RAYBAUD, C., RAMASWAMY, V., TAYLOR, M. D. & LAUGHLIN, S. 2015. Posterior fossa tumors in children: developmental anatomy and diagnostic imaging. *Child's Nervous System,* 31**,** 1661-1676.

REISER, J. & ALTINTAS, M. M. 2016. Podocytes. *F1000Research,* 5.

REZGAOUI, M., HERMEY, G., RIEDEL, I. B., HAMPE, W., SCHALLER, H. C. & HERMANS-BORGMEYER, I. 2001. Identification of SorCS2, a novel member of the VPS10 domain containing receptor family, prominently expressed in the developing mouse brain. *Mechanisms of development,* 100**,** 335-338.

RIVERO-HINOJOSA, S., SAN LAU, L., STAMPAR, M., STAAL, J., ZHANG, H., GORDISH-DRESSMAN, H., NORTHCOTT, P. A., PFISTER, S. M., TAYLOR, M. D. & BROWN, K. J. 2018. Proteomic analysis of medulloblastoma reveals functional biology with translational potential. *Acta neuropathologica communications,* 6**,** 48.

ROADCAP, D. W., CLEMEN, C. S. & BEAR, J. E. 2008. The role of mammalian coronins in development and disease. *The Coronin Family of Proteins.* Springer.

ROBBINS, C. J., BOU-DARGHAM, M. J., SANCHEZ, K., ROSEN, M. C. & SANG, Q. X. A. 2018. Decoding somatic driver gene mutations and affected signaling pathways in human medulloblastoma subgroups. *Journal of Cancer,* 9.

ROBINSON, G., PARKER, M., KRANENBURG, T. A., LU, C., CHEN, X., DING, L., PHOENIX, T. N., HEDLUND, E., WEI, L. & ZHU, X. 2012. Novel mutations target distinct subgroups of medulloblastoma. *Nature,* 488**,** 43-48.

ROBINSON, G. W., RUDNEVA, V. A., BUCHHALTER, I., BILLUPS, C. A., WASZAK, S. M., SMITH, K. S., BOWERS, D. C., BENDEL, A., FISHER, P. G. & PARTAP, S. 2018. Risk-adapted therapy for young children with medulloblastoma (SJYC07): therapeutic and molecular outcomes from a multicentre, phase 2 trial. *The Lancet Oncology,* 19**,** 768-784.

RODRIGUEZ, A., GRIFFITHS-JONES, S., ASHURST, J. L. & BRADLEY, A. 2004. Identification of mammalian microRNA host genes and transcription units. *Genome research,* 14**,** 1902-1910.

ROGG, M., YASUDA-YAMAHARA, M., ABED, A., DINSE, P., HELMSTÄDTER, M., CONZELMANN, A., FRIMMEL, J., SELLUNG, D., BINIOSSEK, M. & KRETZ, O. 2017. The WD40-domain containing protein CORO2B is specifically enriched in glomerular podocytes and regulates the ventral actin cytoskeleton. *Scientific reports,* 7**,** 1-15.

ROWE, R. G. & WEISS, S. J. 2008. Breaching the basement membrane: who, when and how? *Trends Cell Biol,* 18**,** 560-74.

RUTKOWSKI, S., GERBER, N. U., VON HOFF, K., GNEKOW, A., BODE, U., GRAF, N., BERTHOLD, F., HENZE, G. N., WOLFF, J. E. & WARMUTH-METZ, M. 2009. Treatment of early childhood medulloblastoma by postoperative chemotherapy and deferred radiotherapy. *Neuro-oncology,* 11**,** 201-210.

SAUNDERS, J. H., ONION, D., COLLIER, P., DORRINGTON, M. S., ARGENT, R. H., CLARKE, P. A., REECE-SMITH, A. M., PARSONS, S. L. & GRABOWSKA, A. M. 2017. Individual patient oesophageal cancer 3D models for tailored treatment. *Oncotarget,* 8**,** 24224.

SCHENA, M., SHALON, D., DAVIS, R. W. & BROWN, P. O. 1995. Quantitative monitoring of gene expression patterns with a complementary DNA microarray. *Science,* 270**,** 467-470.

SCHRAPPE, M., MÖRICKE, A., REITER, A., HENZE, G., WELTE, K., GADNER, H., LUDWIG, W.-D., RITTER, J., HARBOTT, J. & MANN, G. 2013. Key treatment questions in childhood acute lymphoblastic leukemia: results in 5 consecutive trials performed by the ALL-BFM study group from 1981 to 2000. *Klinische Pädiatrie,* 225**,** S62-S72.

SCHRØDER, T. J., CHRISTENSEN, S., LINDBERG, S., LANGGÅRD, M., DAVID, L., MALTAS, P. J., ESKILDSEN, J., JACOBSEN, J., TAGMOSE, L. & SIMONSEN, K. B. 2014. The identification of AF38469: an orally bioavailable inhibitor of the VPS10P family sorting receptor Sortilin. *Bioorganic & medicinal chemistry letters,* 24**,** 177-180.

SCHROEDER, A., MUELLER, O., STOCKER, S., SALOWSKY, R., LEIBER, M., GASSMANN, M., LIGHTFOOT, S., MENZEL, W., GRANZOW, M. & RAGG, T. 2006. The RIN: an RNA integrity number for assigning integrity values to RNA measurements. *BMC molecular biology,* 7**,** 3.

SCHWALBE, E. C., LINDSEY, J. C., NAKJANG, S., CROSIER, S., SMITH, A. J., HICKS, D., RAFIEE, G., HILL, R. M., ILIASOVA, A. & STONE, T. 2017. Novel molecular subgroups for clinical classification and outcome prediction in childhood medulloblastoma: a cohort study. *The Lancet Oncology,* 18**,** 958-971.

SCHWARZ, A., MÖLLER-HACKBARTH, K., EBARASI, L., JESS, D. U., ZAMBRANO, S., BLOM, H., WERNERSON, A., LAL, M. & PATRAKKA, J. 2019. Coro2b, a podocyte protein downregulated in human diabetic nephropathy, is involved in the development of protamine sulphate-induced foot process effacement. *Scientific reports,* 9**,** 1-11.

SENGUPTA, S., WEERARATNE, S. D., SUN, H., PHALLEN, J., RALLAPALLI, S. K., TEIDER, N., KOSARAS, B., AMANI, V., PIERRE-FRANCOIS, J. & TANG, Y. 2014. α5-GABAA receptors negatively regulate MYC-amplified medulloblastoma growth. *Acta neuropathologica,* 127**,** 593-603.

SHARMA, T., SCHWALBE, E. C., WILLIAMSON, D., SILL, M., HOVESTADT, V., MYNAREK, M., RUTKOWSKI, S., ROBINSON, G. W., GAJJAR, A. & CAVALLI, F. 2019. Second-generation molecular subgrouping of medulloblastoma: an international meta-analysis of Group 3 and Group 4 subtypes. *Acta neuropathologica,* 138**,** 309-326.

SHENDURE, J. 2008. The beginning of the end for microarrays? *Nature methods,* 5**,** 585-587.

SHIRAKI, T., KONDO, S., KATAYAMA, S., WAKI, K., KASUKAWA, T., KAWAJI, H., KODZIUS, R., WATAHIKI, A., NAKAMURA, M. & ARAKAWA, T. 2003. Cap analysis gene expression for high-throughput analysis of transcriptional starting point and identification of promoter usage. *Proceedings of the National Academy of Sciences,* 100**,** 15776-15781.

SHKURNIKOV, M., NIKULIN, S., NERSISYAN, S., POLOZNIKOV, A., BARANOVA, A., SCHUMACHER, U., WICKLEIN, D. & TONEVITSKY, A. 2019. LAMA4-regulating miR-4274 and its host gene SORCS2 play a role in IGFBP6-dependent effects on phenotype of basal-like breast cancer. *Frontiers in molecular biosciences,* 6**,** 122.

SMITH, M. J., BEETZ, C., WILLIAMS, S. G., BHASKAR, S. S., O'SULLIVAN, J., ANDERSON, B., DALY, S. B., URQUHART, J. E., BHOLAH, Z. & OUDIT, D. 2014. Germline mutations in SUFU cause Gorlin syndrome–associated childhood medulloblastoma and redefine the risk associated with PTCH1 mutations. *Journal of Clinical Oncology,* 32**,** 4155-4161.

SMOLL, N. R. & DRUMMOND, K. J. 2012. The incidence of medulloblastomas and primitive neurectodermal tumours in adults and children. *Journal of Clinical Neuroscience,* 19**,** 1541-1544.

SNUDERL, M., BATISTA, A., KIRKPATRICK, N. D., RUIZ DE ALMODOVAR, C., RIEDEMANN, L., WALSH, E. C., ANOLIK, R., HUANG, Y., MARTIN, J. D., KAMOUN, W., KNEVELS, E., SCHMIDT, T., FARRAR, C. T., VAKOC, B. J., MOHAN, N., CHUNG, E., ROBERGE, S., PETERSON, T., BAIS, C., ZHELYAZKOVA, B. H., YIP, S., HASSELBLATT, M., ROSSIG, C., NIEMEYER,

E., FERRARA, N., KLAGSBRUN, M., DUDA, D. G., FUKUMURA, D., XU, L., CARMELIET, P. & JAIN, R. K. 2013. Targeting placental growth factor/neuropilin 1 pathway inhibits growth and spread of medulloblastoma. *Cell,* 152**,** 1065-76.

SOFRONIEW, M. V. 2015. Astrocyte barriers to neurotoxic inflammation. *Nature Reviews Neuroscience,* 16**,** 249-263.

SOOD, D., TANG-SCHOMER, M., POULI, D., MIZZONI, C., RAIA, N., TAI, A., ARKUN, K., WU, J., BLACK, L. D. & SCHEFFLER, B. 2019. 3D extracellular matrix microenvironment in bioengineered tissue models of primary pediatric and adult brain tumors. *Nature communications,* 10**,** 1-14.

SPECTOR, R., SNODGRASS, S. R. & JOHANSON, C. E. 2015. A balanced view of the cerebrospinal fluid composition and functions: focus on adult humans. *Experimental neurology,* 273**,** 57-68.

SPICER, A. P., JOO, A. & BOWLING, R. A. 2003. A Hyaluronan Binding Link Protein Gene Family Whose Members Are Physically Linked Adjacent to Chrondroitin Sulfate Proteoglycan Core Protein Genes THE MISSING LINKS. *Journal of Biological Chemistry,* 278**,** 21083-21091.

STARKE, J., WEHRLE-HALLER, B. & FRIEDL, P. 2014. Plasticity of the actin cytoskeleton in response to extracellular matrix nanostructure and dimensionality. Portland Press Ltd.

SUBRAMANIAN, A., TAMAYO, P., MOOTHA, V. K., MUKHERJEE, S., EBERT, B. L., GILLETTE, M. A., PAULOVICH, A., POMEROY, S. L., GOLUB, T. R. & LANDER, E. S. 2005. Gene set enrichment analysis: a knowledge-based approach for interpreting genome-wide expression profiles. *Proceedings of the National Academy of Sciences,* 102**,** 15545-15550.

SUN, S., XU, M. Z., POON, R. T., DAY, P. J. & LUK, J. M. 2010. Circulating Lamin B1 (LMNB1) biomarker detects early stages of liver cancer in patients. *Journal of proteome research,* 9**,** 70-78.

SUN, T., CHEN, G., LI, Y., XIE, X., ZHOU, Y. & DU, Z. 2015. Aggressive invasion is observed in CD133-/A2B5+ glioma-initiating cells. *Oncology letters,* 10**,** 3399-3406.

SUTHERLAND, R. M., MCCREDIE, J. A. & INCH, W. R. 1971. Growth of multicell spheroids in tissue culture as a model of nodular carcinomas. *Journal of the National Cancer Institute,* 46**,** 113-120.

SWINSCOW, T. D. V. & CAMPBELL, M. J. 2002. *Statistics at square one*, Bmj London.

TALMADGE, J. E. & FIDLER, I. 1982. Evidence for the clonal origin of spontaneous metastases. *Science,* 217**,** 361-363.

TANG, X., MCMULLEN, T. P. & BRINDLEY, D. N. 2019. Increasing the low lipid phosphate phosphatase 1 activity in breast cancer cells decreases transcription by AP-1 and expressions of matrix metalloproteinases and cyclin D1/D3. *Theranostics,* 9**,** 6129.

TAYLOR, M. D., NORTHCOTT, P. A., KORSHUNOV, A., REMKE, M., CHO, Y. J., CLIFFORD, S. C., EBERHART, C. G., PARSONS, D. W., RUTKOWSKI, S., GAJJAR, A., ELLISON, D. W., LICHTER, P., GILBERTSON, R. J., POMEROY, S. L., KOOL, M. & PFISTER, S. M. 2012. Molecular subgroups of medulloblastoma: the current consensus. *Acta Neuropathol,* 123**,** 465-72.

TE BOEKHORST, V., PREZIOSI, L. & FRIEDL, P. 2016. Plasticity of cell migration in vivo and in silico. *Annual review of cell and developmental biology,* 32**,** 491-526.

THAL, D., XAVIER, C. P., ROSENTRETER, A., LINDER, S., FRIEDRICHS, B., WAHA, A., PIETSCH, T., STUMPF, M., NOEGEL, A. & CLEMEN, C. 2008. Expression of coronin‐3 (coronin‐1C) in diffuse gliomas is related to malignancy. *The Journal of pathology,* 214**,** 415-424.

THIERY, J. P. 2002. Epithelial–mesenchymal transitions in tumour progression. *Nature Reviews Cancer,* 2**,** 442-454.

THOMSEN, M. S., ROUTHE, L. J. & MOOS, T. 2017. The vascular basement membrane in the healthy and pathological brain. *Journal of Cerebral Blood Flow & Metabolism,* 37**,** 3300-3317.

TIMPL, R. 1996. Macromolecular organization of basement membranes. *Current opinion in cell biology,* 8**,** 618-624.

TOMMERUP, N., NIELSEN, F. & OPITZ, J. M. 1983. A familial reciprocal translocation t (3; 7)(p21. 1; p13) associated with the Greig polysyndactyly‐craniofacial anomalies syndrome. *American journal of medical genetics,* 16**,** 313-321.

TUTAR, Y. 2012. Pseudogenes. *Comparative and functional genomics,* 2012.

TWIGG, S. R., HUFNAGEL, R. B., MILLER, K. A., ZHOU, Y., MCGOWAN, S. J., TAYLOR, J., CRAFT, J., TAYLOR, J. C., SANTORO, S. L. & HUANG, T. 2016. A recurrent mosaic mutation in SMO, encoding the hedgehog signal transducer smoothened, is the major cause of Curry-Jones syndrome. *The American Journal of Human Genetics,* 98**,** 1256-1265.

VAN OMMEREN, R., GARZIA, L., HOLGADO, B. L., RAMASWAMY, V. & TAYLOR, M. D. 2019. Mini‐symposium: The molecular biology of medulloblastoma metastasis. *Brain Pathology*.

VELCULESCU, V. E., ZHANG, L., VOGELSTEIN, B. & KINZLER, K. W. 1995. Serial analysis of gene expression. *Science,* 270**,** 484-487.

VINCI, M., BOX, C. & ECCLES, S. A. 2015. Three-dimensional (3D) tumor spheroid invasion assay. *JoVE (Journal of Visualized Experiments)***,** e52686.

VINCI, M., GOWAN, S., BOXALL, F., PATTERSON, L., ZIMMERMANN, M., LOMAS, C., MENDIOLA, M., HARDISSON, D. & ECCLES, S. A. 2012. Advances in establishment and analysis of three-dimensional tumor spheroid-based functional assays for target validation and drug evaluation. *BMC biology,* 10**,** 29.

VLADOIU, M. C., EL-HAMAMY, I., DONOVAN, L. K., FAROOQ, H., HOLGADO, B. L., SUNDARAVADANAM, Y., RAMASWAMY, V., HENDRIKSE, L. D., KUMAR, S. & MACK, S. C. 2019. Childhood cerebellar tumours mirror conserved fetal transcriptional programs. *Nature,* 572**,** 67-73.

VON BUEREN, A. O., KORTMANN, R.-D., VON HOFF, K., FRIEDRICH, C., MYNAREK, M., MÜLLER, K., GOSCHZIK, T., ZUR MÜHLEN, A., GERBER, N. & WARMUTH-METZ, M. 2016. Treatment of children and adolescents with metastatic medulloblastoma and prognostic relevance of clinical and biologic parameters. *Journal of Clinical Oncology,* 34**,** 4151-4160.

WALKER, D. A., MEIJER, L., COYLE, B. & HALSEY, C. 2020. Leptomeningeal malignancy of childhood: sharing learning between childhood leukaemia and brain tumour trials. *The Lancet Child & Adolescent Health,* 4**,** 242-250.

WANG, X., ZENG, Y., ZHOU, M., ZHANG, X., XU, A., LIN, J., WU, Z., XIE, C., LUO, J. & DING, S. 2019. SKA1 promotes malignant phenotype and progression of glioma via multiple signaling pathways. *Cancer Cell International,* 19**,** 324.

WASZAK, S. M., NORTHCOTT, P. A., BUCHHALTER, I., ROBINSON, G. W., SUTTER, C., GROEBNER, S., GRUND, K. B., BRUGIÈRES, L., JONES, D. T. & PAJTLER, K. W. 2018. Spectrum and prevalence of genetic predisposition in medulloblastoma: a retrospective genetic study and prospective validation in a clinical trial cohort. *The Lancet Oncology,* 19**,** 785-798.

WATANABE, H., MOGUSHI, K., MIURA, M., YOSHIMURA, R.-I., KURABAYASHI, T., SHIBUYA, H., TANAKA, H., NODA, S., IWAKAWA, M. & IMAI, T. 2008. Prediction of lymphatic metastasis based on gene expression profile analysis after brachytherapy for early-stage oral tongue carcinoma. *Radiotherapy and Oncology,* 87**,** 237-242.

WEERARATNE, S., AMANI, V., TEIDER, N., PIERRE-FRANCOIS, J., WINTER, D., KYE, M., SENGUPTA, S., ARCHER, T., REMKE, M., BAI, A., WARREN, P., PFISTER, S., STEEN, J., POMEROY, S. & CHO, Y.-J. 2012. Pleiotropic effects of miR-183~96~182 converge to regulate cell survival, proliferation and migration in medulloblastoma. *Acta Neuropathologica,* 123**,** 539-552.

WEINBERG, R. & HANAHAN, D. 2000. The hallmarks of cancer. *Cell,* 100**,** 57-70.

WELCH, D. R. & HURST, D. R. 2019. Defining the hallmarks of metastasis. *Cancer research,* 79**,** 3011-3027.

WETMORE, C., EBERHART, D. E. & CURRAN, T. 2001. Loss of p53 but not ARF accelerates medulloblastoma in mice heterozygous for patched. *Cancer research,* 61**,** 513-516.

WILHELM, B. T., MARGUERAT, S., WATT, S., SCHUBERT, F., WOOD, V., GOODHEAD, I., PENKETT, C. J., ROGERS, J. & BÄHLER, J. 2008. Dynamic repertoire of a eukaryotic transcriptome surveyed at single-nucleotide resolution. *Nature,* 453**,** 1239-1243.

WILNE, S., COLLIER, J., KENNEDY, C., KOLLER, K., GRUNDY, R. & WALKER, D. 2007. Presentation of childhood CNS tumours: a systematic review and meta-analysis. *The lancet oncology,* 8**,** 685-695.

WILSON, C. M., NAVES, T., VINCENT, F., MELLONI, B., BONNAUD, F., LALLOUÉ, F. & JAUBERTEAU, M.-O. 2014. Sortilin mediates the release and transfer of exosomes in concert with two tyrosine kinase receptors. *Journal of cell science,* 127**,** 3983-3997.

WU, X., NORTHCOTT, P. A., DUBUC, A., DUPUY, A. J., SHIH, D. J., WITT, H., CROUL, S., BOUFFET, E., FULTS, D. W. & EBERHART, C. G. 2012. Clonal selection drives genetic divergence of metastatic medulloblastoma. *Nature,* 482**,** 529-533.

WU, X., YE, Y., ROSELL, R., AMOS, C. I., STEWART, D. J., HILDEBRANDT, M. A., ROTH, J. A., MINNA, J. D., GU, J. & LIN, J. 2011. Genome-wide association study of survival in non–small cell lung cancer patients receiving platinum-based chemotherapy. *Journal of the National Cancer Institute,* 103**,** 817-825.

XU, J.-Z., ZHANG, J.-L. & ZHANG, W.-G. 2018. Antisense RNA: the new favorite in genetic research. *Journal of Zhejiang University-SCIENCE B,* 19**,** 739-749.

XU, J., MARGOL, A. S., SHUKLA, A., REN, X., FINLAY, J. L., KRIEGER, M. D., GILLES, F. H., COUCH, F. J., AZIZ, M., FUNG, E. T., ASGHARZADEH, S., BARRETT, M. T. & ERDREICH-EPSTEIN, A. 2015. Disseminated Medulloblastoma in a Child with Germline BRCA2 6174delT Mutation and without Fanconi Anemia. *Front Oncol,* 5**,** 191.

YAMAMOTO, N., YANG, M., JIANG, P., XU, M., TSUCHIYA, H., TOMITA, K., MOOSSA, A. & HOFFMAN, R. M. 2003. Determination of clonality of metastasis by cell-

specific color-coded fluorescent-protein imaging. *Cancer research,* 63**,** 7785-7790.

YAMAZAKI, H., BUJO, H., KUSUNOKI, J., SEIMIYA, K., KANAKI, T., MORISAKI, N., SCHNEIDER, W. J. & SAITO, Y. 1996. Elements of neural adhesion molecules and a yeast vacuolar protein sorting receptor are present in a novel mammalian low density lipoprotein receptor family member. *Journal of Biological Chemistry,* 271**,** 24761-24768.

YANG, W., WU, P.-F., MA, J.-X., LIAO, M.-J., WANG, X.-H., XU, L.-S., XU, M.-H. & YI, L. 2019. Sortilin promotes glioblastoma invasion and mesenchymal transition through GSK-3β/β-catenin/twist pathway. *Cell death & disease,* 10**,** 1-15.

YAO, A., STORR, S. J., AL-HADYAN, K., RAHMAN, R., SMITH, S., GRUNDY, R., PAINE, S. & MARTIN, S. G. 2020. Thioredoxin system protein expression is associated with poor clinical outcome in adult and paediatric gliomas and medulloblastomas. *apoptosis,* 11**,** 13.

YURCHENCO, P. & CHENG, Y.-S. 1993. Self-assembly and calcium-binding sites in laminin. A three-arm interaction model. *Journal of Biological Chemistry,* 268**,** 17286-17299.

ZAPOTOCKY, M., MATA-MBEMBA, D., SUMERAUER, D., LIBY, P., LASSALETTA, A., ZAMECNIK, J., KRSKOVA, L., KYNCL, M., STARY, J., LAUGHLIN, S., ARNOLDO, A., HAWKINS, C., TABORI, U., TAYLOR, M. D., BOUFFET, E., RAYBAUD, C. & RAMASWAMY, V. 2018. Differential patterns of metastatic dissemination across medulloblastoma subgroups. *J Neurosurg Pediatr,* 21**,** 145-152.

ZENGEL, P., NGUYEN-HOANG, A., SCHILDHAMMER, C., ZANTL, R., KAHL, V. & HORN, E. 2011. µ-Slide Chemotaxis: a new chamber for long-term chemotaxis studies. *BMC cell biology,* 12**,** 21.

ZHANG, S., GUO, D., LUO, W., ZHANG, Q., ZHANG, Y., LI, C., LU, Y., CUI, Z. & QIU, X. 2010. TrkB is highly expressed in NSCLC and mediates BDNF-induced the activation of Pyk2 signaling and the invasion of A549 cells. *BMC cancer,* 10**,** 43.

ZHOU, L., PICARD, D., RA, Y.-S., LI, M., NORTHCOTT, P. A., HU, Y., STEARNS, D., HAWKINS, C., TAYLOR, M. D. & RUTKA, J. 2010. Silencing of thrombospondin-1 is critical for myc-induced metastatic phenotypes in medulloblastoma. *Cancer research,* 70**,** 8199-8210.

ZHUKOVA, N., RAMASWAMY, V., REMKE, M., PFAFF, E., SHIH, D. J., MARTIN, D. C., CASTELO-BRANCO, P., BASKIN, B., RAY, P. N. & BOUFFET, E. 2013. Subgroup-specific prognostic implications of TP53 mutation in medulloblastoma. *Journal of Clinical Oncology,* 31**,** 2927.

ZIMMERMANN, M., BOX, C. & ECCLES, S. A. 2013. Two-dimensional vs. three-dimensional in vitro tumor migration and invasion assays. *Target Identification and Validation in Drug Discovery.* Springer.

Web references

Cancer Research UK, viewed June 2020, <https://www.cancerresearchuk.org/health-professional/cancer-statistics/childrens-cancers/incidence#heading-Five>

Childhood Cancer Registrations, Great Britain, 1971-2005, viewed June 2020, <http://www.ccrg.ox.ac.uk/datasets/registrations.shtml>

Headsmart Early Diagnosis of Brain Tumours, viewed June 2020, <https://www.headsmart.org.uk/>

Theses referenced

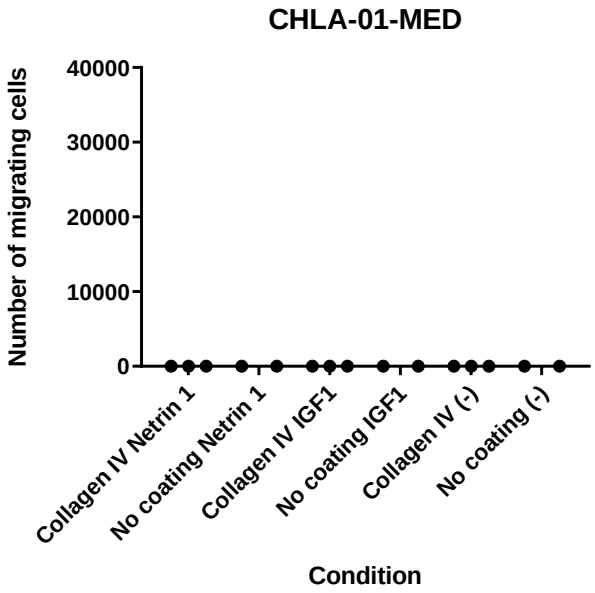
JACKSON, H. K. 2017. *Investigating the role of exosomes in medulloblastoma and their involvement in metastasis.* University of Nottingham.

NASIR, A. 2016. *An investigation of metastatic markers in models of paediatric medulloblastoma*. University of Nottingham.

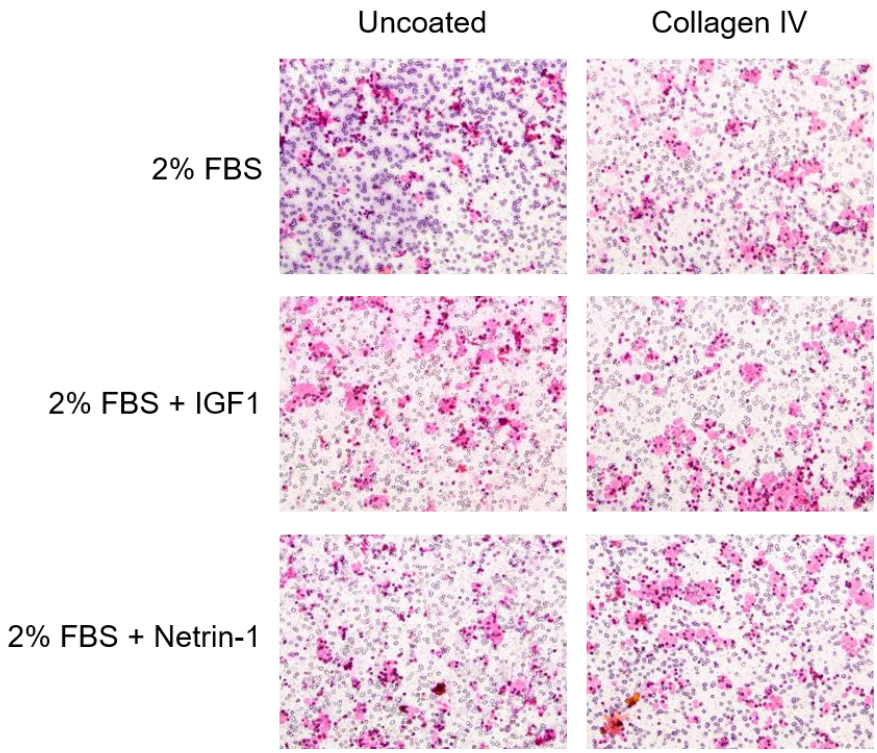
ROPER, S. J. 2019. *Development of three-dimensional spheroid models for the analysis of medulloblastoma drug response and metastatic dissemination*. University of Nottingham.

Appendices

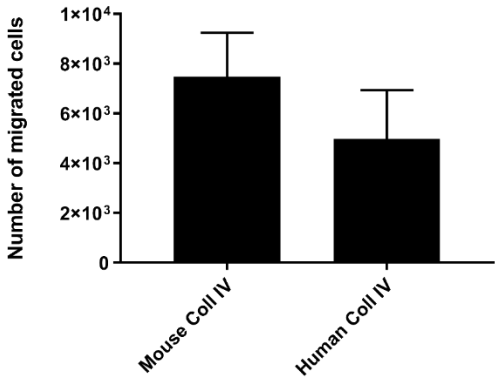
Appendix 1: Chapter 3



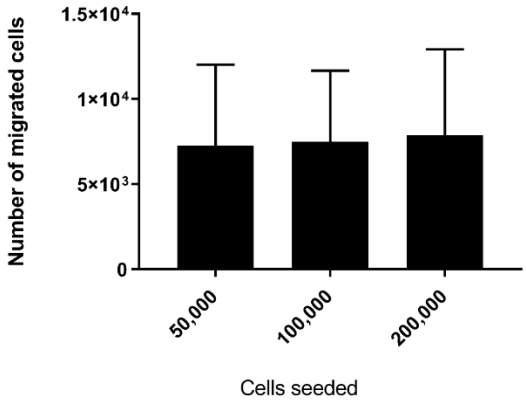
Supp. Figure 1. The number of CHLA-01-MED migrated cells at 72h across trans-wells coated with collagen IV only towards either medium supplemented with 2% FBS and IGF1 or 2% FBS and Netrin-1, or towards 2% FBS only. CHLA-01-MED cells were also exposed to IGF-1 in the top of the trans-well as a treatment (n=1).



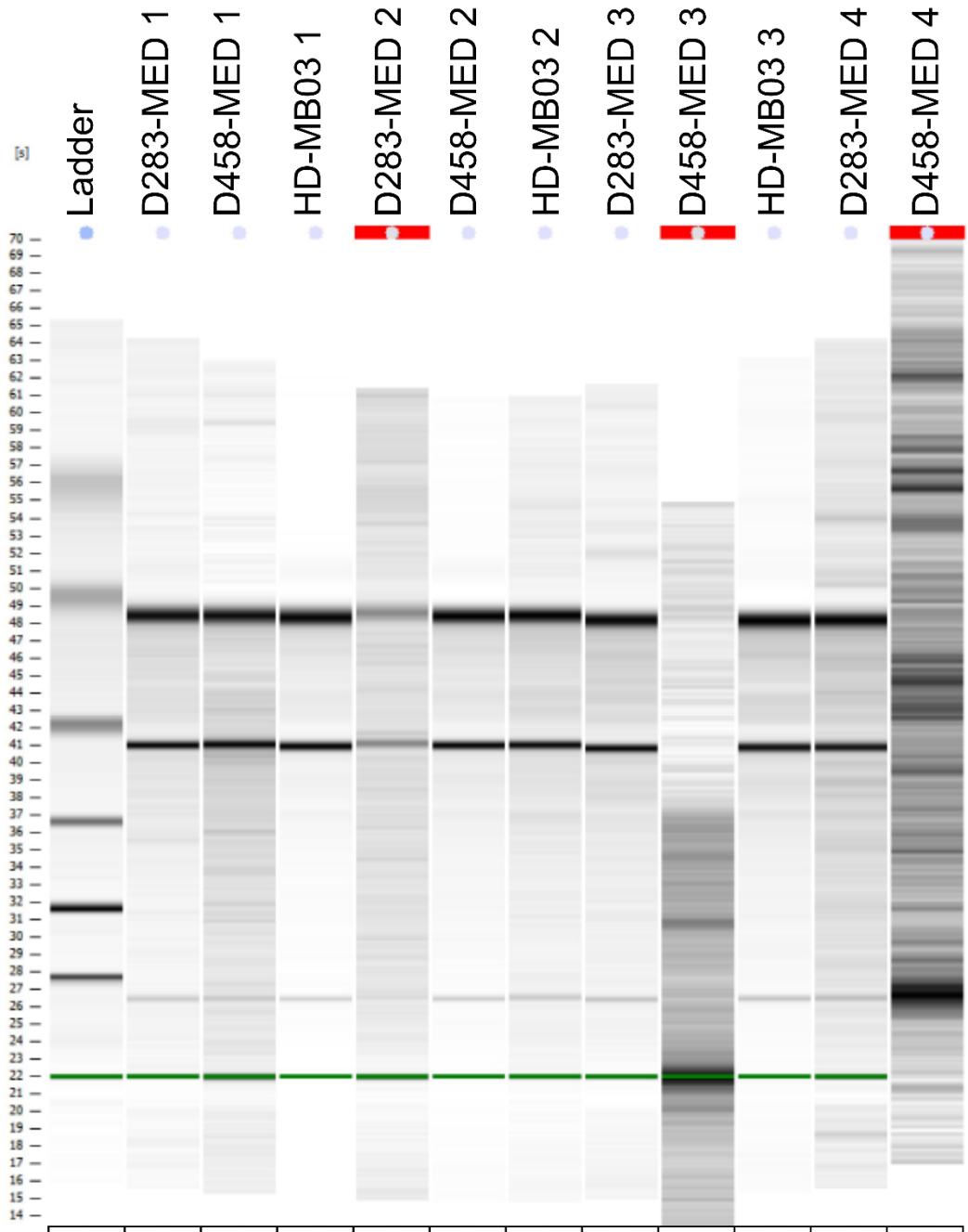
Supp. Figure 2. D283-MED cell migration through an uncoated trans-well or a well coated with Collagen IV (10µg/well) in response to 2% FBS only or 2% FBS supplemented with either IGF1 or Netrin-1.



Supp. Figure 3. The number of HD-MB03 migrated cells at 48h across trans-wells coated with collagen IV of mouse or human origin and Laminin 111 towards aCSF supplemented with 10% FBS (n=1).



Supp. Figure 4. The number of HD-MB03 migrated cells at 48h across trans-wells coated with collagen IV of human origin and Laminin 111 towards aCSF supplemented with 10% FBS (n=1).



ng/µL	0.464	0.290	6.089	0.122	1.948	0.544	0.558	0.255	2.195	0.366	0.295
RIN	7.8	6.9	9.10	N/A	8.4	7.8	7.7	N/A	8	7	2.4

Supp.Figure 5. The RNA concentration (ng/µL) and RNA quality (RIN) were measured for 4 D283-MED migrated (M) samples, 4 D458-MED M samples and 3 HD-MB03 M samples using Bioanalyzer Pico chip. The samples marked in red had an insufficient RIN score.

Appendix 2: Chapter 4

Part 1. Tables expanding on section 4.3.5 Differentially expressed genes between cell compartments.

The top 25 genes for each comparison within each cell line are detailed in Tables 1-18. If fewer than 25 genes were up or downregulated in the cell compartment, the total number of genes is shown.

The prefixes AC or AL indicate novel transcripts. The suffix P indicates a pseudogene, gene copies that have coding-sequence deficiencies but resemble the functional genes (Tutar, 2012). The suffix AS indicates an antisense RNA, small, noncoding, and diffusible molecules that complement mRNA (Xu et al., 2018). The suffix DT indicates a divergent transcript, a transcript that closely resembles a known gene but with modifications.

Supp Table 1 HD-MB03 Migrated > Adherent

Top 25 of 73 genes upregulated in the migrated compartment compared to the adherent compartment. Genes were ordered based on the significant change in expression (Log2FoldChange). Significance was determined using an uncorrected p-value and a Benjamini Hochberg adjusted p-value which is identical with the False Positive Rate (FDR). If a gene has low mean normalized count, then the adjusted p-value was set to NA. The normalized mean of triplicate samples is also show.

Gene	Log2FoldChange	P value	Adjusted p-value	Mean norm counts
RN7SK	2.93	4.80E-26	2.51E-22	436.71
AC100801.1	1.66	2.42E-05	1.15E-02	26.8
TSPAN6	1.61	2.84E-03	NA	10.87
ARL6	1.6	2.90E-03	NA	12.87
AC040162.1	1.57	1.78E-05	9.29E-03	35.21
CTSV	1.53	6.64E-04	8.91E-02	22.17
SORCS2	1.52	2.96E-07	3.87E-04	180.37
SCOC	1.51	3.12E-05	1.16E-02	29.96
SEMA3A	1.48	9.14E-06	5.97E-03	65.99
GCNT1	1.46	1.47E-05	8.53E-03	48.36
MRPL52	1.39	5.41E-04	8.20E-02	21.7
TNNT1	1.38	5.51E-03	NA	16.2
MANEA	1.36	3.60E-03	NA	13.82
MT-TW	1.35	1.89E-02	3.99E-01	536.42
KIF1BP	1.34	1.78E-03	1.65E-01	21.18
SELENOW	1.32	2.60E-06	2.26E-03	70.54
DNLZ	1.32	4.87E-03	NA	15.67
AL591485.1	1.3	2.97E-03	NA	17.3
COA3	1.29	3.48E-05	1.21E-02	63.94
FREM2	1.28	3.27E-04	5.89E-02	41.76
TMEM134	1.28	5.22E-03	NA	14.44
PRPF31	1.27	1.30E-02	NA	11.39
COPS9	1.26	2.69E-05	1.16E-02	63.94
AC244021.1	1.25	1.15E-02	NA	15.41

Supp Table 2 HD-MB03 Adherent > Migrated

Top 25 of 91 genes downregulated in the migrated compartment compared to the adherent compartment. Genes were ordered based on the significant change in expression (Log2FoldChange). Significance was determined using an uncorrected p-value and a Benjamini Hochberg adjusted p-value which is identical with the False Positive Rate (FDR). If a gene has low mean normalized count, then the adjusted p-value was set to NA. The normalized mean of triplicate samples is also show.

Gene	Log2FoldChange	P value	Adjusted p-value	Mean norm counts
MFSD13A	-1.74	8.55E-04	NA	11.1
LMNB1-DT	-1.73	7.65E-06	5.71E-03	32.59
AC006487.1	-1.73	2.93E-05	1.16E-02	32.88
DNAJC27-AS1	-1.7	1.18E-07	2.06E-04	50.25
FLRT2	-1.66	2.36E-03	NA	12.35
EGR1	-1.64	2.12E-04	3.96E-02	29.51
NRSN2-AS1	-1.53	5.11E-03	2.51E-01	32.61
CORO2B	-1.51	1.36E-08	3.56E-05	113.32
UPK3BL1	-1.51	2.02E-03	NA	17.97
RYR1	-1.51	4.34E-03	NA	12.57
SOCS7	-1.5	1.10E-02	NA	10.01
UBALD2	-1.49	5.76E-03	NA	11.57
H6PD	-1.48	9.35E-03	NA	10.45
RIOX1	-1.47	7.03E-03	NA	11.97
RTL10	-1.45	2.68E-03	NA	15.08
CRLF1	-1.43	1.01E-02	3.18E-01	179.84
GIGYF1	-1.42	1.18E-04	2.68E-02	30.58
MVP	-1.41	1.55E-04	3.11E-02	27.55
RASSF3	-1.35	1.25E-06	1.30E-03	115.69
NOL4L	-1.35	5.94E-03	NA	11.92
SUSD1	-1.34	6.59E-03	NA	11.89
SCG3	-1.34	1.08E-02	NA	18.87
AC124283.1	-1.33	3.22E-03	2.22E-01	28.28
MAP3K12	-1.33	1.12E-02	3.26E-01	657.8
SLC22A23	-1.32	4.26E-03	NA	18.53

Supp Table 3 HD-MB03 Adherent > Suspension

Top 25 of 34 genes upregulated in the adherent compartment compared to the suspension compartment. Genes were ordered based on the significant change in expression (Log2FoldChange). Significance was determined using an uncorrected p-value and a Benjamini Hochberg adjusted p-value which is identical with the False Positive Rate (FDR). If a gene has low mean normalized count, then the adjusted p-value was set to NA. The normalized mean of triplicate samples is also show.

Gene	Log2FoldChange	P value	Adjusted p-value	Mean norm counts
LMNB1-DT	-2.62	1.61E-11	3.33E-08	32.59
DNAJC27-AS1	2.13	1.07E-11	2.77E-08	50.25
AL358472.4	2.1	8.70E-06	6.42E-03	11.43
AC006487.1	2.02	5.36E-07	6.15E-04	32.88
GCNT1	1.99	2.81E-07	3.63E-04	48.36
CORO2B	1.96	6.38E-14	3.30E-10	113.32
ANXA8	1.76	4.93E-06	4.12E-03	22.83
PJVK	1.74	5.30E-05	3.42E-02	15.2
CCDC162P	1.73	1.93E-04	9.97E-02	13.37
LSM1	1.64	2.53E-06	2.38E-03	32.62
RASSF3	1.6	3.61E-09	6.22E-06	115.69
AP001781.2	1.56	1.17E-03	4.82E-01	12.15
RN7SK	1.55	7.38E-08	1.09E-04	436.71
MROH8	1.52	2.29E-05	1.58E-02	27.74
PCAT1	1.51	1.56E-12	5.38E-09	685.63
CASC8	1.48	2.81E-15	2.91E-11	625.38
AC016168.2	1.48	1.15E-03	4.82E-01	24.97
SORCS2	1.46	2.34E-06	2.38E-03	180.37
TMEM175	1.29	8.86E-05	5.08E-02	32.47
ZNF302	1.28	1.34E-02	1.00E+00	10.47
ANAPC1	1.27	2.44E-03	8.89E-01	14.85
MCL1	1.18	2.08E-02	1.00E+00	10.95
UFD1	1.17	3.89E-03	1.00E+00	23.41
GALNT7	1.16	8.68E-03	1.00E+00	14.04
DYNC2LI1	1.16	1.29E-02	1.00E+00	11.31

Supp Table 4 HD-MB03 Suspension > Adherent

Top 17 of 17 genes downregulated in the adherent compartment compared to the suspension compartment. Genes were ordered based on the significant change in expression (Log2FoldChange). Significance was determined using an uncorrected p-value and a Benjamini Hochberg adjusted p-value which is identical with the False Positive Rate (FDR). If a gene has low mean normalized count, then the adjusted p-value was set to NA. The normalized mean of triplicate samples is also show.

Gene	Log2FoldChange	P value	Adjusted p-value	Mean norm counts
GABARAPL1	1.41	5.78E-03	1.00E+00	12.72
CBL	1.41	1.01E-02	1.00E+00	10.76
SNORD34	1.34	1.13E-02	1.00E+00	10.33
SRRM5	1.29	1.60E-02	1.00E+00	10.45
DGLUCY	1.28	2.49E-03	8.89E-01	16.65
RTL8C	1.27	6.39E-03	1.00E+00	14.86
NSUN4	1.16	2.45E-02	1.00E+00	10.74
PSTPIP2	1.13	1.40E-02	1.00E+00	13.07
POM121C	1.11	1.08E-02	1.00E+00	13.94
ARL6	1.07	4.33E-02	1.00E+00	12.87
DHCR24	1.04	8.08E-03	1.00E+00	33.68
MAML1	1.04	3.51E-02	1.00E+00	10.44
POLR1E	1.04	3.64E-02	1.00E+00	12.4
BAIAP2-DT	1.03	3.14E-02	1.00E+00	11.57
TCEAL9	1.02	2.27E-02	1.00E+00	17.07
TNNT1	1.02	3.64E-02	1.00E+00	16.2
MEX3C	1.01	4.00E-02	1.00E+00	13.89

Supp Table 5 HD-MB03 Migrated > Suspension

Top 25 of 78 genes upregulated in the migrated compartment compared to the suspension compartment. Genes were ordered based on the significant change in expression (Log2FoldChange). Significance was determined using an uncorrected p-value and a Benjamini Hochberg adjusted p-value which is identical with the False Positive Rate (FDR). If a gene has low mean normalized count, then the adjusted p-value was set to NA. The normalized mean of triplicate samples is also show.

Gene	Log2FoldChange	P value	Adjusted p-value	Mean norm counts
RN7SK	4.48	1.43E-56	3.68E-53	436.71
GCNT1	3.45	2.49E-20	2.13E-17	48.36
SORCS2	2.98	9.17E-23	1.18E-19	180.37
AC100801.1	2.38	1.43E-09	NA	26.8
AP001781.2	2.04	1.57E-05	NA	12.15
ADGRB3	1.82	5.86E-04	NA	10.27
AC016168.2	1.8	6.83E-05	NA	24.97
PCAT1	1.77	1.25E-16	6.43E-14	685.63
CASC8	1.73	3.61E-20	2.32E-17	625.38
C3	1.71	2.10E-04	NA	17.73
SULT1A1	1.61	1.16E-03	NA	10.97
AL358472.4	1.58	1.08E-03	NA	11.43
B3GNT2	1.49	1.37E-03	NA	13.08
MT-TW	1.48	9.85E-03	1.55E-01	536.42
NR2F2-AS1	1.47	2.40E-04	NA	17.71
MT-ND2	1.47	4.22E-03	9.68E-02	6121.81
AFF3	1.46	2.27E-05	5.83E-03	72.53
SPTLC3	1.45	1.13E-03	NA	12.95
RNF181	1.44	1.14E-04	NA	33.83
UFD1	1.42	4.50E-04	NA	23.41
ZFHX4-AS1	1.42	4.51E-03	NA	12.19
BID	1.39	6.99E-06	NA	33.34
C16orf91	1.38	1.60E-03	NA	16.91
UCK1	1.38	7.47E-03	NA	10.54
AC040162.1	1.35	1.10E-04	NA	35.21

Supp Table 6 HD-MB03 Migrated < Suspension

Top 25 of 114 genes downregulated in the migrated compartment compared to the suspension compartment. Genes were ordered based on the significant change in expression (Log2FoldChange). Significance was determined using an uncorrected p-value and a Benjamini Hochberg adjusted p-value which is identical with the False Positive Rate (FDR). If a gene has low mean normalized count, then the adjusted p-value was set to NA. The normalized mean of triplicate samples is also show.

Gene	Log2FoldChange	P value	Adjusted p-value	Mean norm counts
RYR1	-1.92	1.77E-04	NA	12.57
RILPL1	-1.86	7.90E-05	NA	15.6
CRLF1	-1.84	8.99E-04	5.15E-02	179.84
CTBP1-AS	-1.77	3.97E-03	9.53E-02	104.37
SOCS7	-1.74	2.25E-03	NA	10.01
BAIAP2-DT	-1.71	7.22E-04	NA	11.57
THRIL	-1.69	2.68E-03	NA	10.2
PAQR7	-1.65	2.23E-03	NA	10.97
NOL4L	-1.64	5.19E-04	NA	11.92
AL033528.2	-1.63	4.79E-03	NA	10.84
ATN1	-1.59	2.82E-04	NA	16.07
UPK3BL1	-1.48	2.02E-03	NA	17.97
PTPRS	-1.48	2.07E-03	7.14E-02	98.03
AL035587.1	-1.46	1.98E-03	NA	12.26
EGR1	-1.45	9.51E-04	NA	29.51
TGIF2-RAB5IF	-1.42	1.33E-04	NA	25.83
ZC3H6	-1.42	4.59E-04	NA	21.49
CHSY1	-1.41	1.92E-03	NA	16.34
ANKRD13B	-1.41	2.12E-03	NA	26.1
USF3	-1.4	1.46E-03	NA	18.45
AC124283.1	-1.4	1.59E-03	NA	28.28
ZC3H4	-1.4	5.15E-03	1.08E-01	51.05
LBH	-1.39	2.90E-03	NA	14.99
H6PD	-1.39	1.33E-02	NA	10.45
FMNL3	-1.38	9.31E-03	NA	12.29

Supp Table 7 D283 Migrated > Adherent

Top 25 of 80 upregulated genes in the migrated compartment compared to the adherent compartment. Genes were ordered based on the significant change in expression (Log2FoldChange). Significance was determined using an uncorrected p-value and a Benjamini Hochberg adjusted p-value which is identical with the False Positive Rate (FDR). If a gene has low mean normalized count, then the adjusted p-value was set to NA. The normalized mean of duplicate samples is also show.

Gene	Log2FoldChange	P value	Adjusted p-value	Mean norm counts
C1orf21	1.65	9.47E-04	3.07E-01	22.27
CNTRL	1.64	1.90E-03	3.79E-01	13.45
GCNT1	1.53	9.62E-05	8.42E-02	48.36
ARHGAP28	1.51	1.02E-03	3.07E-01	17.68
FIGN	1.5	6.56E-04	2.78E-01	27.37
SORCS2	1.47	3.31E-05	4.73E-02	180.37
ACSL4	1.44	5.20E-03	4.93E-01	13.24
RF01871	1.43	3.24E-03	4.45E-01	395.85
GPCPD1	1.43	1.15E-02	5.78E-01	11.34
EIF2AK3	1.42	1.61E-03	3.68E-01	19.54
LHFPL6	1.42	2.08E-03	3.79E-01	15.28
TPST1	1.42	1.22E-02	5.96E-01	10.23
MAST4	1.37	1.02E-03	3.07E-01	28.32
HUNK	1.34	6.19E-03	5.14E-01	10.52
SLC25A43	1.34	1.84E-02	6.18E-01	10.49
PIGN	1.33	6.65E-04	2.78E-01	28.48
TBC1D32	1.31	7.41E-03	5.29E-01	12.76
DCP1A	1.29	2.46E-03	3.86E-01	20.31
FSTL5	1.29	8.01E-03	5.39E-01	15.01
COL25A1	1.27	6.15E-06	1.41E-02	141.97
KDM5A	1.27	7.85E-04	2.78E-01	43.99
IFT172	1.25	2.37E-02	6.35E-01	11.97
PDE7A	1.24	1.13E-03	3.16E-01	30.44
IFT81	1.22	2.30E-02	6.31E-01	13.51
PRKRIP1	1.21	5.74E-03	5.01E-01	19.93

Supp Table 8 D283 Adherent > Migrated

Top 25 of 98 genes downregulated in the migrated compartment compared to the adherent compartment. Genes were ordered based on the significant change in expression (Log2FoldChange). Significance was determined using an uncorrected p-value and a Benjamini Hochberg adjusted p-value which is identical with the False Positive Rate (FDR). If a gene has low mean normalized count, then the adjusted p-value was set to NA. The normalized mean of duplicate samples is also show.

Gene	Log2FoldChange	P value	Adjusted p-value	Mean norm counts
LMNB1-DT	-2.39	1.74E-07	1.99E-03	32.59
HAS2-AS1	-1.78	7.78E-05	8.42E-02	26.96
HIST1H2BC	-1.72	6.02E-04	2.78E-01	21.58
CORO2B	-1.66	1.55E-06	8.84E-03	113.32
MROH8	-1.63	4.31E-04	2.59E-01	27.74
PCBP2	-1.6	3.63E-06	1.38E-02	874.93
RRP9	-1.59	7.56E-04	5.42E-01	23.01
MTRNR2L3	-1.59	8.69E-03	2.78E-01	31.24
AC005912.1	-1.57	3.25E-05	4.73E-02	143.73
HES1	-1.56	6.16E-03	5.14E-01	10.16
IGHMBP2	-1.55	4.31E-03	4.84E-01	12.43
MAP3K12	-1.51	1.09E-02	5.57E-01	657.8
AL139352.1	-1.5	3.27E-03	4.45E-01	14.52
AC002075.2	-1.47	1.35E-02	6.04E-01	10.33
AL031727.1	-1.43	8.23E-03	5.39E-01	12.06
HIST1H4C	-1.37	2.56E-03	3.86E-01	7339.48
SCARNA12	-1.37	7.45E-03	5.42E-01	47.61
HIST1H3J	-1.37	8.81E-03	5.29E-01	212.8
SNORD38B	-1.34	6.77E-04	2.78E-01	46.78
CDK2	-1.33	1.30E-02	5.96E-01	13.6
MOK	-1.31	7.14E-03	5.25E-01	17.79
HIST1H1D	-1.3	2.25E-02	6.31E-01	15.49
AL137779.2	-1.29	1.02E-04	8.42E-02	47.24
PDE6H	-1.28	2.07E-03	3.79E-01	19.8
NRSN2-AS1	-1.28	3.14E-02	6.63E-01	32.61

Supp Table 9 D283-MED Adherent > Suspension

Top 25 of 25 genes upregulated in adherent compartment compared to the suspension compartment. Genes were ordered based on the significant change in expression (Log2FoldChange). Significance was determined using an uncorrected p-value and a Benjamini Hochberg adjusted p-value which is identical with the False Positive Rate (FDR). If a gene has low mean normalized count, then the adjusted p-value was set to NA. The normalized mean of duplicate samples is also show.

Gene	Log2FoldChange	P value	Adjusted p-value	Mean norm counts
LMNB1-DT	-2.45	2.58E-08	2.95E-04	32.59
MROH8	-1.59	3.14E-04	6.00E-01	27.74
HAS2-AS1	-1.57	3.89E-04	6.36E-01	26.96
AL161716.1	-1.54	1.00E-02	1.00E+00	10.7
SORCS2	-1.46	6.53E-05	2.49E-01	180.37
HIST1H2BC	-1.36	4.02E-03	1.00E+00	21.58
WIPF3	-1.33	1.82E-02	1.00E+00	12.06
BNC2	-1.32	1.38E-02	1.00E+00	10.21
LINC01456	-1.26	5.05E-03	1.00E+00	18.06
ABRAXAS1	-1.24	3.03E-03	1.00E+00	28.9
CNIH3	-1.24	2.26E-02	1.00E+00	10.04
CORO2B	-1.19	2.50E-04	5.91E-01	113.32
RASSF3	-1.18	2.58E-04	5.91E-01	115.69
CCDC58	-1.17	1.12E-02	1.00E+00	32.74
GCNT1	-1.16	6.06E-03	1.00E+00	48.36
WDR92	-1.11	2.28E-02	1.00E+00	13.27
CENPP	-1.1	2.23E-03	1.00E+00	50.22
LAMA1	-1.1	1.80E-02	1.00E+00	24.79
DNAJC27-AS1	-1.09	6.65E-03	1.00E+00	50.25
TBRG4	-1.09	1.64E-02	1.00E+00	22.96
ZHX2	-1.06	3.16E-02	1.00E+00	11.36
BBOX1-AS1	-1.05	8.35E-03	1.00E+00	40.67
FCHO2	-1.03	2.21E-02	1.00E+00	18.24
BMPR1B	-1.01	1.75E-02	1.00E+00	34.43
AL359710.1	-1	3.43E-02	1.00E+00	17.72

Supp Table 10 D283 Suspension > Adherent

6 genes downregulated in the adherent compartment compared to the suspension compartment. Genes were ordered based on the significant change in expression (Log2FoldChange). Significance was determined using an uncorrected p-value and a Benjamini Hochberg adjusted p-value which is identical with the False Positive Rate (FDR). If a gene has low mean normalized count, then the adjusted p-value was set to NA. The normalized mean of duplicate samples is also show.

Gene	Log2FoldChange	P value	Adjusted p-value	Mean norm counts
BAIAP2-DT	-1.24	1.72E-02	1.00E+00	11.57
FAM200B	-1.2	2.27E-03	1.00E+00	26.17
MEF2D	-1.19	1.48E-02	1.00E+00	12.33
LYSMD3	-1.12	4.00E-02	1.00E+00	10.16
RTL8C	-1.09	2.57E-02	1.00E+00	14.86

Supp Table 11 D283-MED Migrated > Suspension

Top 25 of 253 genes upregulated in the migrated compared to the suspension compartment. Genes were ordered based on the significant change in expression (Log2FoldChange). Significance was determined using an uncorrected p-value and a Benjamini Hochberg adjusted p-value which is identical with the False Positive Rate (FDR). If a gene has low mean normalized count, then the adjusted p-value was set to NA. The normalized mean of duplicate samples is also show.

Gene	Log2FoldChange	P value	Adjusted p-value	Mean norm counts
SORCS2	2.93	4.45E-16	2.33E-12	180.37
GCNT1	2.69	2.71E-11	4.73E-08	48.36
ADAMTSL1	2.17	4.68E-10	6.12E-07	39.75
RF01871	2.04	2.78E-05	5.83E-03	395.85
LINC01435	1.92	1.38E-06	7.20E-04	28.44
COL25A1	1.87	2.60E-11	4.73E-08	141.97
AP003049.2	1.8	2.28E-05	5.41E-03	26.65
BNC2	1.79	7.25E-04	NA	10.21
MAST4	1.71	3.36E-05	6.20E-03	28.32
NEAT1	1.67	3.25E-08	3.40E-05	99.7
PDE7A	1.61	1.89E-05	5.15E-03	30.44
AC011586.2	1.61	2.34E-04	NA	13.36
DMGDH	1.59	7.03E-04	NA	18.41
AC026347.1	1.59	1.25E-03	NA	15.83
FAM149A	1.56	7.07E-04	NA	14.56
EGFEM1P	1.55	1.31E-06	7.20E-04	55.5
ARHGAP24	1.53	5.42E-05	8.40E-03	47.49
PARD3B	1.52	8.35E-05	1.18E-02	47.61
CACNB4	1.52	5.15E-03	NA	12.85
MSANTD2	1.5	2.12E-03	NA	11.54
TNS3	1.5	4.40E-03	NA	14.11
MAP3K5	1.49	3.38E-03	NA	10.58
ZFPM2-AS1	1.46	3.70E-04	2.49E-02	35.26
PTPRJ	1.45	1.44E-05	4.70E-03	59.57
RBM5	1.45	5.97E-04	3.46E-02	22.24

Supp Table 12 D283 Suspension > Migrated

Top 25 of 140 genes downregulated in the migrated compartment compared to suspension compartment. Genes were ordered based on the significant change in expression (Log2FoldChange). Significance was determined using an uncorrected p-value and a Benjamini Hochberg adjusted p-value which is identical with the False Positive Rate (FDR). If a gene has low mean normalized count, then the adjusted p-value was set to NA. The normalized mean of duplicate samples is also show.

Gene	Log2FoldChange	P value	Adjusted p-value	Mean norm counts
AC005912.1	-2.02	6.51E-08	5.68E-05	143.73
AC002075.2	-1.84	1.72E-03	NA	10.33
SCARNA12	-1.75	4.89E-04	3.08E-02	47.61
AL139352.1	-1.65	8.93E-04	NA	14.52
RPS27	-1.63	6.49E-07	4.24E-04	1003.9
FKBP7	-1.62	3.85E-03	NA	11.46
HIST1H1D	-1.6	3.94E-03	NA	15.49
AC099560.2	-1.59	2.73E-05	5.83E-03	48.45
TEX30	-1.56	1.01E-03	NA	17.1
HIST1H3J	-1.52	3.70E-03	8.23E-02	212.8
RCOR2	-1.46	7.12E-04	3.81E-02	23.35
PLP2	-1.44	1.33E-03	5.35E-02	19.79
A2MP1	-1.42	5.06E-04	3.13E-02	23.39
TMUB1	-1.42	6.37E-03	NA	13.47
ID1	-1.41	3.44E-05	6.20E-03	59.66
TFAP2C	-1.41	4.79E-03	9.04E-02	19.04
NANOS1	-1.39	9.00E-06	3.14E-03	134.35
AC108110.1	-1.38	1.42E-04	1.55E-02	67.87
BAIAP2-DT	-1.38	8.54E-03	NA	11.57
AC010422.5	-1.33	3.14E-04	2.38E-02	33.75
HCCS	-1.33	7.04E-03	NA	14.97
AL031727.1	-1.33	1.22E-02	NA	12.06
AL137779.2	-1.32	5.46E-05	8.40E-03	47.24
AC099789.1	-1.32	1.97E-03	6.32E-02	36.47
EPHA8	-1.32	6.22E-03	NA	18.15

Supp Table 13 D458 Migrated > Adherent

Top 25 of 38 genes upregulated in the migrated compartment compared to the adherent compartment. Genes were ordered based on the significant change in expression (Log2FoldChange). Significance was determined using an uncorrected p-value and a Benjamini Hochberg adjusted p-value which is identical with the False Positive Rate (FDR). If a gene has low mean normalized count, then the adjusted p-value was set to NA. The mean normalized counts column shows the expression for only one replicate.

Gene	Log2FoldChange	P value	Adjusted p-value	Mean norm counts
Z93403.1	-2.35	2.51E-04	NA	12.43
COL11A1	-2.3	6.95E-05	9.85E-03	23.4
AHI1	-2.17	2.14E-04	2.59E-02	41.67
P3H2	-2.1	1.22E-03	NA	10.44
ANK3	-2.05	1.49E-03	9.98E-02	20.3
TTN-AS1	-1.9	3.05E-03	NA	11.19
PBX3	-1.89	4.61E-04	4.74E-02	56.82
ADAMTSL1	-1.89	8.30E-04	7.36E-02	39.75
CADM2	-1.87	2.81E-03	1.53E-01	19.49
BAZ2A	-1.87	3.13E-03	1.64E-01	17.78
GCNT1	-1.85	1.47E-03	9.98E-02	48.36
CTSV	-1.85	4.39E-03	2.03E-01	22.17
SUCLG1	-1.84	1.61E-04	2.04E-02	182.93
SPRED2	-1.84	3.22E-03	1.68E-01	23.73
TOPBP1	-1.83	2.24E-03	1.35E-01	28.64
VDAC1	-1.82	2.53E-04	2.92E-02	85.21
TBC1D32	-1.82	4.28E-03	NA	12.76
PARPBP	-1.8	3.26E-03	1.68E-01	32.52
NUP107	-1.77	4.06E-03	1.97E-01	27.42
SORCS2	-1.75	5.08E-04	4.89E-02	180.37
CNST	-1.75	4.56E-03	2.07E-01	29.38
ATP6V1A	-1.75	4.15E-03	1.97E-01	23.62
ESD	-1.74	9.99E-04	8.22E-02	76.71
AFF1	-1.74	2.49E-03	1.43E-01	40.87
EGFEM1P	-1.71	1.26E-03	9.35E-02	55.5

Supp Table 14 D458 Adherent > Migrated

Top 25 of 58 genes downregulated in the migrated compartment compared to the adherent compartment. Genes were ordered based on the significant change in expression (Log2FoldChange). Significance was determined using an uncorrected p-value and a Benjamini Hochberg adjusted p-value which is identical with the False Positive Rate (FDR). If a gene has low mean normalized count, then the adjusted p-value was set to NA. The mean normalized counts column shows the expression for only one replicate.

Gene	Log2FoldChange	P value	Adjusted p-value	Mean norm counts
MYH6	-4.13	7.71E-10	NA	10.13
GJD2	-2.78	2.44E-08	2.77E-05	30.97
CYBC1	-2.54	3.83E-05	5.88E-03	18.89
EAF1-AS1	-2.52	1.32E-05	2.49E-03	23.96
COCH	-2.47	7.52E-07	3.71E-04	72.51
AL137779.2	-2.45	8.21E-07	3.71E-04	47.24
AC091133.2	-2.42	5.55E-05	NA	14.23
USP2	-2.4	1.65E-06	6.70E-04	64.2
PNPLA8	-2.39	3.38E-08	1.89E-04	55.22
CORO2B	-2.39	2.33E-07	3.19E-05	113.32
TOB1	-2.31	2.49E-11	1.41E-07	322.32
COLGALT1	-2.28	4.70E-07	3.33E-04	43.28
AC005921.2	-2.27	1.16E-05	2.30E-03	38.98
LMNB1-DT	-2.26	1.32E-04	1.74E-02	32.59
CHP1	-2.23	3.69E-09	1.05E-05	161.19
AC124283.1	-2.21	5.54E-04	5.15E-02	28.28
NUDT19	-2.2	2.13E-08	2.77E-05	140.89
BRD3OS	-2.18	1.75E-08	2.77E-05	99.87
PROCR	-2.18	1.07E-05	2.26E-03	48
B4GALT2	-2.17	5.56E-04	NA	14.48
DTWD1	-2.13	2.58E-04	2.92E-02	24.26
RAP2B	-2.08	2.03E-06	7.19E-04	96.23
HIST1H2BC	-2.08	4.94E-04	4.89E-02	21.58
CNOT9	-2.04	2.92E-06	7.89E-04	178.68
CLPTM1L	-2.03	1.58E-05	2.87E-03	68.26

Supp Table 15 D458 Migrated > Suspension

Top 25 of 260 upregulated genes in the migrated compartment compared to the suspension compartment. Genes were ordered based on the significant change in expression (Log2FoldChange). Significance was determined using an uncorrected p-value and a Benjamini Hochberg adjusted p-value which is identical with the False Positive Rate (FDR). If a gene has low mean normalized count, then the adjusted p-value was set to NA. The mean normalized counts column shows the expression for only one replicate.

Gene	Log2FoldChange	P value	Adjusted p-value	Mean norm counts
ST6GALNAC5	-3.01	5.92E-07	NA	12.47
SORCS2	-2.55	5.25E-08	1.26E-04	180.37
CDK14	-2.4	1.02E-04	NA	16.63
EGFEM1P	-2.3	3.20E-07	4.54E-04	55.5
NLGN1	-2.29	3.29E-06	1.57E-03	27.81
ADAMTSL1	-2.28	1.79E-06	1.07E-03	39.75
P3H2	-2.26	2.26E-04	NA	10.44
RBP7	-2.16	6.87E-06	2.99E-03	38.31
KCTD8	-2.09	5.76E-07	5.51E-04	74.75
ERC2	-2.05	1.74E-04	NA	19.75
GCNT1	-2.03	5.40E-05	1.85E-02	48.36
AP003049.2	-2.01	1.56E-04	2.87E-02	26.65
TBC1D32	-1.9	2.03E-03	NA	12.76
CCDC26	-1.89	3.80E-07	4.54E-04	110.05
EPS8	-1.89	9.54E-05	2.40E-02	43.67
GAB1	-1.89	1.44E-03	9.80E-02	23.11
Z93403.1	-1.89	1.09E-03	NA	12.43
FREM2	-1.85	1.25E-04	2.59E-02	41.76
AC073050.1	-1.83	4.47E-04	5.90E-02	23.07
ADGRB3	-1.83	4.24E-03	NA	10.27
PDE4B	-1.8	1.49E-04	2.87E-02	51.66
ST6GALNAC3	-1.79	9.43E-06	3.76E-03	161.31
COL4A3	-1.78	7.98E-05	2.33E-02	76.82
GULP1	-1.76	1.59E-03	1.02E-01	27.12
MUSK	-1.76	3.25E-03	NA	12.41

Supp Table 16 D458-MED Suspension > Migrated

Top 25 of 161 genes downregulated in the migrated compartment compared to the suspension compartment. Genes were ordered based on the significant change in expression (Log2FoldChange). Significance was determined using an uncorrected p-value and a Benjamini Hochberg adjusted p-value which is identical with the False Positive Rate (FDR). If a gene has low mean normalized count, then the adjusted p-value was set to NA. The mean normalized counts column shows the expression for only one replicate.

Gene	Log2FoldChange	P value	Adjusted p-value	Mean norm counts
GJD2	2.94	1.92E-10	9.21E-07	30.97
AC124283.1	2.94	8.77E-07	6.99E-04	28.28
MYH6	2.59	8.81E-05	NA	10.13
USP2	2.23	3.15E-06	1.57E-03	64.2
MEIOC	2.11	9.24E-05	2.40E-02	24.98
AC114947.2	2.09	1.41E-03	9.80E-02	69.33
EAF1-AS1	2.03	1.01E-04	2.41E-02	23.96
CRX	1.91	6.43E-05	2.05E-02	24.73
SCARNA12	1.9	7.26E-04	7.39E-02	47.61
MYOG	1.86	2.90E-04	NA	18.4
AC005921.2	1.85	1.12E-04	2.56E-02	38.98
LBH	1.83	2.31E-03	NA	14.99
EIF4E	1.72	8.26E-05	2.33E-02	89.12
AC108025.2	1.68	6.24E-04	6.94E-02	30.18
SFR1	1.68	3.98E-03	NA	12.3
AL137779.2	1.62	2.86E-04	4.56E-02	47.24
AC099850.1	1.61	1.67E-03	1.02E-01	119.67
SOX11	1.59	1.03E-03	9.51E-02	199.49
ANKRD40	1.59	2.79E-04	4.56E-02	58.32
PRXL2C	1.59	1.13E-03	9.51E-02	31.86
A2MP1	1.56	2.69E-03	1.40E-01	23.39
AP003096.1	1.54	1.67E-03	1.02E-01	42.91
CYP51A1	1.53	9.66E-04	9.44E-02	295.08
KCNK12	1.53	2.94E-03	1.46E-01	30.36
MRLN	1.53	2.19E-03	1.22E-01	26.41

Supp Table 17 D458-MED Adherent > Suspension

Top 25 of 155 upregulated genes in the adherent compartment compared to the suspensions compartment. Genes were ordered based on the significant change in expression (Log2FoldChange). Significance was determined using an uncorrected p-value and a Benjamini Hochberg adjusted p-value which is identical with the False Positive Rate (FDR). If a gene has low mean normalized count, then the adjusted p-value was set to NA. The mean normalized counts column shows the expression for only one replicate.

Gene	Log2FoldChange	P value	Adjusted p-value	Mean norm counts
GAB1	2.37	2.84E-04	NA	23.11
AC245060.5	2.28	9.28E-04	NA	10.63
LINC02340	2.03	3.35E-03	NA	11.07
CEP95	1.98	4.44E-05	4.79E-02	60.78
PROCR	1.97	7.87E-05	5.16E-02	48
CHMP1A	1.94	3.11E-03	NA	13.43
CYBC1	1.9	2.14E-03	NA	18.89
SLC38A6	1.87	4.26E-03	NA	12.13
CDK5RAP1	1.86	2.27E-03	NA	17.46
MFSD11	1.86	2.35E-03	NA	21.49
TMEM98	1.86	5.40E-03	NA	15.32
C16orf91	1.84	3.68E-03	NA	16.91
DNAJC6	1.8	8.13E-03	NA	11.76
LRIG2	1.79	6.81E-03	NA	12.4
HIST1H2BC	1.78	3.14E-03	NA	21.58
TTC8	1.78	6.35E-03	NA	13.43
DTWD1	1.72	3.37E-03	NA	24.26
PELI1	1.67	5.35E-03	NA	23.16
FBXO3	1.66	1.45E-02	NA	10.45
FLRT2	1.64	1.37E-02	NA	12.35
LIMD1	1.64	1.62E-02	NA	11.05
CWF19L2	1.63	8.59E-04	2.14E-01	55.18
RAB33B	1.63	1.70E-02	NA	10.59
DUBR	1.62	1.70E-02	NA	19.07
ITFG2	1.6	9.96E-03	NA	15.28

Supp Table 18 D458-MED Suspension > Adherent

Top 25 of 193 genes downregulated in the adherent compartment compared to the suspension compartment. Genes were ordered based on the significant change in expression (Log2FoldChange). Significance was determined using an uncorrected p-value and a Benjamini Hochberg adjusted p-value which is identical with the False Positive Rate (FDR). If a gene has low mean normalized count, then the adjusted p-value was set to NA. The mean normalized counts column shows the expression for only one replicate.

Gene	Log2FoldChange	P value	Adjusted p-value	Mean norm counts
OOEP	-2.14	6.65E-04	1.79E-01	49.57
NMNAT2	-2.09	2.49E-03	NA	18.19
C1orf43	-2.02	2.75E-04	9.55E-02	64.53
SUCLG1	-1.9	9.86E-05	5.16E-02	182.93
MYOG	-1.9	2.03E-03	NA	18.4
PPP2R1A	-1.85	1.30E-03	2.69E-01	64.78
ERGIC2	-1.85	2.35E-03	NA	25.77
C12orf73	-1.84	3.02E-03	NA	21.06
LSM8	-1.84	4.35E-03	NA	13.65
TYMS	-1.82	2.80E-03	NA	32.68
C1orf174	-1.78	5.99E-03	NA	17.82
RPL23AP74	-1.77	1.33E-03	2.69E-01	98.66
SH3GL1	-1.76	5.42E-03	NA	18.54
MRPS36	-1.75	2.94E-03	3.86E-01	36.57
KLC2	-1.75	6.55E-03	NA	10.24
RPL39	-1.74	1.45E-05	2.35E-02	617.21
ATP5F1D	-1.73	1.14E-03	2.64E-01	58.23
ACVR2B	-1.7	6.34E-03	NA	24.19
SLC6A6	-1.68	1.00E-02	NA	12.87
VPS4A	-1.64	8.30E-03	NA	24.45
A2MP1	-1.61	9.64E-03	NA	23.39
TPGS1	-1.61	1.22E-02	NA	25.79
BFAR	-1.6	1.04E-02	NA	20.89
COPB2	-1.6	1.17E-02	NA	20.06
PANK2	-1.6	1.25E-02	NA	14.92

Part 2. Expanding on Section 4.3.5 Differentially expressed genes between cell compartments

The GO terms that best describe the functions of genes showing differential expression between two cell compartments are detailed in Supp.Tables 19-22.

Supp Table 19 GSEA Adherent > Suspension across 3 cell lines.

Gene set enrichment analysis (GSEA) was used to identify the top 20 Gene Ontology (GO) gene sets that significantly overlapped with the genes upregulated in the adherent compartment compared to the suspension compartment (A>S). Significance was defined based on a p-value and a p-value adjusted using the Benjamini-Hochberg false Discovery Rate (FDR) method (FDR q-value).

Gene set	Overlap	P-value	FDR q-value
GO Transferase Activity Transferring Phosphorus Containing Groups GO:0016772	17	1.39 e-6	1.27 e-2
GO Leucine Binding GO:0070728	3	3.42 e-6	1.57 e-2
GO UDP Glycosylatransferase Activity GO:0008194	7	7.03 e-6	1.97 e-2
GO Cellular Macromolecule Localization GO:0070727	24	8.56 e-6	1.97 e-2
GO Cellular Response to Leucine GO:0071233	3	1.16 e-5	2.13 e-2
GO Macromolecule Catabolic Process GO:0009057	19	2.45 e-5	3.05 e-2
GO Regulation of Cellular Components Biogenesis GO:0044087	15	2.8 e-5	3.05 e-2
GO Cellular Macromolecule Catabolic Process GO:0044265	17	2.85 e-5	3.05 e-2
GO Glycoprotein Biosynthetic process GO:0009101	9	3.43 e-5	3.05 e-2
GO Response to Leucine GO:0043201	3	3.47 e-5	3.05 e-2
GO Organelle Assembly GO:0070925	14	3.66 e-5	3.05 e-2
GO Modification Dependent Macromolecule Catabolic process GO:0043632	12	4.07 e-5	3.12 e-2
GO Negative Regulation of Intracellular Signal transduction GO:1902532	11	4.82 e-5	3.25 e-2
GO Regulation of Intracellular Signal Transduction GO:1902531	22	5.13 e-5	3.25 e-2
GO Negative Regulation of TORC1 Signaling GO:1904262	3	5.3 e-5	3.25 e-2

Supp Table 20 GSEA Adherent > Migrated across 3 cell lines.

Gene set enrichment analysis (GSEA) was used to identify the top 20 Gene Ontology (GO) gene sets that significantly overlapped with the genes upregulated in the adherent compartment compared to the migrated compartment (A>M). Significance was defined based on a p-value and a p-value adjusted using the Benjamini-Hochberg false Discovery Rate (FDR) method (FDR q-value).

Gene set	Overlap	P-value	FDR q-value
GO Macromolecule Catabolic Process GO:0009057	41	3.3 e-10	3.04 e-6
GO Intracellular Transport GO:0046907	47	1.81 e-9	6.13 e-6
GO Peptidyl Amino Acid Modification GO:0018193	37	2.07 e-9	6.13 e-6
GO Protein Containing Complex Assembly GO:0065003	48	2.67 e-9	6.13 e-6
GO Intracellular Protein Transport GO:0006886	35	5.73 e-9	1.05 e-5
GO Cellular Protein Containing Complex Assembly GO:0034622	34	9.43 e-9	1.44 e-5
GO Macromolecule Catabolic Process GO:0044265	34	1.39 e-8	1.72 e-5
GO Organonitrogen compound catabolic process GO:1901565	36	1.49 e-8	1.72 e-5
GO Chromatin Organization GO:0006325	27	2.77 e-8	2.83 e-5
GO Protein Catabolic process GO:0030163	29	3.68 e-8	3.38 e-5
GO Chromosome Organization GO:0051276	33	1.46 e-7	1.22 e-4
GO Cell Cycle GO:0007049	43	1.61 e-7	1.24 e-4
GO Regulation of Cell Differentiation GO:0045595	43	2.04 e-7	1.44 e-4
GO Mitotic Cell Cycle GO:0000278	29	3.12 e-7	2.05 e-4
GO Organonitrogen Compound Biosynthetic Process GO:1901566	42	3.78 e-7	2.31 e-4
GO RNA Binding GO:0003723	43	4.7 e-7	2.7 e-4
GO Cellular Protein Catabolic Process GO:0044257	24	6.56 e-7	3.54 e-4
GO Cellular Macromolecule Localization GO:0070727	42	8.46 e-7	4.32 e-4
GO Modification Dependent Macromolecule Catabolic Process GO:0043632	21	1.29 e-6	6.22 e-4
GO regulation of Cell Cycle GO:0051726	31	1.44 e-6	6.59 e-4

Supp Table 21 GSEA Suspension > Adherent across 3 cell lines.

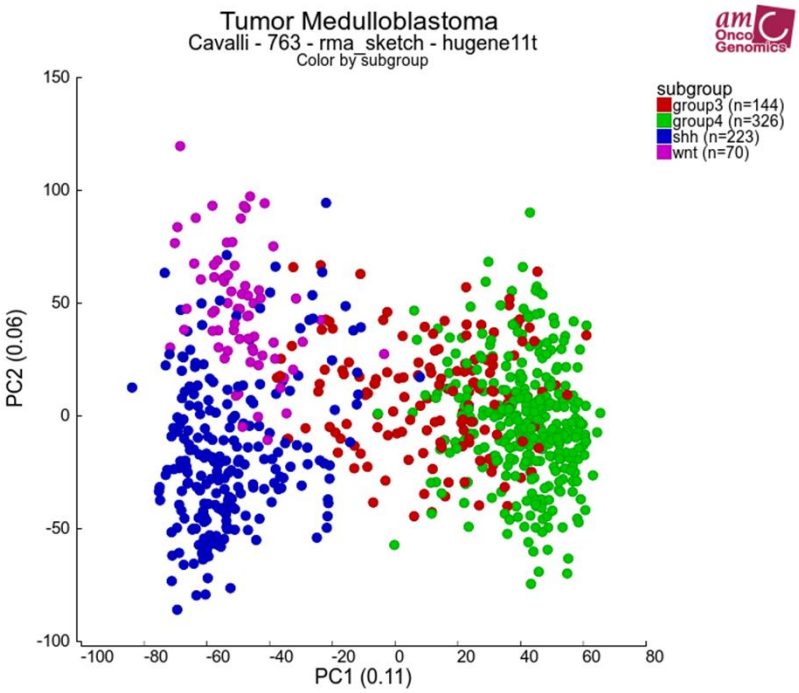
Gene set enrichment analysis (GSEA) was used to identify the top 20 Gene Ontology (GO) gene sets that significantly overlapped with the genes upregulated in the suspension compartment compared to the adherent compartment (S>A). Significance was defined based on a p-value and a p-value adjusted using the Benjamini-Hochberg false Discovery Rate (FDR) method (FDR q-value).

Gene set	Overlap	P-value	FDR q-value
GO RNA Binding	36	1.99 e-13	1.83 e-9
GO Cellular Amide Metabolic Process	23	3.07 e-10	1.41 e-6
GO Organonitrogen Compound Biosynthetic Process	30	7.51 e-10	2.3 e-6
GO Cellular Macromolecule Catabolic Process	23	2.07 e-9	4.75 e-6
GO Intracellular Transport	29	2.72 e-9	4.99 e-6
GO Generation of Precursor Metabolites and Energy	15	9.26 e-9	1.42 e-5
GO Amide Biosynthetic Process	19	1.26 e-8	1.48 e-5
GO Macromolecule Catabolic Process	24	1.29 e-8	1.48 e-5
GO Oxidative Phosphorylation	9	1.52 e-8	1.55 e-5
GO Peptide Biosynthetic Process	17	4.1 e-8	3.77 e-5
GO Nuclear Transcribed mRNA Catabolic Process Nonsense Mediated Decay	8	7.38 e-8	6.17 e-5
GO Structural Constituent of Ribosome	9	1.68 e-7	1.29 e-4
GO Viral Gene Expression	9	2.2 e-7	1.56 e-4
GO Intracellular Protein Transport	20	2.98 e-7	1.93 e-4
GO mRNA Metabolic Process	14	3.15 e-7	1.93 e-4
GO Cellular Macromolecule Localization	26	3.6 e-7	2.07 e-4
GO Interspecies Interaction Between Organisms	17	1.01 e-6	5.48 e-4
GO RNA Splicing	12	1.38 e-6	7.05 e-4
GO Oxidation Reduction Process	17	1.87 e-6	8.74 e-4
GO RNA Catabolic Process	11	1.9 e-6	8.74 e-4

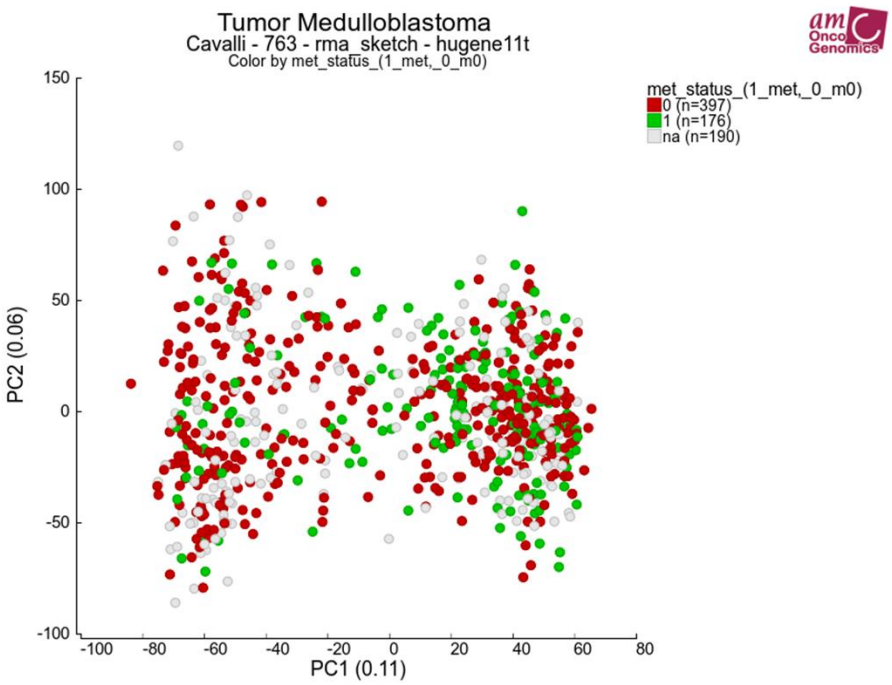
Supp Table 22 GSEA Suspension > Migrated across 3 cell lines.

Gene set enrichment analysis (GSEA) was used to identify the top 20 Gene Ontology (GO) gene sets that significantly overlapped with the genes upregulated in the suspension compartment compared to the migrated compartment (S>M). Significance was defined based on a p-value and a p-value adjusted using the Benjamini-Hochberg false Discovery Rate (FDR) method (FDR q-value).

Gene set	Overlap	P-value	FDR q-value
GO Regulation of Cell Cycle GO:0051726	26	1.39 e-6	7.59 e-3
GO Negative Regulation of RNA Biosynthetic Process GO:1902679	26	2.3 e-6	7.59 e-3
GO Organonitrogen Compound Biosynthetic process GO:1901566	33	2.58 e-6	7.59 e-3
GO Cellular Response to Organic Cyclic Compound GO:0071407	16	3.3 e-6	7.59 e-3
GO Negative Regulation of Biosynthetic Process GO:0009890	30	4.71 e-6	8.67 e-3
GO Regulatory Region Nucleic Acid Binding GO:0001067	21	8.13 e-6	1.03 e-2
GO Rhythmic Process GO:0048511	11	8.37 e-6	1.03 e-2
GO Neurogenesis GO:0022008	29	8.94 e-6	1.03 e-2
GO Positive Regulation of Cell Cycle GO:0045787	13	1.12 e-5	1.11 e-2
GO Muscle Organ Development GO:0007517	13	1.34 e-5	1.11 e-2
GO Protein Modification by Small Protein Conjugation GO:0032446	20	1.36 e-5	1.11 e-2
GO Cellular Response to Endogenous Stimulus GO:0071495	26	1.46 e-5	1.11 e-2
GO Negative Regulation of Signaling GO:0023057	26	1.66 e-5	1.11 e-2
GO Circadian Rhythm GO:0007623	9	1.68 e-5	1.11 e-2
GO Regulation of Cell Differentiation GO:0045595	31	2.31 e-5	1.36 e-2
GO Regulation of Protein Autophosphorylation GO:0031952	5	2.52 e-5	1.36 e-2
GO Protein Modification by Small Protein Conjugation or Removal GO:0070647	22	2.63 e-5	1.36 e-2
GO Neuron Differentiation GO:0030182	25	2.66 e-5	1.36 e-2
GO E Box Binding GO:0070888	5	3.42 e-5	1.58 e-2
GO Double Stranded DNA Binding GO:0003690	20	3.44 e-5	1.58 e-2



Supp. Figure 1 PCA of patients in the dataset by Cavalli *et al* showing the 4 molecular subgroups (Group 3, group 4, SHH, WNT). The plot was generated using the PCA Meta analysis option on the R2: Genomics Analysis and Visualization Platform.



Supp. Figure 2 PCA of patients in the dataset by Cavalli *et al* showing the metastatic status (M0 or M+). The plot was generated using the PCA Meta analysis option on the R2: Genomics Analysis and Visualization Platform

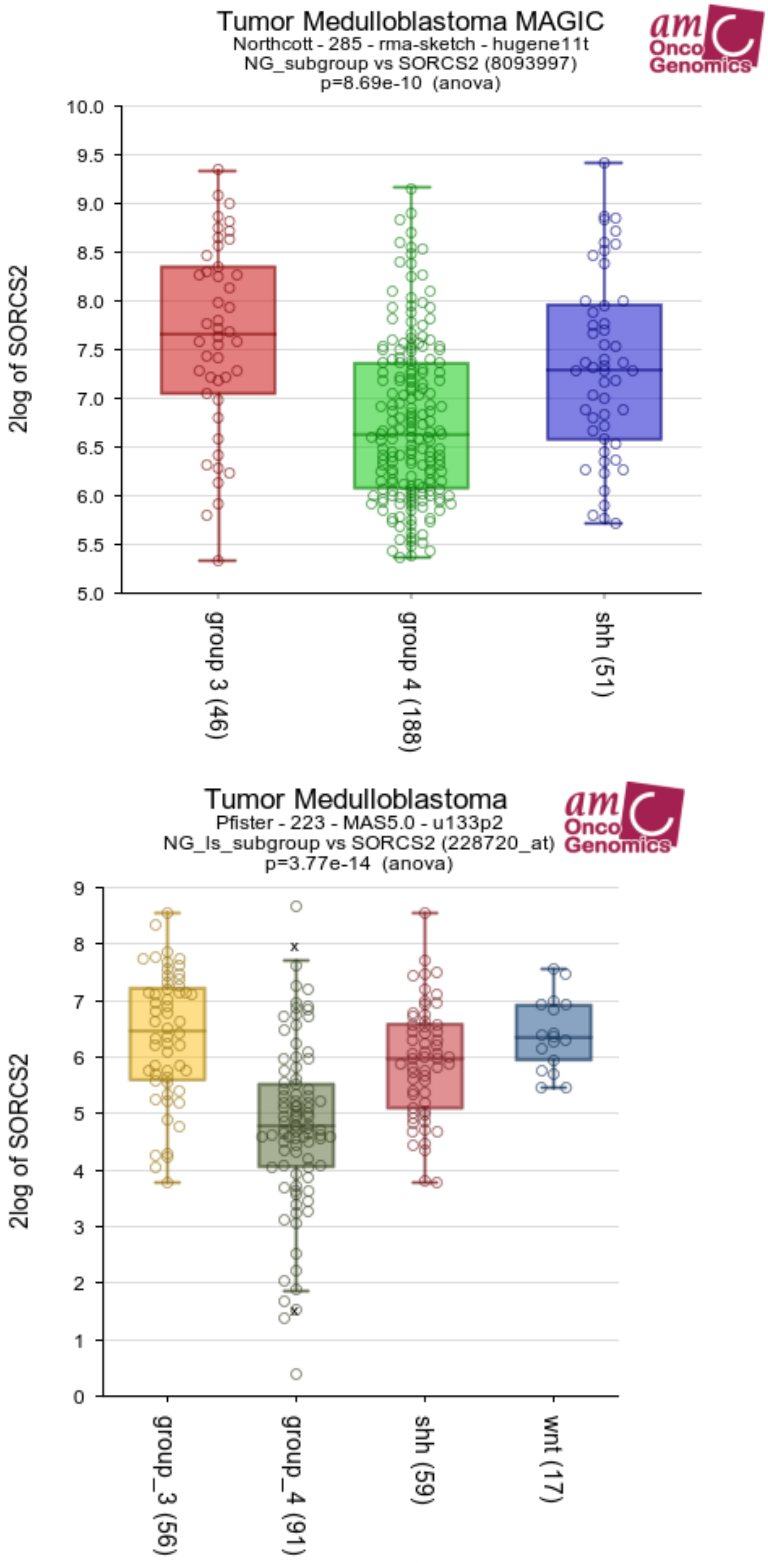
Appendix 3: Chapter 5 & Discussion

A)	G3	G4	SHH	WNT
G3	/	****	****	****
G4		/	****	****
SHH			/	****
WNT				/

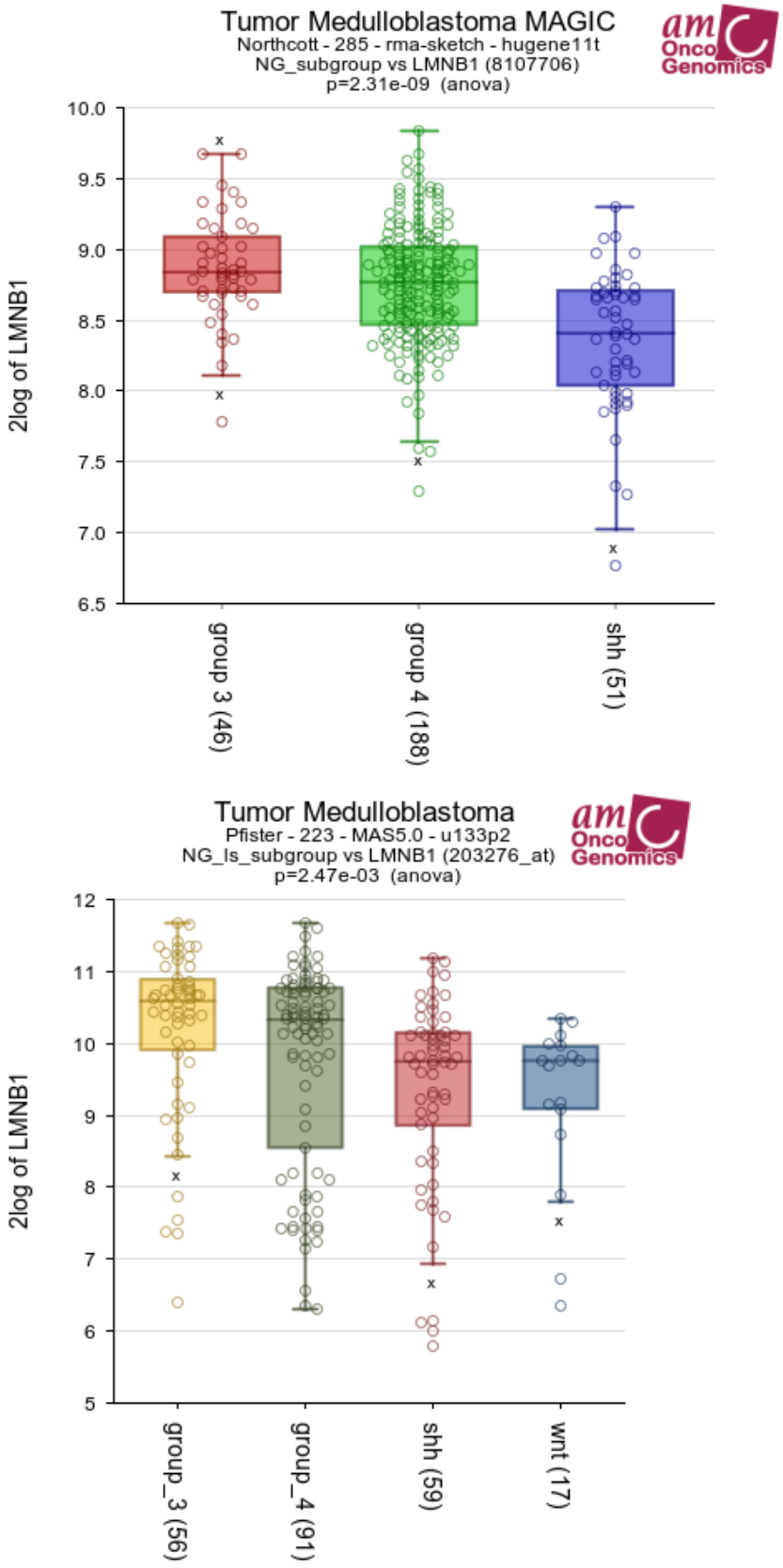
B)	G3	G4	SHH	WNT
G3	/	***	****	****
G4		/	****	****
SHH			/	ns
WNT				/

C)	G3	G4	SHH	WNT
G3	/	ns	ns	****
G4		/	ns	****
SHH			/	****
WNT				/

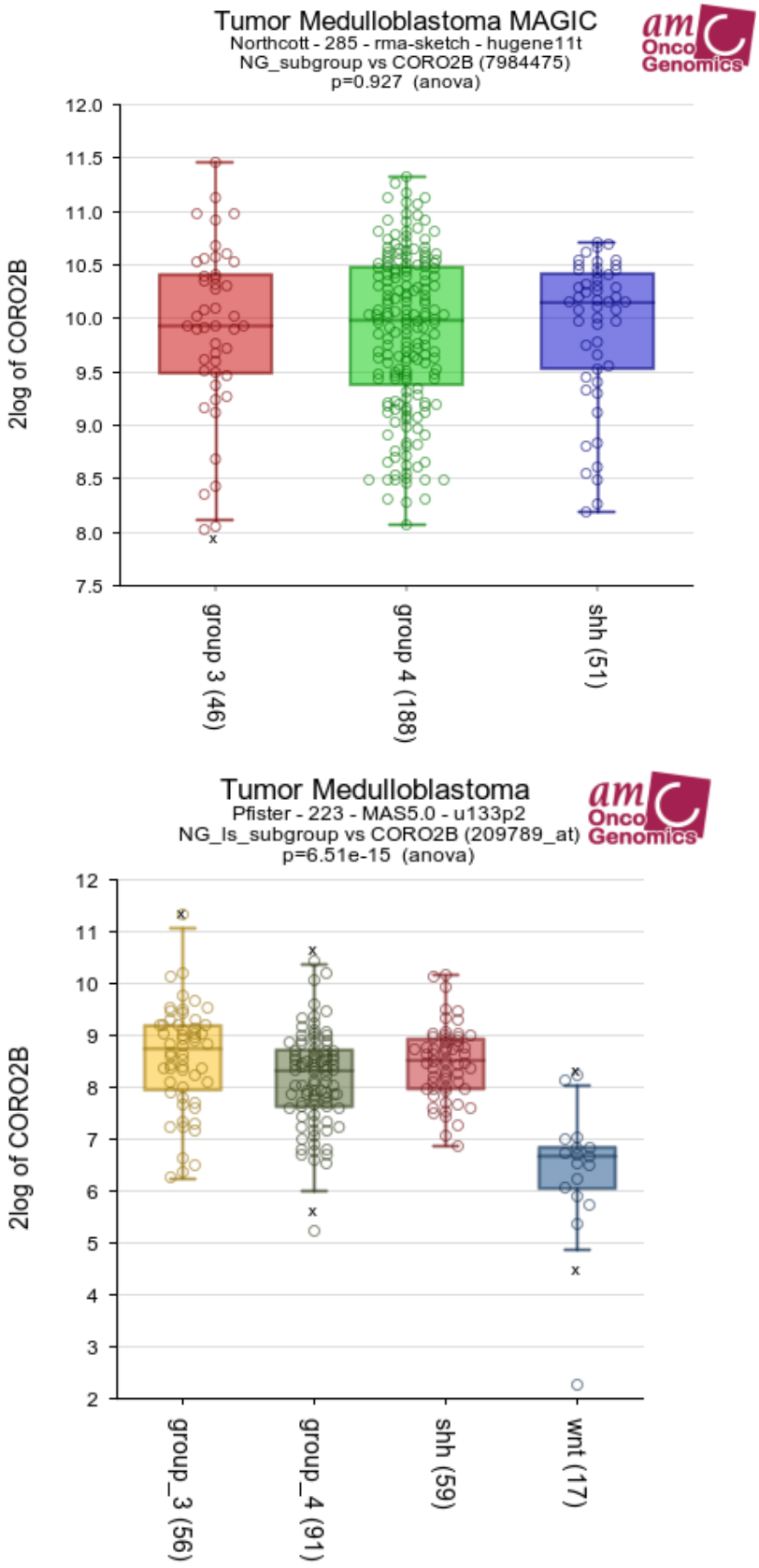
Supp. Fig. 1 Significant differences in expression between each group were calculated using one-way ANOVA with Tukey's multiple comparisons of geneexpression values in **A)** SORCS2, **B)** LMNB1 and **C)** CORO2B in the 4 molecular subgroups of medulloblastoma from the Cavalli et al., dataset in Figure 5.1.



Supp. Fig. 2 Gene expression (Log2) of *SORCS2* was assessed using the R2 Genomics Analysis and Visualization Platform using the **A)** Northcott *et al*., 2012 and **B)** Northcott *et al*., 2017 datasets.



Supp. Fig. 3 Gene expression (Log2) of *LMNB1* was assessed using the R2 Genomics Analysis and Visualization Platform using the **A)** Northcott *et al*., 2012 and **B)** Northcott *et al*., 2017 datasets.



Supp. Fig. 4 Gene expression (Log2) of *CORO2B* was assessed using the R2 Genomics Analysis and Visualization Platform using the **A)** Northcott *et al*., 2012 and **B)** Northcott *et al*., 2017 datasets.

	G3 α	G3 β	G3 γ	G4 α	G4 β	G4 γ	Shh α	Shh β	Shh γ	Shh ∆	Wnt α	Wnt β
G3 α	/	****	ns	****	****	****	****	****	ns	***	****	ns
G3 β	****	/	****	ns	ns	ns	ns	***	****	**	ns	****
G3 γ			/	****	****	****	****	****	ns	***	****	ns
G4 α				/	****	ns	ns	*	****	ns	ns	****
G4 β					/	***	****	****	****	****	*	****
G4 γ						/	*	****	****	****	ns	****
Shh α							/	ns	****	ns	Ns	****
Shh β								/	*	ns	****	**
Shh γ									/	Ns	***	*
Shh ∆										/	****	NS
Wnt α											/	****
Wnt β												/

Supp. Fig. 3 Significant differences in expression between each group were calculated using one-way ANOVA with Tukey's multiple comparisons of the SORCS2 expression values for 12 medulloblastoma subtypes in Figure 5.3.

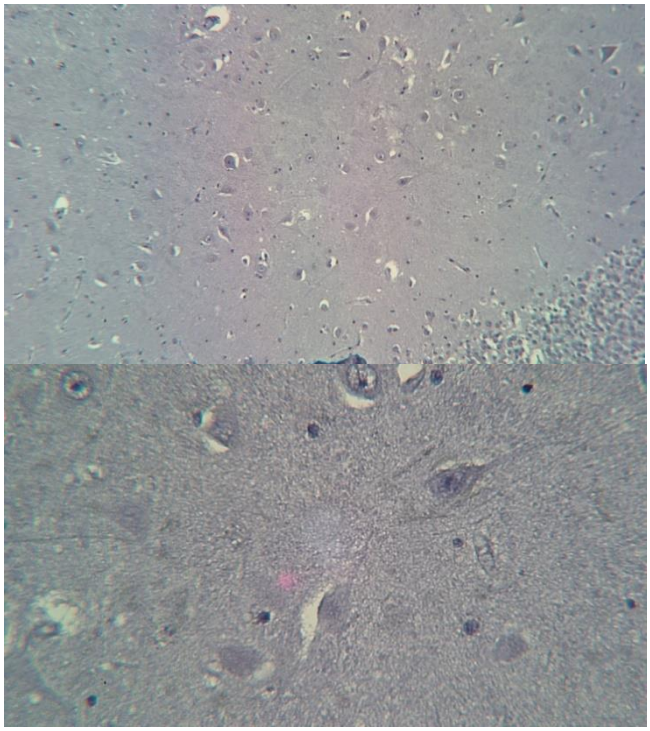
	G3 α	G3 β	G3 γ	G4 α	G4 β	G4 γ	Shh α	Shh β	Shh γ	Shh Δ	Wnt α	Wnt β
G3 α	/	ns	ns	**	ns	ns	****	****	****	****	****	****
G3 β		/	ns	ns	ns	ns	**	ns	****	****	****	****
G3 γ			/	**	ns	ns	****	****	****	****	****	****
G4 α				/	ns	ns	*	ns	****	****	****	****
G4 β					/	ns	****	*	****	****	****	****
G4 γ						/	****	**	****	****	****	****
Shh α							/	ns	****	****	**	**
Shh β								/	****	****	**	***
Shh γ									/	ns	ns	ns
Shh Δ										/	ns	ns
Wnt α											/	ns
Wnt β												/

Supp. Fig. 4 Significant differences in expression between each group were calculated using one-way ANOVA with Tukey's multiple comparisons of the LMNB1 expression values for 12 medulloblastoma subtypes in Figure 5.4.

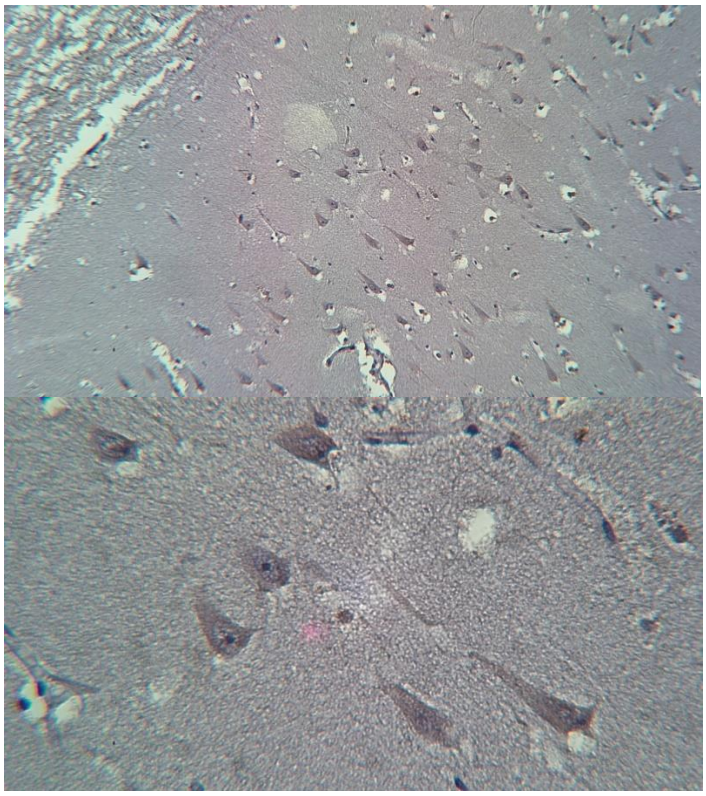
	G3 α	G3 β	G3 γ	G4 α	G4 β	G4 γ	Shh α	Shh β	Shh γ	Shh Δ	Wnt α	Wnt β
G3 α	/	****	****	**	ns	ns	****	****	****	****	****	****
G3 β		/	ns	ns	ns	ns	**	ns	****	****	****	****
G3 γ			/	**	ns	ns	****	****	****	****	****	****
G4 α				/	ns	ns	*	ns	****	****	****	****
G4 β					/	ns	****	*	****	****	****	****
G4 γ						/	****	**	****	****	****	****
Shh α							/	ns	****	****	**	**
Shh β								/	****	****	**	***
Shh γ									/	ns	ns	ns
Shh Δ										/	ns	ns
Wnt α											/	ns
Wnt β												/

Supp. Fig. 5 Significant differences in expression between each group were calculated using one-way ANOVA with Tukey's multiple comparisons of the CORO2B expression values for 12 medulloblastoma subtypes in Figure 5.5.

A) Negative staining control



B) Positive staining control



Supp. Fig. 6 Controls for the IHC staining of medulloblastoma TMAs in Figures 5.11-5.13. Pyramid cells in normal Hippocampus tissue stained with **A)** secondary antibody only or **B)** SORCS2 antibody.

Supp. Table 1 A) Clinical information on the patients whose tumours were included in the TMA analysis which had some SORCS2 staining.

SORCS2 score	Subgroup	Met status	survival time*	Gender	Age**	Details of metastasis or recurrence***
3	n/a	4	13	M	8.58	Widespread bone metastasis
2.33	G4	0	n/a	F	10.2	
2.25	WNT	0	n/a	M	10.11	
2.2	SHH	1	n/a	M	n/a	Recurrence in the spine after 10 months
2.16	WNT	n/a	n/a	F	8.6	
2	n/a	n/a	n/a	M	4.8	
2	n/a	0	n/a	n/a	13.08	
1.25	n/a	0	n/a	M	6.69	Recurrence in the leptomeninges
1	G4	3	n/a	M	5.9	Recurrence in the spine after 3 years
1	SHH	0	n/a	F	8.5	Recurrence at primary site after 2 years
1	WNT	0	n/a	n/a	n/a	
1	n/a	0	n/a	M	11.25	
1	n/a	n/a	n/a	n/a	n/a	
1	n/a	n/a	n/a	n/a	n/a	
0.92	WNT	0	n/a	M	n/a	
0.75	G4	2	n/a	M	8.2	Recurrence in the bone after 4 years
0.67	G4	3	n/a	n/a	n/a	
0.67	SHH	1	n/a	n/a	n/a	
0.5	G4	1	n/a	M	2.11	
0.5	G4	3	n/a	M	9.5	
0.5	G4	n/a	n/a	n/a	n/a	Leptomeningeal spread of disease also involving spinal cord and pituitary
0.5	n/a	n/a	n/a	n/a	n/a	Fourth ventricle tumour with extensive leptomeningeal tumour spread intracranially and in the spine.
0.5	n/a	n/a	n/a	n/a	n/a	
0.49	G4	2	n/a	n/a	12.1	
0.37	n/a	3	n/a	M	n/a	Recurrence in the leptomeninges
0.34	n/a	n/a	n/a	n/a	n/a	
0.33	G4	3	n/a	M	5.1	Recurrence after 2 years
0.33	G3	0	n/a	M	2.1	
0.25	G4	0	n/a	M	6.75	
0.25	SHH	3	n/a	M	10.58	Residual leptomeningeal disease but no spinal disease, recurrence after 3 years
0.25	n/a	n/a	n/a	n/a	n/a	
0.25	n/a	n/a	n/a	n/a	n/a	
0.17	G3	0	n/a	M	3.5	
0.17	G4	3	n/a	M	4.93	Recurrence after 8 months
0.17	G4	0	n/a	n/a	n/a	
0.17	SHH	0	n/a	M	17.6	
0.17	n/a	n/a	n/a	n/a	n/a	
0.16	n/a	n/a	n/a	n/a	n/a	

Supp. Table 2 B) Clinical information on patients whose tumours were included in the TMA analysis which did not have any SORCS2 staining.

SORCS2 score	Sub group	Met status	survival time*	Gender	Age**	Details of metastasis or recurrence***
0	G3	0	n/a	M	2.46	
0	G3	1	n/a	M	5.5	
0	G3	0	n/a	M	4.11	Recurrence after 10 months
0	G3	n/a	n/a	M	4.1	Recurrence in leptomeninges after 4 years
0	G3	2	n/a	F	4.17	Extensive leptomeningeal spread on MRI but no spinal leptomeningeal spread, recurrence after 2 months
0	G4	0	n/a	F	4.7	
0	G4	0	72	M	9.3	
0	G4	2	n/a	M	12.06	
0	G4	1	n/a	M	3.5	
0	G4	n/a	n/a	M	5.1	Recurrence in spine and intracranial after 1 year
0	G4	0	n/a	F	1.9	Intracranial and spinal recurrence after 3 years
0	G4	0	n/a	F	4.58	Recurrence after 1 year
0	G4	0	n/a	M	12.42	
0	SHH	0	n/a	F	3.6	
0	SHH	0	n/a	n/a	n/a	
0	SHH	0	n/a	M	12.9	
0	SHH	n/a	n/a	M	12.5	
0	SHH	n/a	n/a	n/a	n/a	
0	SHH	2	n/a	F	n/a	
0	WNT	0	n/a	M	6.1	
0	WNT	0	n/a	n/a	n/a	
0	n/a	0	n/a	F	n/a	Recurrence after 3 years
0	n/a	0	n/a	M	2.97	Recurrence after 1.5 years
0	n/a	0	n/a	M	n/a	
0	n/a	1	n/a	M	n/a	
0	n/a	0	44	F	5	
0	n/a	1	n/a	M	2.92	Medulloblastoma cells seen in CSF
0	n/a	n/a	n/a	n/a	n/a	
0	n/a	n/a	n/a	n/a	n/a	
0	n/a	n/a	n/a	n/a	n/a	
0	n/a	n/a	n/a	n/a	n/a	
0	n/a	0	14	M	12.4	
0	n/a	n/a	n/a	n/a	n/a	Intracranial recurrence after 5 years
0	n/a	n/a	n/a	n/a	n/a	

*Survival time in months

**Age at diagnosis

***Details of metastasis and recurrence are included if known

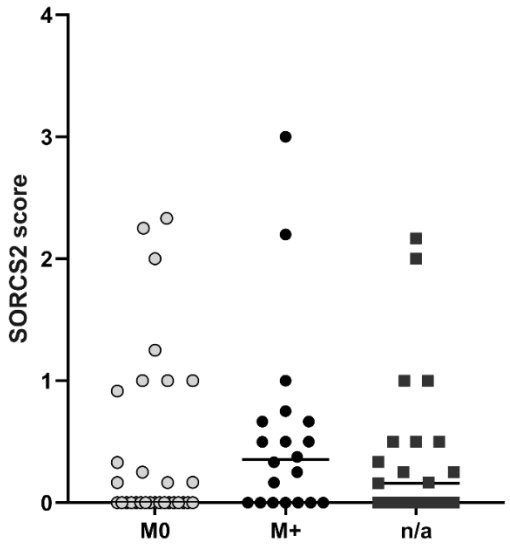
A)

	G3	G4	Shh	Wnt	n/a
G3	/	ns	ns	ns	ns
G4		/	ns	ns	ns
Shh			/	ns	ns
Wnt				/	ns
n/a					/

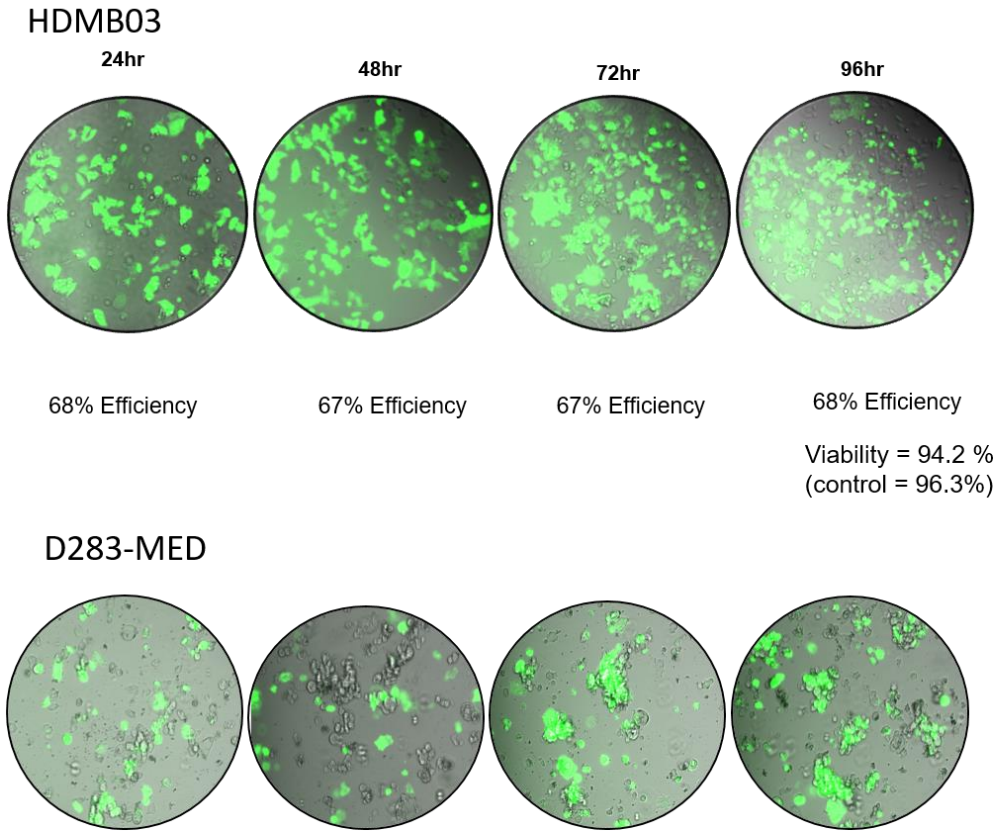
B)

	M0	M1	M2	M3	M4	n/a
M0	/	ns	ns	ns	**	ns
M1		/	ns	ns	**	ns
M2			/	ns	**	ns
M3				/	**	ns
M4					/	ns
n/a						/

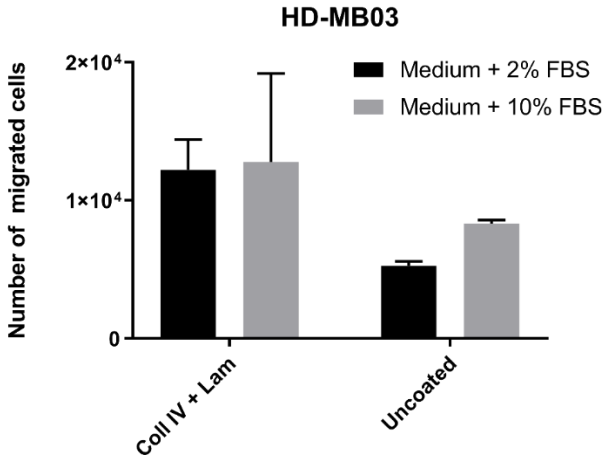
Supp. Fig. 7 Significant differences in expression between each group were calculated using one-way ANOVA with Tukey's multiple comparisons of the score according to **A)** molecular subgroup or **B)** Chang's staging system in Figure 5.14.



Supp. Fig. 8 SORCS2 protein expression in tumour cores from non-metastatic patients (M0), metastatic patients (M+) or unknown (n/a) patients. The metastatic status was determined using Chang's metastatic groups (M1-M4), and the 4 metastatic groups were combined under M+ in this figure, showing the same data as Figure 5.11.

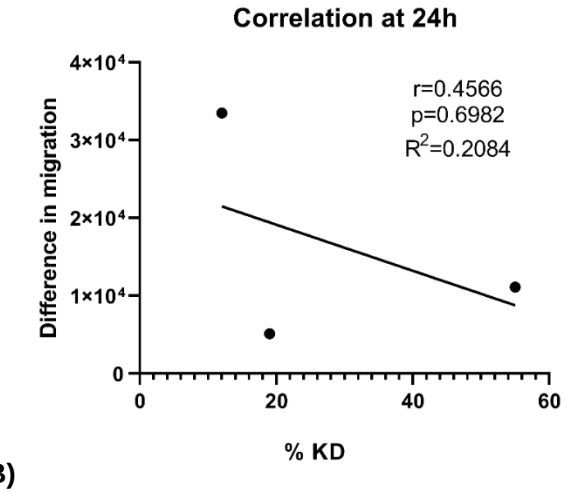


Supp. Fig. 9 Transfection efficiency in HD-MB03 and D283-MED cell lines using Mouse NSC Nucleofector Kit (Lonza) was used with the programme A0-33 on $0.5x10^6$ cells .

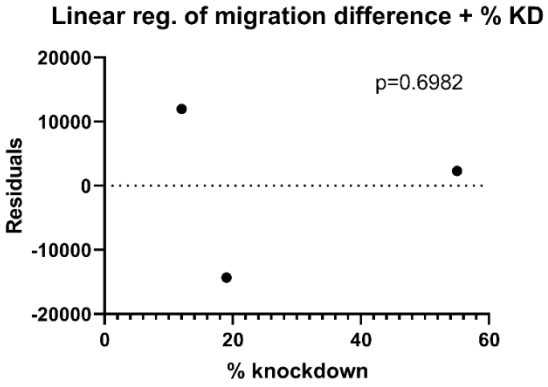


Supp. Fig. 10 The number of migrated cells treated with starved overnight in 2% FBS medium 5 hours after nucleofection or left in 10% FBS medium overnight after nucleofection. Metabolic activity assay results for each condition were plotted against a standard curve of known cell numbers in order to derive the exact number of migrated cells.

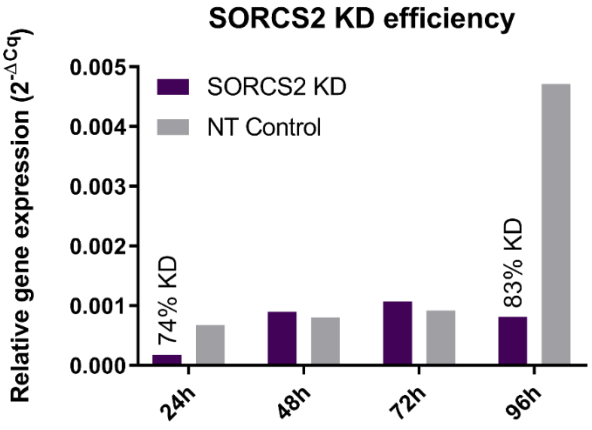
A)



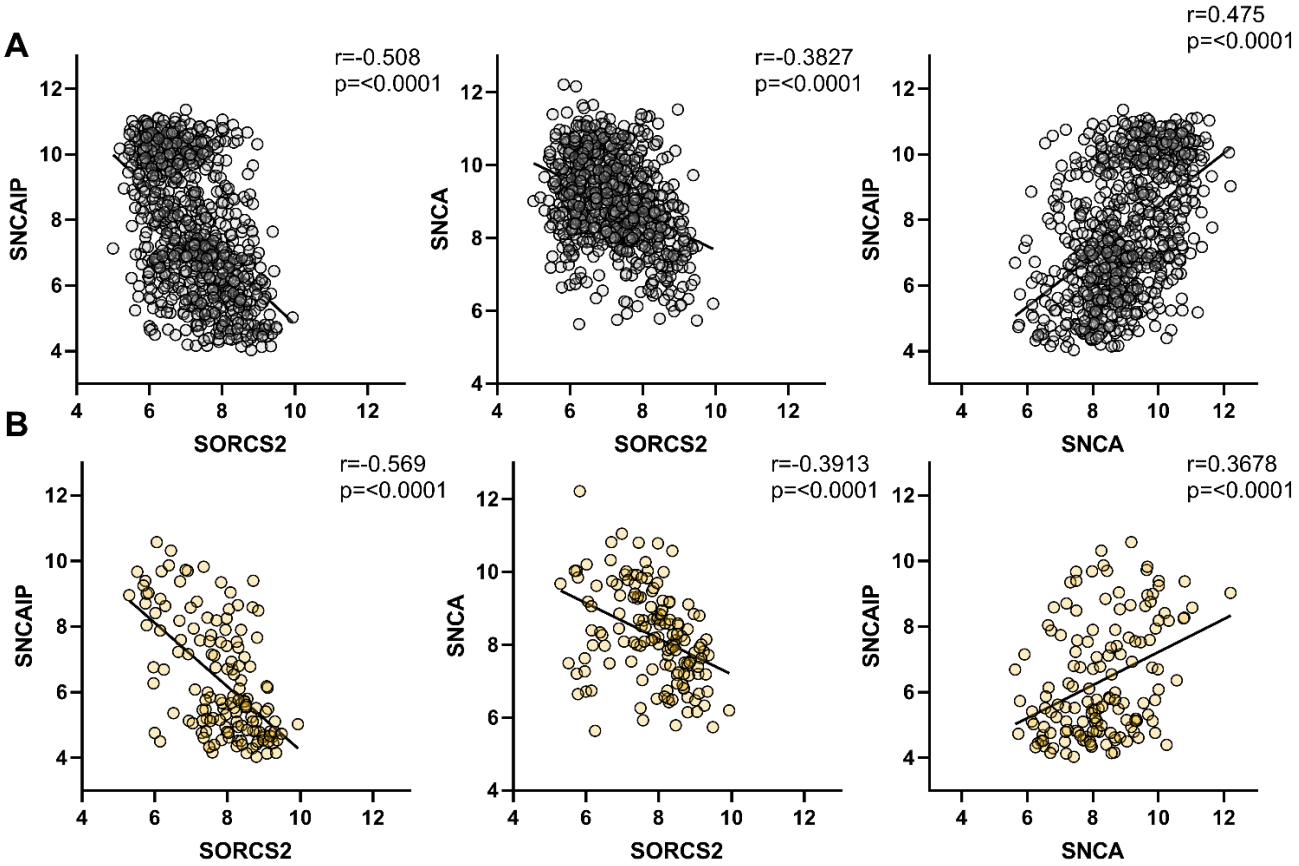
B)



Supp. Fig. 11 A) Pearson's correlation analysis and **B)** linear regression analysis of residuals for the difference in number of migrated cells as compared to a non-targeting control, with the percent (%) decrease in SORCS2 expression quantified by qRT-PCR.



Supp. Fig. 12 The mean of RNA expression in cells treated with SORCS2 siRNA or a non-targeting control siRNA quantified by qRT-PCR corresponding to the Western Blot in Figure 5.19.



Supp. Figure 13 Correlation analysis of SORCS2, SNCAIP and SNCA gene expression in medulloblastoma patients.

A) Pearson's correlation (r) analysis was performed using gene expression of patients in the Cavalli *et al*., dataset using the R2 database. *SORCS2* expression was inversely correlated with *SNCAIP* expression (r -0.508, p<0.0001) and SNCA expression (r-0.3827, p<0.0001), in patients of all subgroups n=763. The expression of *SNCAIP* and *SNCA* was correlated in the same patients (r=0.475, p<0.0001). **B)** *SORCS2* expression inversely correlated with *SNCAIP* expression (r -0.569, p<0.0001) and SNCA expression (r-0.3913, p<0.0001) in Group 3 patients only in the same dataset. The expression of *SNCAIP* and *SNCA* was correlated in the same patients (r=0.3678, p<0.0001) in Group 3 patients only in the same dataset, n=144.